Post-Buckling Behaviour of Prestressed Steel Stayed Columns

A thesis submitted to the University of London

for the degree of Doctor of Philosophy

by

Daisuke Saito

B.Eng M.Eng

Department of Civil and Environmental Engineering,

Imperial College of Science, Technology & Medicine,

London SW7 2AZ, UK

February 2008

Abstract

A prestressed steel stayed column is a structural component that is reinforced by either cable stays or rods such that its strength is increased in axial compression. This system provides a considerable increase in axial strength due to the restriction from the stay of the primary buckling movement.

In the past, greater emphasis was placed on its higher critical load, and hence, extensive studies were performed on this. However, knowledge of the post-buckling behaviour is rather important for designers to ensure the safety and the cost-effectiveness of the structure. Despite its potential importance, the post-buckling response has not previously been investigated satisfactorily. Therefore, the primary aim of the current study was to investigate the theoretical post-buckling behaviour of stayed columns.

A geometrically nonlinear model accounting for the post-buckling behaviour of a single-crossarm stayed column was formulated using the Rayleigh–Ritz method; then, the model was validated using the finite element method. Geometrical imperfections and the occurrence of possible material failure were also considered to account for realistic behaviour in addition to the theoretical behaviour of the component in a perfect state.

As part of the study, finite element models were developed to account for interactive buckling. The results suggest that interactive buckling gains practical importance when higher modes become critical. Using the same model, the optimal value of prestress was also investigated through the application of more rational structural

optimization indicators proposed in the thesis. It was revealed that the optimal level of the prestress was higher than that previously thought based on linear buckling analysis. Furthermore, comparisons of the optimization indicators for different cases allowed the ideal configuration of the stayed column to be inferred.

Acknowledgements

This work was carried out under the supervision of Dr Ahmer Wadee, Senior Lecturer in the Department of Civil and Environmental Engineering. I am extremely grateful for all of his expert help and advice and his continuous encouragement throughout the project.

I would like to acknowledge the financial support for the project provided by the Overseas Research Students Award Scheme (ORSAS).

I would also like to acknowledge The Royal Academy of Engineering for partially funding the attendance of the third international conference on structural engineering, mechanics and computation in Cape Town, South Africa in September 2007.

I would like to thank John Hughes, the coordinator of the English Language Support Programme (ELSP) for his dedicated language support throughout the course of my studies.

I am also grateful to my colleagues, Arash Soleiman Fallah, Miguel Castro, Rafee Mukbol, Tak Ming Chan, Jason Treadway, Alan Nip, Mohammad Reza Haidarali, Alexandre Delsavio and Michal Jandera for valuable suggestions about various subjects together with their emotional support.

Finally, I will be grateful to my wife, Mami and parents for their support and encouragement throughout the course of my studies.

Contents

List of Figures

Notation

Coordinates, Stress, Strains, Loads and Energy

x	Longitudinal direction along column length
y	Transverse direction along crossarm length
ε_{ciX}	Axial strain in column
ε_{siXj}	Axial strain in stay
σ_s	Axial stress in stay
ε_{st}	initial strain in stay
ε_{ct}	initial strain in column
ε_{at}	initial strain in crossarm
T	Initial prestress force in stay
T_c	Initial prestress force in column
T_a	Initial prestress force in crossarm
T_{iXj}	Axial force in stay
C_{iX}	Compression force in column
S_{iX}	Shear force in column
M_{iX}	Bending moment in column
M_{aX}	Bending moment in crossarm
R_{hX}	Horizontal reaction force at crossarm tip
R_{vX}	Horizontal reaction force at crossarm tip
$\mathrm{d}F_{X3},\ \mathrm{d}F_{X4}$	Axial force changes in stays
V_{iX}	Total potential energy

U_{cbi}	Strain energy of bending in column
U_{ab2X}	Strain energy of bending in crossarm
U_{caiX}	Axial strain energy in column
U_{caiX}	Axial strain energy in column
$P\mathcal{E}_{iX}$	Work dove by load
P	External load
P^{C}	Critical buckling load
$P^{\mathrm{C}i}_{\mathrm{Zone1}}$, $P^{\mathrm{C}}_{\mathrm{Zone2}}$, $P^{\mathrm{C}i}_{\mathrm{Zone3}}$	Critical buckling load for each zone
$P^{\mathrm{C}}_{\mathrm{max}}$	Maximum buckling load
P_{E}	Euler load
T_{opt}	Initial prestress at the maximum buckling load
T_{min}	Minimum-required initial prestress to increse buckling load

Prestressed Stayed Column Properties

Geometry

L	Column length
a	Crossarm length
L_s	Stay length
α	Angle between column and crossarm
ϕ_{co}	Outside diameter of the column
ϕ_{ci}	Inside diameter of the column
ϕ_{ao}	Outside diameter of the crossarm
ϕ_{ai}	Inside diameter of the crossarm
ϕ_s	Stay diameter

Material Properties

E	Young's modulus of column
E_a	Young's modulus of crosssarm
E_s	Young's modulus of stay
A	Cross sectional area of column
A_a	Cross sectional area of crosssarm
A_s	Cross sectional area of stay
I	Cross-sectional second moment of area of column
I_a	Cross-sectional second moment of area of crossarm

Stiffness

K_c	Axial stiffness of a column
K_s	Axial stiffness of a stay
K_a	Axial stiffness of a crossarm

Displacements and Degrees of Freedom

Post-buckling

$W_1(x),\ W_2(x)$	Displacement functions of column
$\Theta_1(x),\ \Theta_2(x)$	Angle functions of column
$w_{2X}(y)$	Displacement functions of crossarm
h_X	Tip displacement of crossarm
$c_B,\ c_C$	Tip displacement coefficients
L_{siXj}	Stay length under loading

α_{iXj}	Stay angle under loading
$q_1,\ q_3,\ q_{2m-1}$	Amplitudes for Mode 1 buckling
$q_2,\ q_4,\ q_{2m}$	Amplitudes for Mode 2 buckling
Δ_{iX}	End-shortening of column
$b_{pX},\ b_{tX},\ b_{mX},\ b_{mlX}$	End-shortening coefficients
γ	Angle between the horizontal and crossarm
β_i	Angle between the vertical and column end

Imperfections

$W_{1\delta},\ W_{2\delta}$	Imperfection displacements of a column
$\delta,\ \delta_1,\ \delta_2$	Amplitude of imperfection
L_{sij}	Initial stay length with imperfection
α_{ij}	Initial stay angle with imperfection
$\mathcal{E}_0$	Mean square measure end-shortening of total initial imperfection
$\mu_1,\ \mu_2$	Coefficients for imperfection combinations

Optimal level of prestress

$P_{\text{el,max}}$	Elastic maximum load capacity of a stayed column
$f_{\text{y,req}}$	Required column yield stress
$f_{\text{s,Rd,req}}$	Required stay design stress
η	Ratio of the elastic maximum load capacity to the required structural resitance for the column
η_s	Ratio of the elastic maximum load capacity to the required structural resitance for the stay
T_{ropt}	Optimal level of prestress

T_{ropt1}	Optimal level of prestress obteined from η
T_{ropt2}	Optimal level of prestress obteined from η_s
χ	Buckling reduction factor

Chapter 1

Introduction

1.1 Background

A prestressed steel stayed column (Figure 1.1) is a structural component that is reinforced by either cable stays or rods such that its strength is increased in axial compression. Ordinary columns have a propensity to buckle under axial compression primarily due to their characteristic of being slender. To counter this, a prestressed steel stayed column is equipped with pre-tensioned stay systems; these restrain the column buckling displacement through horizontal crossarms placed at some intermediate distance from the column ends. Consequently, this additional system acts to prevent the principal movement during conventional column buckling and potentially provides a considerable increase in axial strength.

An application of this column type can be found where slender supports or towers are required; for example, it was used as a temporary support during the erection phase of the main stage of the "Rock in Rio III" stadium in Rio de Janeiro, Brazil (De Andrade *et al.*, 2003a; De Andrade *et al.*, 2003b)—see Figure 1.2. In this project, it was required to support the large roof structures as high as 36 metres above ground level. Conventional construction methods would have required a massive and complicated shoring system with a commensurate time penalty. To counter

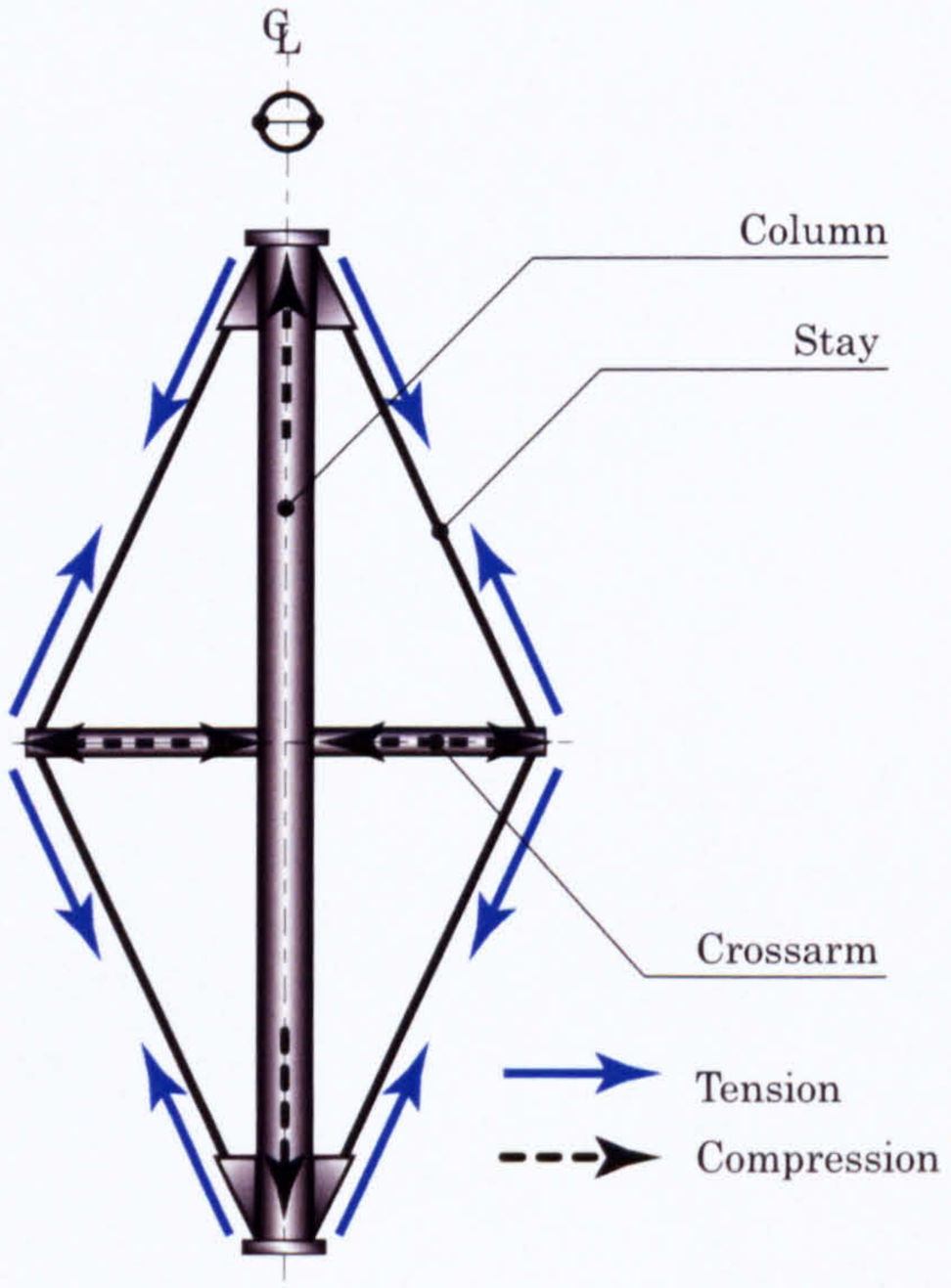

Figure 1.1: Principle of the prestress steel stayed column: stays are pretensioned to provide lateral restraint against overall buckling.

this, the engineers decided to adopt stayed columns as the shoring system. Owing to its structural simplicity and superiority in resisting axial loads, this choice allowed the engineers to save significant time in the construction process.

Another example can be found in Building 5 at Chiswick Park, London as shown in Figure 1.3. Owing to an aesthetic requirement, the columns that support aluminium solar shading fins were designed to be slender. In order to achieve this requirement, the stayed column system was adopted.

In addition to these practical uses, a number of research works on stayed columns have existed since the 1960s, such as those evaluating critical buckling loads (Chu & Berge, 1963; Mauch & Felton, 1967; Smith *et al.*, 1975; Temple, 1977; Belenya, 1977; Hafez *et al.*, 1979), imperfection sensitivity studies (Wong & Temple, 1982; Chan *et al.*, 2002), and examining the column's maximum axial strength (Temple *et al.*, 1984; Smith, 1985).

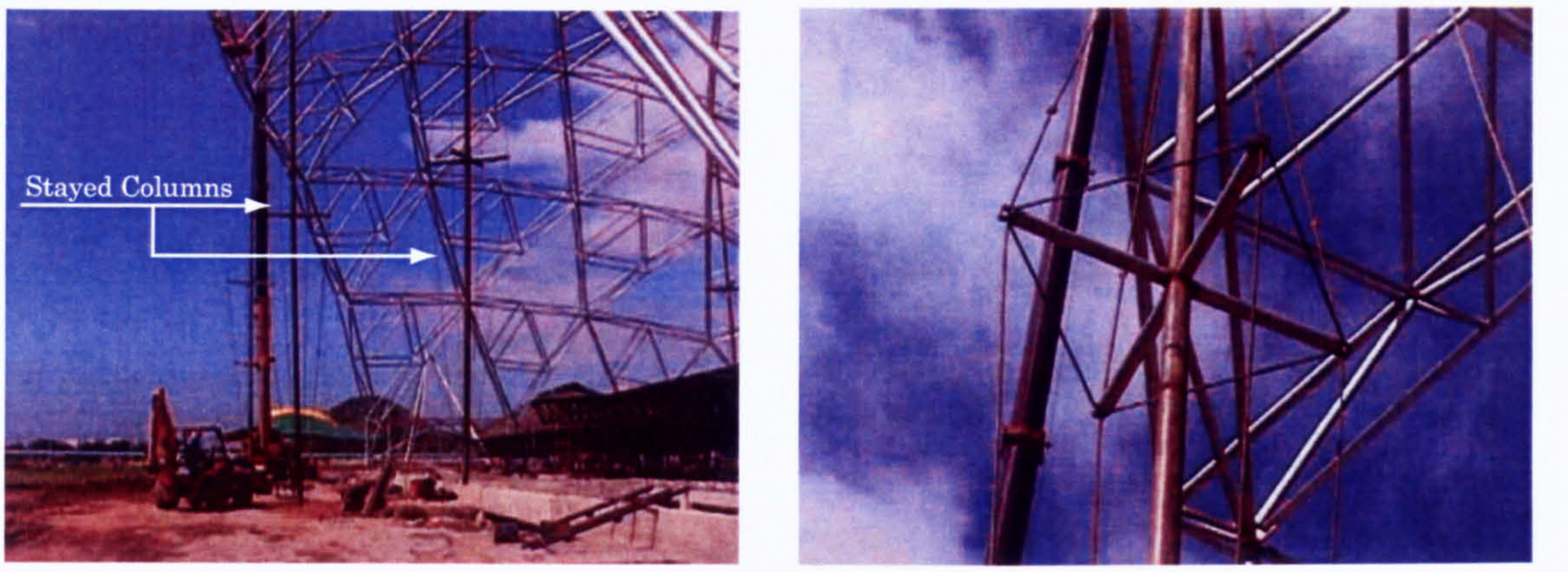

(a) stayed column as a temporary shoring (b) crossarm in detail

Figure 1.2: Use of stayed columns in the construction phase of Rock in Rio III main stage.

Despite this progress, to the best knowledge of the author, the post-buckling response has not been investigated satisfactorily. This information is crucial to make the design safer and more efficient; stability in the post-buckling range implies that the design load could potentially be set higher in consideration for the post-buckling stiffness; conversely, instability in the post-buckling range means the design load should be significantly reduced in order to ensure safety and the potentiality of the structure being sensitive to imperfections (Thompson & Hunt, 1973).

With the background mentioned above, the aims of the research presented herein are as follows:

1. To reveal the post-buckling response of stayed columns, in particular the stability of the equilibrium response after buckling.

2. To propose design recommendations for stayed columns in the light of the results obtained.

In the current study, the post-buckling response was investigated by developing analytical models using energy principles and numerical models using the finite element method (FEM).

Figure 1.3: Building 5 at Chiswick Park, London—the stayed column system was adopted for the façade in conjunction with the shading fins.

1.2 Methodology

1.2.1 Object of the study

There are many possible forms of stayed columns, as can be seen from Figure 1.4. With large numbers of crossarms, the effective length of the column can become even shorter, which provides the structure with a much higher axial resistance in compression. In the current work, a two-dimensional[1], single-crossarm stayed column, the simplest type, shown in Figure 1.1, was modelled. It is known from previous work that investigating the stayed column with an analytical procedure inevitably involves mathematically sophisticated formulations; therefore, modelling the simplest structure is a rational first step to revealing its post-buckling response. Moreover, the majority of the literature deals with this single-crossarm type; hence, validation and comparisons with previous research are possible.

[1]In a three-dimensional case, the buckling direction does not occur in the same plane as the one where the stays exists, which would render the analytical model even more sophisticated

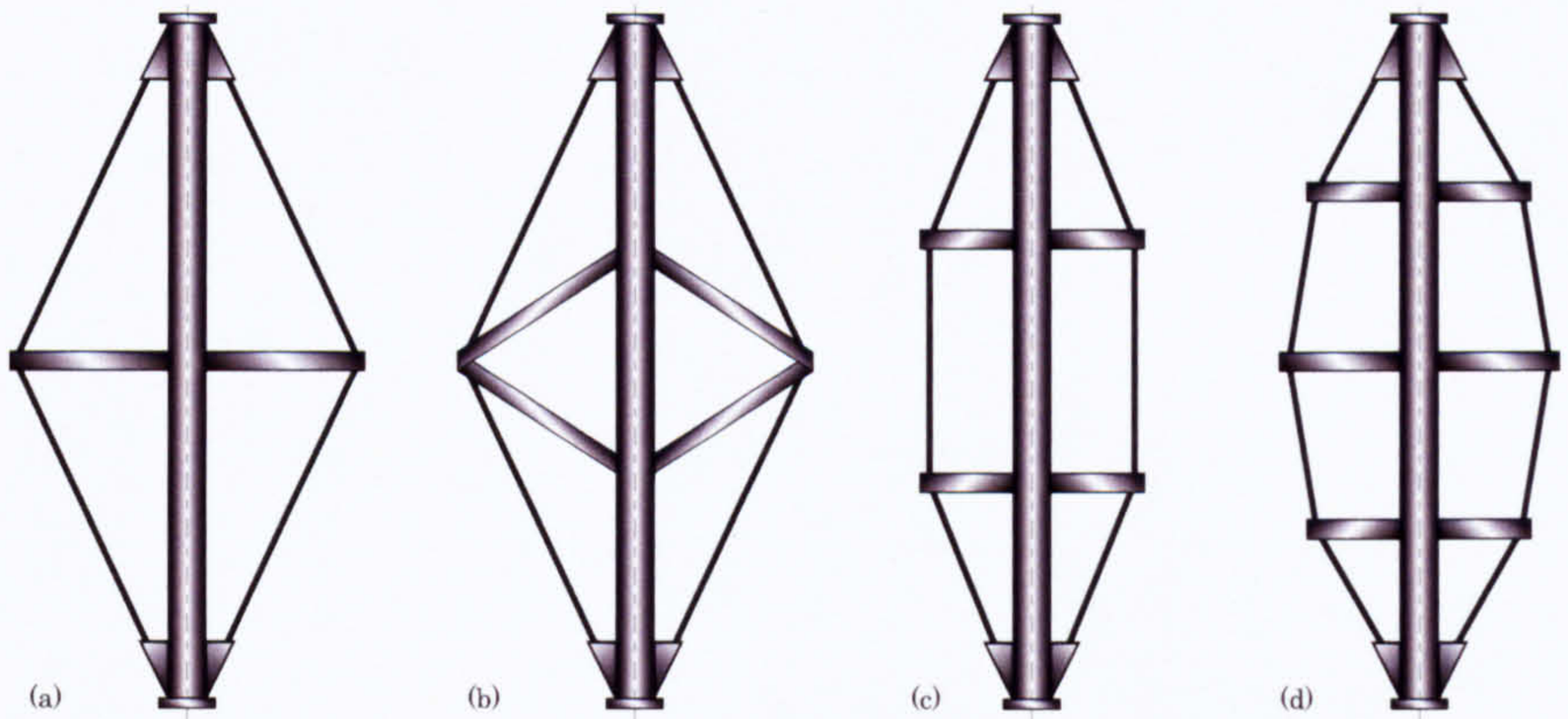

Figure 1.4: Variation of stayed column: (a) single-crossarm, (b) split-up (bipod) crossarm, (c) double crossarm, rectangular, (d) triple crossarm, bowstring. Note that by increasing the number of crossarms, the effective length of the column will be reduced; thereby, even higher buckling loads can be achieved.

1.2.2 Overview of analysis methods

In order to perform post-buckling analysis with an analytical method, the total potential energy principle was applied with the use of the Rayleigh–Ritz method, which is covered in some textbooks (Thompson & Hunt, 1973; Thompson & Hunt, 1984; Simitses, 1976; Allen & Bulson, 1980). Although this is a classic approach compared with a numerical approach such as the nonlinear FEM, and sometimes, inevitably involves considerable error due to its approximation, this method does not require imposing geometrical initial imperfections onto the model to investigate equilibrium paths, which allows us to understand the buckling responses of a structure more systematically. The details of this analytical method are described in §1.4.

Finite element (FE) analysis was also conducted for validation and parametric study purposes, expecting to evaluate the behaviour of the stayed column accurately. As the main focus of the research is overall scale buckling, not local buckling of the main column element, the model was developed on a two-dimensional basis with the use of beam and truss elements, which allows the model to be less computationally expensive than fully three-dimensional models. By taking this advantage, a large number of parametric studies were conducted, including investigation into interactive buckling behaviour. Further details of the numerical model are described at the

relevant stage in the thesis.

1.3 Introduction to Post-Buckling Analysis

1.3.1 Post-buckling stability

From the viewpoint of design engineers, post-buckling analysis might seem less important, because ordinary columns can be designed largely with consideration of only their critical loads and their yield stress (Dowling *et al.*, 1988; Trahair *et al.*, 2001). In fact, the ordinary column has an almost flat but slightly stable post-buckling response; thus there is no significant post-buckling strength nor stiffness, which means that any consideration towards its post-buckling response is basically unnecessary. Despite the response of ordinary columns, when a structure is thin-walled or stiffened, the post-buckling response usually gains importance. In plated structures, significant stable paths can be found in their post-buckling response (see Figure 1.5); therefore, plated structures can be designed with the thought that they can carry a larger load than their critical load. Further examples are restrained columns

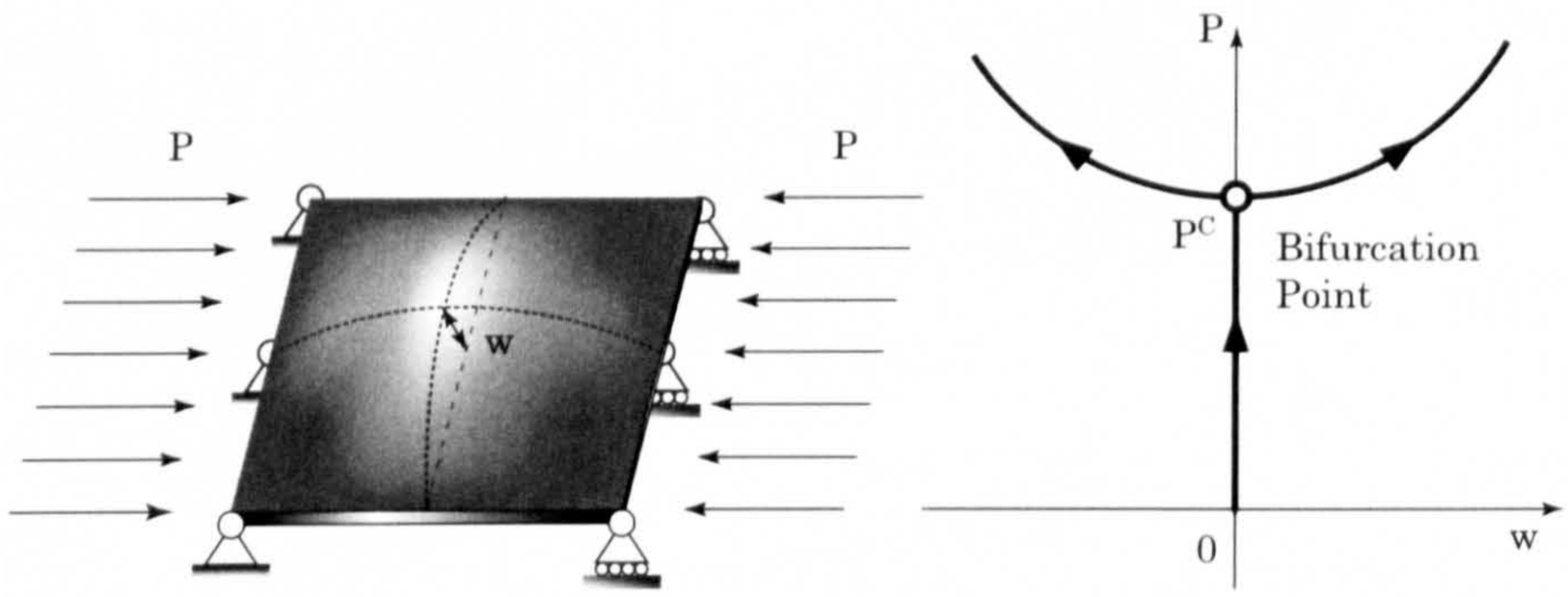

Figure 1.5: Stable post-buckling response of a simply-supported plate.

(see Figure 1.6); in this case, the critical load P^C can be sent higher thanks to its supporting spring, but unstable paths can emerge after buckling (Tsien, 1942; Hunt, 1989). In such cases, safety factors and sensitivities to initial imperfections should be carefully examined to ensure structural safety and integrity. As the stayed column

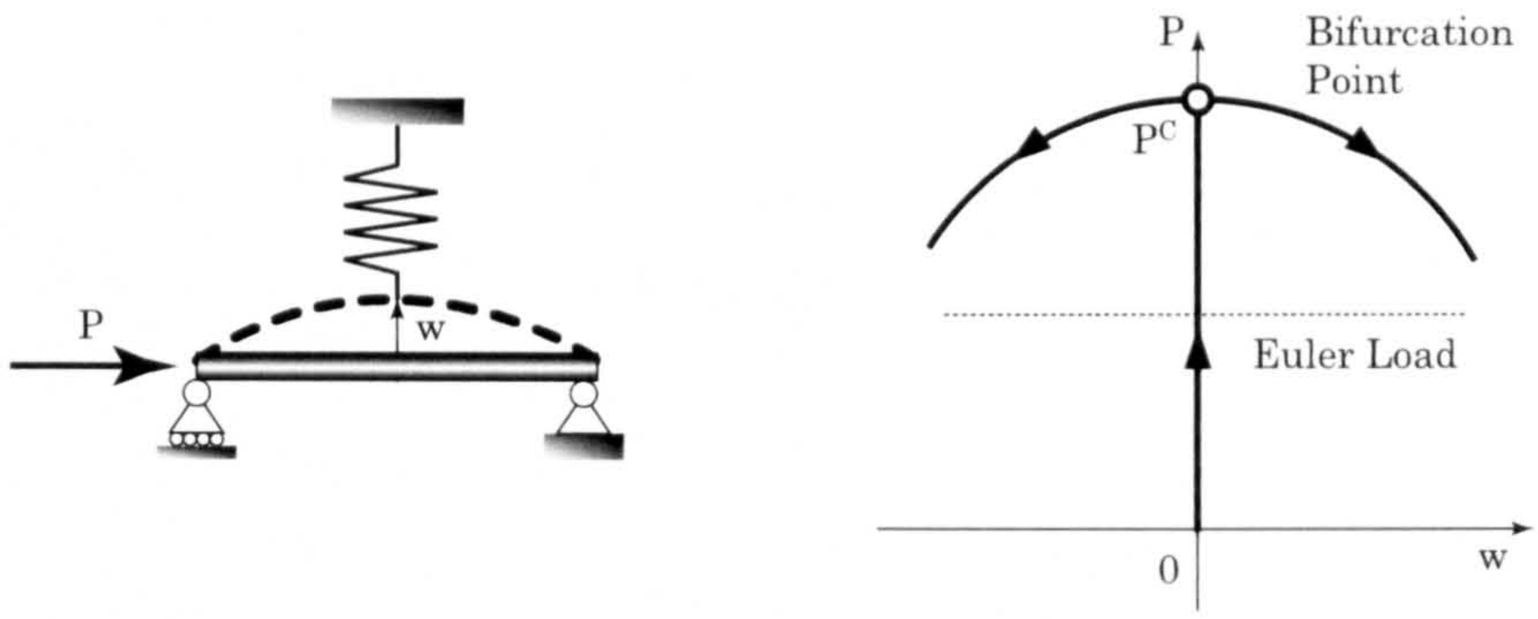

Figure 1.6: Unstable post-buckling response of a restrained column.

is an example of a stiffened structure, a complicated and significant post-buckling response can be expected. Thus, information about its post-buckling response is essential, either to make the most of structural strength when the post-buckling path is stable, or to ensure structural safety when the post-buckling path is unstable.

1.3.2 Interactive buckling

Different wavelengths of buckling may occur within the same structure; in the case of the restrained column shown in Figure 1.6, a half wave and a full length wave can be observed, depending on the stiffness of the spring. Different wavelengths of buckling create the possible problem of "interactive buckling", which is a phenomenon in which different modes of buckling occur simultaneously. It has been reported as quite a notorious phenomenon for structural safety in previous work. When a structure is compressed, typically overall buckling, buckling along the total length of the structure, occurs as the first failure mode. If afterwards the compression is maintained, i.e. if the structure goes into a post-buckling state, a different mode of buckling may emerge at some point, depending on the shape of the structure. This new mode combines with the overall buckling and results in a new rather complicated interactive buckling mode shape. Catastrophic structural failure can be triggered by this interactive buckling through a sudden loss of structural stiffness; therefore, avoiding interactive buckling is considered to be one of the most impor-

tant issues for the safety of structures. Since interactive buckling seems to be one of the important issues in the current work because of the structural configuration, more examples of this phenomenon are reviewed in this section.

A relatively simple type of interactive buckling can be found in ordinary plates. As shown in Figure 1.7, two different wavelengths of overall buckling can be combined (Supple, 1970). Furthermore, with large deflections, the interaction with other modes also occurs (Everall & Hunt, 1999), resulting in a further complicated post-buckling response.

Arches—beams initially deflected upwards whose horizontal movements are restricted at both ends—have similar interactive mode shapes to plates though an unstable post-buckling response occurs rather than a stable response (Huseyin, 1974; Zeeman, 1977; Thompson & Hunt, 1984). An asymmetric buckling profile is observed after buckling; the configuration consists of two different wavelengths of overall buckling, as can be seen from Figure 1.8, the asymmetry being a key feature indicating interactive buckling.

Cylindrical shells (Hutchinson & Koiter, 1970; Hunt *et al.*, 1986; Hunt *et al.*, 1997) have a more complicated type of interactive buckling system than ordinary plates and arches. Different wavelengths of local buckling appear consecutively due to the interruption of the longitudinal deflection caused by the cross sectional deformation. Despite the perfect symmetry of each buckling mode in isolation, in combination they can account for the diamond pattern of buckling, as shown in Figure 1.9, where the symmetric breaking mode is observed axially. Interactive buckling is also found in skin-stringer stiffened plates (Murray, 1973; Koiter & Pignataro, 1976; Luongo & Pignataro, 1988; Sridharan & Peng, 1989; Ronalds, 1989; Azhari & Bradford, 1995; Falzon & Cerini, 2006), which are commonly used in aeronautical and bridge structures. In this case, overall skin buckling can induce localized stiffener buckling (local buckling, known as *tripping*), as shown in Figure 1.10.

The reticulated column (Thompson & Hunt, 1973), shown in Figure 1.11, is also an interesting example illustrating interactive buckling. This structure is composed of

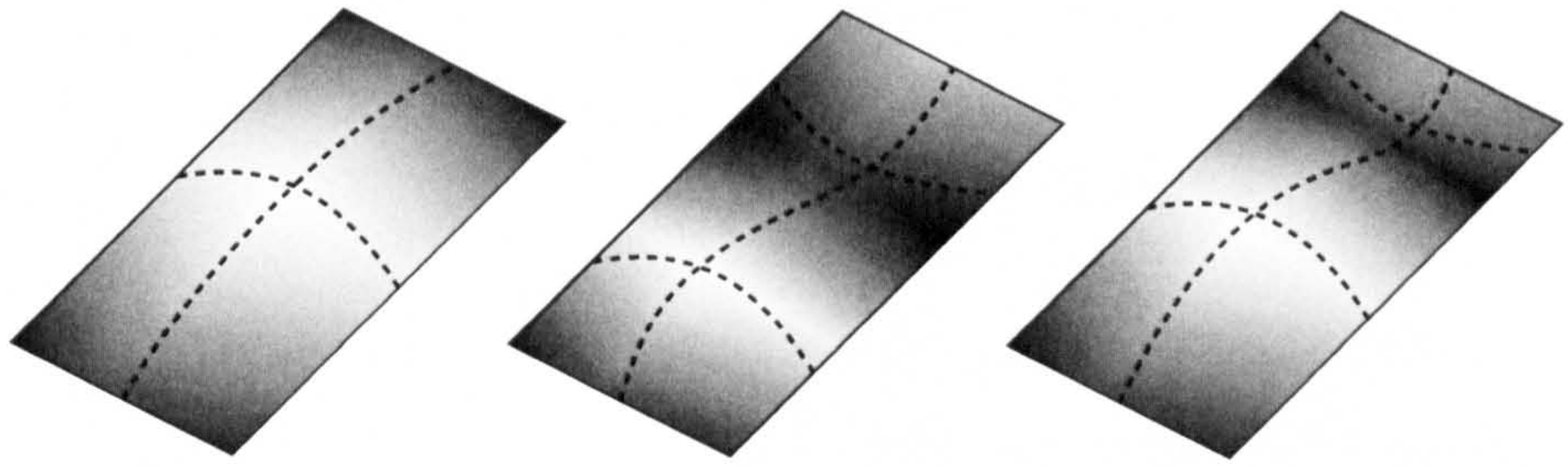

(i) one half-wave (ii) two half-waves (iii) coupled waves (interactive buckling)

(a) buckling mode

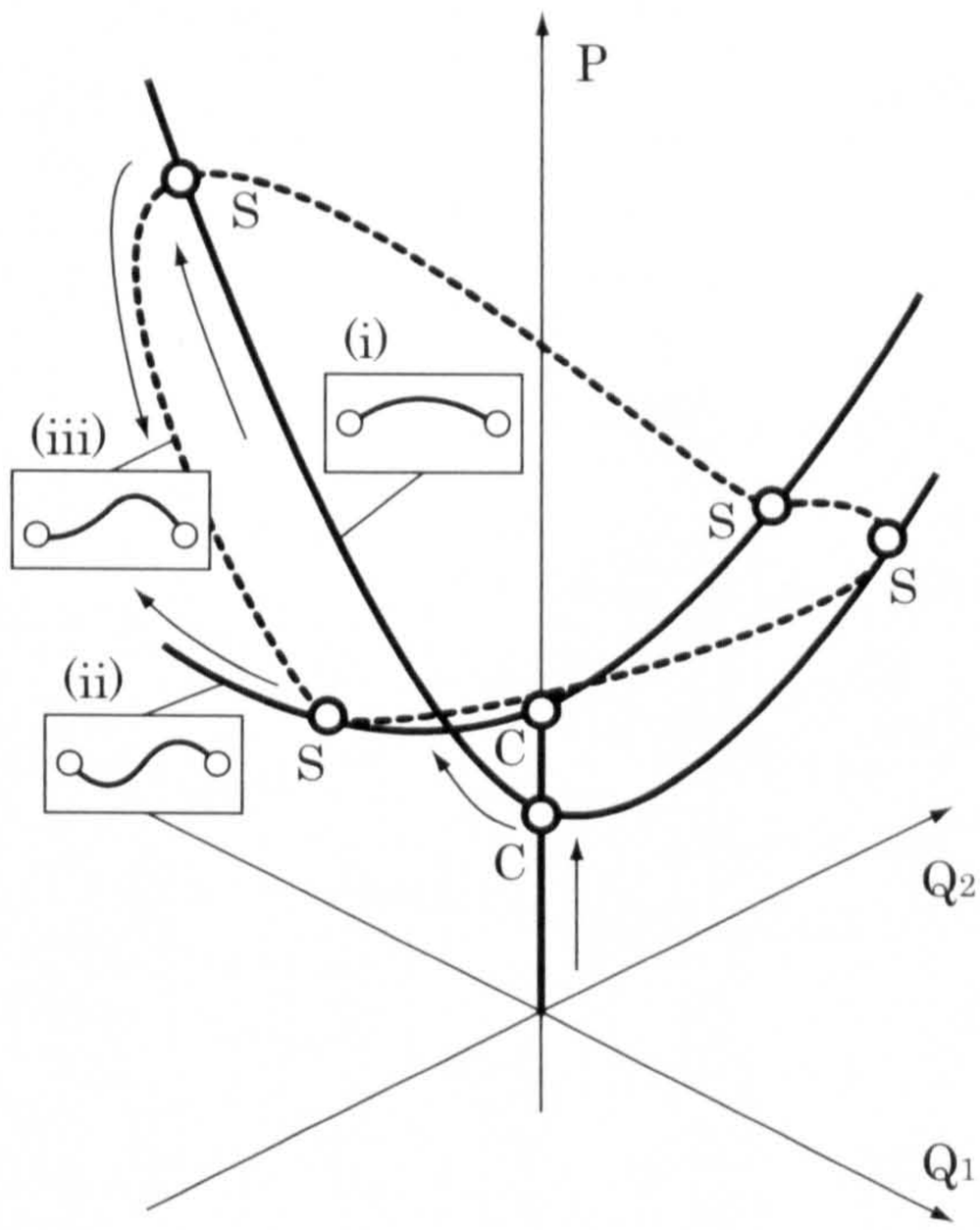

(b) post-buckling equilibrium path

Figure 1.7: Interactive buckling in a plate, after Everall (1999). Note that the existence critical (C) and secondary (S) bifurcations occur when equilibrium paths cross.

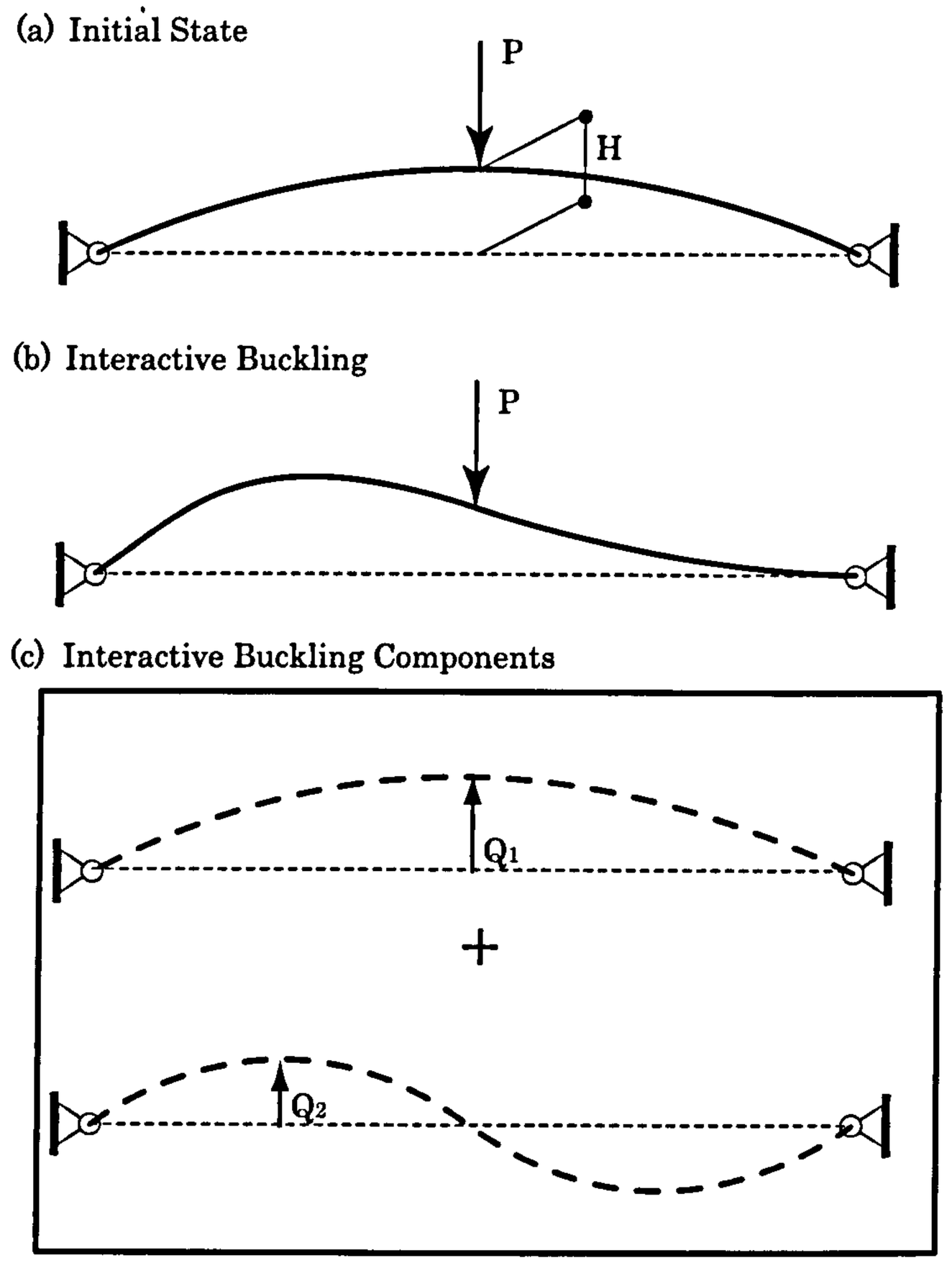

Figure 1.8: Interactive buckling in an arch—(b) consists of the components in (c).

small members, forming a truss. When the structure is compressed, as illustrated in Figure 1.11(c), overall buckling along the total length and local buckling in individual truss members may occur simultaneously. The local buckling causes a sudden loss of the structural rigidity, and together with overall buckling, the structure fails catastrophically.

Sandwich structures, with two stiff face plates separated by softer core material (Allen, 1969; Hunt *et al.*, 1988; Hunt & Wadee, 1998; Wadee, 1999), can also suffer an interaction between overall and local buckling. Overall buckling of the structure in combination with local buckling of the face plates is shown in Figure 1.12. This instability behaviour is responsible for severe destiffening in the post-buckling range and a consequent sensitivity to geometrical imperfections.

Figure 1.9: Interactive buckling in a cylindrical shell.

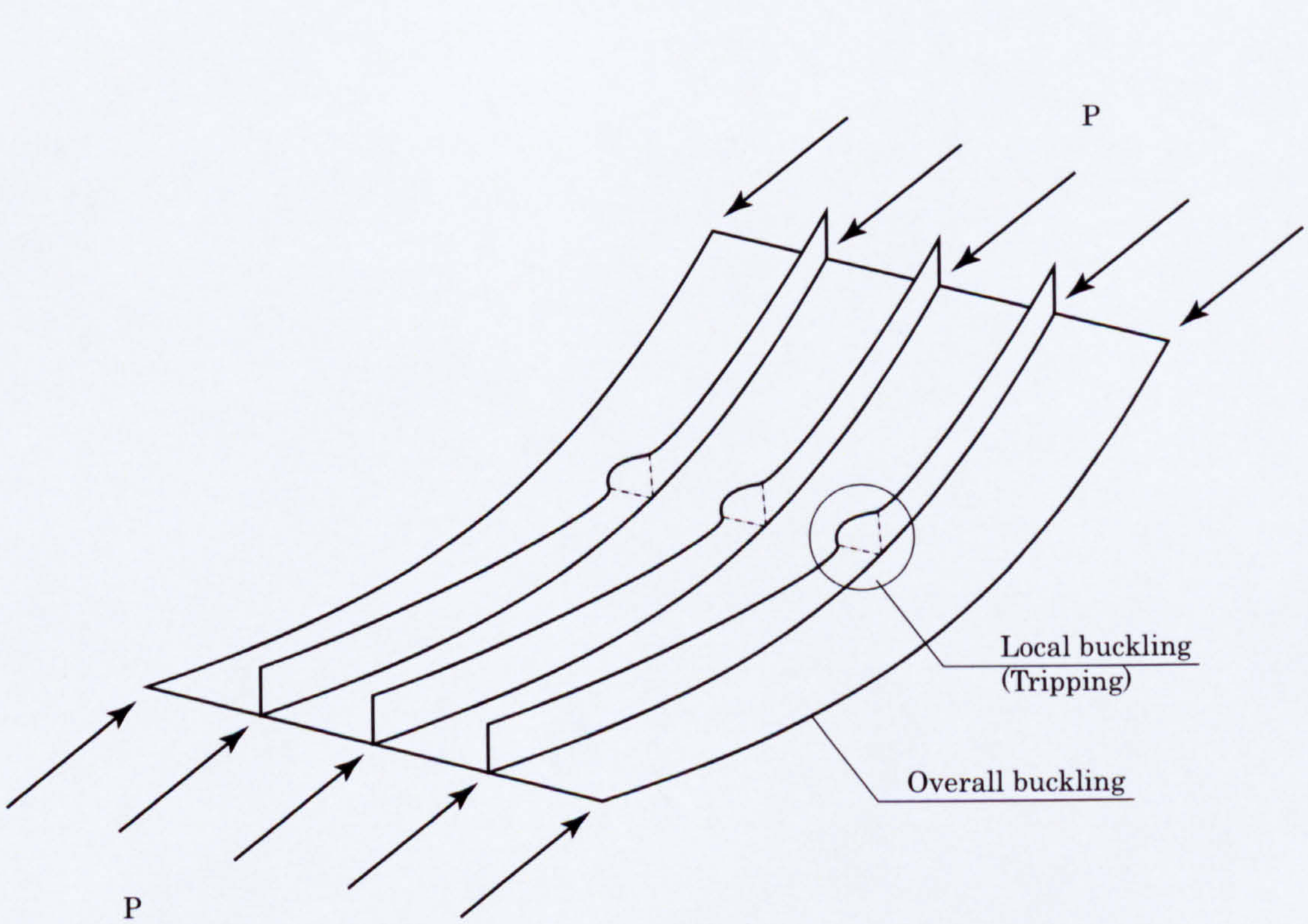

Figure 1.10: Interactive buckling in a stiffened plate.

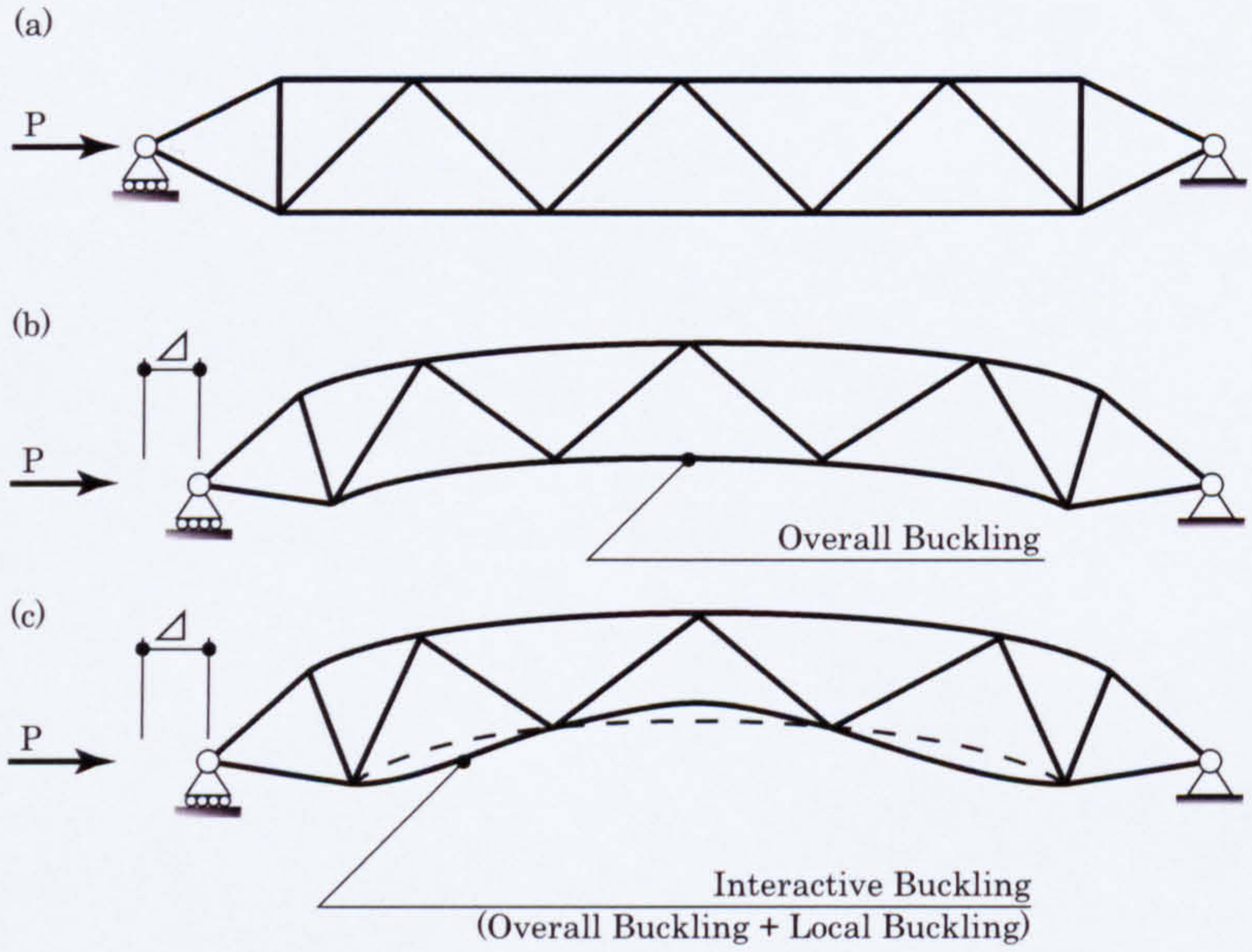

Figure 1.11: Structural model of a reticulated column, showing the interaction between overall and local buckling.

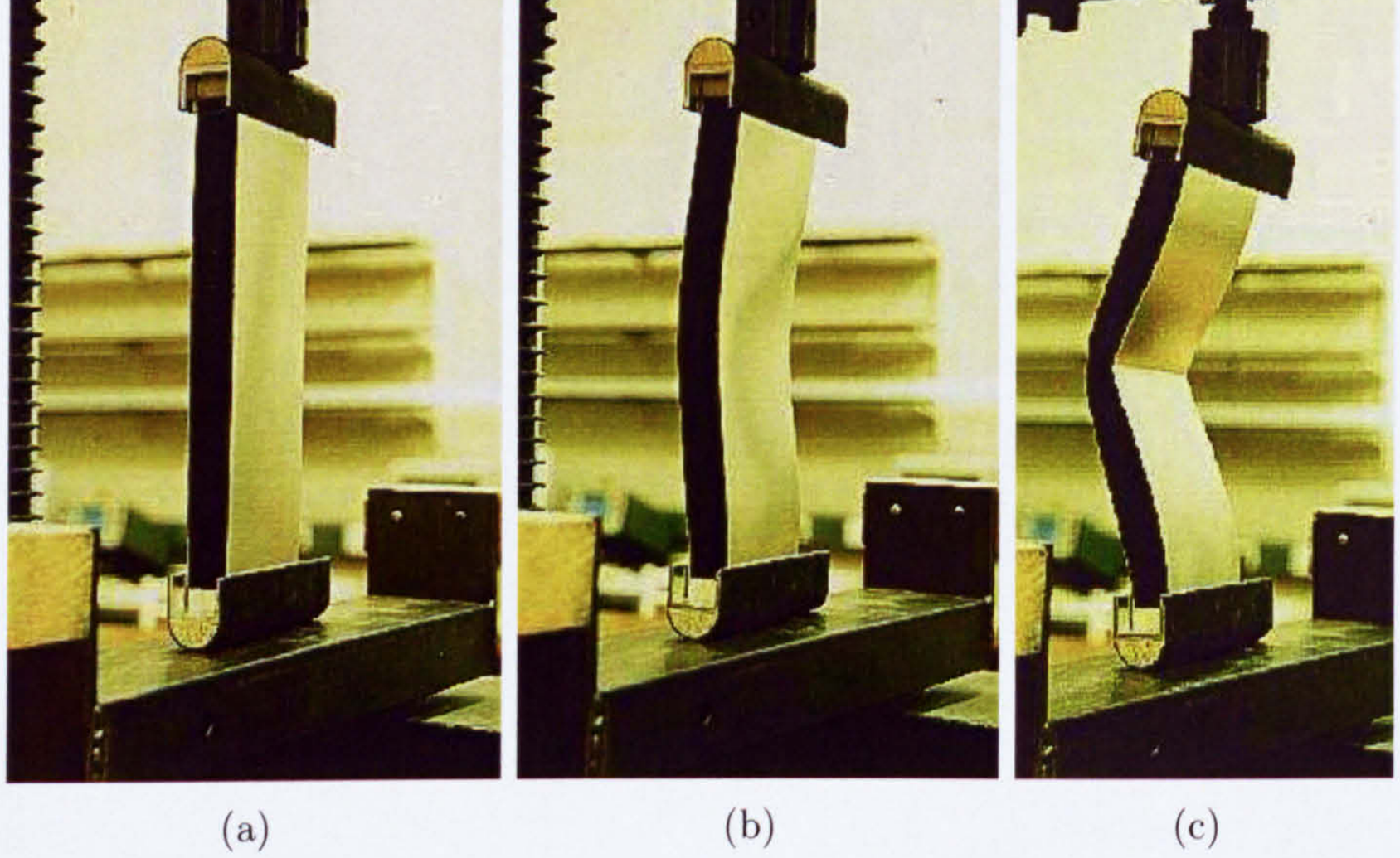

Figure 1.12: Interactive buckling in a compressed sandwich panel: (a) pre-buckling; (b) overall buckling; (c) interactive buckling (Wadee, 1999).

In the work presented herein, combinations of different wavelengths of overall buckling are to be considered, as discussed later; thus, the interactive buckling in plates and arches described above is more relevant to the current work.

1.3.3 Naïve optimum

It is also worth mentioning that, when the configuration of a structure allows two separate buckling modes to occur together, i.e. an initial buckling mode coincides with a secondary mode, the critical load for design become the highest, which is sometimes regarded as design optimization for instability. However, at the expense of the maximized critical load, significant instability can be observed in the post-buckling response (Johns & Chilver, 1971; Thompson & Lewis, 1972; Thompson & Supple, 1973; Thompson & Hunt, 1973; Wadee, 2000).

The buckling of thin walled members, shown in Figure 1.13, is a suitable example of this design optimization dilemma (Thompson & Lewis, 1972). In this case, overall buckling and local buckling possibly occur, and an increase in the dimension b allows a rise in the critical load for overall buckling, but simultaneously reduces the load for local buckling. The design load for buckling is defined as the lesser load from these two loads; the highest design load can be obtained when overall buckling and local buckling loads are at the same value, which is the case for point A in Figure 1.13. At the expense of this increase, the most unstable response can be observed in its post-buckling response. Consequently, this point cannot simply be defined as the optimized point, and this dilemma is sometimes noted as the "naïve" optimum (Koiter & Pignataro, 1976).

In the current work, this problem is also seen in relation to the initial prestress. In fact, the most significant instability can be seen at the prestress which maximizes the buckling load, which is described in Chapter 3.

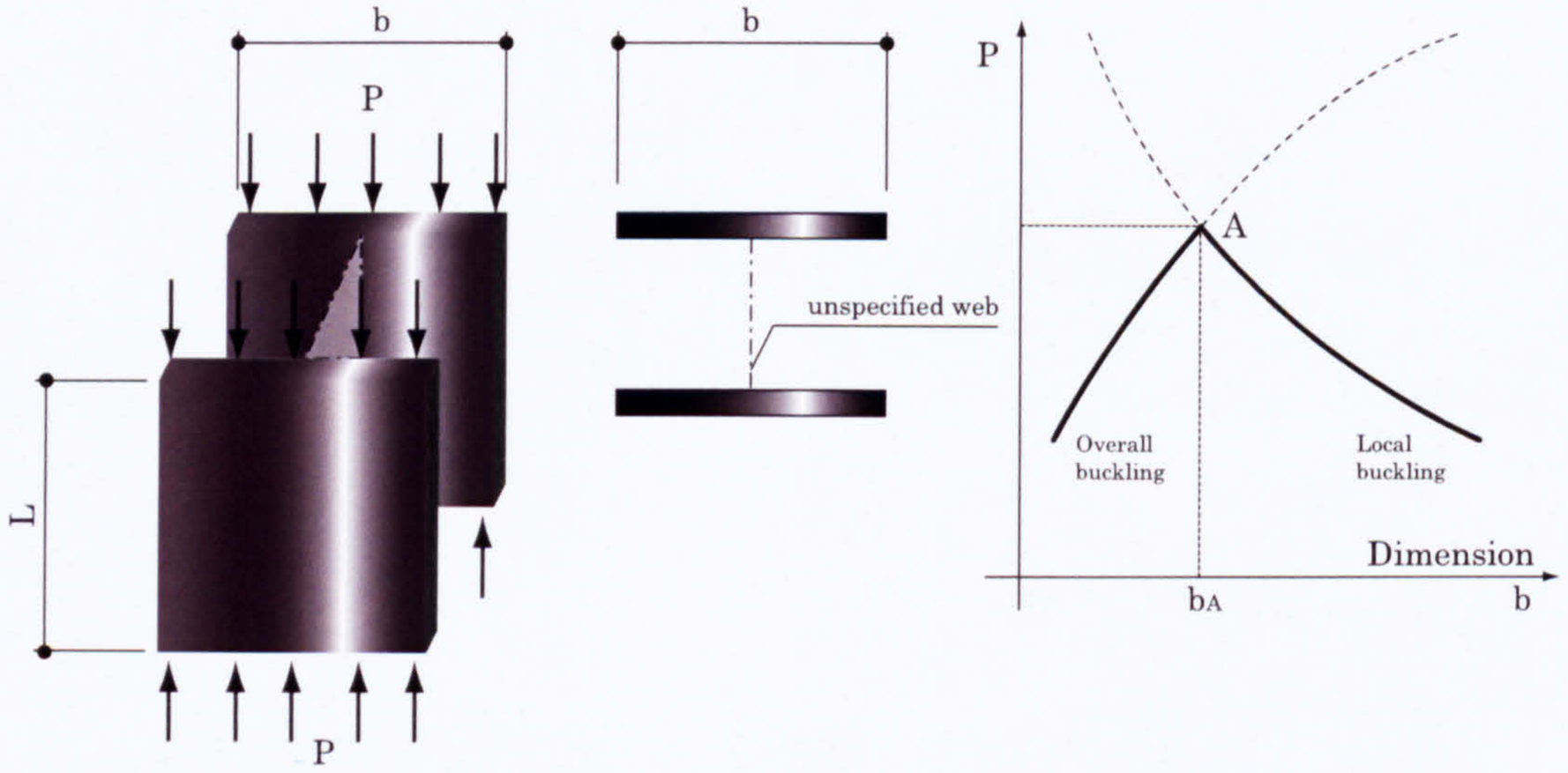

Figure 1.13: Optimum design for thin walled members represented by the van der Neut model—a thin walled member which has an idealized section comprising two load-carrying flange plates with an unspecified web which simply serves to maintain the structural integrity of the strut without contributing to the transmission of axial stresses: the flange plates are assumed to be simply-supported along their edges—after Thompson and Lewis (1972). The "naïve" optimum occurs when the dimension $b = b_A$. Note that the overall buckling load is associated with a increasing function of b, while the local buckling load corresponding to the walls of the section is associated with a decreasing function of b.

1.4 Energy Principles

In this section, applied energy methods—the total potential energy principle with the Rayleigh–Ritz method—for post-buckling analysis are presented. Firstly, the basic approach for formulating the total potential energy is presented. This is followed by the methodology involved in investigating the post-buckling response with the total potential energy. As with most practical structural systems, it is difficult to express a buckling shape function precisely with a simple mathematical expression without a complicated analytical process such as the calculus of variations from a continuum formulation. Hence, the Rayleigh–Ritz method, one of the well-known approximate methods, needs to be introduced.

1.4.1 Total potential energy

As it is assumed that the model of the current work is a static conservative system, the total potential energy, V, stored in the system consists of internal (strain) energy and the work done by an external load. Thus

$$V = U - P\mathcal{E}, \tag{1.1}$$

where U is the strain energy stored in the structure and $P\mathcal{E}$ is the work done by a load, which is given as the load P multiplied by the distance $\mathcal{E}$ that the load moves in the direction of P.

1.4.2 Post buckling analysis with total potential energy

The first general approach for the modelling of post-buckling behaviour was developed by Koiter (1945). He used the calculus of variations to minimize the potential energy of a structure V; the formulation of his theory is given as follows:

$$V = \int \mathcal{L}\, \mathrm{d}x, \tag{1.2}$$

where $\mathcal{L}$ is equivalent to the Lagrangian function in dynamical systems (Fox, 1987) and x is the spatial coordinate. When the first variation of V vanishes, this equation gives the stationary points, which, as will be shown later, can reveal the post-buckling equilibrium behaviour.

This work was extended considerably by Thompson & Hunt (1973), introducing generalized coordinates in conjunction with Koiter's pioneering work. It was assumed that post-buckling profiles can be expressed as a series of modes, and that each mode can be expressed with generalized coordinates Q_m, which define amplitudes of distinct buckling mode shapes. The subscript m represents an arbitrary integer number. For instance, it is known that the buckling mode for the simply-supported plate shown in Figure 1.14 can be expressed as a truncated Fourier series:

$$w = \left(Q_1 \sin\frac{\pi x}{L} + Q_2 \sin\frac{\pi x}{L} + \cdots + Q_n \sin\frac{n\pi x}{L}\right) \sin \pi y, \tag{1.3}$$

where n represents the number of degrees of freedom in the model.

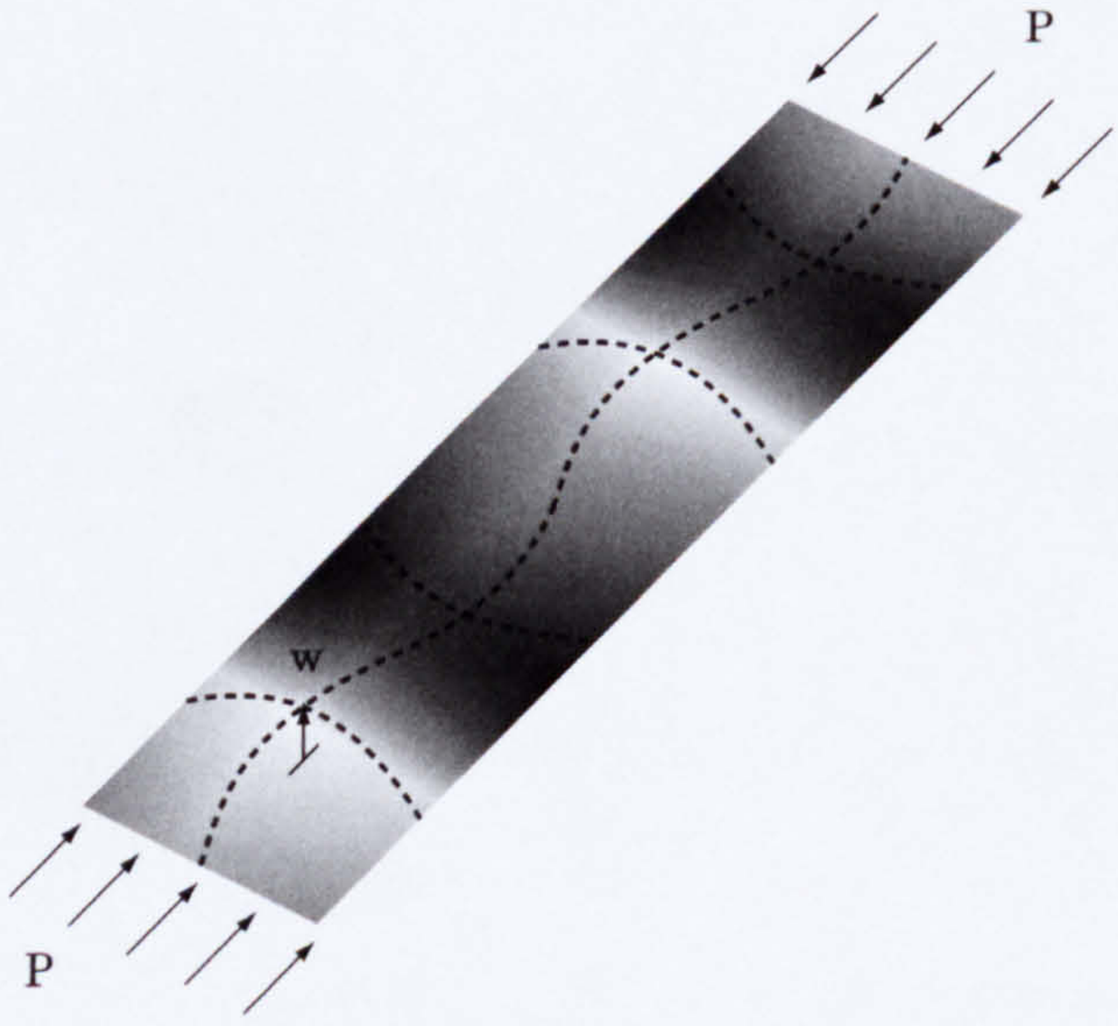

Figure 1.14: Periodic deflection of the axially-compressed plate.

With reference to equation (1.2), and using general coordinates Q_m, the total po-

tential energy is expressed as

$$V = V(Q_1, Q_2, Q_3, \cdots, Q_n, P), \tag{1.4}$$

where P is the applied load. Applying Koiter's theory to the equation above, an equilibrium state can be expressed as

$$\frac{\partial V}{\partial Q_m} = 0. \tag{1.5}$$

Thompson & Hunt also discussed the stability and instability of post-buckling behaviour; a stable path appeared when energy is a locally minimized. A single degree-of-freedom (SDOF) system is appropriate to illustrate their theory. Defining a generalized coordinate as Q, the potential energy as $V = V(Q)$, and a perturbation for Q as ϵ, and using a Taylor series expansion, for the perturbed potential energy $V(Q+\epsilon)$, the following expression is obtained:

$$V(Q+\epsilon) = V(Q) + \frac{\mathrm{d}V}{\mathrm{d}Q}\epsilon + \frac{1}{2!}\frac{\mathrm{d}^2V}{\mathrm{d}Q^2}\epsilon^2 \cdots + \frac{1}{n!}\frac{\mathrm{d}^nV}{\mathrm{d}Q^n}\epsilon^n + \cdots. \tag{1.6}$$

As we consider the equilibrium state of the system, we can obtain the following equation from (1.5):

$$\frac{\mathrm{d}V}{\mathrm{d}Q} = 0. \tag{1.7}$$

Hence, equation (1.6) can be rewritten as

$$V(Q+\epsilon) - V(Q) = \frac{1}{2}\frac{\mathrm{d}^2V}{\mathrm{d}Q^2}\epsilon^2 + \cdots + \frac{1}{n!}\frac{\mathrm{d}^nV}{\mathrm{d}Q^n}\epsilon^n + \cdots. \tag{1.8}$$

In order that $V(Q)$ is minimized, the equation above has to be positive for any small ϵ, which would imply that the system is stable. In the first instance, the sign of the equation is controlled by the terms of the second derivative of V, as can be seen. When the second derivative of V vanishes, it implies that it is a bifurcation or critical state because the energy level is locally flat. A small energy change is made when the system is perturbed by ϵ; in the neighbourhood of such states, the

second derivative of V cannot give the stability of equilibrium, and thus the higher derivatives of the energy must be examined (Wadee, 2007).

From the discussion above, Thompson & Hunt's work presented the two famous axioms that allow the use of V for analysing the structural stability of a system:

Axiom 1 *A stationary value of the total potential energy with respect to the generalized coordinates is necessary and sufficient for the equilibrium of the system.*

Axiom 2 *A complete relative minimum of the total potential energy with respect to the generalized coordinates is necessary and sufficient for the stability of an equilibrium state.*

In the current work, the first axiom is used to describe all equilibrium states and the second axiom is used to find the critical load and the stability of the post-buckling equilibrium states.

1.4.3 Rayleigh–Ritz method

The Rayleigh–Ritz method is an approximate method which can be used to investigate any type of structural deflections through the calculation of the total potential energy; this method is covered in some textbooks (Bažant & Cedolin, 1991; Allen & Bulson, 1980). In general, the more complicated a structure is, such as the stayed column, the more difficult it is to express the post-buckling behaviour of the structure precisely with a continuum formulation. In such cases, applying the Rayleigh–Ritz method along with the energy formulation is a useful approach to obtain approximate mathematical equations which express the equilibrium states. Owing to the structural complexity of the stayed column, the Rayleigh–Ritz approximation is used in the current work. The general concept of this method is discussed in this section.

For the Rayleigh–Ritz method in structural analysis, an approximate function for a deflected shape $f(x)$ is generally assumed as follows:

$$f(x) = Q_1\phi_1(x) + Q_2\phi_2(x) + Q_3\phi_3(x) + \cdots + Q_n\phi_n(x), \tag{1.9}$$

where Q_1, Q_2, Q_3, $\cdots$, Q_n are generalized coordinates, and $\phi_1(x)$, $\phi_2(x)$, $\phi_3(x)$, $\cdots$, $\phi_n(x)$ are arbitrary functions to express the units of the post-buckling shape along a structure, and which are usually defined as sinusoidal or polynomial functions. In general, the higher the number of these generalized coordinates and arbitrary functions become, the more accurate the post-buckling profile $f(x)$ becomes.

With this function of $f(x)$, the strain energy U and the work done $P\mathcal{E}$ can be obtained, which leads directly to the total potential energy V. Subsequently, by Axiom 1, the first derivative of V with respect to each Q_m can be set equal to zero; this condition produces n simultaneous equations expressing the relationship between the applied load P and Q_m. By solving these equations, it is possible to express the relationship between P and $f(x)$, which implies that the approximate post-buckling deflection can be obtained by substituting a certain value to the applied load P.

The major benefit of this method is that an approximate post-buckling shape in relation to loading can be obtained without resorting to purely numerical methods, such as the FEM[2], just by executing differentiations and solving simultaneous equations. In addition to this, as a deflected shape $f(x)$ is obtained as an analytical expression, it can provide more comprehensive and qualitative meaning. It is also a great advantage that $f(x)$ can be obtained without imposing geometrical initial imperfections onto the model; the behaviour obtained by this method is able to show the principal behaviour of the structure in a perfect state.

Although these conveniences and advantages should be fully appreciated, there are

[2]Note that the FEM also adopts the Rayleigh–Ritz method to determine the deformation of each element. However, since a large number of elements are used in the FEM—this is of assistance in increasing the accuracy of the analysis—it quickly becomes cumbersome to understand the effects of individual modes in conjunction with each element shape function, and hence the FEM is regarded as a purely numerical method.

also some disadvantages. First of all, being an approximate method, the Rayleigh–Ritz method is not accurate unless it is a case in which $f(x)$ can express the actual shape accurately. Hence, the Rayleigh–Ritz method usually underestimates the displacement of structures in their post-buckling states due to its in-built approximation in $f(x)$. The consequence of this is that if the assumed post-buckling shape $f(x)$ does not have reasonable accuracy, the obtained solution finishes far away from the actual post-buckling behaviour. If $f(x)$ is not realistic, $f(x)$ has to be modified with an increase in the number of Q_m and $\phi_m(x)$ or by changing the arbitrary function $\phi_m(x)$. However, in order to achieve accuracy, sometimes it is necessary to increase the number of Q_m and $\phi_m(x)$ by an excessive amount. In that case, the Rayleigh–Ritz method is no longer a practical procedure; consequently, other numerical solution processes, most commonly the FEM, have to be considered.

From the discussion, it can be seen that in practice, the Rayleigh–Ritz method can be generally applied to the case in which the shape function $f(x)$ is reasonably accurate with a relatively small numbers of Q_m and $\phi_m(x)$. Despite this limitation on its application, in this work, as discussed later, each mode shape of the stayed column is approximated with few sinusoidal functions; thus the Rayleigh–Ritz method is considered to be effective, and its advantage will be shown in the results.

1.5 Outline of Thesis

This chapter has provided a concise introduction to prestressed stayed columns, post-buckling behaviour including interactive buckling and the analysis methods. Also the broad aim of this research has been stated.

Chapter 2 describes a review of the literature that is relevant to this research project. The review is intended to given an overview of the development of theory for the stayed column, with some of the important papers being introduced, which are discussed later in the thesis.

Chapter 3 contains the formulation of the analytical model, which illuminates the theoretical post-buckling behaviour of the stayed column. Subsequently, Chapter 4 describes necessary modifications to the analytical model to account for imperfections and possible material failure. These analytical models presented in Chapters 3 and 4 are validated by comparing them against previous research and results from the FEM.

Chapter 5 presents work on modelling interactive buckling; the results were obtained from FE analysis. Parametric studies are also presented in order to find the structural configuration for which interactive buckling gains importance.

Chapter 6 presents parametric studies using the validated FE model to seek the optimal design of the stayed column. The concept of the ratio of the maximum elastic load capacity to the structural resistance of each component is introduced, and the optimal prestress and configuration which maximize this ratio is presented.

A summary of the important findings from the project, conclusions and suggestions for further work are provided in Chapter 7.

Chapter 2

Development of Theory for Prestressed Stayed Columns

There is a considerable body of literature on the behaviour of prestressed stayed columns; each has a different method of analysis as mentioned in the previous chapter. In this chapter, the literature on stayed columns is divided into four types and reviewed: on the critical loads, on imperfections, on the maximum strength, and on miscellaneous topics.

2.1 Studies on the Critical Load

The earliest published research on stayed columns seems to have been conducted by Chu and Berge (1963). They developed a general solution for the elastic buckling load of stayed columns with multiple pin-connected crossarms (see Figure 2.1). The solution indicated that regardless of the number of symmetrically placed intermediate crossarm supports, the maximum possible buckling load would be a four-fold strength increase over the Euler load of the simply-supported column without any stays. Although their work should be regarded as significant and the first attempt to find the critical load of stayed columns, it has to be mentioned that pin-connected

crossarms are not common in practice, and that with rigidly-connected crossarms to the column, stayed columns can provide more strength; the practical application of their work is therefore limited.

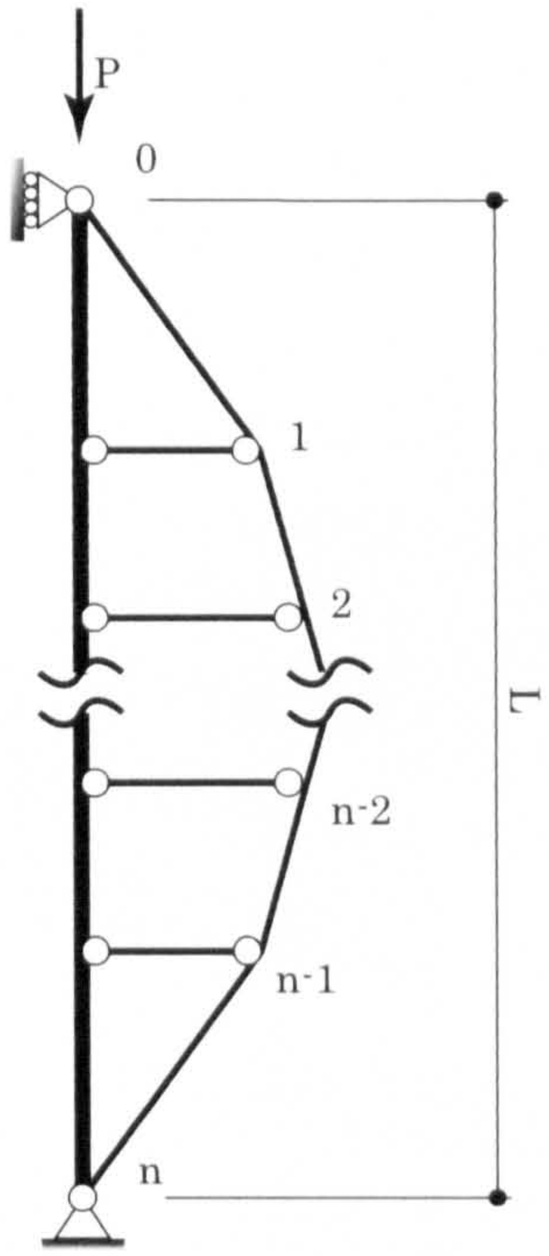

Figure 2.1: Model investigated by Chu et al. (1963)—crossarms are pin-connected to the stays and to the column.

Subsequently, Mauch and Felton (1967) continued the work of Chu and Berge, developing an analytical foundation. Their indication was that at low values of the structural index, defined as P/L^2, the use of stayed columns offered a potential saving in steel weight of up to 50% compared with ordinary tubular columns. The efficiency of stayed columns was firstly evaluated with Mauch and Felton's work, which should be noted. However, they were still working with the assumption of pin-connected crossarms, which reduces the value of their contribution somewhat.

Smith et al. (1975) developed an analytical expression for the buckling load of stayed columns with a single-crossarm, which was ideally pin-connected to the stays and fixed to the column, by solving the governing differential equations. Also, the critical loads in different modes were revealed in relation to the structural dimensions. Their work showed in an analytical way that stayed columns have even higher potential

efficiency as an axial load carrier in compression than had been thought previously.

Belenya (1977) presented previous work on stayed columns which was conducted in the Soviet Union in the early 1970s. In order to find the critical load of stayed columns with arbitrary numbers of crossarms, ordinary differential equations were presented with the assumption that the initial prestress was zero. These equations were solved in the case of a single-crossarm; the procedure for predicting the critical load in relation to its dimensions was presented. Despite its success, the assumption of zero prestress is hardly considered to be realistic. The result of experimental work was also presented, and according to his statement, the critical load was 2.5 to 3 times larger than that of an ordinary column.

Temple (1977) worked on the buckling loads and modes of stayed columns with multiple crossarms, which were ideally pinned to the stays and fixed to the column, using the FEM. He pointed out those rigid connections of the crossarms yield much higher critical loads in general, and that the multiple crossarms result in more complicated modes of buckling. The advantage of the use of multiple crossarms was numerically presented, but being numerical work, their work is meaningful only in a quantitative sense for a limited number of cases.

Important features of stayed columns were discovered by Hafez et al. (1979); they found how the buckling load changed in relation to the level of the initial prestress. For all of the models discussed earlier in this section, it was assumed that all of the stays keep their residual tension at the instant of buckling, and hence the relationship between the critical load and the initial prestress remained undiscovered. The solution presented by Hafez et al. indicated that the critical load would be divided into three zones in relation to the prestress as shown in Figure 2.2. Parametric studies were also conducted for the buckling loads. Despite their achievement, the FEM was still required to determine the maximum critical loads in relation to its initial prestress; thus their work did not consist of complete analytical procedures, which implied the critical loads were still not obtainable with an purely analytical process. To determine the maximum critical loads using an analytical process is to

be one of the important contributions of the current work.

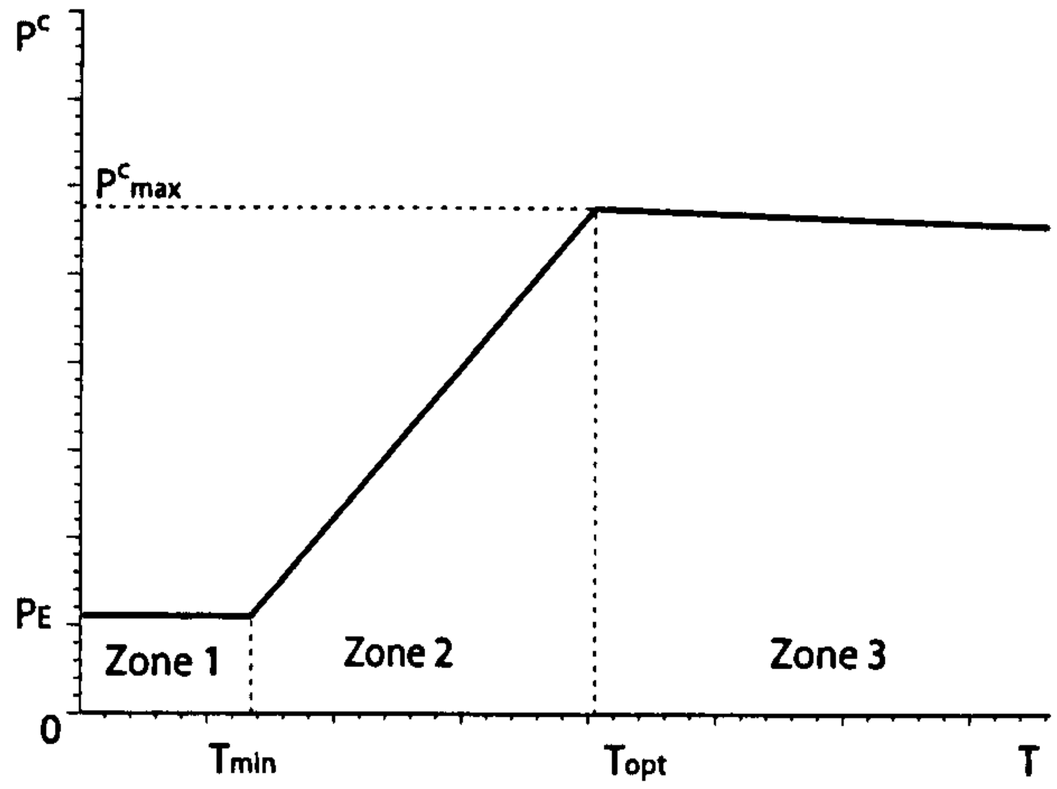

Figure 2.2: Critical buckling load P^C versus initial prestress T as found by Hafez et al. (1979).

Howson and Williams (1980) worked on critical loads for ten different types of stayed columns using a specific plane frame program to find the optimum structural type for design. By measuring the ratio of the steel weight saving for each structure, the type of stayed column that required the least steel material was successfully discovered.

Howson and Williams continued their work (1984), dealing with the optimum structural type of the stayed column discovered from their earlier research mentioned above (1980). They varied certain structural parameters, such as the crossarm length and the number of joints, in order to find the values of the structural parameters that minimized the steel weight. Also, the effect of the residual prestress of the stays after buckling was examined with the conclusion that it did not make a significant difference in values of the buckling loads. Although the optimum shape and structural dimensions of stayed columns had been discovered by Howson and Williams, their attention was only paid to the critical load. The effect of post-buckling was ignored, which should be included in the argument for optimized design, as discussed in the previous chapter and investigated later in this thesis.

2.2 Imperfection Studies

Imperfection studies on stayed columns were conducted by Wong et al. (1982) for the first time. They examined the effect of initial out-of-straightness of the column element on the buckling load of a single-crossarm stayed column in conjunction with the FEM. The result indicated that the initial out-of-straightness significantly reduces the buckling load of the stayed column[1] (see Figure 2.3), which gave good agreement between the theoretical and experiment results. As imperfections are essential factors in practical behaviour, their contribution ought to deserve proper attention; however, as they did not perform parametric studies, sensitivities to imperfections could not be established from their work.

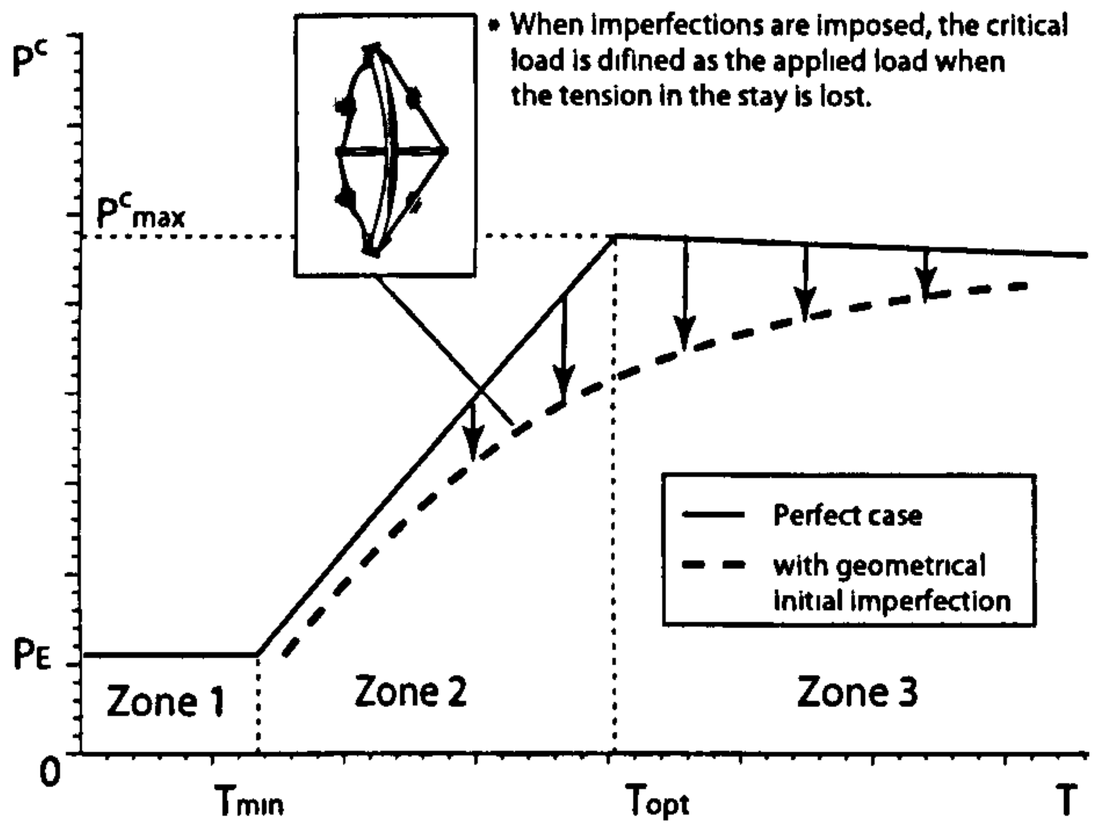

Figure 2.3: Critical buckling load P^C versus initial prestress T with imperfections imposed, arising from the results of Wong et al. (1982).

Chan et al. (2002) examined the sensitivity of the buckling load[2] to changing initial imperfections and other structural dimensions; this research was conducted by using the FEM with nonlinear elements called the point wise equilibrium polynomial (PEP) element. They illuminated the sensitivities of the critical load to imperfections in relation to the dimensions of stayed columns, which is definitely useful for calculating the buckling load of real structures. It was therefore concluded that

[1]Note that in their analysis, the buckling load was defined as the load at which the tension in the concave side of the stays is lost, not the maximum load capacity of the structure.

[2]The same as the above.

the stayed column was quite a sensitive structure to initial imperfections. However, it should be noted again that their contribution does not include sensitivities to post-buckling behaviour, which is to be discussed in the current work.

2.3 Studies on Maximum Strength

There are studies on the maximum strength after the buckling of stayed columns. Although these did not investigate post-buckling responses in detail, they indicated that with a certain condition, maximum strength emerged after the critical buckling load. This finding implies the importance of post-buckling studies, even though they did not seem to mention it explicitly. The earliest work was carried out by Temple et al. (1984)—they sought the maximum axial load capacity of a single crossarm stayed column by means of the FEM and experiments. The results indicated that the stayed column with lower values of prestress possess a much greater strength than the critical buckling load as shown in Figure 2.4. Their work deserves attention; however, as being numerical and experimental work, their work is only meaningful in a quantitative way for a limited number of cases.

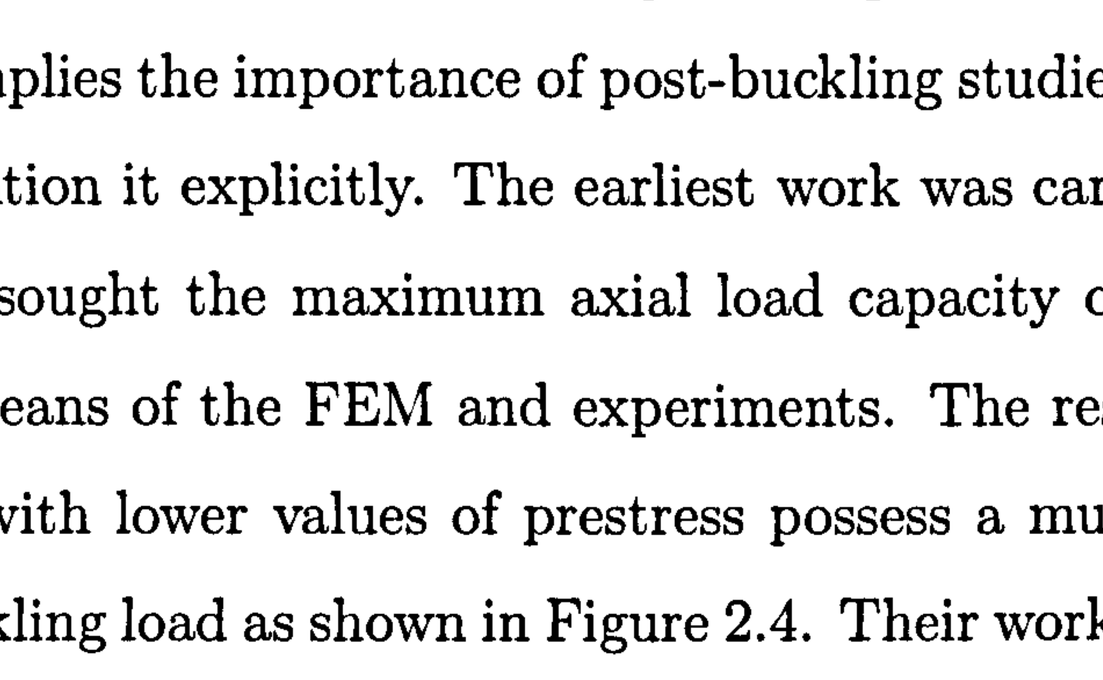

Figure 2.4: Maximum load capacity versus initial prestress T, arising from the results of Temple et al. (1984).

Smith (1985) sought an analytical solution for the maximum axial load capacity of stayed columns by solving differential equations. He also included the effect of initial

out-of-straightness to their formulation to take imperfections into account. The analytical model accounting for initial imperfections to find the maximum strength of stayed columns was successfully presented. Despite this achievement, his analytical solution requires a trial and error procedure to determine the values of the buckling loads; thus the result may be considered to be too complicated to serve practical design purposes.

2.4 Miscellaneous

Jemah and Williams (1990) presented experimental work on stayed columns that had three frames of stays and bipod-crossarms (see Figure 1.4(b)) subject to all practical prestress levels. The result indicated that the obtained critical load was typically 10% below the theoretical buckling load of the perfect column, and that, with relatively low prestress, this difference tended to be larger. It was also shown that a method known as the "Southwell plot" (Southwell, 1932) was effective for predicting experimental critical loads.

Steirteghem et al. (2005) also worked on stayed columns with the bipod-crossarms in conjunction with the FEM. They discovered that because the bipod-crossarms provided a rather large rotational stiffness, they frequently led to a symmetrical mode of buckling. Furthermore, parametric studies were conducted for investigating sensitivity to the buckling loads with a variation in crossarm length, stay diameter, crossarm properties and the opening angle of the bipods. It was concluded that with the bipod crossarms, the efficiency of a stayed column as a load carrier is increased by more than 20% when compared to a single-crossarm stayed column. Although the current work is not dealing with bipod-crossarms, the potential advantage of its use should be noted.

Araujo et at al. (2006) presented experimental work on full-scale three-dimensional stayed columns for the first time in conjunction with FEM simulations. It was shown that the actual stayed columns can provide more strength than ordinary columns

with the actual experiments conducted. Despite their achievement, the presented FEM results showed less good agreement with their experimental results in load versus displacement curves. Improvement in their experimental tests, such as replacing the provided semi-rigid boundaries by reasonably ideal hinges and eliminating large amounts of the initial deflection arising from the self-weight displacement of the column in the test owing to the test specimen being in the horizontal plane, may be necessary in order to gain good agreement between the two.

Liew et al. (2006) investigated the maximum strength of three-dimensional stayed columns with a number of horizontal crossarms in a part of the paper using the FEM. The optimal level of pretension was examined along with the adequate length and number of crossarms for certain cases using the maximum load capacity as an indicator for the design optimum. Despite work on the design optimum, the number of studies is limited; their work is meaningful only for the cases they examined. For generalization, more numbers of studies in conjunction with a more generalized indicator for the design optimum rather than the maximum load capacity would be necessary. The current research also aims to tackle this issue.

Table 2.1 gives a summary of all experimental tests conducted on stayed columns; all of the tests listed in the table have already been presented in the current chapter. Although this thesis focuses upon theoretical work, the imprtance of laboratory tests should be not be understressed.

Publication	Structural Type	Column Length (m)	No. of tests
Hafez et al. (1979)	2D, single crossarm	3.05	U
Wong et al. (1982)	2D, single crossarm	3.05	7
Temple et al. (1984)	2D, single crossarm	0.813	8
Jemah and Williams (1990)	3D, bipod-crossarm	0.820	203
Araujo et al. (2006)	3D, single crossarm	12	2

Table 2.1: Experimental works in literature. "2D" and "3D" represent two-dimensional and three-dimensional respectively. In the 2D experiments, the structures were only allowed to deflect in one plane only. "U" represents the number of tests being unspecified.

2.5 Remarks

This chapter has presented an overview of the development of theory for prestressed stayed columns, which allows further detail of the literature to be referred to at the appropriate stage. It can be seen that, although significant progress has been made to understand the buckling load of the system including imperfection effects, post-buckling analysis has not been attempted satisfactorily, and interactive buckling effects have not been investigated at all. Illuminating these areas and deriving design recommendations from the results, which enables a more efficient and safer approach to the structural design of stayed columns, are the aims of the research.

Chapter 3

Formulation of Analytical Post-Buckling Model

3.1 Introduction

As stated in Chapter 1, a number of research works on the stayed column have been conducted. Although previous studies (Wong & Temple, 1982; Temple *et al.*, 1984; Smith, 1985; De Araujo *et al.*, 2006) also had a look at the post-buckling response of the stayed column in either an implicit or explicit way, they did not provide the comprehensive theoretical post-buckling response of the stayed column. This chapter aims to illuminate the theoretical post-buckling response of the stayed column by developing analytical models using energy methods, the results of which were validated by the FEM.

3.1.1 Methodology

As stated in Chapter 1, in the current work, a single-crossarm stayed column, the simplest type shown in Figure 3.1, was modelled. In order to formulate the model, the total potential energy principle was applied in conjunction with the Rayleigh–

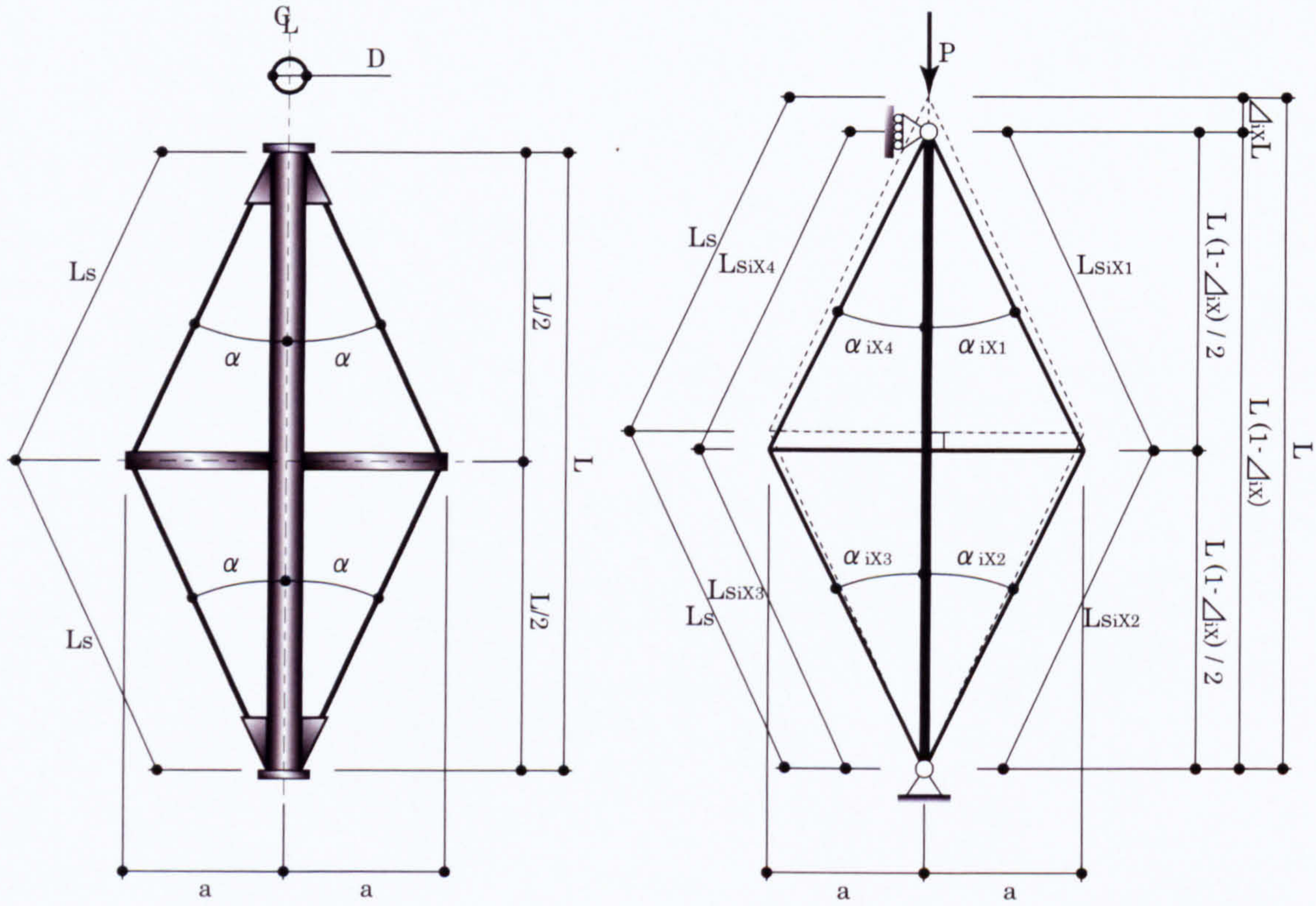

(a) Profile (b) Structural model

Figure 3.1: Structural model of the stayed column: column length L, crossarm length a, axial load P, angle between the stay and the vertical α and stay length L_s. The quantity Δ_{iX} represents the end-shortening of the column, where subscripts i and X represent a buckling mode number (1 or 2), and a buckling type (A, B or C) respectively. Subscripts 1, 2, 3 and 4 after X represent the number of the individual stays.

Ritz method (Thompson & Hunt, 1973). The total potential energy V for the prestressed stayed column was developed as a multiple degree-of-freedom (MDOF) system. A set of algebraic equilibrium equations was derived from minimizing V using the symbolic computation software MAPLE (Heck, 2003). The structural response was revealed by this process, and was subsequently validated by the FEM using the well-established code ABAQUS (ABAQUS, 2006). For the analytical modelling, the following assumptions were made.

1. The column is simply-supported.

2. The connections between the stays and the column, and between the stays and the crossarms, are ideal hinges. The connections between the crossarm and the column are rigid.

3. The column is centrally loaded and perfectly straight, i.e. imperfections are not taken into account in the analysis at this stage.

4. The axial deformation of the crossarm and the bending deformation of the stays are both ignored.

5. The stay goes slack the instant it goes into compression; hence it does not carry any stresses in compression.

6. The analysis is purely elastic; hence, the stress–strain relationship is completely linear apart from the stay slackening.

7. Changes in geometries from applying the prestress are ignored, i.e. the initial configuration is kept after the introduction of the initial prestress.

Changes in geometries from the prestress do not yield significant effects unless the initial prestress has the same level as the Euler load of the column. As this level of prestress leads to a considerable amount of compressive force in the column, which significantly diminishes the axial buckling resistance, this situation is considered to be impractical.

3.2 Model Formulation

In this section, the MDOF system is developed by considering, in turn, the displacements of each component and the geometrical changes after applying the prestress. This leads to the total potential energy function.

3.2.1 Displacement functions for the column

Two different buckling mode shapes for the column are considered: a symmetric shape (Mode 1, $W_1(x)$) and an antisymmetric shape (Mode 2, $W_2(x)$) about the column midspan, as shown in Figure 3.2; these are the basic possible deflection

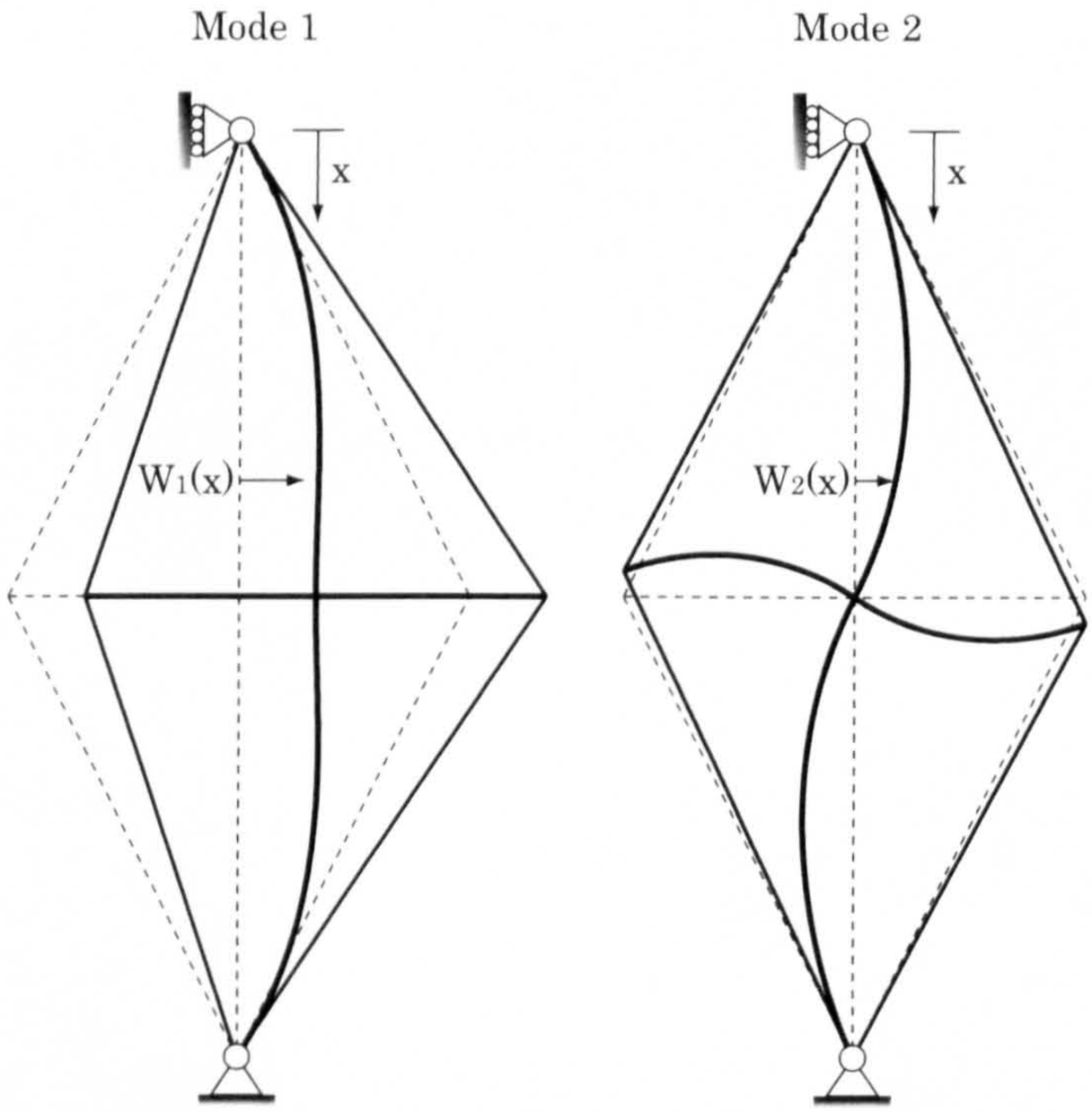

Figure 3.2: Buckling Modes 1 (symmetric) and 2 (antisymmetric).

shapes for buckling in the single-crossarm stayed column. In Mode 1, zero curvature can be found at both ends; in Mode 2, zero curvature can be found at the column midspan and both ends. Each mode can be expressed as a summation of sinusoidal waves. Defining the column length as L (see Figure 3.1) and the generalized coordinates as q_m, where the subscript m is an integer representing a degree of freedom for a sinusoidal wave that has a wavelength of $2L/m$, the displacement

functions for the column W_1 and W_2 can be assumed to be as follows:

$$\begin{aligned} W_1(x) &= q_1 L \sin\frac{\pi x}{L} + q_3 L \sin\frac{3\pi x}{L} + \dots \\ &= \sum_{m=1}^{n} q_{2m-1} L \sin\frac{(2m-1)\pi x}{L}, \end{aligned} \tag{3.1}$$

$$\begin{aligned} W_2(x) &= q_2 L \sin\frac{2\pi x}{L} + q_4 L \sin\frac{4\pi x}{L} + \dots \\ &= \sum_{m=1}^{n} q_{2m} L \sin\frac{2m\pi x}{L}, \end{aligned} \tag{3.2}$$

where n represents the number of degrees of freedom in the model. As the individual components of the stayed column tend to be long and thin, Euler–Bernoulli bending theory can be applied; the angles of the members to the vertical $\Theta_1(x)$ and $\Theta_2(x)$ are therefore approximated as the first derivative of the displacement with respect to x:

$$\begin{aligned} \Theta_1(x) &= q_1 \pi \cos\frac{\pi x}{L} + 3\pi q_3 \cos\frac{3\pi x}{L} + \dots \\ &= \sum_{m=1}^{n} (2m-1) q_{2m-1} \pi \cos\frac{(2m-1)\pi x}{L}, \end{aligned} \tag{3.3}$$

$$\begin{aligned} \Theta_2(x) &= 2q_2 \pi \cos\frac{2\pi x}{L} + 4\pi q_4 \cos\frac{4\pi x}{L} + \dots \\ &= \sum_{m=1}^{n} 2m q_{2m} \pi \cos\frac{2m\pi x}{L}. \end{aligned} \tag{3.4}$$

3.2.2 Displacement functions for the crossarm

3.2.2.1 Buckling type distinction

The deflected shape of the crossarm and the function for the end shortening of the column depend on the stress state of the stays (see Figure 3.3). To account for these effects in the current model, the following three states are considered:

1. Type A: all of the stays are slack in compression.

2. Type B: all of the stays are active in tension.

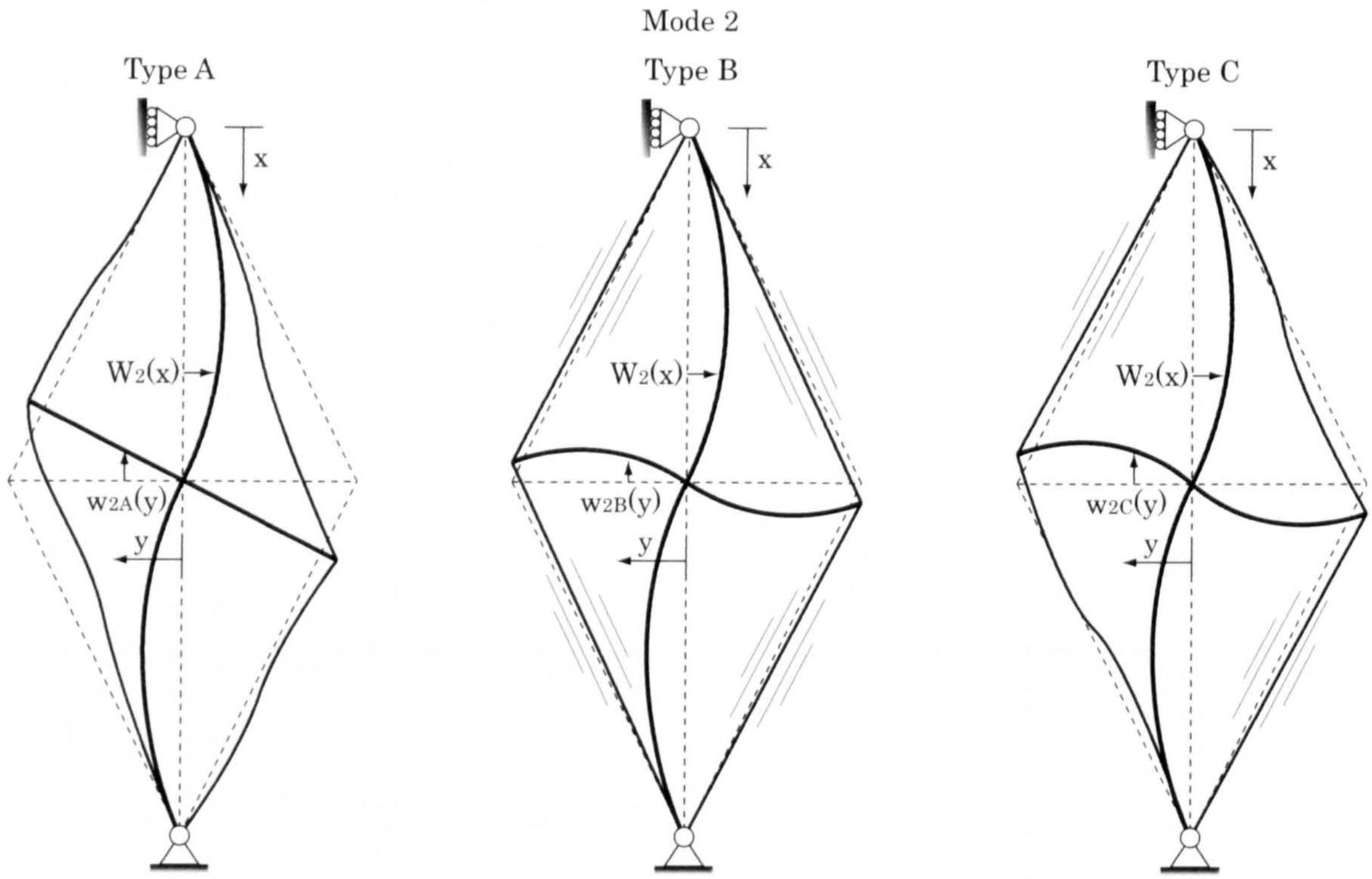

Figure 3.3: Buckling types in Mode 2.

3. Type C: two stays are active in tension.

Note that Type A occurs with a small value of the initial prestress; Type B occurs with a sufficient amount of the initial prestress which allows the stays not to slacken until buckling; Type C buckling can occur either after Type A, B or the fundamental (pre-buckling) state. Shape functions for the crossarm for each type can be obtained by solving differential equations reflecting each type of stress state in the stays and the reaction forces developed in the crossarm.

3.2.2.2 Shape functions

First, the bending moment for $y \geqslant 0$ in the crossarm M_{aX} (see Figure 3.4) is given by

$$M_{aX} = -R_{hX}[h_X - w_{2X}(y)] + R_{vX}(a - y), \tag{3.5}$$

where R_{hX} and R_{vX} are horizontal and vertical reaction forces respectively at the tip of the crossarm; h_X is the displacement at the tip of the crossarm; y is the horizontal axis; and $w_{2X}(y)$ is the deflection of the crossarm perpendicular to the coordinate. Ignoring higher-order terms and the effect of the end-shortening of the

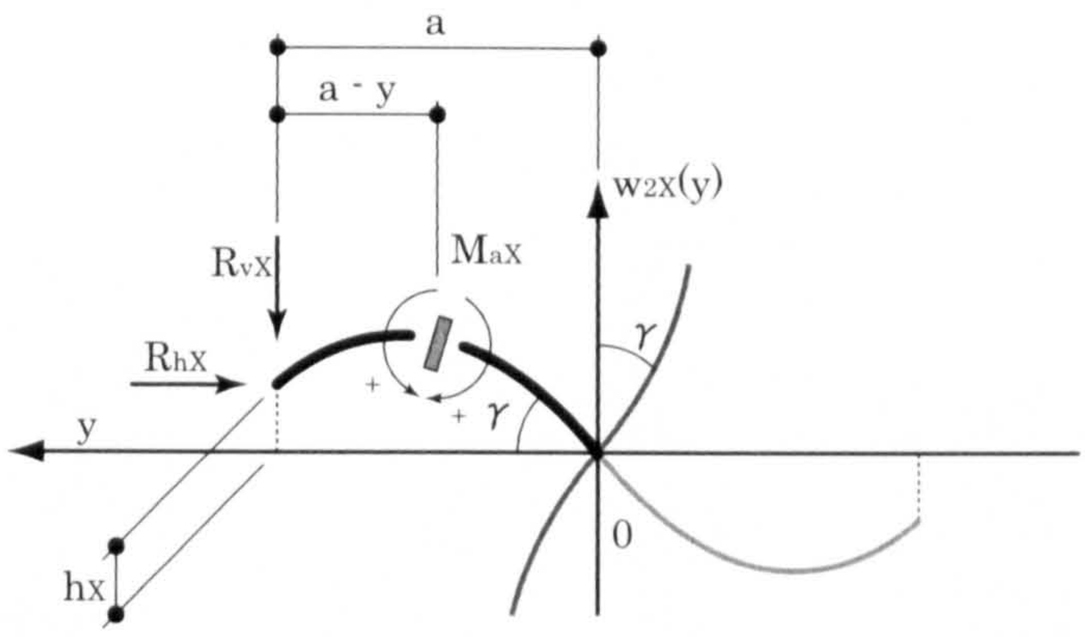

Figure 3.4: Free body diagram to determine the bending moment at an arbitrary cross section ($y \geqslant 0$) of the crossarm. Note that the subscript X represents the buckling type classification which can be either B or C.

crossarm, the basic differential equation for the bending of the crossarm takes the form:

$$M_{aX} = -E_a I_a w''_{2X}(y), \tag{3.6}$$

where primes represent differentiation with respect to the indicated independent variable, in this case y, and E_a and I_a are the Young's modulus and the cross-sectional second moment of area of the crossarm respectively. Substituting equation (3.6) into (3.5) leads to

$$w''_{2X}(y) + k_X^2 w_{2X}(y) = -\frac{R_{vX}}{E_a I_a}(a - y) + h_X k_X^2, \tag{3.7}$$

where

$$k_X = \sqrt{\frac{R_{hX}}{E_a I_a}}. \tag{3.8}$$

The general solution of differential equation (3.7) is

$$w_{2X}(y) = H_X \sin k_X y + K_X \cos k_X y - \frac{R_{vX}}{k_X^2 E_a I_a}(a - y) + h_X, \tag{3.9}$$

where H_X and K_X are constants of integration that are determined from the boundary conditions, thus:

$$w_{2X}(0) = 0, \quad w'_{2X}(0) = \gamma, \quad w_{2X}(a) = h_X, \tag{3.10}$$

where γ is the angle between the horizontal and the crossarm at the midpoint, defined as

$$\gamma = -\Theta_2(L/2) = 2q_2\pi - 4q_4\pi + \cdots = \sum_{m=1}^{n}(-1)^{m-1}\,2m\,q_{2m}\pi. \tag{3.11}$$

The second condition comes from the assumption that $W_2(x)$ intersects the crossarm at right angles. Applying this condition yields the following expressions:

$$H_X = \frac{1}{k_X}\left(-\frac{R_{vX}}{k_X^2 E_a I_a} + \gamma\right), \tag{3.12}$$

$$K_X = \frac{R_{vX}a}{k_X^2 E_a I_a} - h_X, \tag{3.13}$$

$$h_X = \frac{(\gamma E_a I_a k_X^2 - R_{vX})\sin k_X a + k_X R_{vX} a \cos k_X a}{k_X^3 E_a I_a \cos k_X a}. \tag{3.14}$$

In order to find the actual shape of the crossarm with equation (3.9), it is also necessary to establish equations for R_{vX} and R_{hX}. With reference to Figure 3.5 and then by taking the leading terms of Δ_{2X} and h_X, the changes in the axial force in Stays 3 and 4 $\mathrm{d}F_{X3}$ and $\mathrm{d}F_{X4}$, resulting from the structural displacement, can be expressed as follows:

$$\begin{aligned}\mathrm{d}F_{X3} &= E_s A_s \frac{L_{s2X3} - L_s}{L_s} \\ &\approx (-\Delta_{2X} + \frac{2h_X}{L})\cos^2\alpha,\end{aligned} \tag{3.15}$$

$$\begin{aligned}\mathrm{d}F_{X4} &= E_s A_s \frac{L_{s2X4} - L_s}{L_s} \\ &\approx -(\Delta_{2X} + \frac{2h_X}{L})\cos^2\alpha,\end{aligned} \tag{3.16}$$

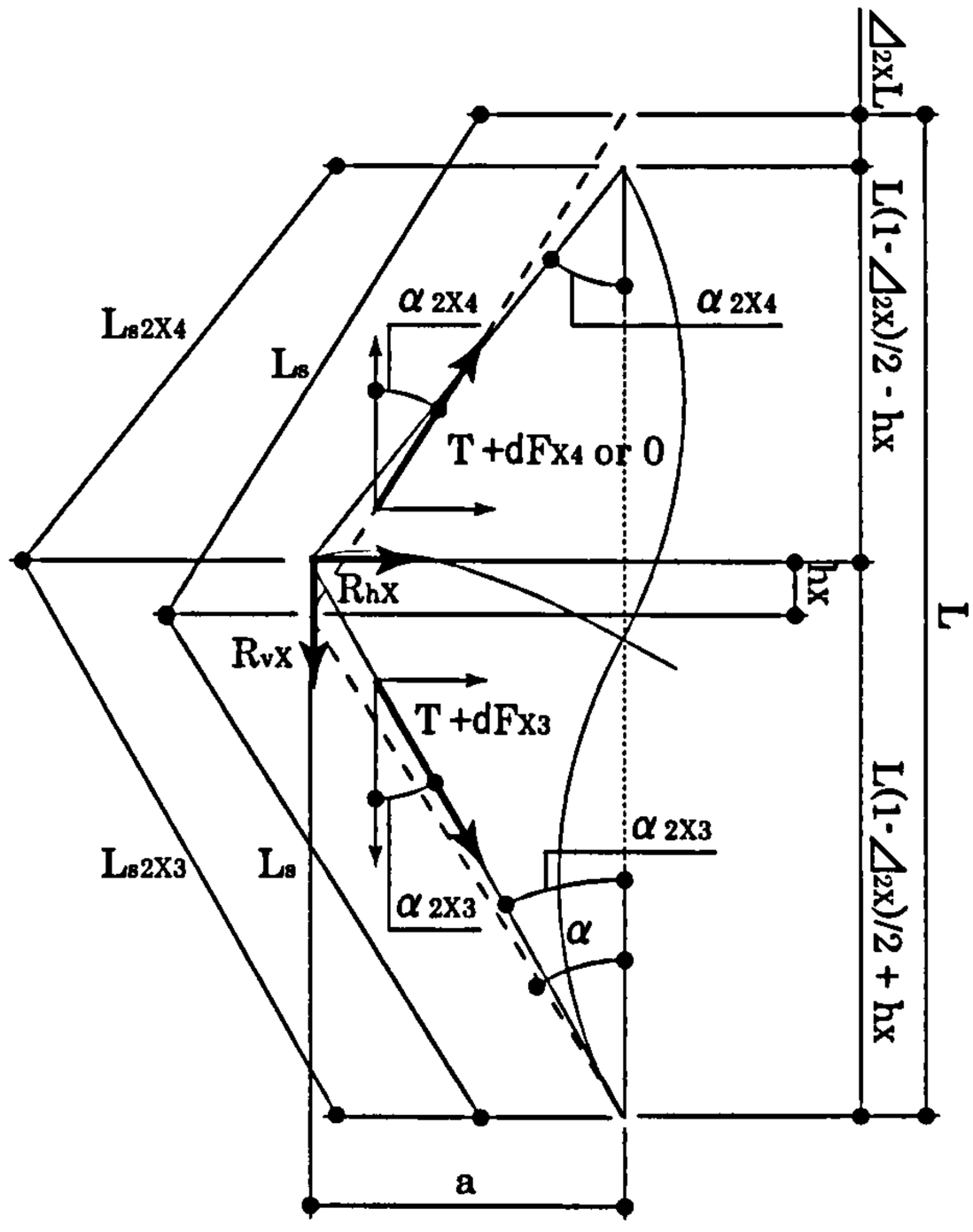

Figure 3.5: Elongation of the stays and reaction forces at the tip of the crossarm.

where A_s is the cross sectional area of the stay with E_s being the Young's modulus. From the expression for $\mathrm{d}F_{X3}$ and $\mathrm{d}F_{X4}$, the vertical and the horizontal reaction forces for Type B, R_{vB} and R_{hB}, can be obtained thus:

$$\begin{aligned} R_{vB} &= (T + \mathrm{d}F_{B3}) \cos \alpha_{2B3} - (T + \mathrm{d}F_{B4}) \cos \alpha_{2B4} \\ &= \frac{4h_B}{L}(T \sin^2 \alpha + E_s A_s \cos^2 \alpha) \cos \alpha, \end{aligned} \tag{3.17}$$

$$\begin{aligned} R_{hB} &= (T + \mathrm{d}F_{B3}) \sin \alpha_{2B3} + (T + \mathrm{d}F_{B4}) \sin \alpha_{2B4} \\ &= 2\left[T + (T - E_s A_s)\Delta_{2B} \cos^2 \alpha\right] \sin \alpha. \end{aligned} \tag{3.18}$$

As only one stay is active on each side in Type C, R_{vC} and R_{hC}, can thus be obtained from $\mathrm{d}F_{C3}$. However, including the h_C term in the R_{hC} equation causes a computation problem that leaves the governing equation untractable[1]. To rectify this we apply the approximation $h_C = 0$ in R_{hC}, which applies when the stays first

[1]Note that in the R_{hB} expression, the h_B term does not exist as this drops out in the process of summing the horizontal components of $\mathrm{d}F_{B3}$ and $\mathrm{d}F_{B4}$.

slacken, thereby enabling us to obtain an approximate expression for R_{hC}:

$$\begin{aligned} R_{vC} &= (T + \mathrm{d}F_{C3}) \cos \alpha_{2C3} \\ &= \left[1 - \left(\Delta_{2C} - \frac{2h_C}{L}\right)\left(\sin^2 \alpha + \frac{E_s A_s}{T} \cos^2 \alpha\right)\right] T \cos \alpha, \end{aligned} \tag{3.19}$$

$$\begin{aligned} R_{hC} &= (T + \mathrm{d}F_{C3}) \sin \alpha_{2C3} \\ &= \left[1 + \left(\Delta_{2C} - \frac{2h_C}{L}\right)\left(1 - \frac{E_s A_s}{T}\right) \cos^2 \alpha\right] T \sin \alpha \\ &\approx \left[\left(1 + \Delta_{2C} \cos^2 \alpha\right) T - E_s A_s \Delta_{2C} \cos^2 \alpha\right] \sin \alpha. \end{aligned} \tag{3.20}$$

Note that in the following energy formulation, equation (3.9) adopts approximated equations of h_X, later shown in equations (3.23) and (3.26) for Types B and C respectively, and the leading terms with respect to Δ_{2X} and γ were taken in that equation in order to render the analytical model tractable.

3.2.3 Stress and geometrical changes in the structure

Stress and geometric changes in the structure are investigated prior to the energy formulation presented in the following section. The investigation includes items such as the stress changes by the prestress, the elongation of the stays and the end-shortening of the column.

3.2.3.1 Initial stress of the column with prestress

With reference to Figure 3.6, the initial prestresses that are introduced to the column T_c and the crossarm T_a are

$$T_c = 2T \cos \alpha, \quad T_a = 2T \sin \alpha. \tag{3.21}$$

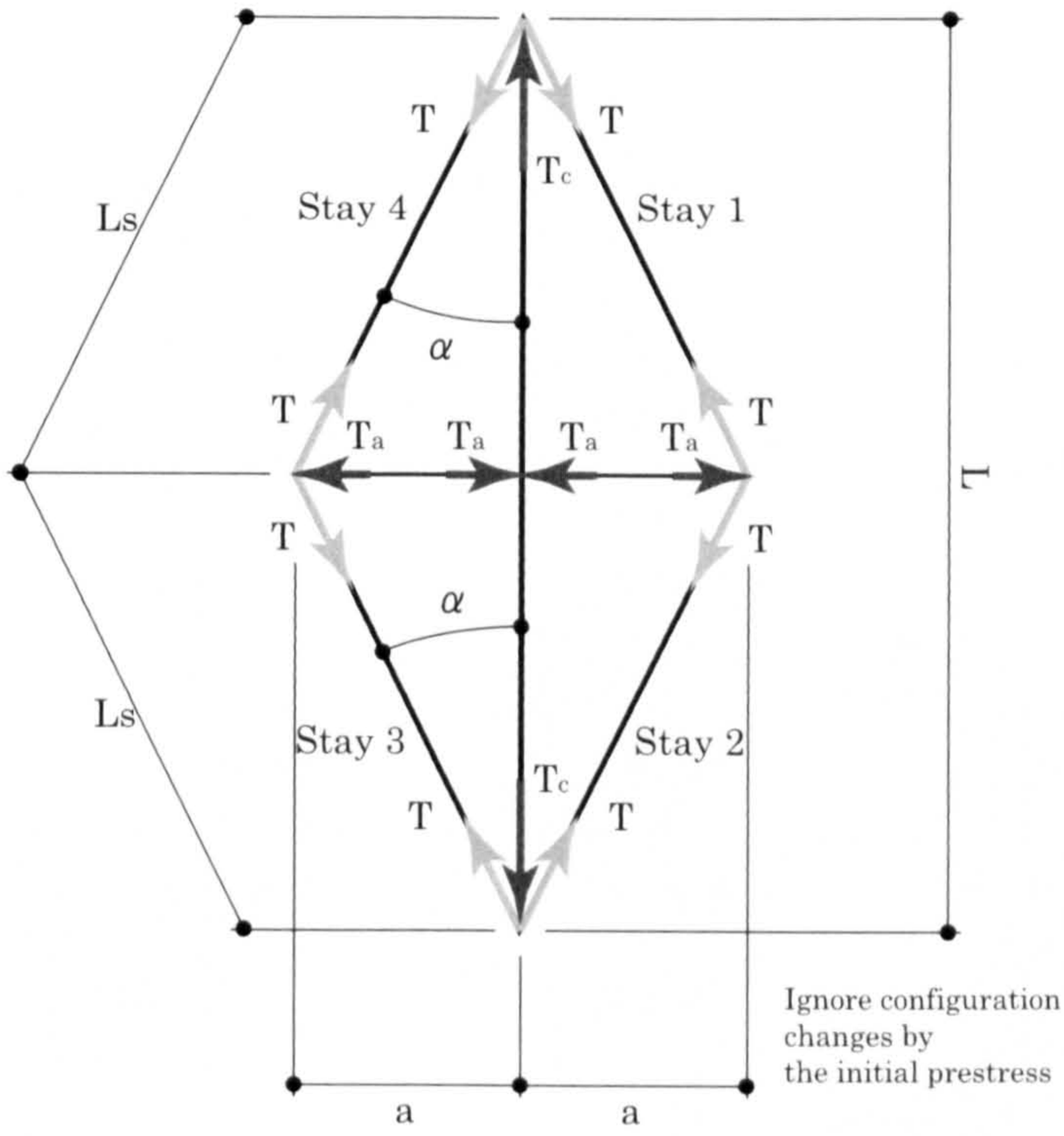

Figure 3.6: Effect of the initial prestress.

Therefore, the strains in the stay ε_{st}, the column ε_{ct}, and the crossarm ε_{at} are respectively:

$$\varepsilon_{st} = \frac{T}{E_s A_s}, \quad \varepsilon_{ct} = \frac{2T\cos\alpha}{EA}, \quad \varepsilon_{at} = \frac{2T\sin\alpha}{E_a A_a}, \tag{3.22}$$

where A and A_a are defined as the cross sectional areas with E and E_a being the Young's moduli of the column and the crossarm respectively.

3.2.3.2 Tip displacement coefficient

The tip displacement of the crossarm is necessary to find the elongation of the stays. This displacement is already presented in equation (3.14). However, as the direct expressions that can be obtained from that expression are too complicated for the analytical model, these are simplified by using a Taylor expansion.

In the case of Type B buckling, h_B is expanded to the third order with respect to Λ_B, and then, in that equation, the leading order terms with respect to Δ_{2B} and γ

are taken, which yields the following:

$$h_B = c_B a\gamma, \tag{3.23}$$

where c_B is a factor expressing the magnitude of the tip displacement of the crossarm for Type B:

$$c_B = \left[1 + \frac{2E_sA_s}{3E_aI_a}a^2 \sin\alpha\cos^2\alpha\right]^{-1}. \tag{3.24}$$

and Λ_B is

$$\Lambda_B = ak_B. \tag{3.25}$$

The same expression of the tip displacement can be obtained using the work of Smith et al. (1975). In the case of Type C, similarly, h_C is expanded to the fifth order with respect to Λ_C, and then, in that equation, the leading order terms with respect to Δ_{2C} and γ are taken, which yields the following:

$$h_C = c_C\, a\gamma + c_{C\Delta}\, a\Delta_{2C} + c_{C0}\, a, \tag{3.26}$$

where c_C, $c_{C\Delta}$ and c_{C0} are factors expressing the magnitude of the tip displacement of the crossarm in Type C:

$$c_C = \frac{(15E_aI_a - E_sA_sa^2\sin\alpha)\, a^2T\sin\alpha\cos^2\alpha + 15\zeta E_aI_a}{5\zeta^2}, \tag{3.27}$$

$$c_{C\Delta} = \frac{\left[(3E_aI_a + 2E_sA_sa^2\sin\alpha\cos^2\alpha)\, T\sin^2\alpha + \zeta E_sA_s\cos^2\alpha\right] a^2\cos\alpha}{\zeta^2}, \tag{3.28}$$

$$c_{C0} = -\frac{a^2T\cos\alpha}{\zeta}, \tag{3.29}$$

where

$$\zeta = \left(3E_aI_a + E_sA_sa^2\sin\alpha\cos^2\alpha\right), \tag{3.30}$$

and Λ_C is

$$\Lambda_C = ak_C. \tag{3.31}$$

Note that this simplification becomes less accurate as the initial prestress T becomes larger.

The accuracy of the third and fifth order approximations for h_B and h_C are discussed in the validation section later in this chapter.

3.2.3.3 Elongation of the stays

The post-buckling shapes are sketched in Figure 3.7; these geometries allow the new stay length L_{siXj}, where the subscript j refers to the stay number as indicated in Figure 3.6, to be evaluated through Pythagoras's theorem, which leads to the strain in the stays purely arising from the applied load P in the stays. Subsequently, this equation is expanded as a Taylor series up to second order with respect to q_m and Δ_{iX}. In this process, the cross and quadratic terms of Δ_{iX} such as $\Delta_{iX}q_m$ and Δ_{iX}^2 are dropped, as these terms are considered to be small from numerical observation. By combining the expanded strain φ_{iXj} with the initial prestress T, the total strains in the stays ε_{siXj} can be obtained, giving a sequence of expressions, here written in a compact format:

$$\varepsilon_{siXj} = \varphi_{iXj} + \varepsilon_{st}. \tag{3.32}$$

3.2.3.4 End-shortening of the column

In order to find the end-shortening expression of the column Δ_{iX}, equilibrium is considered at the end of the column where the external load P is applied with the free body diagram approach shown in Figure 3.8. Vertical force equilibrium and moment equilibrium around the point O give the following equations:

$$T_{iX1}\cos\alpha_{iX1} + T_{iX4}\cos\alpha_{iX4} + P - C_{iX}\cos\beta_i - S_{iX}\cos\beta_i = 0, \tag{3.33}$$

$$M_{iX} - \xi S_{iX}\cos\beta_{iX} - W_i(\xi)S_{iX}\sin\beta_i - W_i(\xi)C_{iX}\cos\beta_i + \xi C_{iX}\sin\beta_i = 0, \tag{3.34}$$

where T_{iXj} is the axial force in stay j with C_{iX}, S_{iX} and M_i being an axial force, a shear force and a bending moment respectively in the column at a point which is a small distance ξ away from O; β_i is the angle between the column and the vertical;

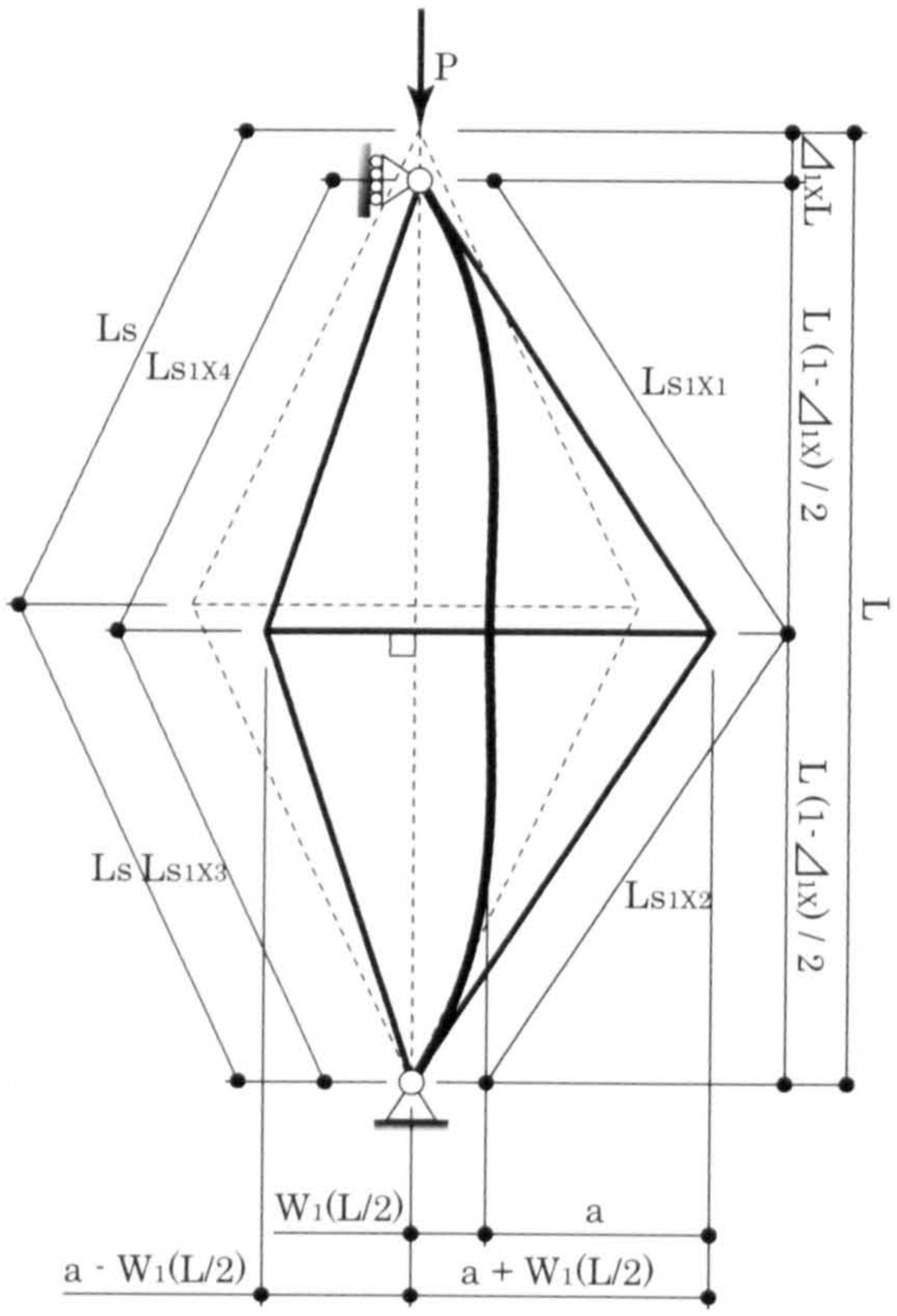

(a) Mode 1

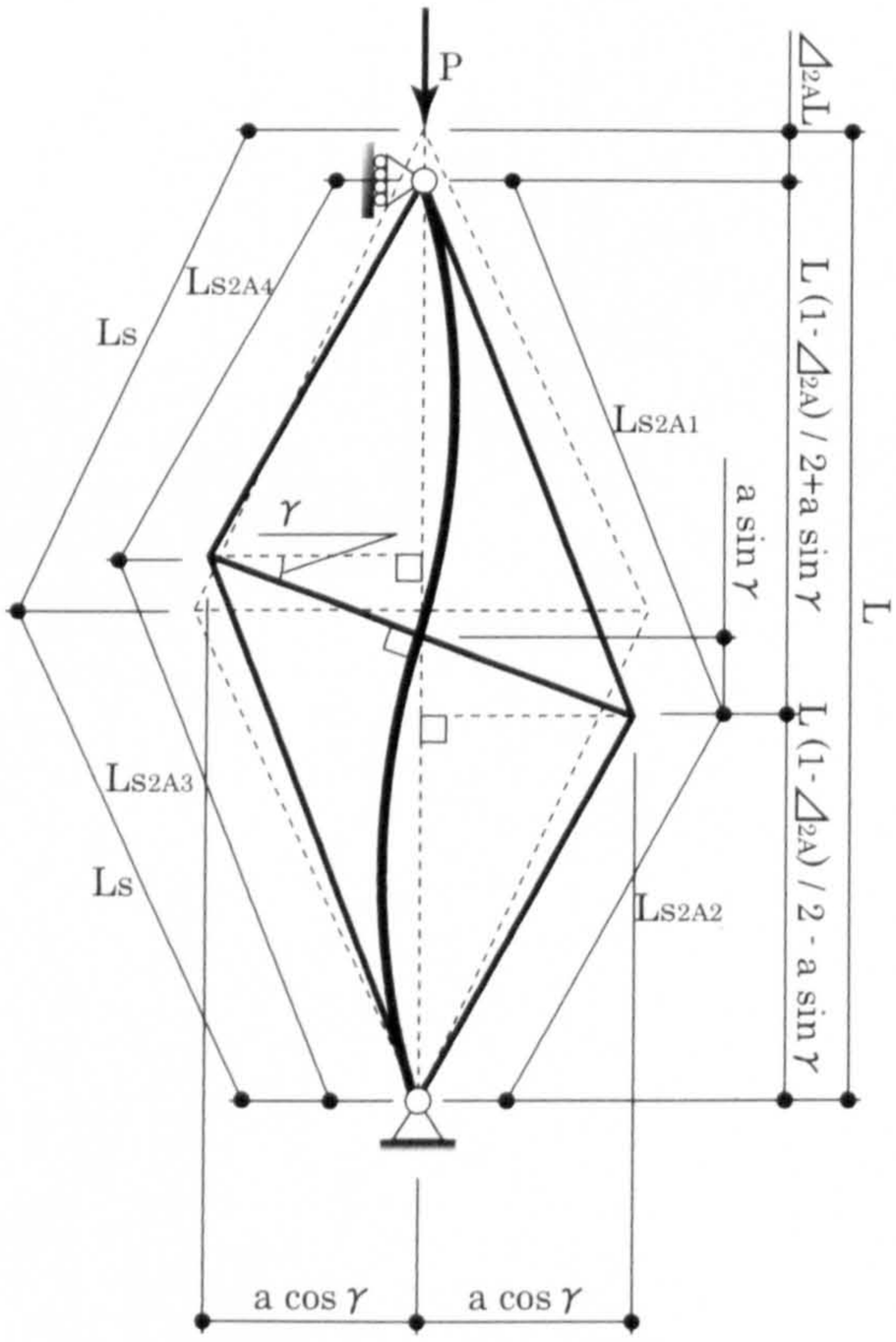

(b) Mode 2 Type A

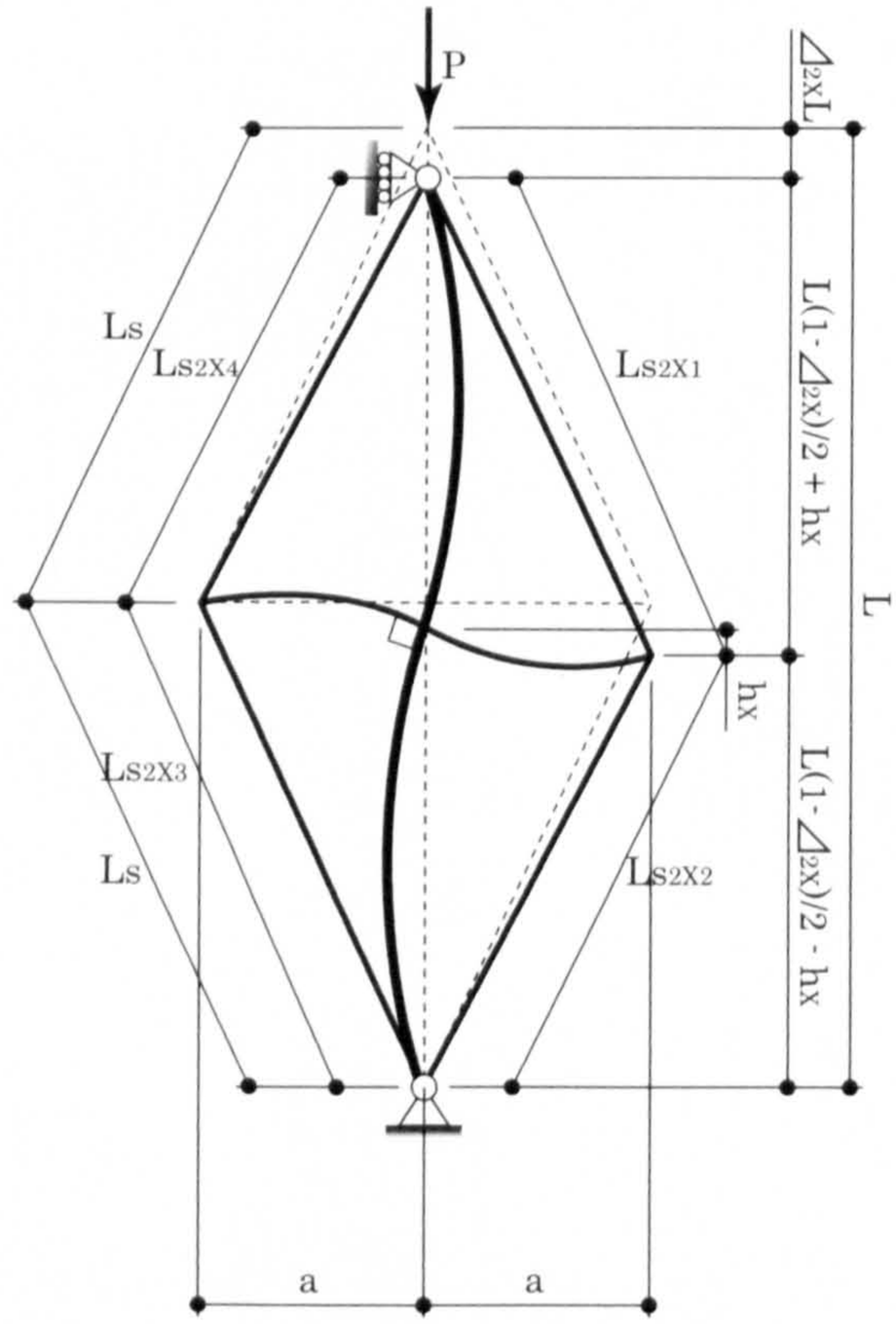

(c) Mode 2 Type B–C

Figure 3.7: Geometry of the stayed column in buckling modes 1 and 2.

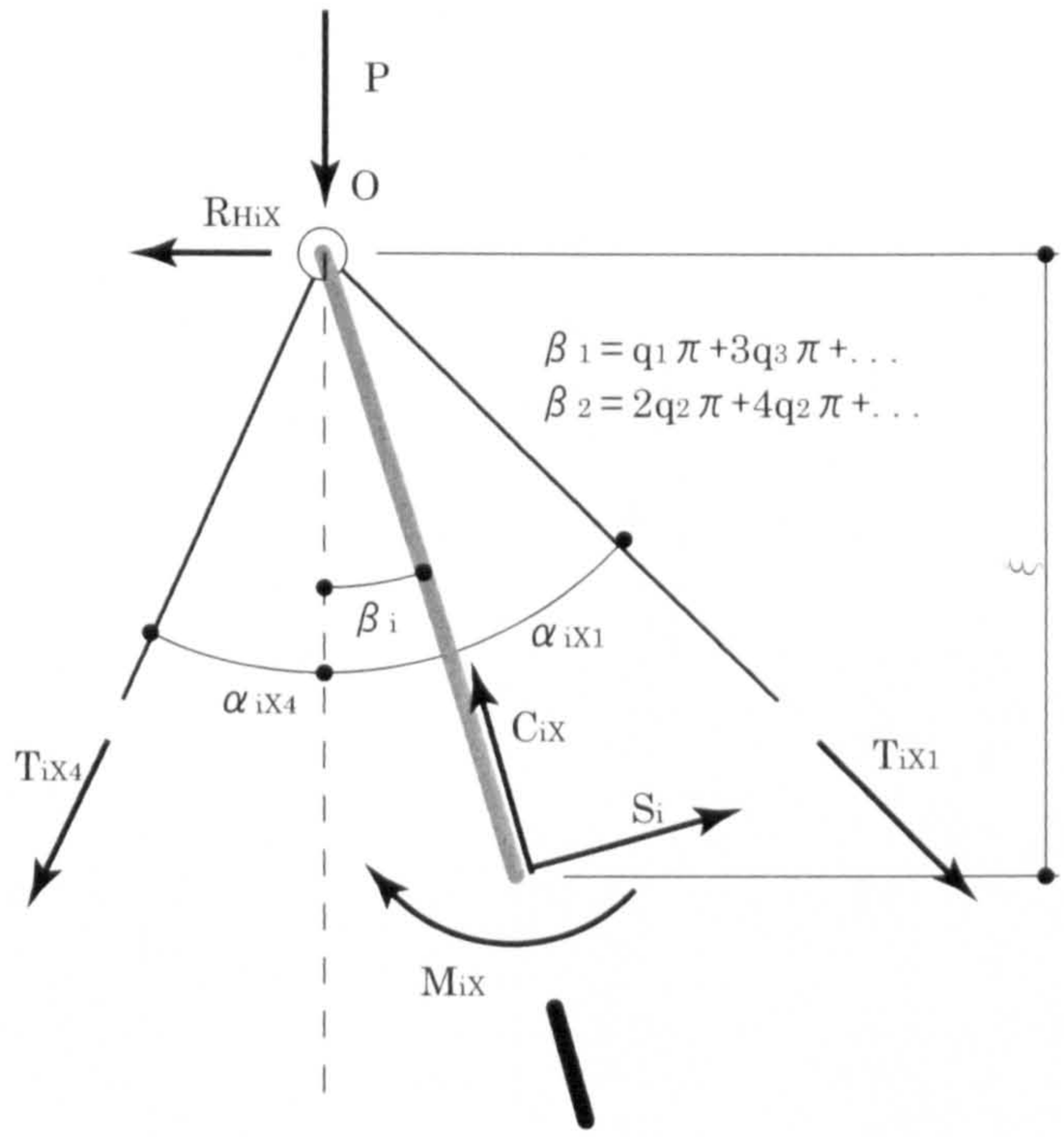

Figure 3.8: Equilibrium free body diagram for the column. Note that R_{HiX} is the horizontal reaction force at the end of the column.

α_{iX1} and α_{iX4} are the angles between each stay and the vertical. These angles, internal forces and moments need to be defined in order to solve the equilibrium equations and to obtain an expression for Δ_{iX}. Firstly, β_i can be obtained by substituting $x = 0$ into $\Theta_i(x)$ defined in equations (3.3) and (3.4):

$$\beta_1 = \Theta_1(0) = q_1\pi + 3q_1\pi + \cdots = \sum_{m=1}^{n} (2m-1)\, q_{2m-1}\pi, \tag{3.35}$$

$$\beta_2 = \Theta_2(0) = 2q_2\pi + 4q_1\pi + \cdots = \sum_{m=1}^{n} 2m\, q_{2m}\pi. \tag{3.36}$$

With reference to Figures 3.7(a)–(c), $\cos\alpha_{iX1}$ and $\cos\alpha_{iX4}$ are obtained through trigonometry; subsequently, those relationships are expressed to the leading order

with respect to q_m and Δ_{iX}. For example, $\cos\alpha_{1X1}$ is given as

$$\cos\alpha_{1X1} = \frac{\frac{1}{2}L(1-\Delta_{1X})}{\sqrt{\left[\frac{1}{2}L(1-\Delta_{1X})\right]^2 + \left[\sum_{m=1}^{n} L(-1)^{m-1}q_{2m-1} + a\right]^2}} \tag{3.37}$$
$$\approx (1-\Delta_{1X}\sin^2\alpha)\cos\alpha.$$

As all of the required angles are defined, the forces and bending moments T_{iX}, C_{iX}, S_{iX}, and M_{iX} in the free body diagram then need to be investigated. Firstly, with the strain expressions of the stays shown in the previous section and the assumption that the stays do not resist compression, the axial forces in the stays T_{iX1} and T_{iX4} are defined as follows:

$$\begin{aligned} &T_{iA1} = T_{iA4} = T_{iC4} = 0, \\ &T_{iB1} = \varepsilon_{siB1}E_sA_s, \quad T_{iB4} = \varepsilon_{siB4}E_sA_s, \quad T_{iC1} = \varepsilon_{siC1}E_sA_s. \end{aligned} \tag{3.38}$$

The axial strain in the column ε_{ciX} is expressed as a summation of the components Δ_{iX} and ε_{ct} minus the effect of the relaxation from the buckling displacement. Therefore, the axial strain for each mode is expressed as follows:

$$\begin{aligned} \varepsilon_{c1X} &= \Delta_{1X} + \varepsilon_{ct} - \frac{1}{L}\int_0^L \frac{1}{2}W_1'^2(x)\mathrm{d}x \\ &= \Delta_{1X} + \frac{2T\cos\alpha}{EA} - \sum_{m=1}^{n}\frac{(2m-1)^2\pi^2 q_{2m-1}^2}{4}, \end{aligned} \tag{3.39}$$

$$\begin{aligned} \varepsilon_{c2X} &= \Delta_{2X} + \varepsilon_{ct} - \frac{1}{L}\int_0^L \frac{1}{2}W_2'^2(x)\mathrm{d}x \\ &= \Delta_{2X} + \frac{2T\cos\alpha}{EA} - \sum_{m=1}^{n} m^2\pi^2 q_{2m}^2. \end{aligned} \tag{3.40}$$

Thus, the axial force C_{iX} is expressed as

$$C_{iX} = EA\varepsilon_{ciX}. \tag{3.41}$$

With linear bending theory, the bending moments M_i are expressed as follows:

$$M_1 = -EIW_1''(\xi) = \sum_{m=1}^{n} \frac{(2m-1)^2\pi^2 EIq_{2m-1}}{L} \sin\frac{(2m-1)\pi\xi}{L}, \tag{3.42}$$

$$M_2 = -EIW_2''(\xi) = \sum_{m=1}^{n} \frac{(2m)^2\pi^2 EIq_{2m}}{L} \sin\frac{2m\pi\xi}{L}, \tag{3.43}$$

where I represents the cross-sectional second moment of area of the column. The shear force S_{iX} can be defined by substituting equations (3.41) and either equation (3.42) for Mode 1 or equation (3.43) for Mode 2 into equation (3.34) and then by taking the limit $\xi \to 0$.

By substituting equations (3.38), (3.41) and an expression for the shear force, either (3.42) for Mode 1 or (3.43) for Mode 2, into equation (3.33), expressions for Δ_{iX} can be obtained. Subsequently, the solution is expressed as a Taylor series with respect to T, P and q_m up to second order, which gives the following simplified expressions:

$$\begin{aligned}\Delta_{1X} &= b_{pX}P + b_{tX}T + b_{1X}q_1 + b_{3X}q_3 + \cdots + b_{11X}q_1^2 + b_{13X}q_1q_3 + b_{33X}^2q_3^2 + \cdots \\ &= b_{pX}P + b_{tX}T + \sum_{m=1}^{n} b_{2m-1\,X}q_{2m-1} + \sum_{m=1,l=1,m\leqslant l}^{n} b_{2m-1\,2l-1\,X}q_{2m-1\,2l-1}q_{2m-1\,2l-1},\end{aligned} \tag{3.44}$$

$$\begin{aligned}\Delta_{2X} &= b_{pX}P + b_{tX}T + b_{2X}q_2 + b_{4X}q_4 + \cdots + b_{22X}q_2^2 + b_{24X}q_2q_4 + b_{44X}^2q_4^2 + \cdots \\ &= b_{pX}P + b_{tX}T + \sum_{m=1}^{n} b_{2m\,X}q_{2m} + \sum_{m=1,l=1,m\leqslant l}^{n} b_{2m\,2l\,X}q_{2m\,2l}q_{2m\,2l},\end{aligned} \tag{3.45}$$

where b_{pX}, b_{tX}, b_{mX} and b_{mlX} are coefficients for P, T, q_m, and q_mq_l respectively.

3.2.4 Energy formulation

The total potential energy V_{iX} comprises components of the strain energy and the work done by the load. In a general state of deflection, there are four components of strain energy: from bending in the column (U_{cbi}) and the crossarm (U_{abiX}) with

axial strains in the column (U_{caiX}) and stays (U_{siX}). Note that the bending energy in the crossarm (U_{abiX}) only exists for Mode 2 in buckling Types B and C as the crossarm does not bend in the other cases.

3.2.4.1 Bending energy

The bending energy components in the column U_{cbi} arise from a linear curvature expression for W_i, thus:

$$\begin{aligned} U_{cb1} &= \frac{1}{2}EI\int_0^L W_1''^2(x)\mathrm{d}x - U_{cb0} \\ &= \sum_{m=1}^{n}\frac{(2m-1)^4 EIq_{2m-1}^2\pi^4}{4L} - U_{cb0}, \end{aligned} \tag{3.46}$$

$$\begin{aligned} U_{cb2} &= \frac{1}{2}EI\int_0^L W_2''^2(x)\mathrm{d}x - U_{cb0} \\ &= \sum_{m=1}^{n}\frac{(2m)^4 EIq_{2m}^2\pi^4}{4L} - U_{cb0}, \end{aligned} \tag{3.47}$$

where U_{cb0} is the existing column bending energy at the beginning of each buckling type.

In a similar way, the bending energy in the crossarm for Mode 2 Types B and C can be obtained. Note that the crossarm symmetry accounts for the doubling of the standard bending energy expression:

$$\begin{aligned} U_{ab2X} &= E_a I_a \int_0^a w_{2X}''^2(y)\,\mathrm{d}y - U_{ab0} \\ &= E_a I_a k_B^3\{2H_X K_X - H_X^2\cos k_X a\sin k_X a + H_X^2 k_X a + K_X^2 k_X a \\ &\quad + K_X^2\cos k_X a\sin k_X a - 2H_X K_X\cos^2 k_X a\}/2 - U_{ab0}, \end{aligned} \tag{3.48}$$

where U_{ab0} is the existing crossarm bending energy at the beginning of each buckling type. Note that U_{cb0} and U_{ab0} have independent values from q_m, and therefore, they do not affect the critical load nor the post-buckling path as they simply vanish on differentiation. Although these terms vanish, as shown later, in Type C buckling,

the column and the crossarm are not necessarily straight at the onset of the buckling type; hence, the existing bending energies U_{cb0} and U_{ab0} should be expressed in the formulation of the total potential energy V.

3.2.4.2 Axial energy

The axial energy U_{caiX} in the column accounts for the energy gained through the axial compression from the load P together with the effect of the relaxation from the buckling displacement; using equations (3.39) and (3.40) as the ending points of integration for each mode, the axial energy is obtained as

$$U_{caiX} = \int_{\varepsilon_{cX0}}^{\varepsilon_{ciX}} EAL\varepsilon \mathrm{d}\varepsilon = \frac{1}{2} EAL(\varepsilon_{ciX}^2 - \varepsilon_{cX0}^2), \tag{3.49}$$

where ε_{cX0} is the existing strain at the beginning of each type.

The axial energy in the stays is obtained by integrating the stress–strain relationship over the stay volume—written as the product of the cross-sectional area A_s and the length L_s:

$$U_{siX} = \sum_{j=1}^{4} U_{siXj} = \sum_{j=1}^{4} \int_{\varepsilon_{sX0}}^{\varepsilon_{siXj}} A_s L_s \sigma(\varepsilon_{siXj}) \, \mathrm{d}\varepsilon, \tag{3.50}$$

where U_{siXj} is the strain energy stored in stay j for Mode i Type X, and ε_{sX0} is the existing strain at the commencement of each buckling type. The stress–strain curve of the stays is assumed to be piecewise linear as shown in Figure 3.9, thus:

$$\sigma_s(\varepsilon_{siXj}) = \begin{cases} E_s \varepsilon_{siXj} & \text{for} \quad \varepsilon_{siXj} > 0, \\ 0 & \text{for} \quad \varepsilon_{siXj} \leqslant 0. \end{cases} \tag{3.51}$$

From equations (3.50) and (3.51), the total stay energy for Mode i Type X in stay j is given as follows:

$$U_{siXj} = \begin{cases} \frac{1}{2} E_s A_s L_s \left(\varepsilon_{siXj}^2 - \varepsilon_{sX0}^2\right) & \text{for} \quad \varepsilon_{siXj} \geqslant 0, \\ 0 & \text{for} \quad \varepsilon_{siXj} \leqslant 0. \end{cases} \tag{3.52}$$

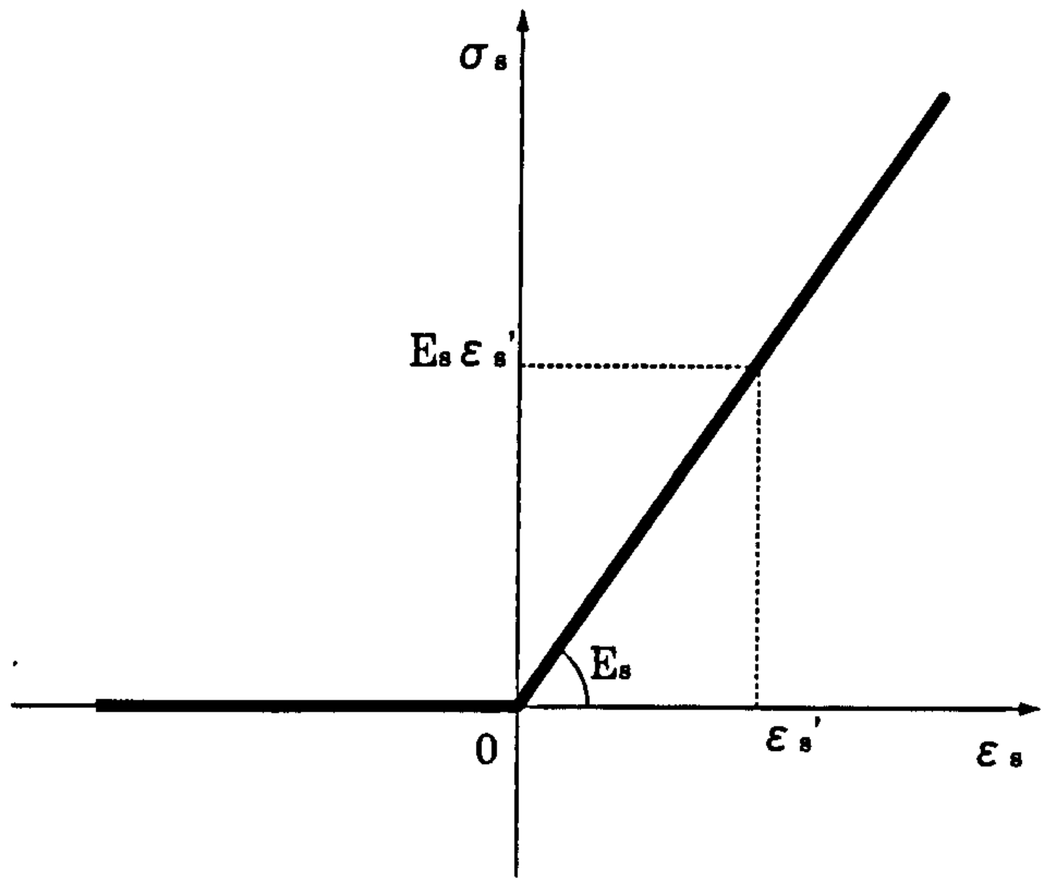

Figure 3.9: Stress–strain relationship of the stays.

Note that ε_{cX0} and ε_{sX0} affect neither the critical load nor the post-buckling path, because they are independent of q_m and vanish on differentiation.

3.2.4.3 Work done by the load

The work done by the load $P\mathcal{E}_{iX}$ is defined as the external axial load P multiplied by the corresponding end-shortening $\Delta_{iX}L$:

$$P\mathcal{E}_{iX} = P\Delta_{iX}L - P\mathcal{E}_{0X}, \tag{3.53}$$

where $P\mathcal{E}_{0X}$ is the work done by the load before the commencement of each buckling type. Note that, again, this value affects neither the critical load nor the post-buckling path for the same reason as stated in the previous section.

3.2.4.4 Total potential energy function

The total potential energy is a summation of the bending and axial strain energies minus the work done, thus:

$$V_{iX} = U_{cbi} + U_{abiX} + U_{caiX} + U_{siX} - P\mathcal{E}_{iX}. \tag{3.54}$$

In the Mode 2 Type C analysis, higher terms of P are then truncated as they are not the dominant terms in the function and leave the governing equation untractable. For equilibrium, the total potential energy V_{iX} must be stationary with respect to the generalized coordinates q_m. Therefore, the equilibrium paths can be computed from the condition:

$$\frac{\partial V_{iX}}{\partial q_m} = 0, \tag{3.55}$$

which is derived from Axiom 1 in §1.4.2.

3.3 Critical Buckling

Having formulated the total potential energy, the critical buckling load of the stayed column is investigated using linear eigenvalue analysis. From the earlier work of Hafez et al. (1979), it is known that the critical load is divided into three zones in relation to the magnitude of the initial pretension in the stays.

Zone 1 The tension in the stays disappears completely before the external load reaches the buckling load. Therefore, the critical load is exactly the Euler load (Type A buckling).

Zone 2 The strain in the stays becomes zero when the applied load reaches the critical load, i.e. the structure resists buckling until the tension in the stays becomes zero. Thus, all the stays remain effective until buckling, which sends the critical load potentially to a level that is significantly higher than the Euler

load (Type C buckling).

Zone 3 The tension in the stays is nonzero at the instant of buckling. As a large amount of the pretension has been introduced, all the stays remain effective for some while after buckling. The value of the critical load falls somewhat as the initial prestress increases because the initial compressive stress in the column diminishes its axial load capacity (Type B buckling).

As the formulation of the model ensures that the profile of the structure maintains perfect symmetry during the fundamental state, a bifurcation point can be observed when $q_m = 0$. With the type B formulation, conventional linear eigenvalue analysis, i.e. finding when the Hessian matrix for V_{iB} becomes singular, yields the critical load for Zone 3 P^{Ci}_{Zone3} directly. The details on the process and equations obtained can be seen in Appendix A.

For Zones 1 and 2, it is necessary to consider geometrical nonlinearities in order to find the critical load. In these zones, the end-shortening of the column releases the axial energy in the stays during the fundamental stage, which does not allow linear eigenvalue analysis to yield the critical load. Moreover, linear buckling analysis in the FEM does not detect the critical load for Zones 1 and 2 either, the analytical method being therefore essential to find the critical load in this range of T.

In Zone 1, where the axial energy in the stays is already lost before buckling, this problem can be simply resolved by adopting the Type A buckling energy formulation and then following the same process as for Zone 3. Because in Zone 1 (Type A buckling) all of the stays are slack at the instant of buckling, no substantial changes in the way of determining the critical load are necessary. As the stays are therefore effectively absent, the critical loads for Zone 1 for Mode i are

$$P^{Ci}_{\text{Zone1}} = \frac{i^2\pi^2 EI}{L^2}. \tag{3.56}$$

As can be seen from this equation, the critical load for Zone 1 is the exactly same as the Euler buckling load P_{E}.

For Zone 2, the critical load can be found from utilizing the condition that the strain in the stays becomes zero at the instant of buckling. As all of the stays are active during the pre-buckling stage, substituting $q_m = 0$ and $h_B = 0$ into equation (3.32) with the adoption of subscript B and solving the equation for P gives the following critical load for Zone 2 for Mode i:

$$P^{\mathrm{C}}_{\mathrm{Zone2}} = \frac{T}{b_{pB} E_s A_s \cos^2 \alpha}, \tag{3.57}$$

where

$$b_{pB} = \left[2E_s A_s \cos^3 \alpha + EA\right]^{-1}. \tag{3.58}$$

Note that Modes 1 and 2 have the same expression for the Zone 2 critical load. In fact, the instability behaviour in Zone 2 is not a classic bifurcation response: at the point of "buckling" there is a sudden release of the axial energy of the column, forcing the column to buckle, which is immediately followed by the reactivation of the convex side stays as the column displaces laterally.

By plotting the critical loads against T, the relationship between the buckling load and the initial prestress, which was first presented by Hafez et al. (1979), can be reproduced. This relationship is shown in Figure 3.10, where T_{min} represents the initial prestress at the boundary between Zones 1 and 2—the minimum effective pretension required to raise the buckling load above the Euler load P_{E}. $P^{\mathrm{C}}_{\mathrm{max}}$ represents the theoretical maximum buckling load that is observed at the boundary between Zones 2 and 3, and T_{opt} represents the initial prestress where $P^{\mathrm{C}}_{\mathrm{max}}$ is exhibited.

3.3.1 Numerical results

In this section the aim is to compare theoretical $P^{\mathrm{C}}_{\mathrm{max}}$ values obtained from the previous section with those from the Hafez model as a benchmark for validation. In the Hafez model, $P^{\mathrm{C}}_{\mathrm{max}}$ was obtained by the FEM, so that the accuracy of the current model in terms of the critical load can be evaluated. In the Hafez model, $P^{\mathrm{C}}_{\mathrm{max}}$ was

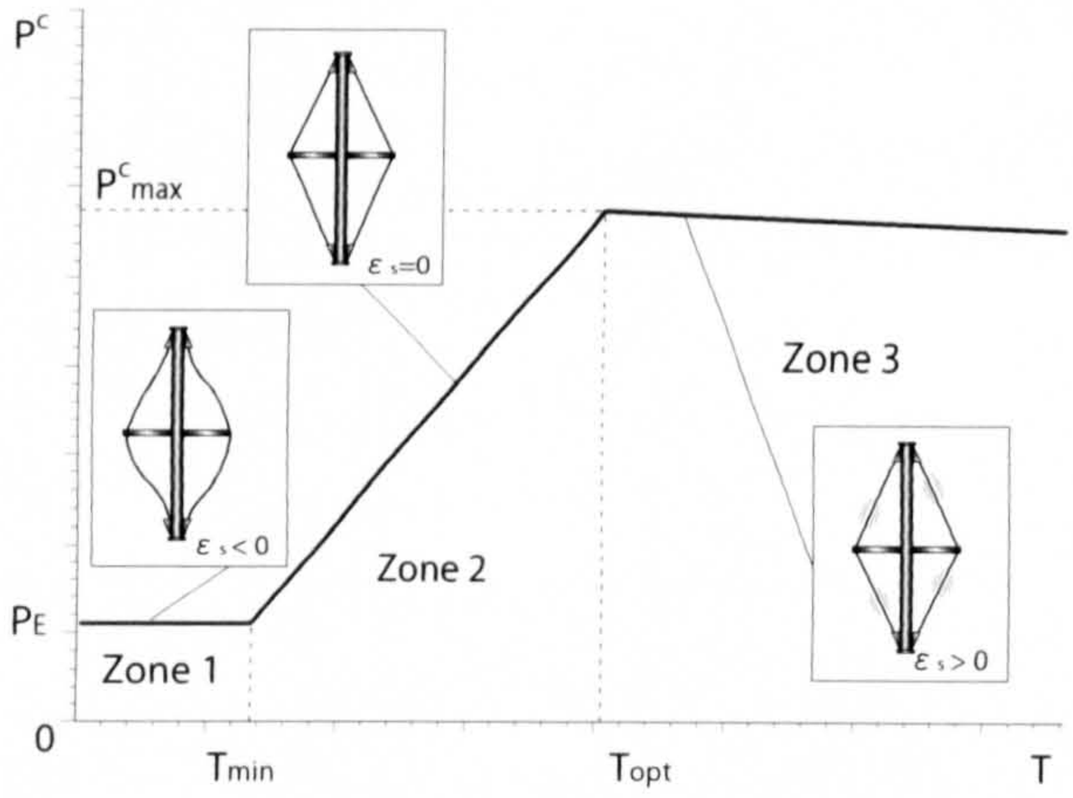

Figure 3.10: Critical buckling load P^{C} versus initial prestress T. The state of the stays and their strains ε_s at the instant of buckling are also shown.

sought with a variation in three parameters: crossarm length, stay diameter and stay Young's modulus; for the current model, the same parameters are varied. The dimensions of the structure used in the Hafez model were as follows:

column Young's modulus:	$E = 201\,\mathrm{kN/mm^2}$
crossarm Young's modulus:	$E_a = 201\,\mathrm{kN/mm^2}$
stay Young's modulus:	$E_s = 202\,\mathrm{kN/mm^2}$
column length:	$L = 3.05\,\mathrm{m}$
crossarm length:	$a = 0.305\,\mathrm{m}$
outside diameter of the column:	$\phi_{co} = 38.1\,\mathrm{mm}$
inside diameter of the column:	$\phi_{ci} = 25.4\,\mathrm{mm}$
outside diameter of the crossarm:	$\phi_{ao} = 38.1\,\mathrm{mm}$
inside diameter of the crossarm:	$\phi_{ai} = 25.4\,\mathrm{mm}$
stay diameter:	$\phi_s = 3.2\,\mathrm{mm}$ or $\phi_s = 4.8\,\mathrm{mm}$.

While the crossarm length a is varied from $0.305\,\mathrm{m}$ to $3.05\,\mathrm{m}$, the stay diameter is fixed to $\phi_s = 3.2\,\mathrm{mm}$; when the stay Young's modulus E_s is varied from $64.8\,\mathrm{kN/mm^2}$ to $204\,\mathrm{kN/mm^2}$, the stay diameter is fixed to $\phi_s = 4.8\,\mathrm{mm}$. Figures 3.11(a), (b) and (c) respectively show $P^{\mathrm{C}}_{\mathrm{max}}$ varying with each parameter along with that of the Hafez model. In the case of the SDOF model for Mode 1, there is a certain degree of error

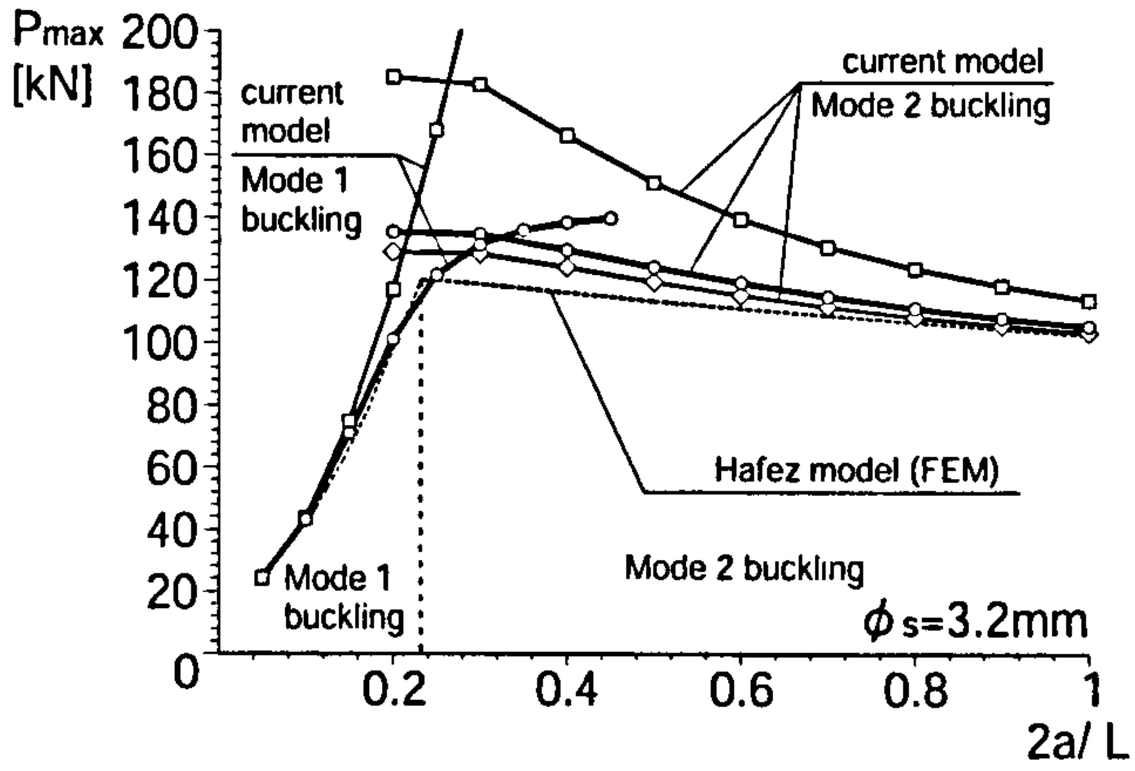

(a) crossarm length

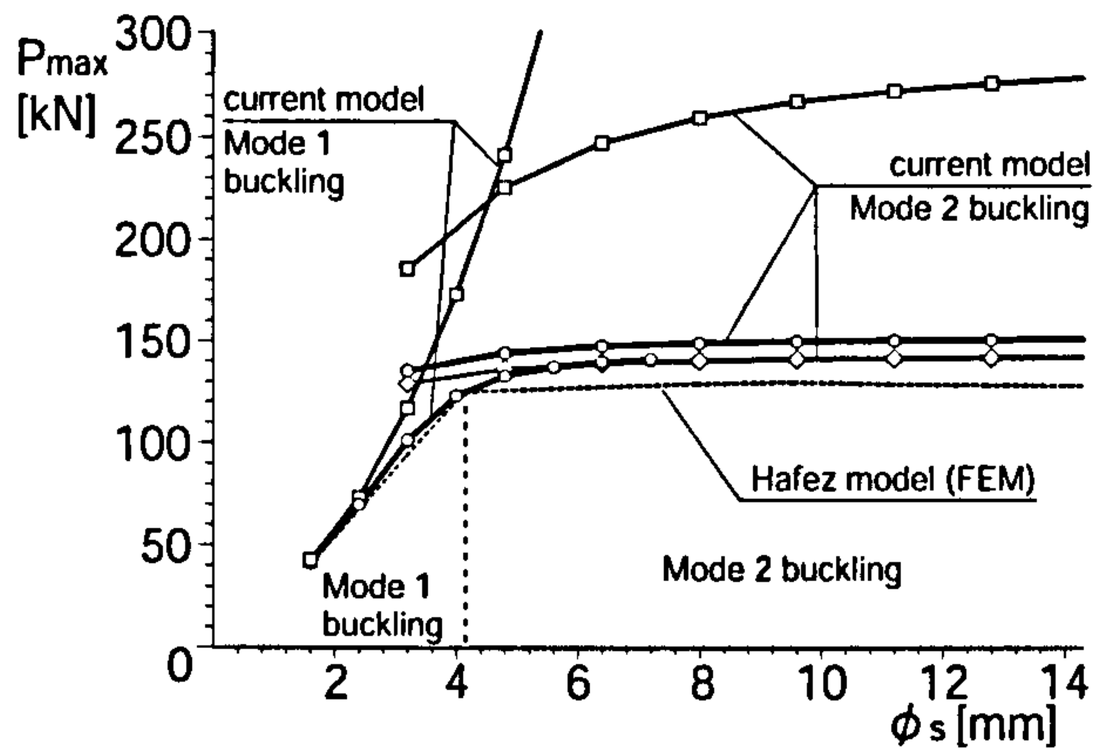

(b) stay diameter

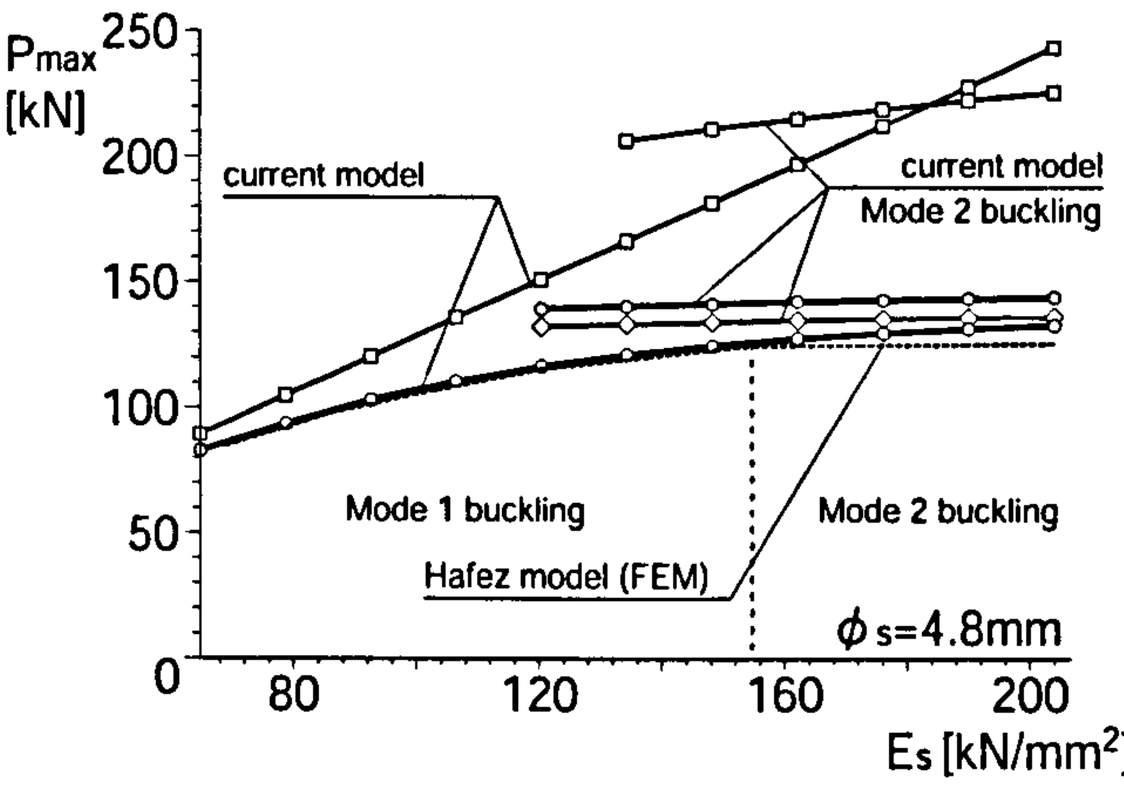

(c) stay Young's modulus

Figure 3.11: Comparison of P_{max}^{C} values with those of the Hafez model: (a) varying crossarm length, (b) varying stay diameter, (c) varying Young's modulus. Symbols (□), (○) and (◇) represent the cases of $n = 1$, $n = 2$ and $n = 3$ respectively.

shown in Figure 3.11 between the Hafez and the current model. However, with the two degree-of-freedom (2DOF) model, this error between the two becomes almost negligible. In Mode 2, however, gaps between the Hafez model and the current model can be seen to be more significant. With the three degree-of-freedom (3DOF) model, which is the most sophisticated model presented and therefore is expected to have the least error, some differences are still evident. Although these figures show relatively less good agreement compared with those of Mode 1, the trend is that increasing the number of freedoms increases the accuracy but with computational expense and analytical complexity.

Considering that the difference between the 2DOF and the 3DOF models is not significant, and that the solutions from the 2DOF model are relatively close to the benchmark solutions, the 2DOF model will be used in order to obtain reasonably accurate solutions for the post-buckling behaviour without it being excessively demanding computationally.

3.4 Post-Buckling Response

Equation (3.55) expresses the equilibrium states after buckling, which can be solved using the symbolic computation package MAPLE. In Mode 1, the same dimensions and properties as in §3.3.1 were also applied for the post-buckling analysis, with the stay diameter, $\phi_s = 4.8\,\text{mm}$ being chosen. The critical buckling loads obtained with those dimensions against the initial prestress are shown in Figure 3.12. As illustrated, eight points are selected from each diagram to investigate changes in the post-buckling response as T changes, the selection criteria being shown in Table 3.1.

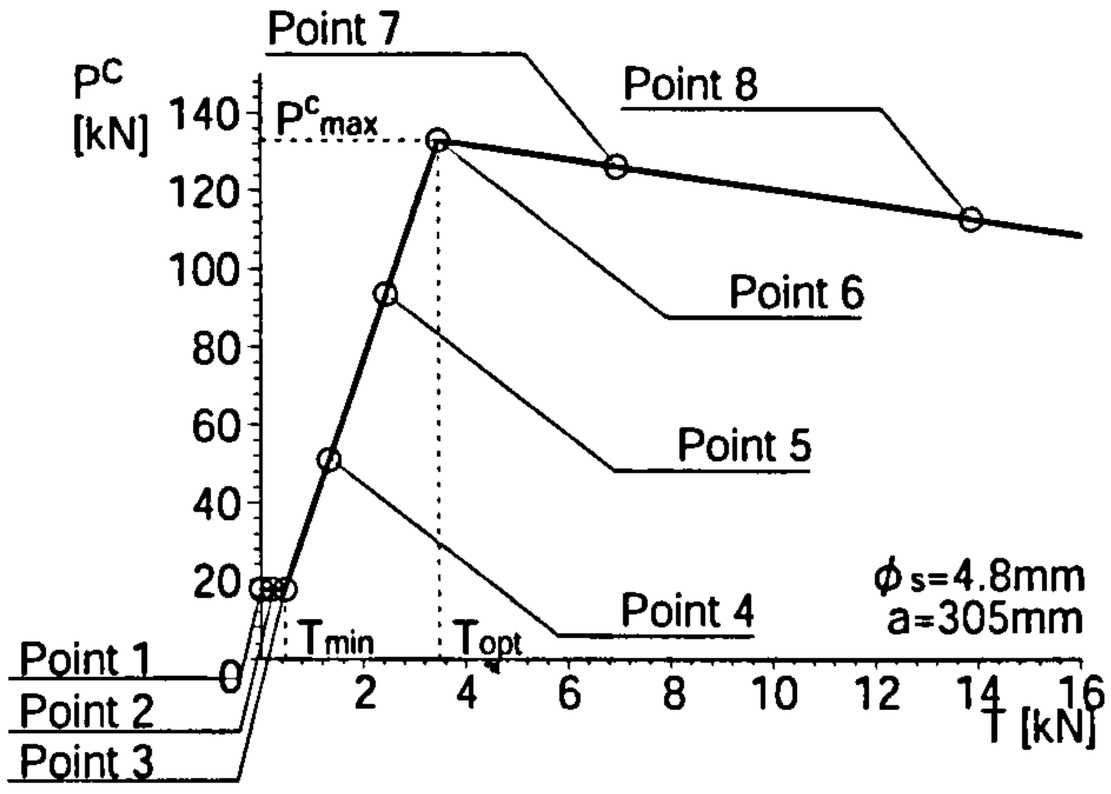

(a) Mode 1

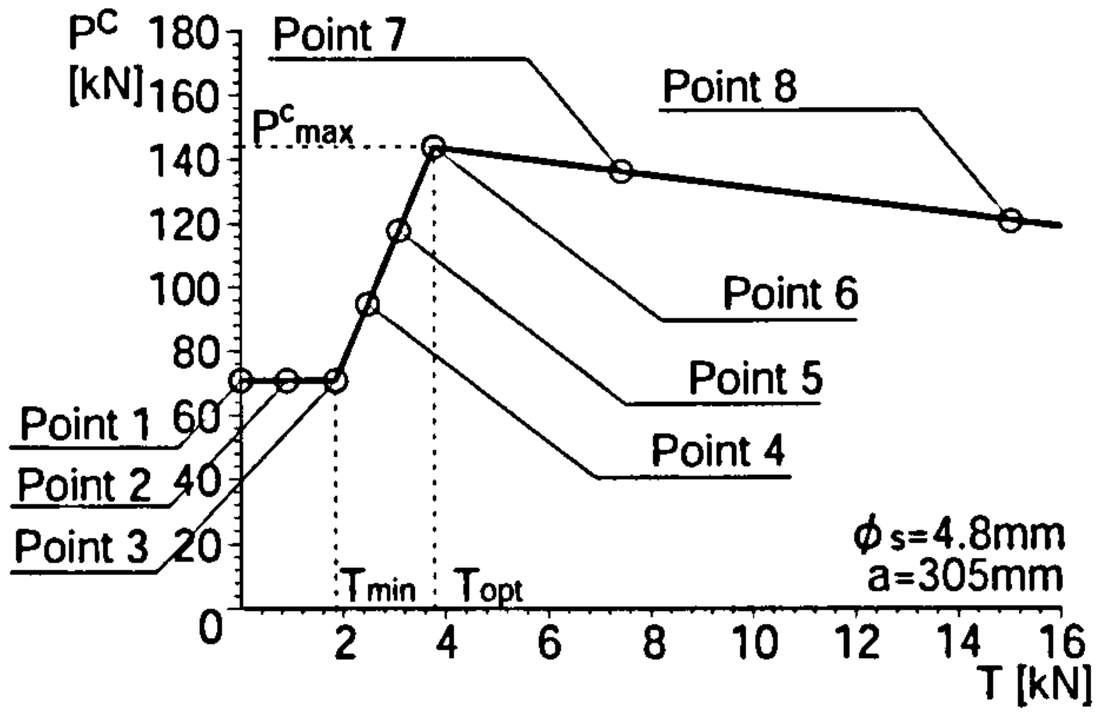

(b) Mode 2

Figure 3.12: Critical buckling load P^C versus the initial prestress T showing the selected points for the study.

Point	Initial prestress T		
	Criterion expression	Mode 1 (kN)	Mode 2 (kN)
1	0	0.00	0.00
2	$T_{\min}/2$	0.23	0.93
3	$T_{\min}$	0.46	1.86
4	$(T_{\text{opt}} - T_{\min})/3 + T_{\min}$	1.47	2.50
5	$2(T_{\text{opt}} - T_{\min})/3 + T_{\min}$	2.48	3.14
6	T_{opt}	3.48	3.78
7	$2T_{\text{opt}}$	6.97	7.55
8	$4T_{\text{opt}}$	13.93	15.10

Table 3.1: Selected points for the post-buckling investigation.

3.4.1 Zones of behaviour

The post-buckling responses for Modes 1 and 2 in each zone are represented in Figures 3.13 and 3.14. For Mode 1, the relationship between P and $q_1 - q_3$ is shown, the latter quantity being the normalized horizontal displacement at the column midspan, obtained by evaluating $W_1(L/2)/L$. For Mode 2, the relationship between P and $q_2 - 2q_4$ is shown, the latter quantity being the normalized rotation at the column midspan, obtained by evaluating $\Theta_2(L/2)/2\pi$.

For both modes the post-buckling path in Zone 1 has two distinct stages, as shown in (a) and (b) in Figures 3.13 and 3.14 respectively; P remains practically at the critical load in Type A buckling (all stays slack) for a while, then the equilibrium path stabilizes with Type C buckling (convex side stays reactivated). Note that, as shown in (b) in Figures 3.13 and 3.14, the initially flat range becomes shorter as the prestress T is increased.

As shown in the graphs in (c) of Figures 3.13 and 3.14, in Zone 2, stable paths can be observed in the initial post-buckling range with relatively low values of the prestress, such as for Points 3, 4 and 5, whereas unstable paths can be observed with relatively high values of the prestress, such as for Point 6. The initial prestress at the transition from stability to instability can be found when $T = 2.79\,\text{kN}$ for Mode 1. The reason for this transition in Zone 2 can be considered as follows: with

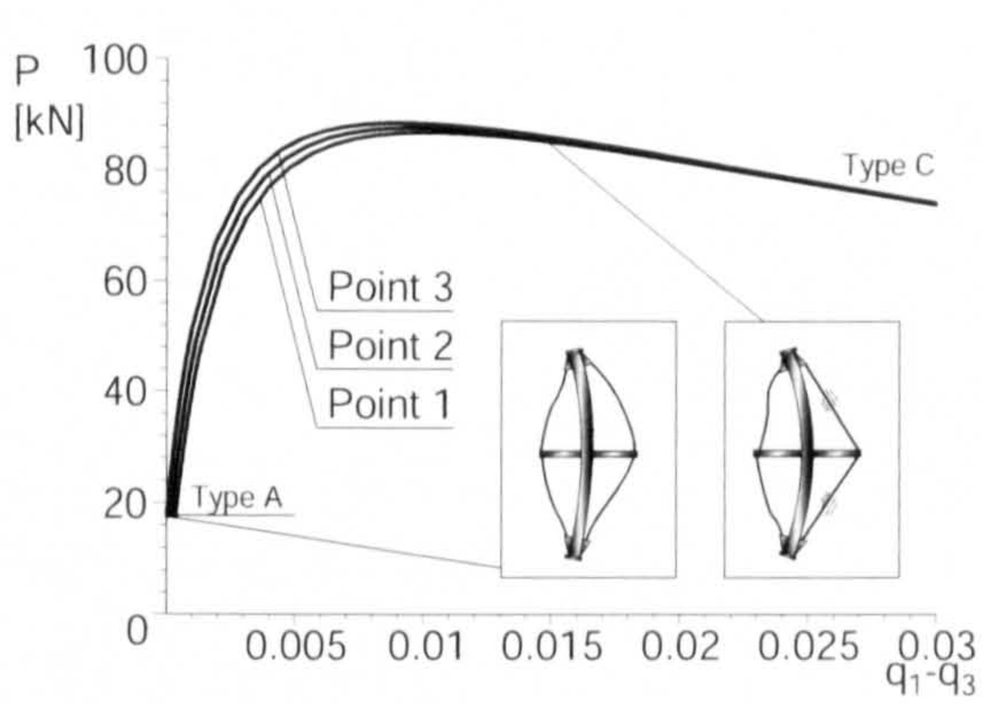

(a) Zone 1

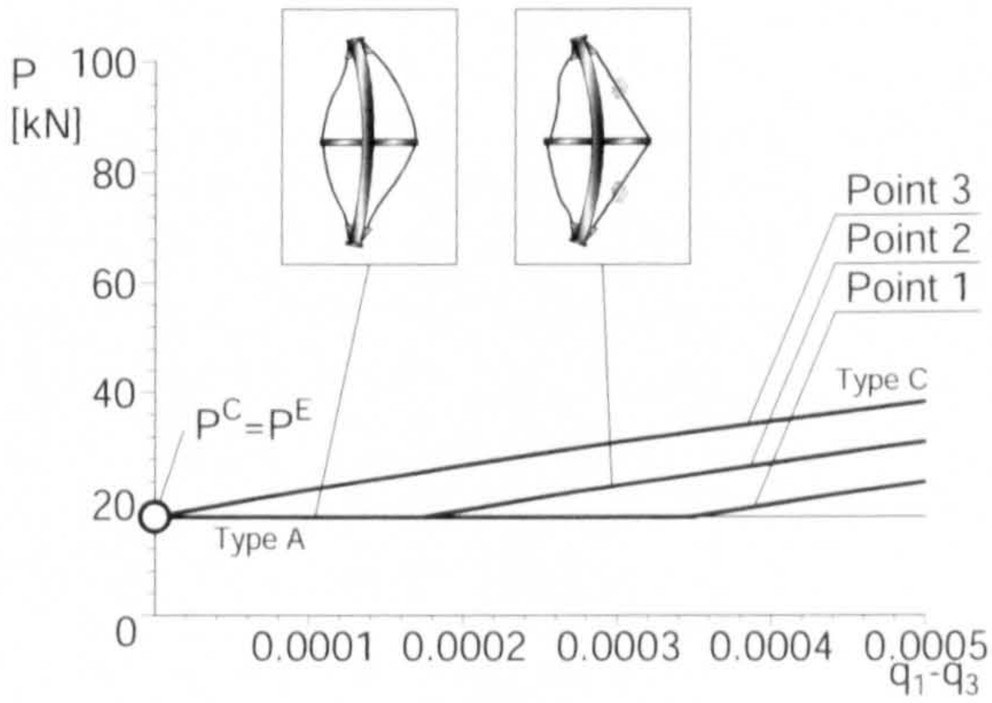

(b) initial part of zone 1

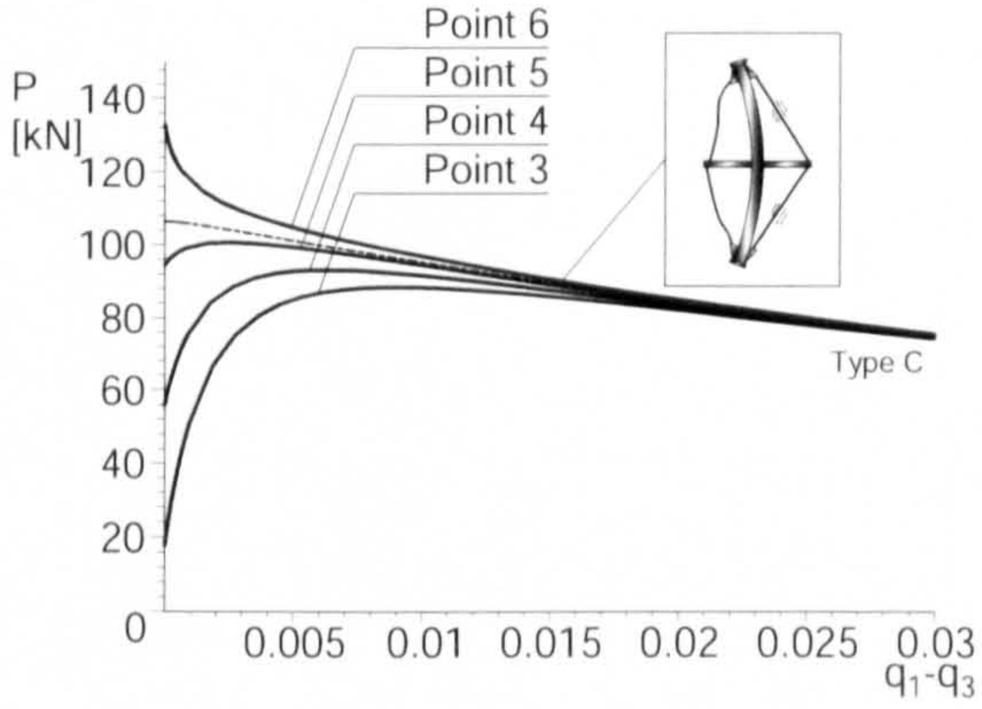

(c) Zone 2

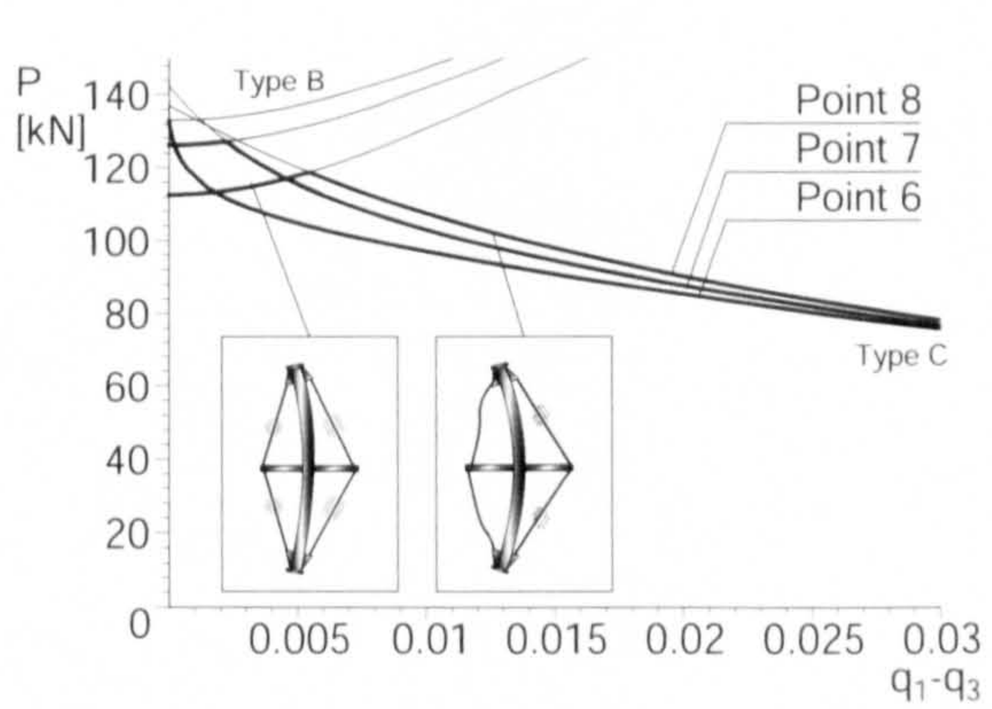

(d) Zone 3

Figure 3.13: Post-buckling responses for Mode 1 represented by axial load P versus midspan buckling displacement $q_1 - q_3$.

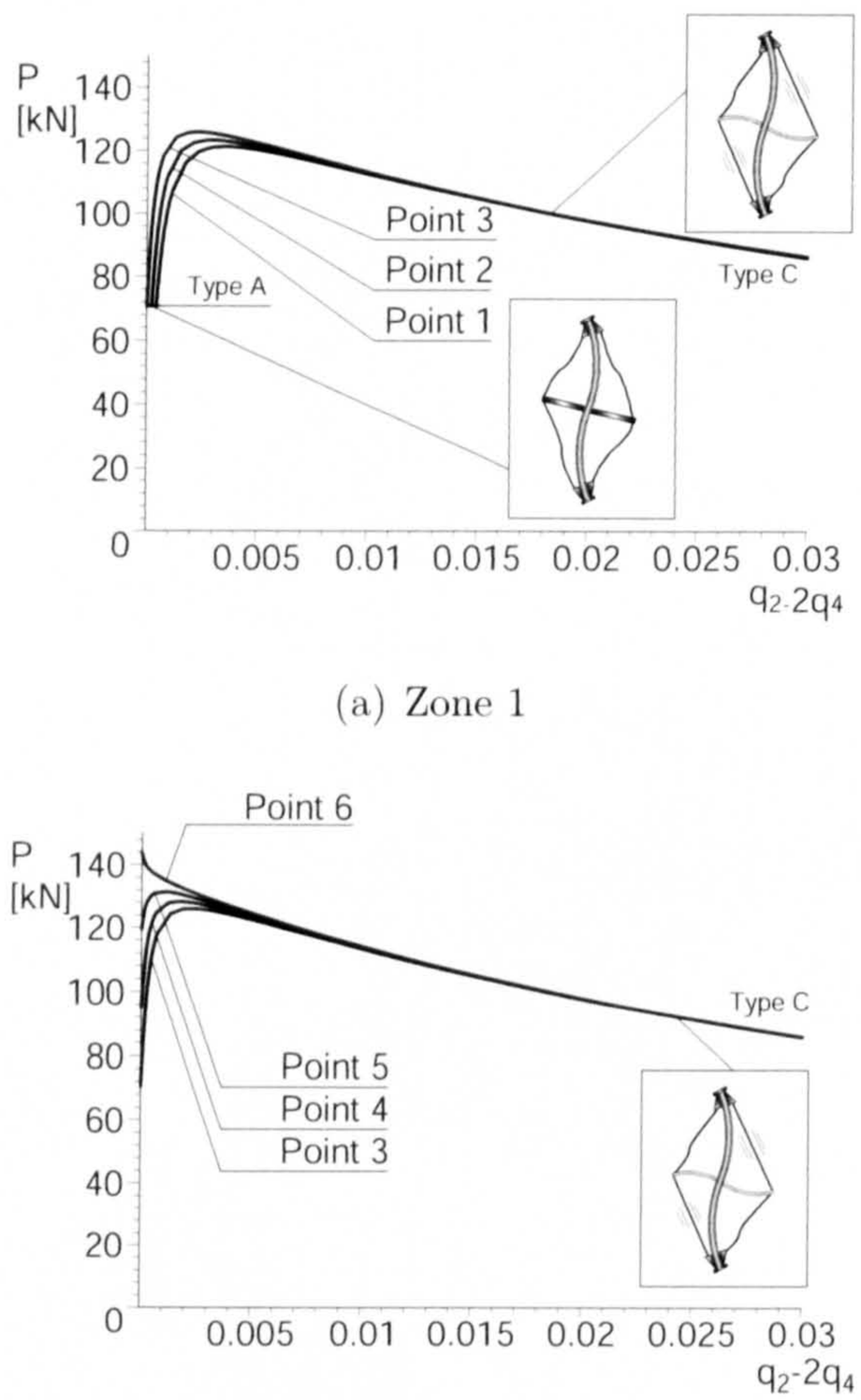

(a) Zone 1

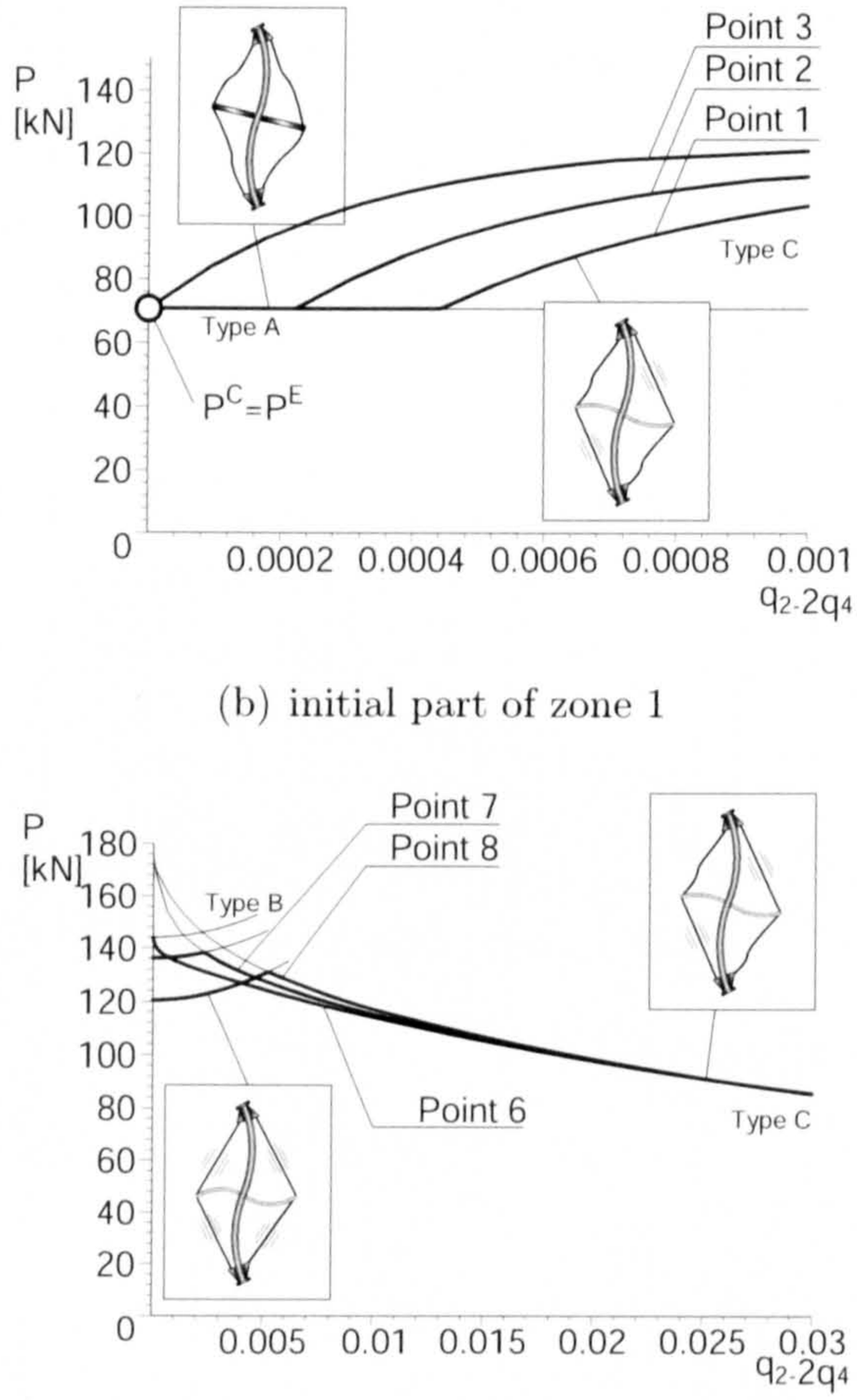

(b) initial part of zone 1

(c) Zone 2

(d) Zone 3

Figure 3.14: Post-buckling responses for Mode 2 represented by axial load P versus midspan buckling rotation $q_2 - 2q_4$.

a relatively large value of the prestress in Zone 2, a large amount of the axial energy can be stored in the fundamental state due to the presence of effective axial forces in the stays, which prevents the release of axial energy from the column. Therefore, this excessive amount of the energy is suddenly released at the instant of buckling, which is conjectured to cause the unstable responses. By contrast, with a relatively small value of the prestress, although the axial energy has been able to be stored in the fundamental state, more than in the case of Zone 1, this additional energy can be absorbed completely into the stays after buckling; therefore, stable paths are seen. Despite this difference within the zone, for any case in Zone 2 post-buckling response, the convex side stays are active throughout the post-buckling range, with

the stays on the concave side being slack, which implies that in Zone 2 the post-buckling response has Type C characteristics.

As shown in the graphs in (d) of Figures 3.13 and 3.14, there is also a discontinuity in the post-buckling response in Zone 3. The load P remains nearly at the critical load in Type B buckling for a while, and this initial stage is followed by Type C buckling with a sudden loss of the stability; unstable paths are then observed when the concave side stays go slack. The discontinuity of Zone 3 is basically a mirror image of the response in Zone 1, where slackening of the stays occurs rather than their reactivation.

Also these two diagrams suggest that the most unstable paths after the critical loads occurs when the prestress level is equal to T_{opt} (Point 6), which is located at the boundary of Zones 2 and 3. Since the prestress T_{opt} gives the highest value of the critical load as shown in 3.10, T_{opt} was considered to be the optimal level of the prestress (Hafez *et al.*, 1979). Despite that statement, this unstable response is not favourable at all and often renders the maximum load capacity extremely sensitive to geometrical imperfections. Hence, a greater level of the prestress than T_{opt} would be recommended for design as a stable path appears with a higher level of prestress, which allows the system to be more reliable when buckling may occur.

For all of the zones, the only difference between Modes 1 and 2 is the active stays in the Type C buckling response: the active stays are 1 and 2 for Mode 1 with 1 and 3 for Mode 2.

3.4.2 Validation for the tip displacement coefficients

In order to investigate the tip displacement coefficients for the crossarm, the third and fifth order expansions with respect to Λ_X were formulated for buckling Types B and C respectively. Although this approximation gives much computational advantage to the analytical model, the accuracy of the process has not yet been estimated. Hence, in this section, the numerical values of the approximated tip displacements

h_X, which can be obtained from equations (3.23) and (3.26), and the exact shape functions for the crossarm $w_{2X}(y)$, which can be obtained from equation (3.9), are presented and then compared against each other.

To examine the actual values of h_X and $w_{2X}(y)$, equilibrium points were selected from the post-buckling response at the prestress level of Point 7, as shown in Figure 3.15. Points EB1–EB4 are from the path in Type B, and Points EC1–EC4 are from the path in Type C.

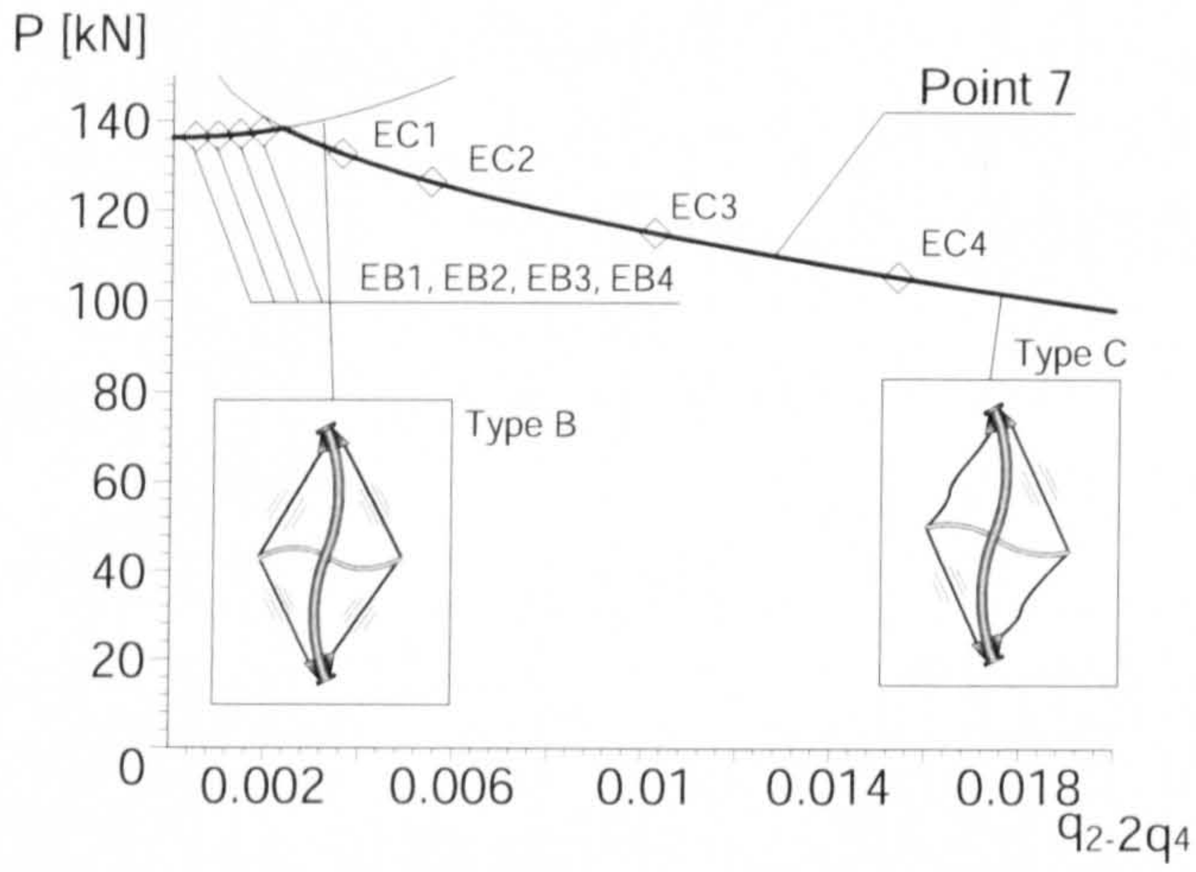

Figure 3.15: Selected points for the validation of the tip displacement coefficients.

Figure 3.16 plots h_X and $w_{2X}(y)$ at those selected points from the equilibrium path shown in Figure 3.15. As can be seen, not much difference is observed between these two curves at the tip of the crossarm for all points. Thus, it can be said that the approximation for h_X is appropriate and has been validated with the presented comparison.

3.4.3 Validation for the post-buckling response

Using the FEM program ABAQUS, a purely numerical model was developed and the post-buckling response was revealed by nonlinear Riks analysis to validate the results presented in the previous section. In this procedure, the column and the crossarm were modelled as beam elements and the stays were modelled as truss elements. The

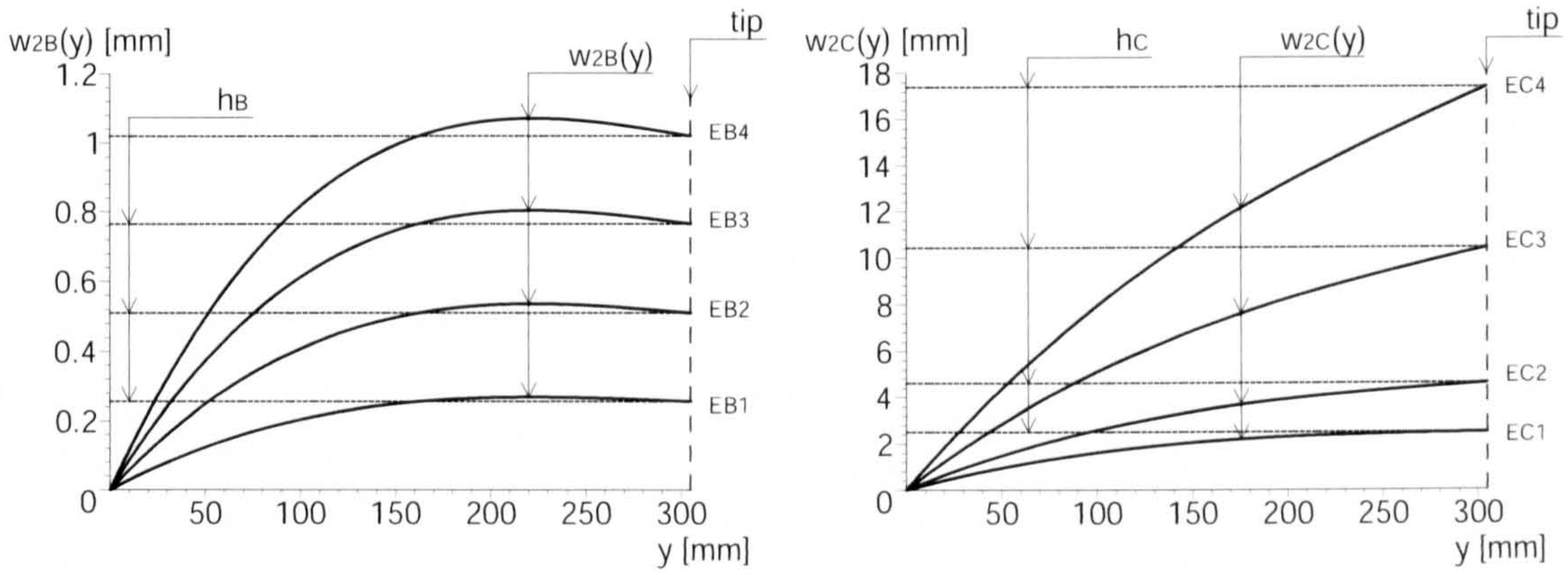

(a) Type B

(b) Type C

Figure 3.16: Comparison of $w_{2X}(y)$ and h_X. Note that the values of $w_{2X}(y)$ and h_X coincides at the tip of crossarm, $y = 305\,\text{mm}$.

"No compression option", which prevents any compression force entering the truss elements, was also adopted to simulate any slackening in the stays. Furthermore, it is essential in this type of nonlinear analysis to introduce a geometrical imperfection. In the current study, this was achieved using the Euler buckling displacement generated by eigenvalue analysis. The magnitude of the imperfection was intended to be deliberately small such that the perfect response would be approximated. To trigger Mode 1, an out-of-straightness of $L/10000$ was imposed at the middle of the column. To trigger Mode 2, an out-of-straightness of $L/14142$ was imposed at the quarter and the three-quarter points along the column such that the horizontal displacement at those points would be the same as that in Mode 1.

3.4.3.1 Comparisons

Figures 3.17 and 3.18 show the post-buckling responses from the FEM along with those from the analytical models at Points 1, 3, 6, 7 and 8. As can be seen in Figure 3.17, for Mode 1, the post-buckling paths of the FEM model almost coincide with those of the analytical model. However, Figure 3.18 shows less good agreement between the FEM and the analytical models in Mode 2. Regardless of the less

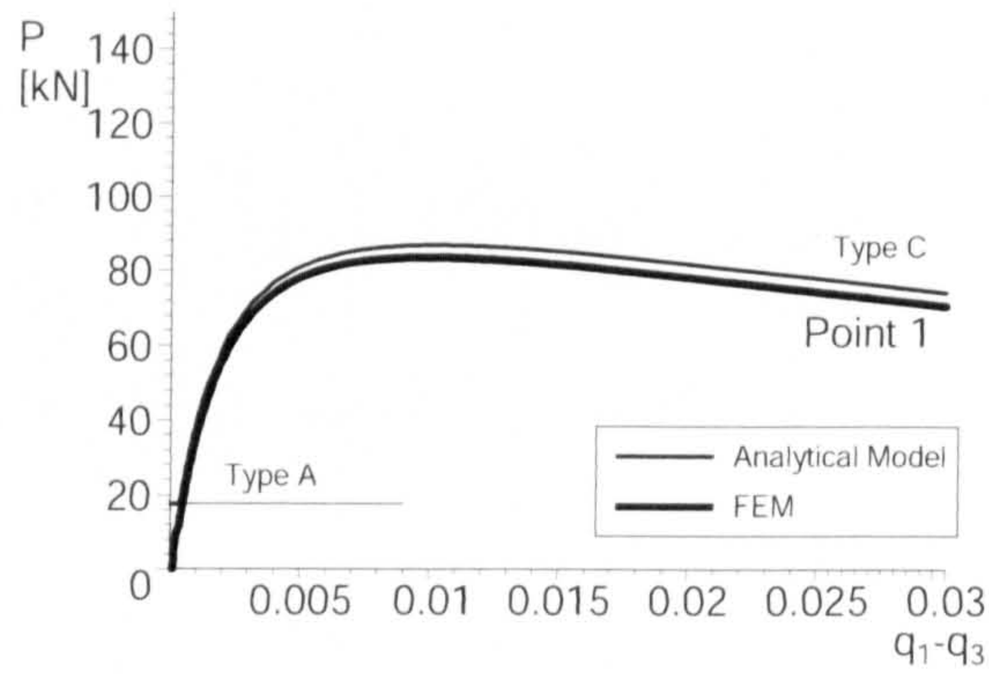

(a) Zone 1

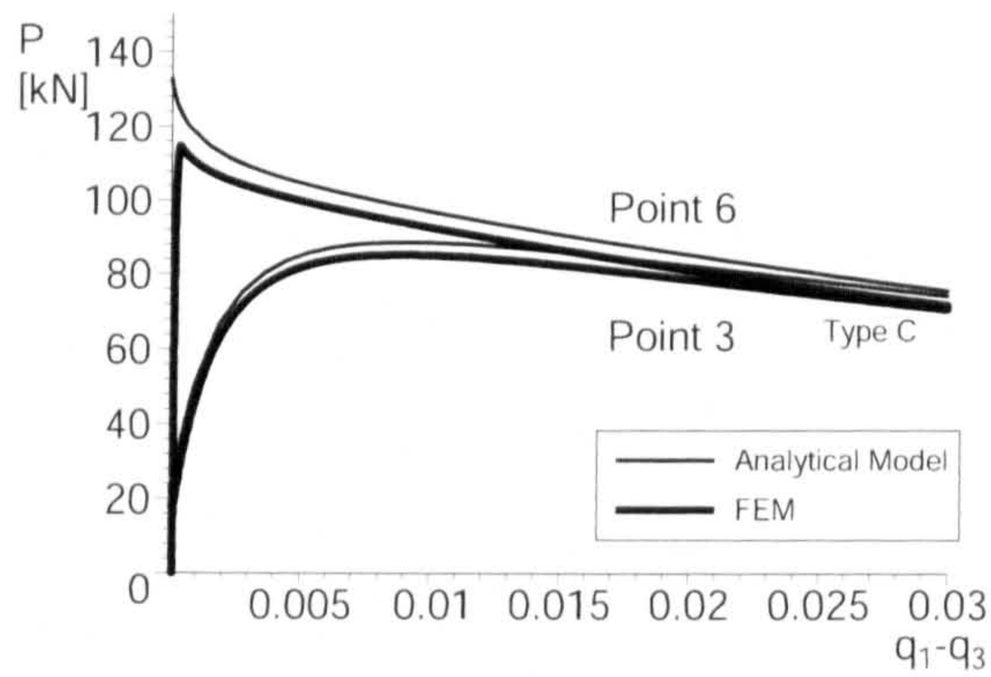

(b) Zone 2

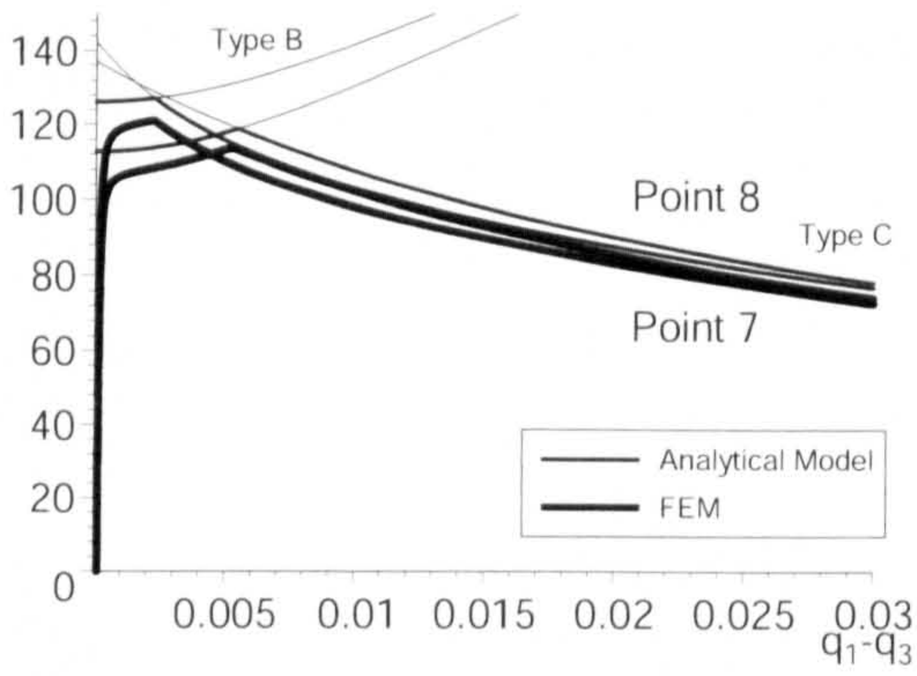

(c) Zone 3

Figure 3.17: Equilibrium paths for Mode 1 comparing the FEM and the analytical models.

good agreement in Mode 2, the same trend can still be detected from these two models; therefore, the analytical models for Mode 2 are still useful for predicting the qualitative buckling behaviour.

These comparisons suggest that using the current 2DOF analytical modelling, the Mode 1 buckling behaviour of the stayed column can be simulated with excellent accuracy. It is also shown that the current analytical 2DOF model can yield the approximated Mode 2 post-buckling response; it has to be admitted that the analytical model involves a certain discrepancy with the numerical model. This inaccuracy can be reduced by increasing the number of degrees of freedom, but this process is computationally demanding as discussed earlier.

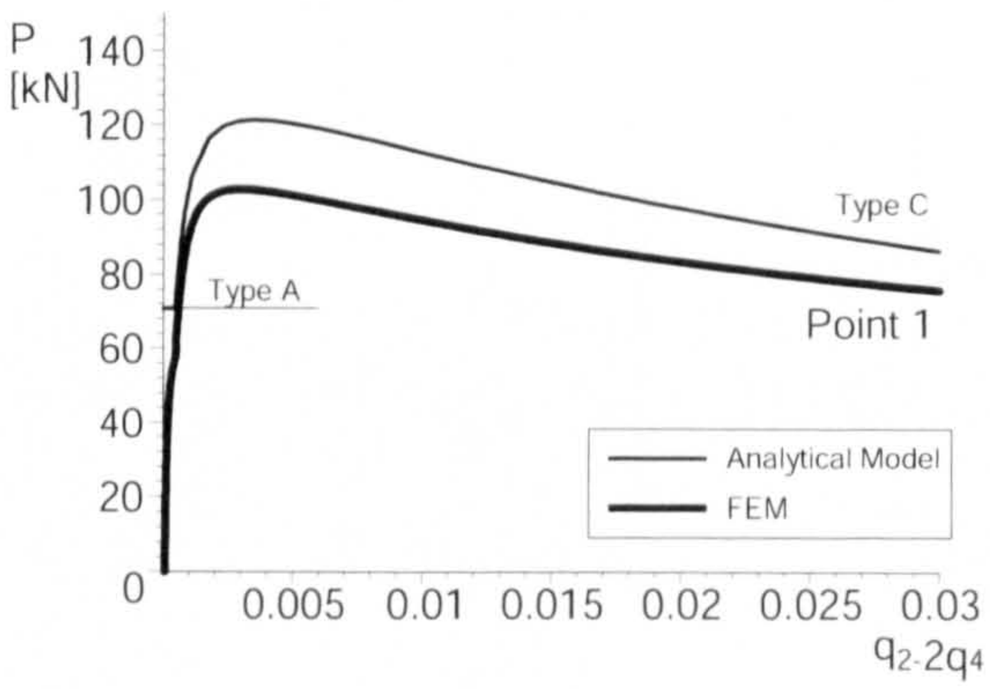

(a) Zone 1

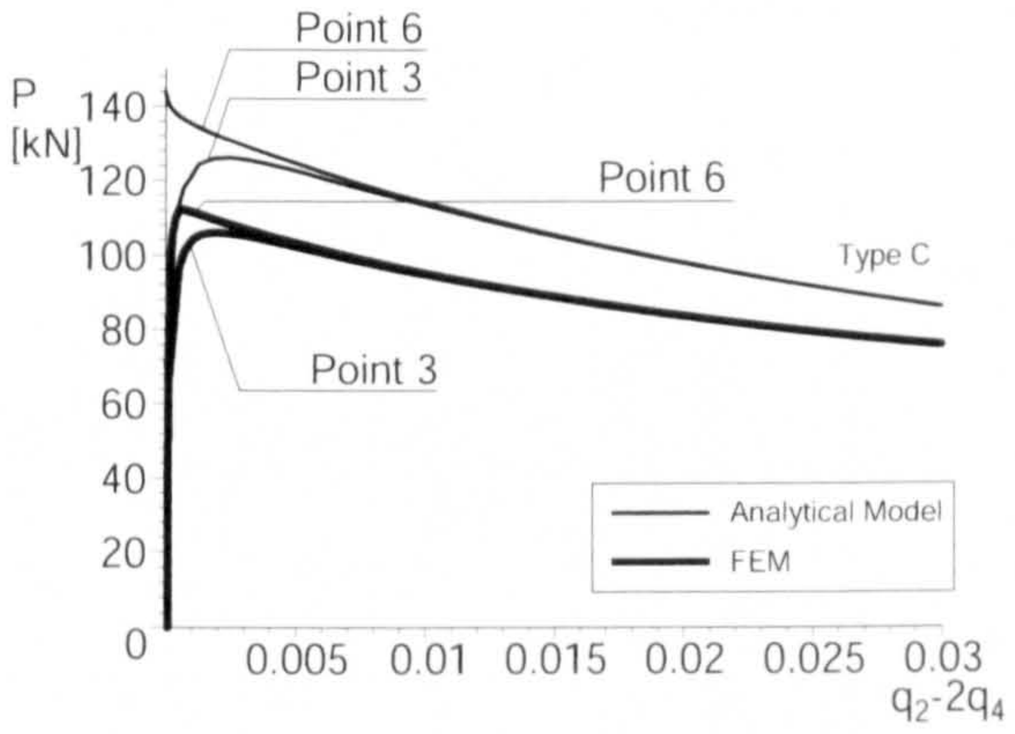

(b) Zone 2

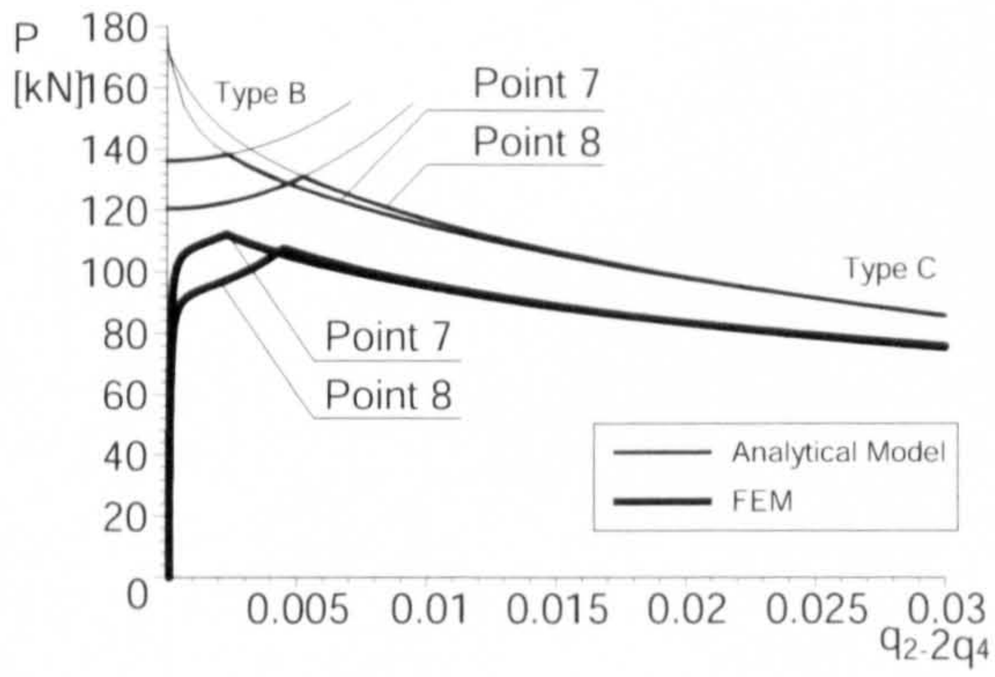

(c) Zone 3

Figure 3.18: Equilibrium paths for Mode 2 comparing the FEM and the analytical models.

3.5 Remarks

This chapter has described the theoretical post-buckling behaviour of the prestressed steel stayed column, especially focused on the relationship between the equilibrium response and the initial prestress. Previous studies (Wong & Temple, 1982; Temple *et al.*, 1984; Smith, 1985; De Araujo *et al.*, 2006) also investigated a limited number of the post-buckling responses of the stayed column in their work, but they did not work on a theoretical model, nor on a relationship between the post-buckling response and the initial prestress since their focus was placed upon on the ultimate strength.

The results indicate that the post-buckling response is strongly linked to the zone distinction of the critical loads that was found by Hafez et al. (1979) for the first two buckling modes. In Zone 1, the response is initially similar to that of Euler buckling, which is followed by a rather stable path thanks to the reactivation of the convex side stays. In Zone 2, the critical load is increased to more than the Euler load, and either a stable or an unstable path emerges after buckling; the stability of the response depends on the level of the prestress. In Zone 3, the critical load reaches its theoretical maximum, and the post-buckling path becomes unstable, after an initially flat but slightly stable response, due to some of the stays slackening. These results have been validated using the FEM. It has been shown that the current analytical model for Mode 1 has excellent agreement with the FEM model; however it is less accurate for Mode 2 when compared to Mode 1, even though the model is still useful to find approximate post-buckling responses for that mode.

It has also been shown that the most unstable path occurs at the prestress level T_{opt}. This implies that this level of the prestress is not favourable; hence the greater level of the prestress would be recommended as a stable path occurs with a higher level of the prestress.

Despite these findings, geometrical imperfections and plasticity in the materials were neglected in the current analytical formulation. These are important factors to

predict the actual response of the stayed column. Further work is needed to reflect these factors in the current models, and these modifications are presented in the following chapter.

Chapter 4

Imperfection and Failure Model

4.1 Introduction and Methodology

In the previous chapter, the post-buckling behaviour of the stayed column was modelled analytically, and the accuracy of the results was validated using the FEM. Although a good correlation was found between these two models, the analyses were based on the assumption that all the materials were purely elastic; the models therefore did not account for any plasticity in the materials. Furthermore, component geometries were assumed to be perfect. Hence, it should be noted that the model did not necessarily reflect the real response of the stayed column.

In order to predict a more realistic structural response, a modified model was developed; geometrical imperfections were incorporated in terms of an out-of straightness of the column, and possible failure modes—column yielding and stay fracture—were also investigated using the symbolic computation software MAPLE (Heck, 2003). In addition, FE analysis was conducted in order to ensure that the obtained results were sufficiently accurate using the code ABAQUS (ABAQUS, 2006).

Certainly, other types of imperfection, such as unequal stay tensions and unequal size of the crossarm, geometrical imperfections in the crossarm are neglected. Although

this issue is also considered to be important,

4.2 Methodology

The analytical model was modified from that presented in Chapter 3 to account for the out-of-straightness, column yielding and stay fracture. The procedure to formulate the modified analytical models also follow that outlined in §3.1.1. The same assumptions were also included for this model modification as those in that section, except that in the current chapter the column is not perfectly straight. Furthermore, the following additional assumptions were made.

1. The column has an idealized elastic, perfectly–plastic relationship.

2. The stay has an idealized elastic, brittle relationship.

3. Imperfections other than an out-of-straightness of the column is ignored.

As for assumption 3, taking into account other types of imperfections, especially ones that are specific to the stayed column, such as unequal stay tensions and crossarms of unequal size, are considered to be important but secondary to the present discussion; therefore, it was assumed that an out-of-straightness of the column suffices.

For the column failure in FE analysis, bilinear behaviour was assumed: linearly elastic behaviour until the stress reaches the yield stress σ_y, followed by a flat yield plateau, as shown in Figure 4.1(a). This model forms the basis for the current European design code (EN1993-1-1, 2005). As for the stay, linear behaviour was assumed in the FEM, terminating with the stress reaching the stay fracture stress σ_u (see Figure 4.1(b)) for the following reasons: (1) stays have a mostly high yield strength, which tends to show brittle fracture without any significant plastic behaviour, and (2) the plastic region is not usually considered for tension members in design of practice (EN1993-1-1, 2005; EN1993-1-11, 2006).

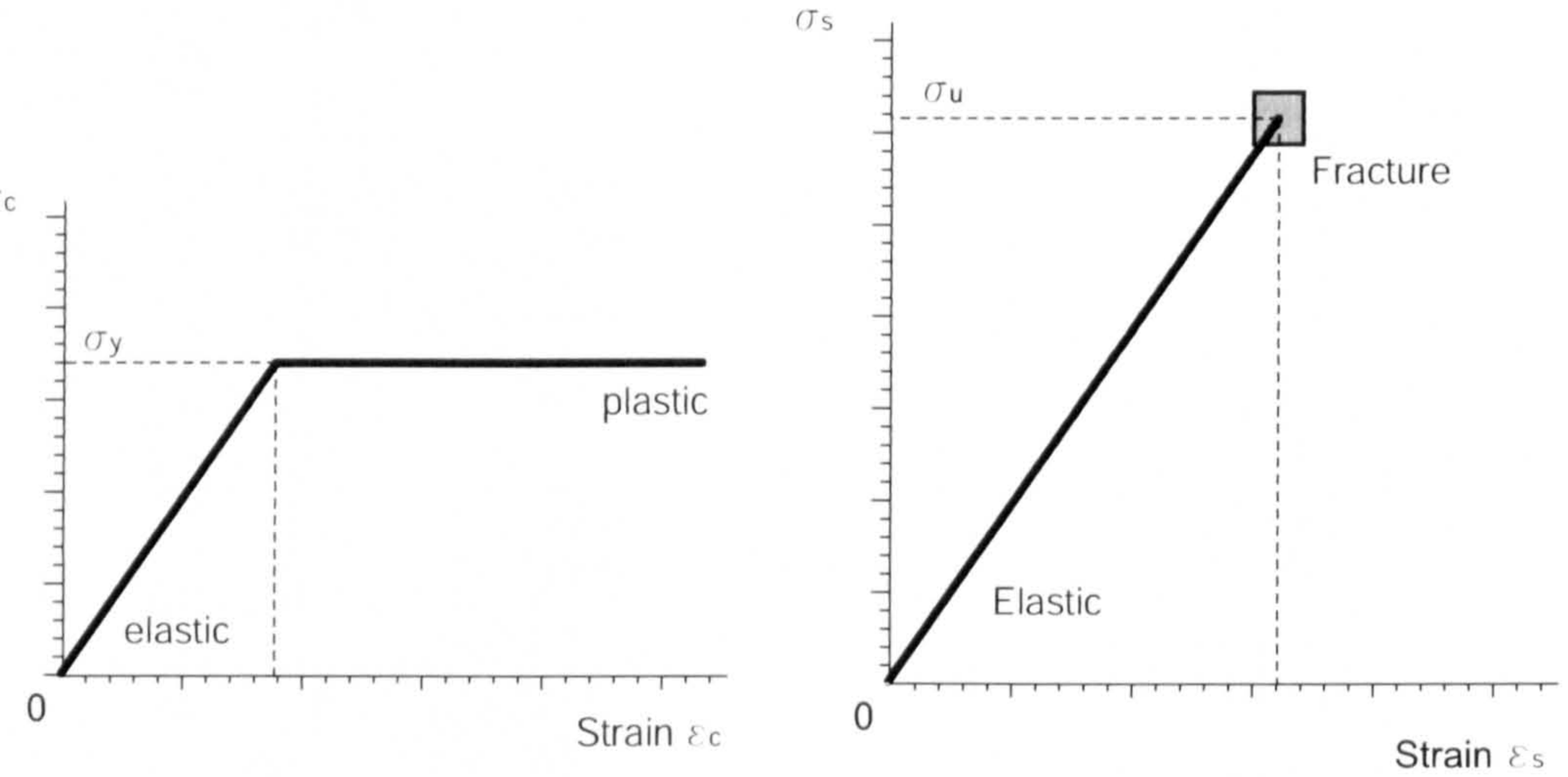

(a) column (b) stay

Figure 4.1: Stress–strain curves for column and stay.

The shape functions for geometrical imperfections were based on sinusoidal functions reflecting the same type as seen in previous works (Wong & Temple, 1982; Smith, 1985). In the process of modelling, the two degree-of-freedom (2DOF) model was adopted as it was shown in the previous chapter that this is reasonably accurate and not excessively demanding computationally. The structural failure modes were found by calculating the stresses in the structural components using Euler–Bernoulli beam theory.

4.3 Formulation

In this section, the 2DOF system accounting for initial geometrical imperfections is developed by considering, in turn, the displacements of each component and the geometrical changes after applying the prestress. This, again, leads to the total potential energy function. A formulation to find the conditions for the chosen failure criteria in the course of axial loading—column yielding and stay fracture— is also established.

4.3.1 Imperfections

Two different initial out-of-straightness buckling modes are considered for geometrical imperfections: a half-sinusoidal wave for Mode 1 and a full sinusoidal wave for Mode 2 as shown in Figure 4.2. The shape functions for these types of out-of-

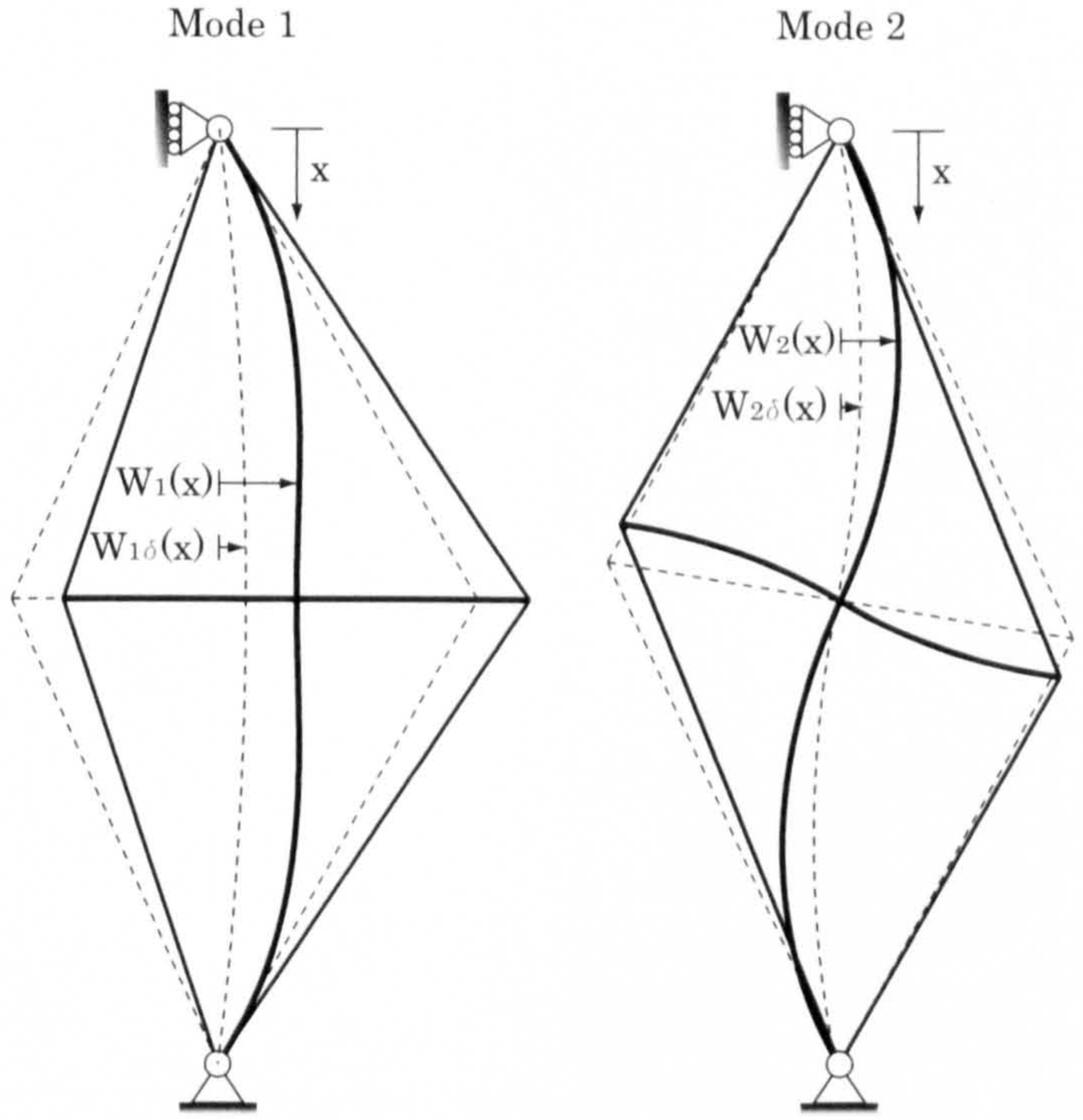

Figure 4.2: Buckling Modes 1(symmetric) and 2 (antisymmetric) with initial out-of-straightness.

straightness $W_{1\delta}$ and $W_{2\delta}$ are expressed as follows:

$$W_{1\delta}(x) = \delta L \sin \frac{\pi x}{L}, \tag{4.1}$$

$$W_{2\delta}(x) = \delta L \sin \frac{2\pi x}{L}, \tag{4.2}$$

where δ represents a nondimensional horizontal displacement, either at the middle of the column for Mode 1 or at the quarter point for Mode 2.

4.3.2 Displacement functions for the column

As the number of degrees of freedom is set at 2, the displacement functions for the column W_1 and W_2 can be given by substituting $n = 2$ in equations (3.1) and (3.2) respectively, thus:

$$W_1(x) = q_1 L \sin\frac{\pi x}{L} + q_3 L \sin\frac{3\pi x}{L}, \tag{4.3}$$

$$W_2(x) = q_2 L \sin\frac{2\pi x}{L} + q_4 L \sin\frac{4\pi x}{L}. \tag{4.4}$$

Substituting $n = 2$ in equations (3.3) and (3.4) yields the angles of the members to the vertical $\Theta_1(x)$ and $\Theta_2(x)$ respectively as follows:

$$\Theta_1(x) = q_1 \pi \cos\frac{\pi x}{L} + 3\pi q_3 \cos\frac{3\pi x}{L}, \tag{4.5}$$

$$\Theta_2(x) = 2q_2 \pi \cos\frac{2\pi x}{L} + 4\pi q_4 \cos\frac{4\pi x}{L}. \tag{4.6}$$

With reference to Figure 4.3, the original lengths of the stays for each mode L_{sij} are defined as follows:

$$L_{s11} = L_{s12} = \sqrt{\frac{L^2}{4} + (a + \delta L)^2}, \tag{4.7}$$

$$L_{s13} = L_{s14} = \sqrt{\frac{L^2}{4} + (a - \delta L)^2}, \tag{4.8}$$

$$L_{s21} = L_{s23} = \sqrt{\left(\frac{L}{2} + a\sin 2\pi\delta\right)^2 + (a\cos 2\pi\delta)^2}, \tag{4.9}$$

$$L_{s22} = L_{s24} = \sqrt{\left(\frac{L}{2} - a\sin 2\pi\delta\right)^2 + (a\cos 2\pi\delta)^2}. \tag{4.10}$$

Thus, the initial angles α_{ij} between the stays and the vertical are expressed as

$$\alpha_{ij} = \arccos\left(\frac{L/2}{L_{sij}}\right). \tag{4.11}$$

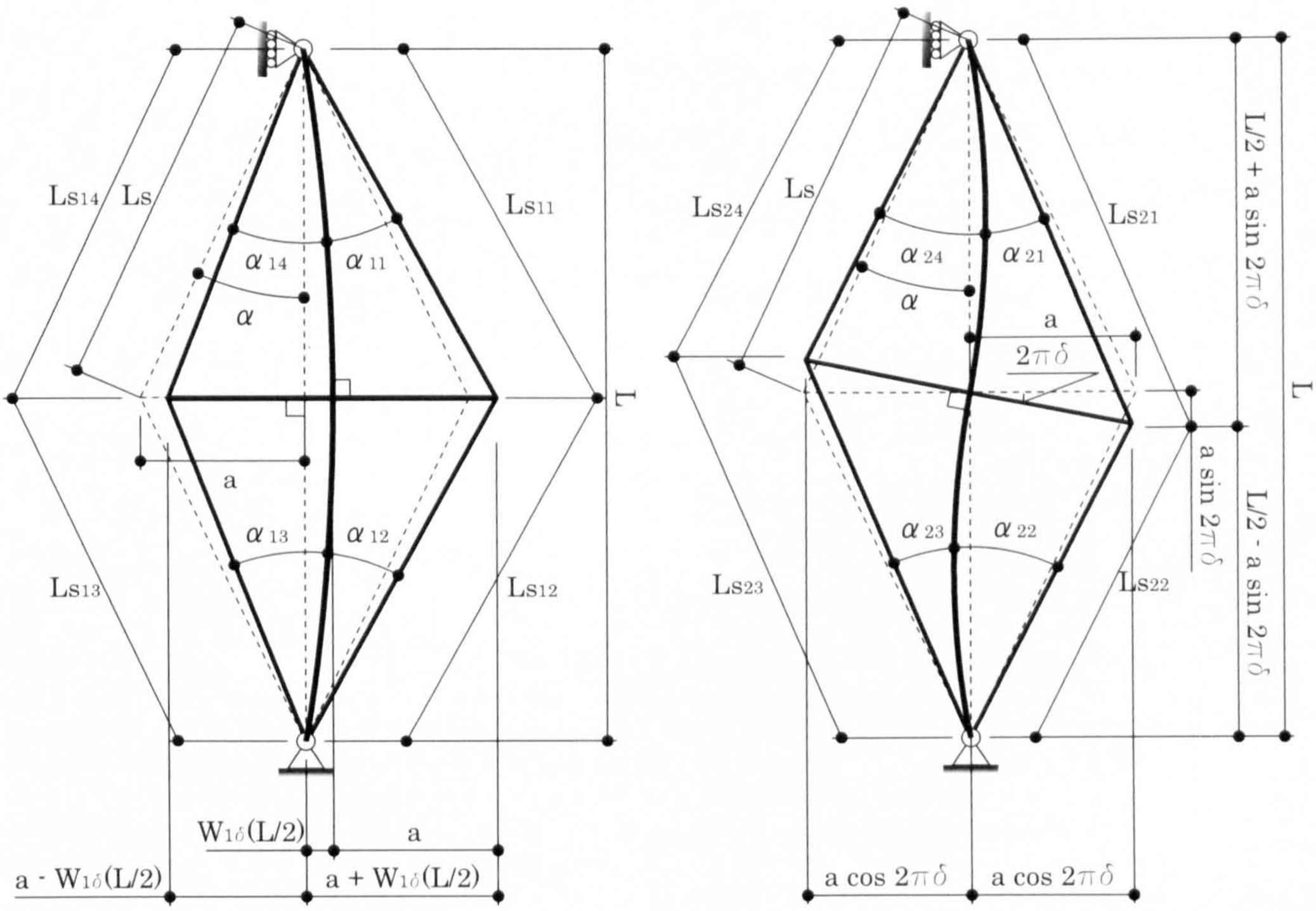

(a) Mode 1

(b) Mode 2

Figure 4.3: Initial profiles. Note that α_{ij} shows the angle between the column and each stay at the ends of the column.

4.3.3 Displacement functions for the crossarm

4.3.3.1 Shape functions

The general shape function for the crossarm is already given in equation (3.9):

$$w_{2X}(y) = H_X \sin k_X y + K_X \cos k_X y - \frac{R_{vX}}{k_X^2 E_a I_a}(a - y) + h_X. \tag{4.12}$$

Note that, in this chapter, y is the coordinate which coincides with the centre of the initial crossarm profile reflecting the geometrical imperfection; $w_{2X}(y)$ is the deflection of the crossarm perpendicular to that coordinate (see Figure 4.4). With

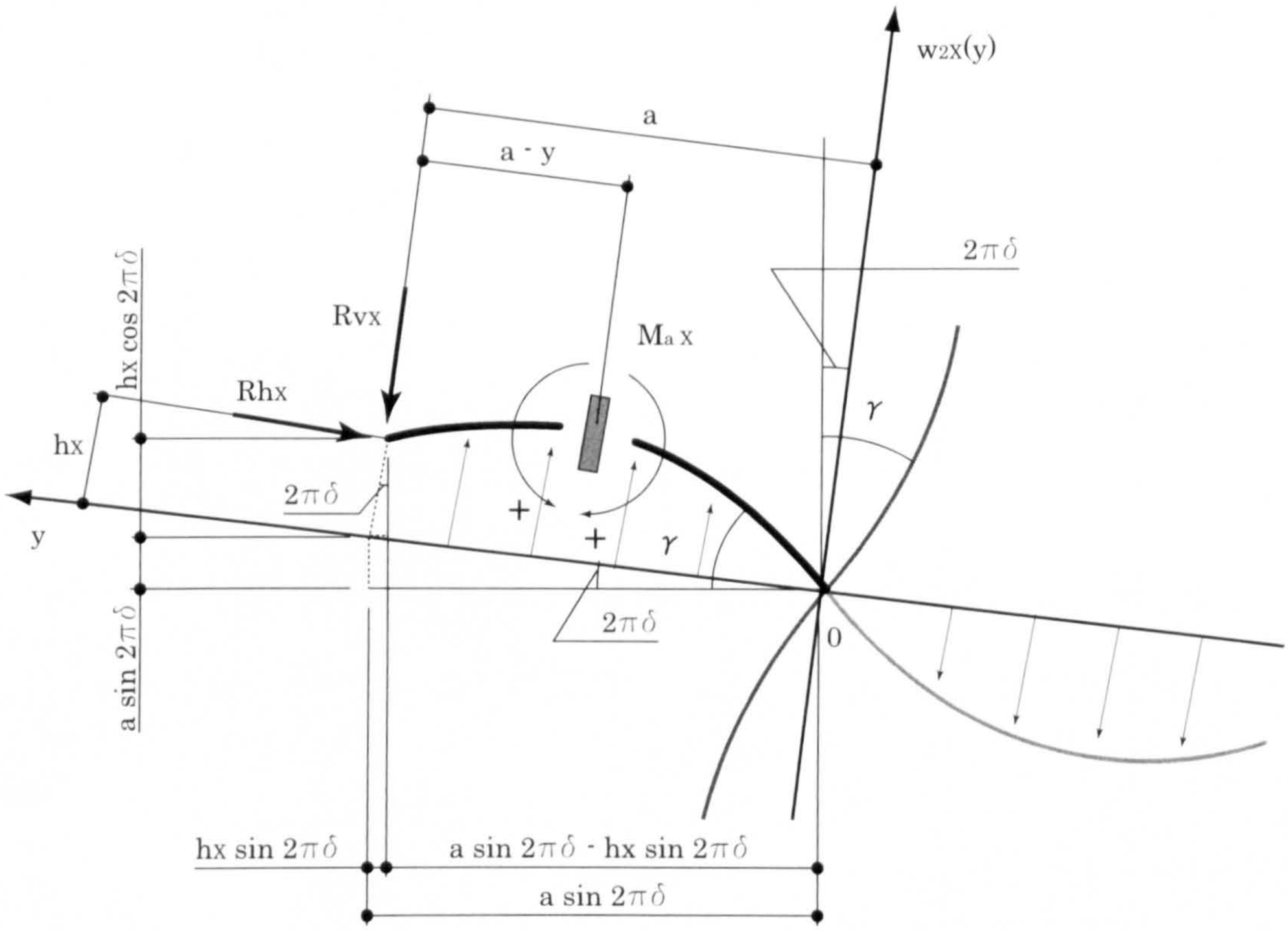

Figure 4.4: Free body diagram to determine the bending moment at an arbitrary cross section ($y \geqslant 0$) of the crossarm. Note that the subscript X represents the buckling type classification which can be either B or C.

reference to Figure 4.4, the boundary conditions are given, thus:

$$w_{2X}(0) = 0, \quad w'_{2X}(0) = \gamma - 2\pi\delta, \quad w_{2X}(a) = h_X, \tag{4.13}$$

where γ is the angle between the horizontal and the crossarm at the midpoint, defined as

$$\gamma = -\Theta_2(L/2) = 2q_2\pi - 4q_4\pi. \tag{4.14}$$

The second condition comes from the assumption that $W_2(x)$ intersects the crossarm at right angles. Applying this condition yields the following expressions:

$$H_X = \frac{1}{k_X}\left(-\frac{R_{vX}}{k_X^2 E_a I_a} + \gamma - 2\pi\delta\right), \tag{4.15}$$

$$K_X = \frac{R_{vX}a}{k_X^2 E_a I_a} - h_X, \tag{4.16}$$

$$h_X = \frac{\left[(\gamma - 2\pi\delta)\, E_a I_a k_X^2 - R_{vX}\right]\sin k_X a + k_X R_{vX} a \cos k_X a}{k_X^3 E_a I_a \cos k_X a}. \tag{4.17}$$

In order to find the actual shape of the crossarm with equation (4.12), it is also necessary to establish equations for R_{vX} and R_{hX}. With reference to Figure 4.5 and then by taking the leading terms of Δ_{2X}, h_X and δ, the changes in the axial force in Stays 3 and 4, $\mathrm{d}F_{X3}$ and $\mathrm{d}F_{X4}$ resulting from the structural displacement can be expressed as follows:

$$\begin{aligned} \mathrm{d}F_{X3} &= E_s A_s \frac{L_{s2X3} - L_{s23}}{L_{s23}} \\ &\approx \left(-\Delta_{2X} + \frac{2h_X}{L}\right)\cos^2\alpha, \end{aligned} \tag{4.18}$$

$$\begin{aligned} \mathrm{d}F_{X4} &= E_s A_s \frac{L_{s2X4} - L_{s24}}{L_{s24}} \\ &\approx \left(-\Delta_{2X} - \frac{2h_X}{L}\right)\cos^2\alpha. \end{aligned} \tag{4.19}$$

With reference to (b) and (c) in Figure 4.5 along with the expressions for $\mathrm{d}F_{X3}$ and $\mathrm{d}F_{X4}$, the reaction forces for Type B, R_{vB} and R_{hB}, can be defined, which are then

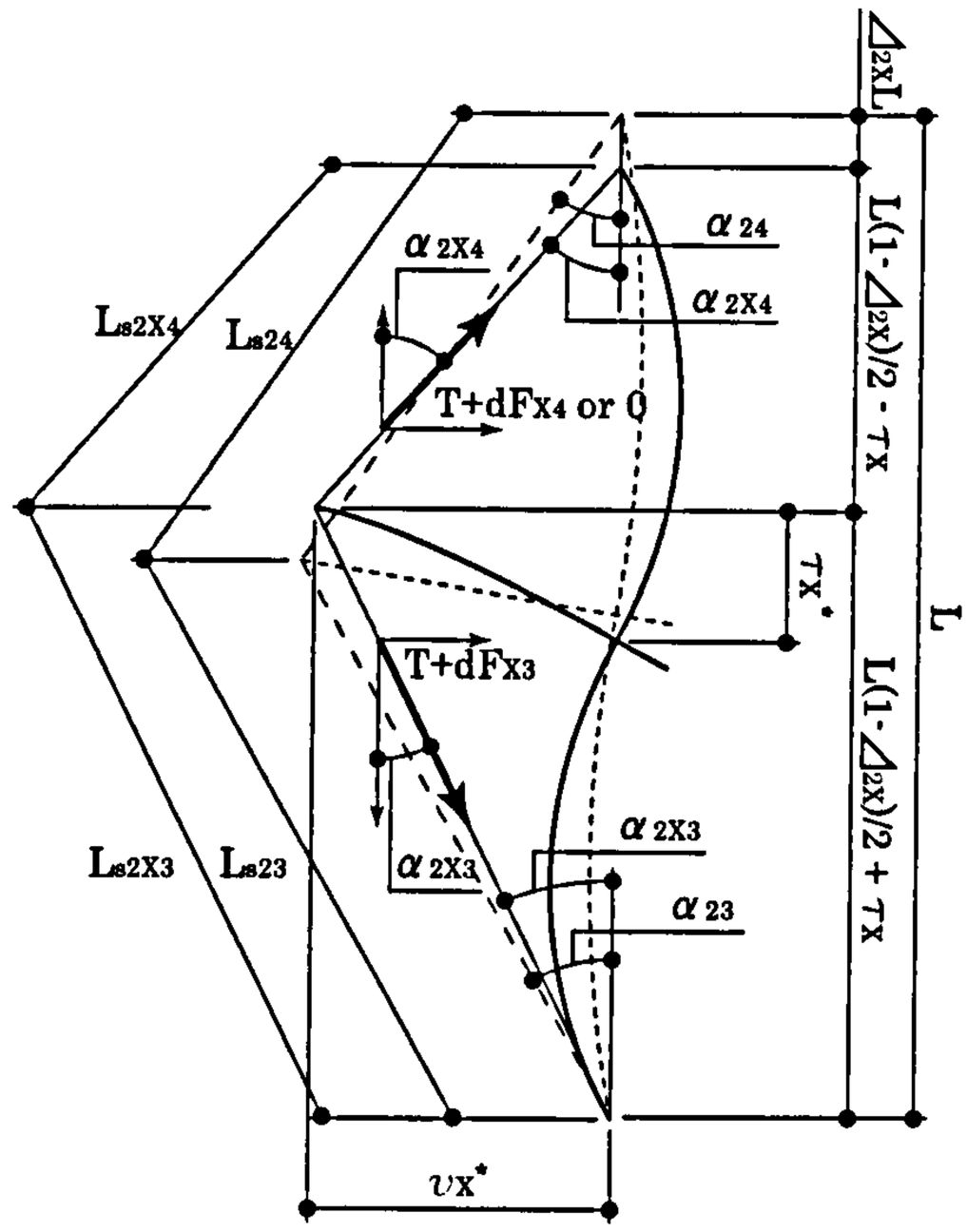

*τx= hx cos 2πδ + a sin 2πδ
*υx= a sin 2πδ · hx cos 2πδ

(a) elongation of the stays

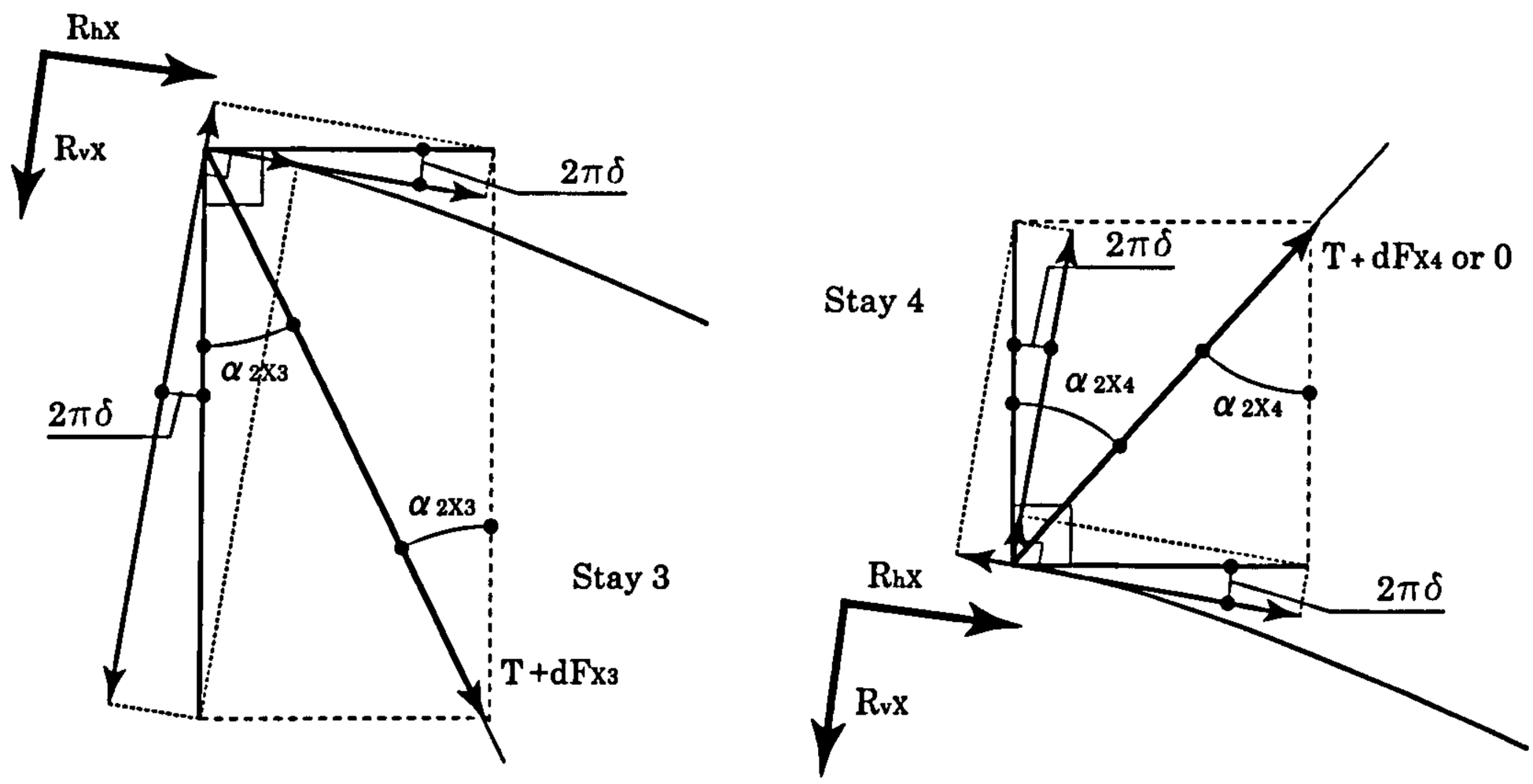

(b) reaction forces in stay 3

(c) reaction forces in stay 4

Figure 4.5: Elongation of the stays and reaction forces at the tip of the crossarm.

approximated by taking the leading terms of Δ_{2X}, h_X and δ.

$$\begin{aligned} R_{vB} &= (T + \mathrm{d}F_{B3})(\cos\alpha_{2B3}\cos 2\pi\delta - \sin\alpha_{2B3}\sin 2\pi\delta) \\ &\quad - (T + \mathrm{d}F_{B4})(\cos\alpha_{2B4}\cos 2\pi\delta + \sin\alpha_{2B4}\sin 2\pi\delta) \\ &\approx 4\left[\left(\frac{h_B}{L}\sin\alpha - \pi\delta\cos\alpha\right)T\sin\alpha + E_sA_s\frac{h_B}{L}\cos^2\alpha\right], \end{aligned} \tag{4.20}$$

$$\begin{aligned} R_{hB} &= (T + \mathrm{d}F_{B3})(\sin\alpha_{2B3}\cos 2\pi\delta + \cos\alpha_{2B3}\sin 2\pi\delta) \\ &\quad + (T + \mathrm{d}F_{B4})(\sin\alpha_{2B4}\cos 2\pi\delta - \cos\alpha_{2B4}\sin 2\pi\delta) \\ &\approx 2\left[\left(1 + \Delta_{2B}\cos^2\alpha\right)T - E_sA_s\Delta_{2B}\cos^2\alpha\right]\sin\alpha. \end{aligned} \tag{4.21}$$

As only one stay is active on each side in Type C buckling, with reference to Figure 4.5(c) R_{vC} and R_{hC} can thus be obtained from the expression for $\mathrm{d}F_{X3}$. The same approximation as in §3.2.2.2 is applied, as including the h_C term in the R_{hC} equation causes a computation problem that leaves the governing equation untractable[1].

$$\begin{aligned} R_{vC} &= (T + \mathrm{d}F_{C3})(\cos\alpha_{2C3}\cos 2\pi\delta - \sin\alpha_{2C3}\sin 2\pi\delta) \\ &\approx \left[1 - 2\pi\delta\cos\alpha\sin\alpha - \left(\Delta_{2C} - \frac{2h_C}{L}\right)\left(\sin^2\alpha + \frac{E_sA_s}{T}\cos^2\alpha\right)\right]T\cos\alpha, \end{aligned} \tag{4.22}$$

$$\begin{aligned} R_{hC} &= (T + \mathrm{d}F_{C3})(\sin\alpha_{2C3}\cos 2\pi\delta + \cos\alpha_{2C3}\sin 2\pi\delta) \\ &\approx \left\{\left[1 + \left(\Delta_{2C} - \frac{2h_C}{L}\right)\left(1 - \frac{E_sA_s}{T}\right)\cos^2\alpha\right]\sin\alpha + 2\pi\delta\cos^3\alpha\right\}T \\ &\approx \left\{\left[1 + \Delta_{2C}\left(1 - \frac{E_sA_s}{T}\right)\cos^2\alpha\right]\sin\alpha + 2\pi\delta\cos^3\alpha\right\}T. \end{aligned} \tag{4.23}$$

Note that in the energy formulation, equation (4.12) adopted approximated equations of h_X—later shown in equations (4.27) and (4.28)—, and the leading terms with respect to Δ_{2X}, γ and δ were taken in that equation in order to render the analytical model tractable.

[1]Note that in the R_{hB} expression, the h_B term does not exist as this drops out in the process of summing the horizontal components of $\mathrm{d}F_{B3}$ and $\mathrm{d}F_{B4}$.

4.3.4 Stress and geometrical changes in the structure

Stress and geometrical changes in the structure are exhibited prior to the energy formulation presented in the following section. The investigation includes items such as the stress changes caused by the prestress, the elongation of the stays and the end-shortening of the column.

4.3.4.1 Stress in the column from prestress

The initial strain ε_{st} in each stay from prestressing is

$$\varepsilon_{st} = \frac{T}{E_s A_s}. \tag{4.24}$$

With reference to Figure 4.6, the initial stress ε_{ct} that is introduced to the column can be obtained by solving the following force equilibrium equation:

$$T_{ci}\cos(i\pi\delta) = T\cos\alpha_{i1} + T\cos\alpha_{i4}. \tag{4.25}$$

As δ is a small value, by taking the leading term with respect to δ, ε_{ct} is approximated as

$$\varepsilon_{ct} \approx \frac{2T\cos\alpha}{EA}. \tag{4.26}$$

Note that this expression is exactly the same as the perfect case.

4.3.4.2 Tip displacement coefficient

The tip displacement of the crossarm is necessary to determine the elongation of the stays. This displacement has already been presented in equation (4.17). However, as the direct expression is too complicated for the analytical model, these are simplified by using a Taylor expansion.

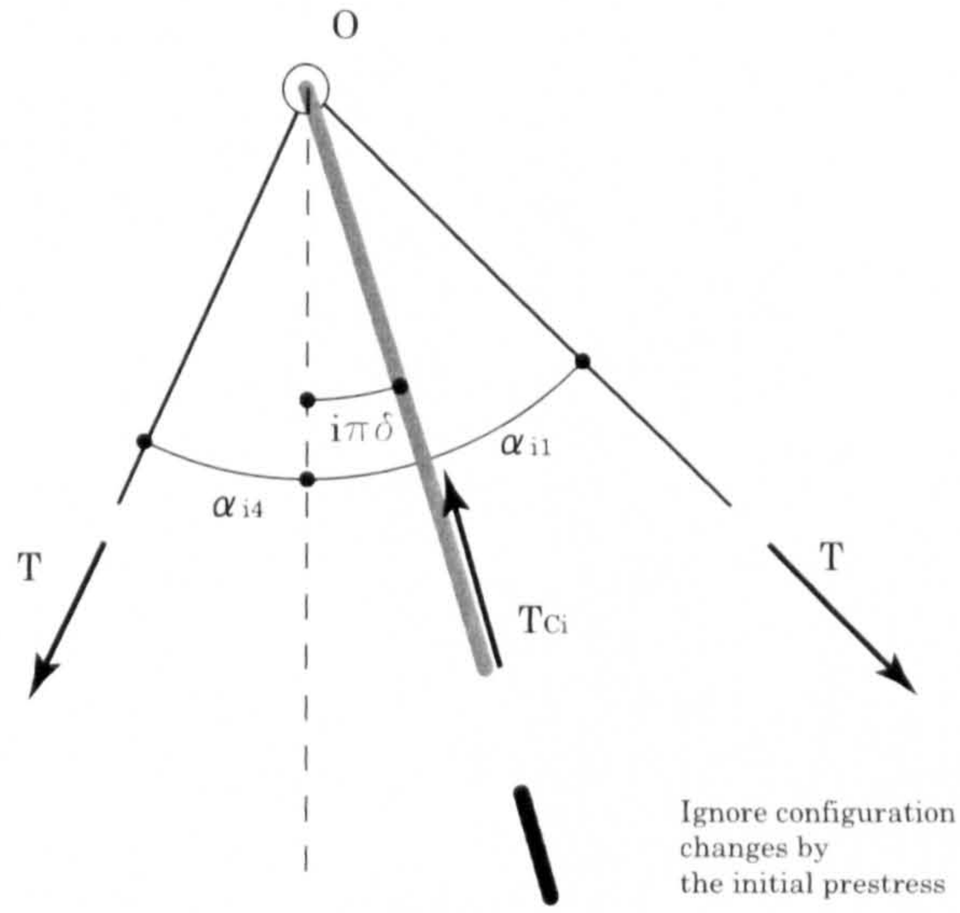

Figure 4.6: Effect of the initial prestress.

In the case of Type B buckling, h_B is expanded to the third order with respect to Λ_B, and then, in that equation, the leading order terms with respect to Δ_{2B}, γ and δ are taken, which yields the following:

$$h_B = c_B a(\gamma - 2\pi\delta), \tag{4.27}$$

where c_B is already expressed in equation (3.24), and Λ_B has the same form expression as equation (3.25).

In the case of Type C, similarly, h_C is expanded to the fifth order with respect to Λ_C, and then, in that equation, the leading order terms with respect to Δ_{2C}, γ and δ are taken, which yields the following:

$$h_C = c_C\, a\gamma + c_{C\Delta}\, a\Delta_{2C} + c_{C0}\, a + c_{C\delta}\, a\delta, \tag{4.28}$$

where $c_{C\delta}$ is the factor expressing the magnitude of the tip displacement of the crossarm in Type C associated with the imperfection amplitude δ:

$$c_{C\delta} = \frac{E_s A_s a^4 \sin^2\alpha \cos^2\alpha \left(\cos^2\alpha + 1/5\right) T - 3E_a I_a \zeta}{\zeta^2}, \tag{4.29}$$

with c_C, $c_{C\Delta}$ and c_{C0} being already expressed in equations (3.27), (3.28) and (3.29) respectively. As for the quantity Λ_C, this also has the same form as equation (3.31). Note that this simplification becomes less accurate as the initial prestress T becomes larger. The accuracy of the third and fifth order approximations for h_B and h_C are discussed in the validation section later in this chapter.

4.3.4.3 Elongation of the stays

The post-buckling profiles of the stayed column are sketched in Figure 4.7. These geometries allow the new stay length L_{siXj}, where the subscript j refers to the stay number as indicated in Figure 3.6, to be evaluated through Pythagoras's theorem, and leads to the strain in the stays purely arising from the applied load P. Subsequently, this equation is expanded as a Taylor series up to second order with respect to q_m, Δ_{iX}, and δ, depending on the buckling type. In this process, the cross and quadratic terms of Δ_{iX}, such as $\Delta_{iX}q_m$, $\Delta_{iX}\delta$ and Δ_{iX}^2 are dropped, as these terms are considered to be small from numerical observation. By combining the expanded strain φ_{iXj} with the initial prestress T, the total strains in the stays ε_{siXj} can be obtained, giving a sequence of expressions, here written in a compact format:

$$\varepsilon_{siXj} = \varphi_{iXj} + \varepsilon_{st}. \tag{4.30}$$

4.3.4.4 End-shortening of the column

In order to determine the end-shortening expression of the column Δ_{iX}, equilibrium is considered at the end of the column where the external load P is applied with the free body diagram approach shown in Figure 4.8. Vertical force equilibrium and moment equilibrium around the point O give the same equations as those in (3.33) and (3.34), where β_i can be obtained by substituting $x = 0$ into $\Theta_i(x)$ defined in

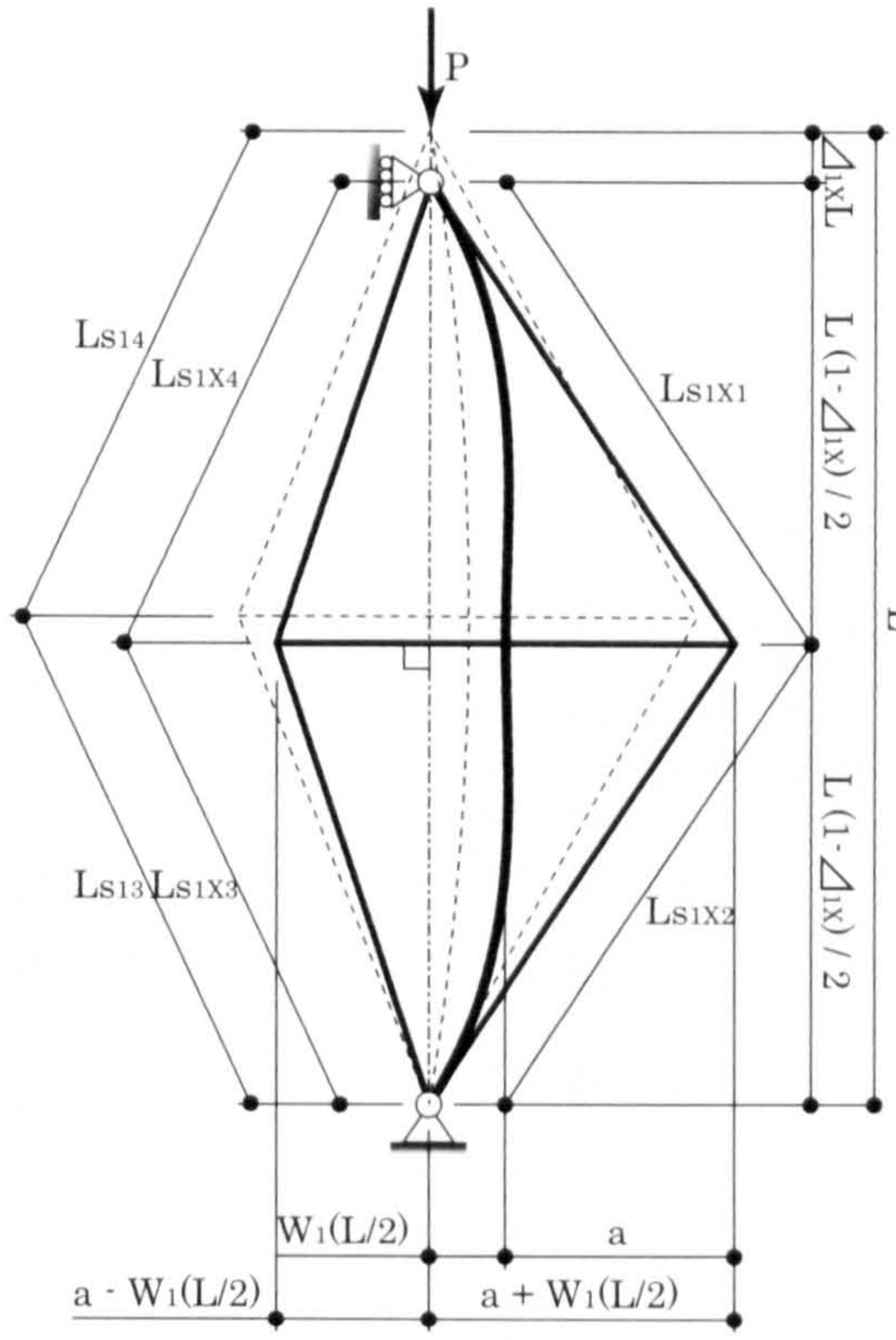

(a) Mode 1

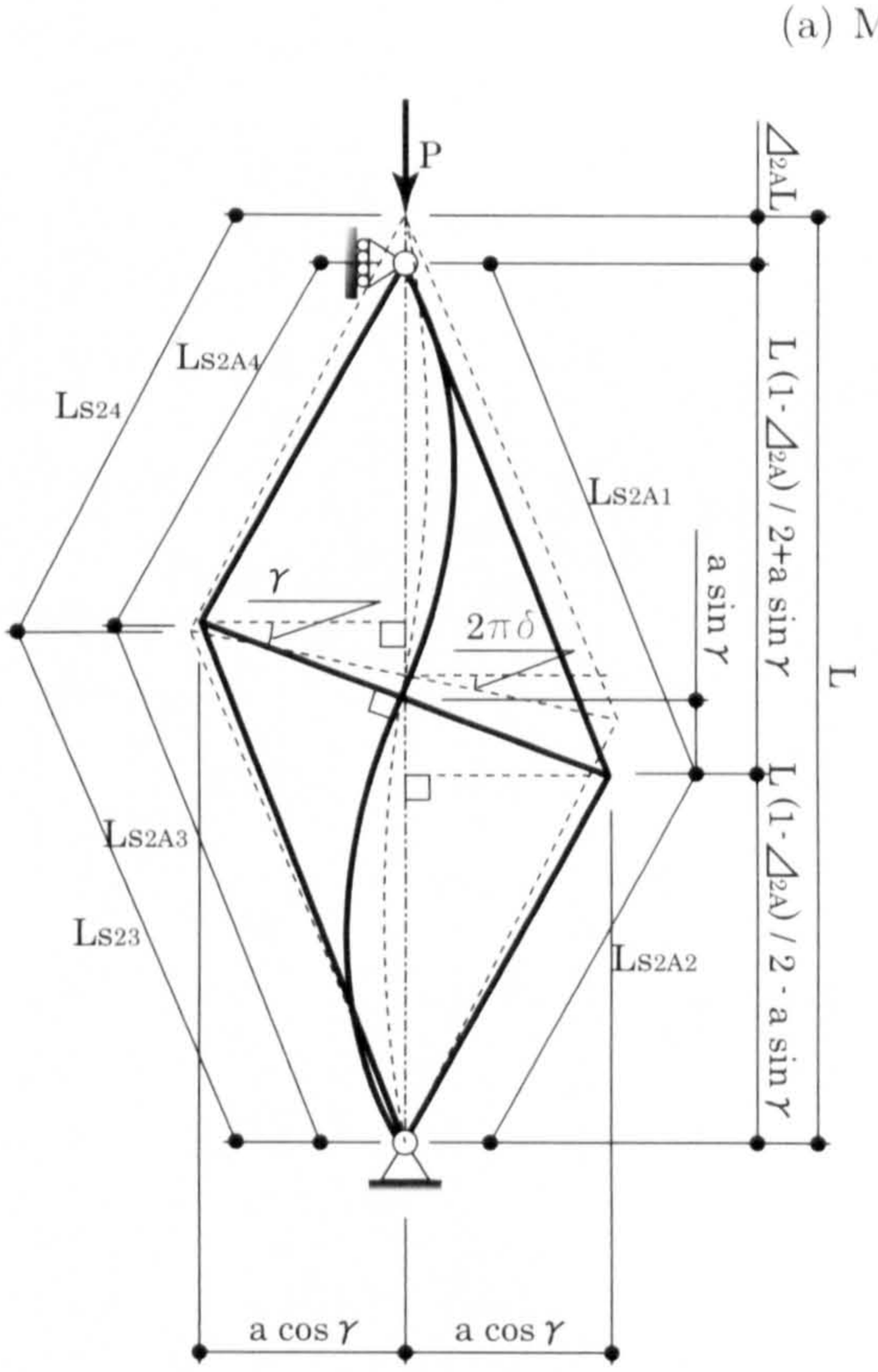

(b) Mode 2 Type A

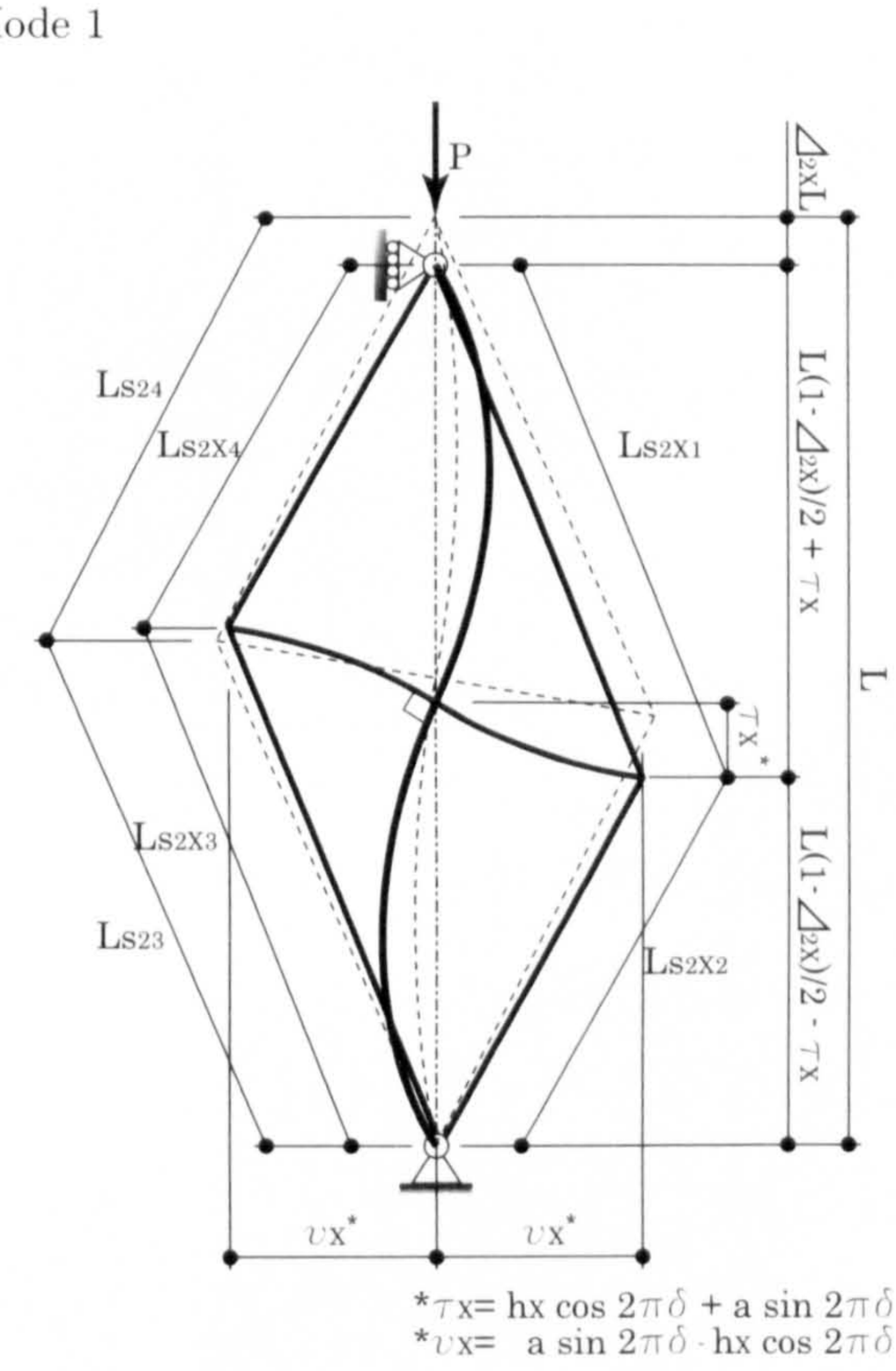

(c) Mode 2 Type B–C

Figure 4.7: Geometry of the stayed column in buckling modes 1 and 2.

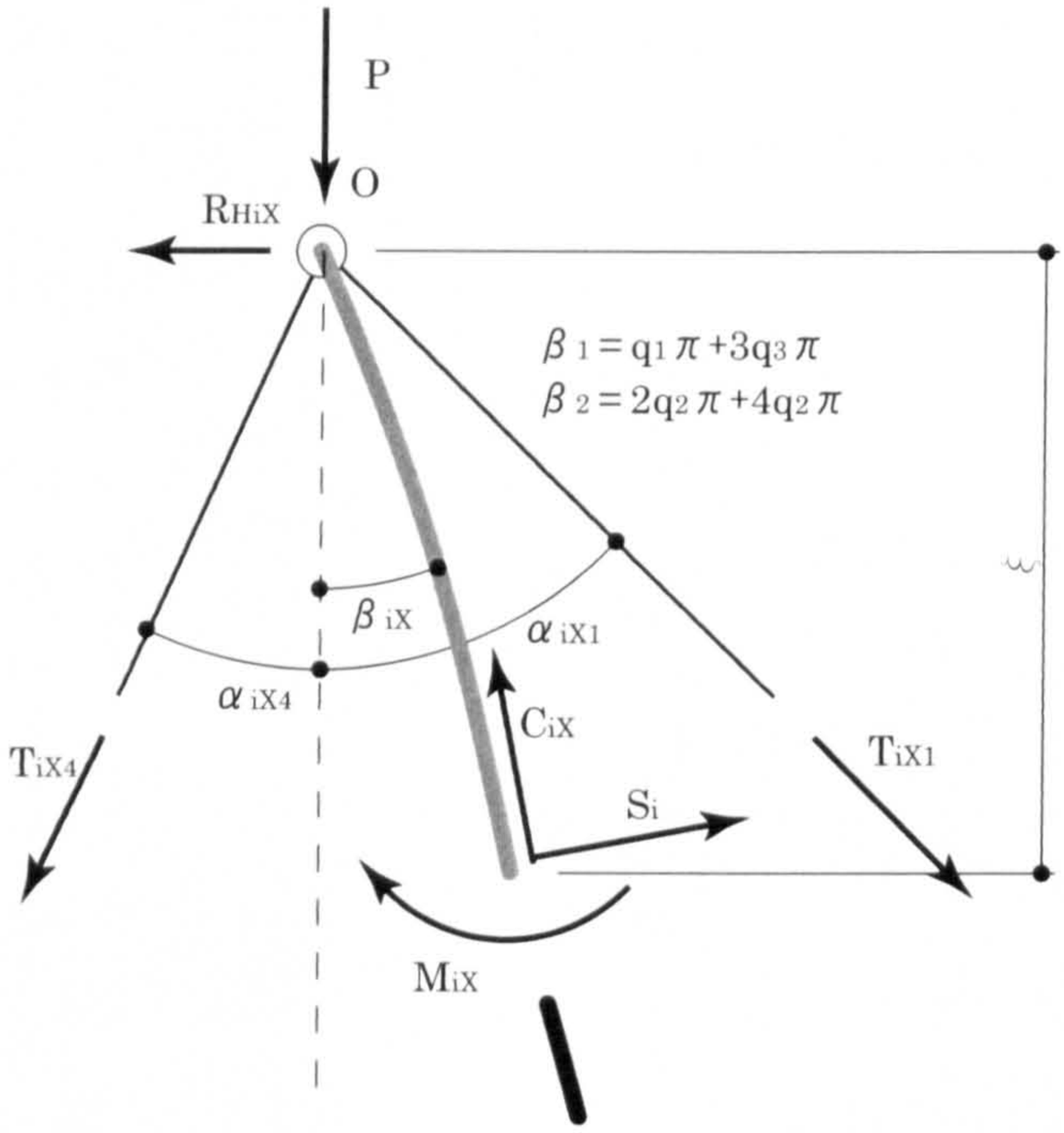

Figure 4.8: Equilibrium free body diagram for the column. Note that R_{HiX} is the horizontal reaction force at the end of the column.

equations (4.5) and (4.6):

$$\beta_1 = \Theta_1(0) = q_1\pi + 3q_1\pi, \qquad \beta_2 = \Theta_2(0) = 2q_2\pi + 4q_1\pi. \tag{4.31}$$

With reference to Figures 4.7(a)–(c), $\cos\alpha_{iX1}$ and $\cos\alpha_{iX4}$ are obtained through trigonometry; subsequently, those relationships are expressed to the leading order with respect to q_m, Δ_{iX}, and δ.

As all of the required angles are defined, the forces and bending moments T_{iX}, C_{iX}, S_{iX}, and M_{iX} in the free body diagram need to be investigated. Firstly, with the strain expressions of the stays shown in the previous section and the assumption that the stays do not resist compression, the axial forces in the stays T_{iX1} and T_{iX4} are defined as follows:

$$\begin{aligned} &T_{iA1} = T_{iA4} = T_{iC4} = 0, \\ &T_{iB1} = \varepsilon_{siB1}E_sA_s, \quad T_{iB4} = \varepsilon_{siB4}E_sA_s, \quad T_{iC1} = \varepsilon_{siC1}E_sA_s. \end{aligned} \tag{4.32}$$

The axial strain in the column ε_{ciX} is expressed as a summation of the components Δ_{iX} and ε_{ct} minus the effect of the relaxation from the buckling displacement. Therefore, the axial strain for each mode is expressed as follows:

$$\begin{aligned}\varepsilon_{ciX} &= \Delta_{iX} + \varepsilon_{ct} - \frac{1}{2L}\int_0^L \left[W_i'^2(x) - W_{i\delta}'^2(x)\right] \mathrm{d}x \\ &= \begin{cases} \Delta_{1X} + \dfrac{2T\cos\alpha}{EA} - \dfrac{1}{4}\pi^2\left(q_1^2 + 9q_3^2 - \delta^2\right) & \text{for Mode 1,} \\ \Delta_{2X} + \dfrac{2T\cos\alpha}{EA} - \pi^2\left(q_2^2 + 4q_4^2 - \delta^2\right) & \text{for Mode 2.} \end{cases}\end{aligned} \tag{4.33}$$

Thus, the axial force C_{iX} is expressed as

$$C_{iX} = EA\varepsilon_{ciX}. \tag{4.34}$$

With linear bending theory, the bending moments M_i are expressed as the following:

$$\begin{aligned}M_i &= -EI[W_i''(\xi) - W_{i\delta}''(\xi)] \\ &= \begin{cases} \dfrac{\pi^2 EI}{L}\left[(q_1 - \delta)\sin\dfrac{\pi\xi}{L} + 9q_3\sin\dfrac{3\pi\xi}{L}\right] & \text{for Mode 1,} \\ \dfrac{4\pi^2 EI}{L}\left[(q_2 - \delta)\sin\dfrac{2\pi\xi}{L} + 4q_4\sin\dfrac{4\pi\xi}{L}\right] & \text{for Mode 2.} \end{cases}\end{aligned} \tag{4.35}$$

The shear force S_{iX} can be defined by substituting equations (4.34) and (4.35) into equation (3.34) and then by taking the limit $\xi \to 0$.

By substituting equations (4.32), (4.34), (4.35) and an expression for the shear force into equation (3.33), expressions for Δ_{iX} can be obtained. Subsequently, the solution is expressed as a Taylor series with respect to T, P, q_m, and δ up to second order, which gives the following simplified expressions:

$$\begin{aligned}\Delta_{1X} =& b_{pX}P + b_{tX}T + b_{1X}q_1 + b_{3X}q_3 + b_{\delta X}\delta + b_{11X}q_1^2 + b_{13X}q_1q_3 + b_{33X}^2q_3^2 \\ &+ b_{1\delta X}q_1\delta + b_{3\delta X}q_3\delta + b_{\delta\delta X}^2\delta^2,\end{aligned} \tag{4.36}$$

$$\begin{aligned}\Delta_{2X} =& b_{pX}P + b_{tX}T + b_{2X}q_2 + b_{4X}q_4 + b_{\delta X}\delta + b_{22X}q_2^2 + b_{24X}q_2q_4 + b_{44X}^2q_4^2 \\ &+ b_{2\delta X}q_2\delta + b_{4\delta X}q_4\delta + b_{\delta\delta X}^2\delta^2,\end{aligned} \tag{4.37}$$

where b_{pX}, b_{tX}, $b_{\delta X}$, b_{mX}, b_{mlX}, $b_{m\delta}$ and $b_{\delta\delta}$ are coefficients for P, T, δ, q_m, $q_m q_l$, $q_m\delta$, δ^2 respectively.

4.3.5 Energy formulation

The total potential energy V_{iX} comprises components of the strain energy and the work done by the load. In a general state of deflection, there are four components of the strain energy: from bending in the column (U_{cbi}) and the crossarm (U_{abiX}) with axial strains in the column (U_{caiX}) and stays (U_{siX}). Except for the bending in the column, all of the components have the same expressions as in Chapter 3. Hence, only the bending energy in the column is described in this section, please refer to §3.2.4 for the other components.

4.3.5.1 Bending energy

The bending energy components in the column arise from a linear curvature expression; thus, W_i give the following expressions for U_{cbi}:

$$\begin{aligned} U_{cbi} &= \frac{1}{2}EI\int_0^L [W_i''(x) - W_{i\delta}''(x)]^2\,\mathrm{d}x - U_{cb0} \\ &= \begin{cases} \dfrac{EI\pi^4\left(q_1^2 + 81q_3^2 - 2q_1\delta + \delta^2\right)}{4L} - U_{cb0} & \text{for Mode 1,} \\ \dfrac{4EI\pi^4\left(q_2^2 + 16q_4^2 - 2q_2\delta + \delta^2\right)}{L} - U_{cb0} & \text{for Mode 2,} \end{cases} \end{aligned} \tag{4.38}$$

where U_{cb0} is the existing column bending energy at the beginning of each buckling type.

4.3.5.2 Total potential energy function

The total potential energy is a summation of U_{cbi}, U_{abiX}, U_{caiX}, U_{siX} minus $P\mathcal{E}_{iX}$:

$$V_{iX} = U_{cbi} + U_{abiX} + U_{caiX} + U_{siX} - P\mathcal{E}_{iX}. \tag{4.39}$$

In the Mode 2 Type C analysis, higher terms of P are then truncated as they are not the dominant terms in the function and leave the governing equation untractable. For equilibrium, the total potential energy V_{iX} must be stationary with respect to the generalized coordinates q_m. Therefore, the equilibrium paths can be computed from the condition:

$$\frac{\partial V_{iX}}{\partial q_m} = 0. \tag{4.40}$$

4.3.6 Failure criteria

In order to model more practically realistic behaviour, certain failure criteria are defined; column yielding and stay fracture are included in the study as they are considered to be the principal failure criteria, apart from instability, in the design of such structural components.

4.3.6.1 Column yielding

The bending moment along the column can be obtained by substituting x for ξ in equation (4.35). Locating the maximum bending moment in the total length of the column at each numerical increment $M_{iX,\max}(q_i)$, which is uniquely determined by q_i, and applying Euler–Bernoulli beam theory, the maximum stress can be found by calculating the fibre stress using $M_{iX,\max}(q_i)$ and the axial force $C_{iX}(q_i)$ thus:

$$\sigma_{fiX,\max}(q_i) = \frac{M_{iX,\max}(q_i)\phi_{co}}{2I} + \frac{C_{iX}(q_i)}{A}. \tag{4.41}$$

Increasing the value of q_i leads the value of $\sigma_{fiX,\max}(q_i)$ to rise; when the fibre stress reaches the yielding stress σ_y, the plasticity in the column begins to be observed. This approach is in line with the Perry–Robertson formula (Coates *et al.*, 1988), which has been used for strut design in the UK for many years.

4.3.6.2 Stay fracture

Defining the ultimate strength of the stays σ_u and assuming that the stays are purely linearly elastic until they reach the fracture stress, the fracture strength of the stays can be defined as

$$T_u = \sigma_u A_s. \tag{4.42}$$

When the axial force in Stay 1 (T_{iX1})—the convex side stay for both modes—reaches T_u, fracture of the stay would be expected.

4.4 Equilibrium Path with Imperfections

The main purpose of this work was to investigate the buckling response of the stayed column with geometrical imperfections and to present the occurrence of material failure on the elastic response. With the modified formulated total potential energy and the failure criteria, the post-buckling behaviour of the stayed column together with failure points can be investigated. The same dimensions and properties as in §3.3.1 were also applied for the post-buckling analysis, with the stay diameter, $\phi_s = 4.8\,\text{mm}$ being chosen. The column yield and stay fracture stresses were defined as $\sigma_y = 338\,\text{N/mm}^2$ and $\sigma_u = 614\,\text{N/mm}^2$ respectively. These values also originate from the Hafez model (Hafez *et al.*, 1979). Five different values of the initial prestress were selected from the zones discussed before to investigate changes in the mechanical response as T changes, the selection criteria being expressed in Table 4.1.

As for the initial out-of-straightness, the following seven different values of δ shown

Point	Initial prestress T			
	Criterion expression	Mode 1 (kN)	Mode 2 (kN)	Zone
1	0	0.00	0.00	1
2	$(T_{\text{opt}} - T_{\text{min}})/3 + T_{\text{min}}$	1.47	2.50	2
3	T_{opt}	3.48	3.78	2/3 boundary
4	$2T_{\text{opt}}$	6.97	7.55	3
5	$2.75T_{\text{opt}}$	9.58	10.38	3

Table 4.1: Selected prestress levels for the study.

in Table 4.2 were adopted in the analysis. A value of 1/1500 originates from experimental measurements (Wong & Temple, 1982; De Araujo *et al.*, 2006); 1/500 originates from manufacturing tolerances (EN10210-2, 2006); values of 1/300 and 1/200 are derived from the values of the recommended initial local bow imperfection in the global analysis of frames for hot-rolled and cold-formed hollow sections respectively in Eurocode 3, the European design code for steel structures (EN1993-1-1, 2005).

No	Initial out of straightness	
	Mode 1	Note
0	0	perfect
1	1/10000	nearly perfect
2	1/3000	
3	1/1500	experimental measurements
4	1/1000	
5	1/500	manufacturing tolerance
6	1/300	Eurocode 3 design value for hot-rolled sections
7	1/200	Eurocode 3 design value for cold-formed sections

Table 4.2: Selected amplitudes for the initial out-of-straightness.

In Mode 2, amplitudes of the imperfections were selected in order that the end-shortening caused by the initial out-of-straightness would be the same as in Mode 1 (Wadee, 2000), thus

$$\int_0^L \frac{1}{2} W_{1\delta}'^2(x)\mathrm{d}x = \int_0^L \frac{1}{2} W_{2\delta}'^2(x)\mathrm{d}x = \mathcal{E}_0, \tag{4.43}$$

where $\mathcal{E}_0$ is the first order approximation of the end-shortening caused by the initial out-of-straightness, which gives the following equation:

$$\delta_2 = \frac{1}{2}\delta_1, \tag{4.44}$$

where δ_1 and δ_2 are imperfection amplitudes for Modes 1 and 2 respectively. Thereby, the imperfection values shown in Table 4.2 were divided by 2 for Mode 2.

4.4.1 Buckling behaviour

The equilibrium equations accounting for the imperfections are expressed in equation (4.40), which were solved using MAPLE. In addition, the yielding points of the column and the fracture points of the stays were investigated to find the structural failure points. These analyses would be expected to facilitate the prediction of more realistic structural response than the previous purely elastic analysis performed for the perfect system. Figures 4.9 and 4.10 represent the equilibrium paths with the imperfection for Modes 1 and 2 respectively at each point.

At Point 1, with lower amplitudes of the imperfection (1/10000 and 1/3000 for Mode 1, and 1/20000, 1/6000, 1/3000, and 1/2000 for Mode 2), the response begins with Type A buckling; then, at a certain value of horizontal deflection, the convex side of the stays reactivate, which leads to the conversion of the buckling types to Type C. This response pattern is exactly the same as the one seen in the perfect case. However, when the imperfection becomes large—greater than 1/3000 for Mode 1 and 1/2000 for Mode 2—the response starts immediately with Type C buckling. The reason for this difference may be related to the fact that a large value of the out-of-straightness allows the structure to bend easily even at the beginning of loading, which renders the convex side stays immediately active after loading.

At the other points, the buckling response starts with Type B, and afterwards the concave side stays slacken at a certain value of horizontal deflection, which leads to the conversion of the buckling types to Type C. As can be seen from (c)–(f) in

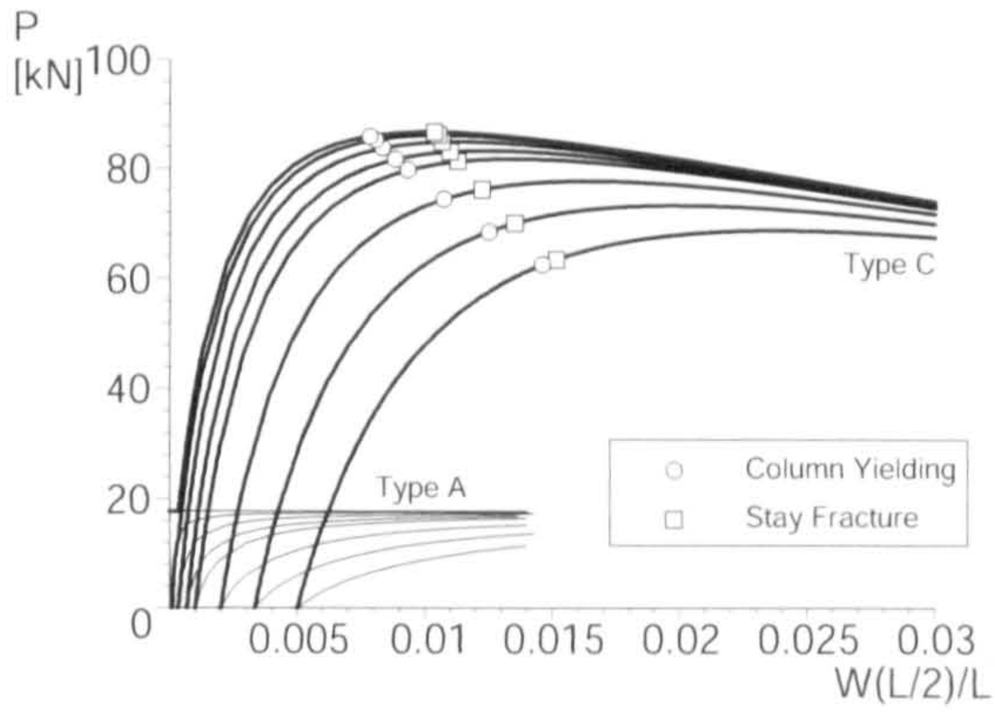

(a) Point 1

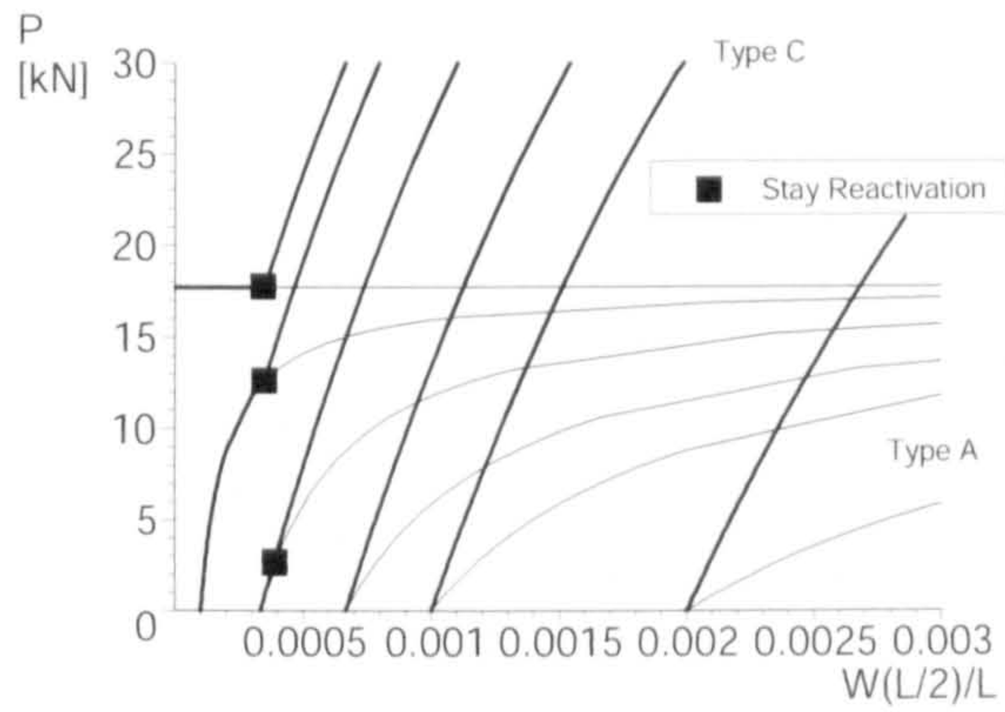

(b) initial part of Point 1

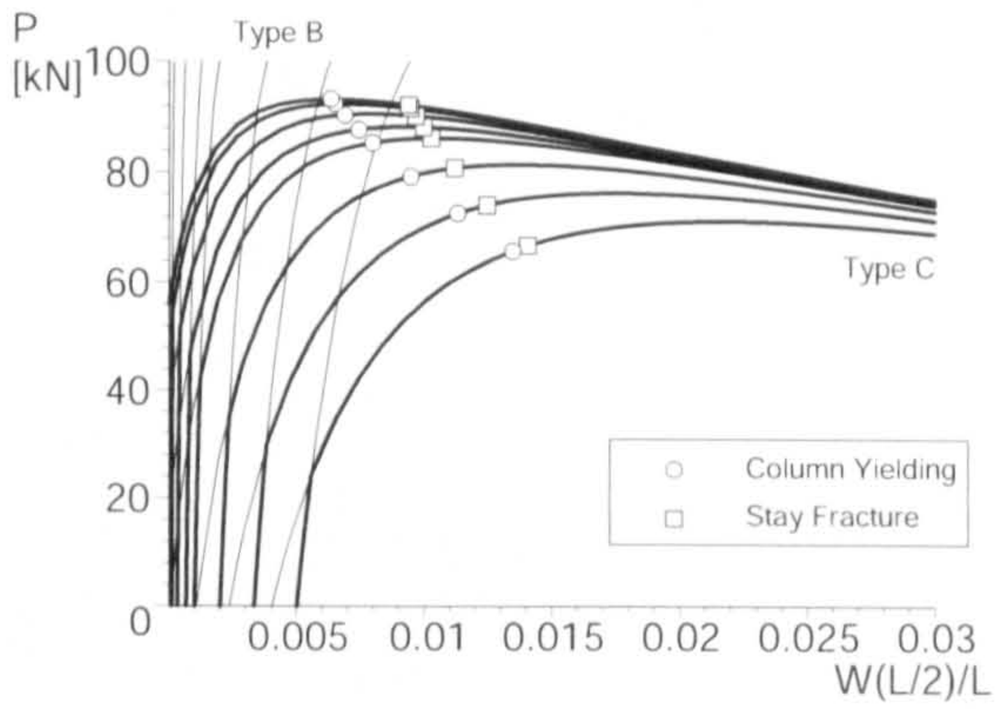

(c) Point 2

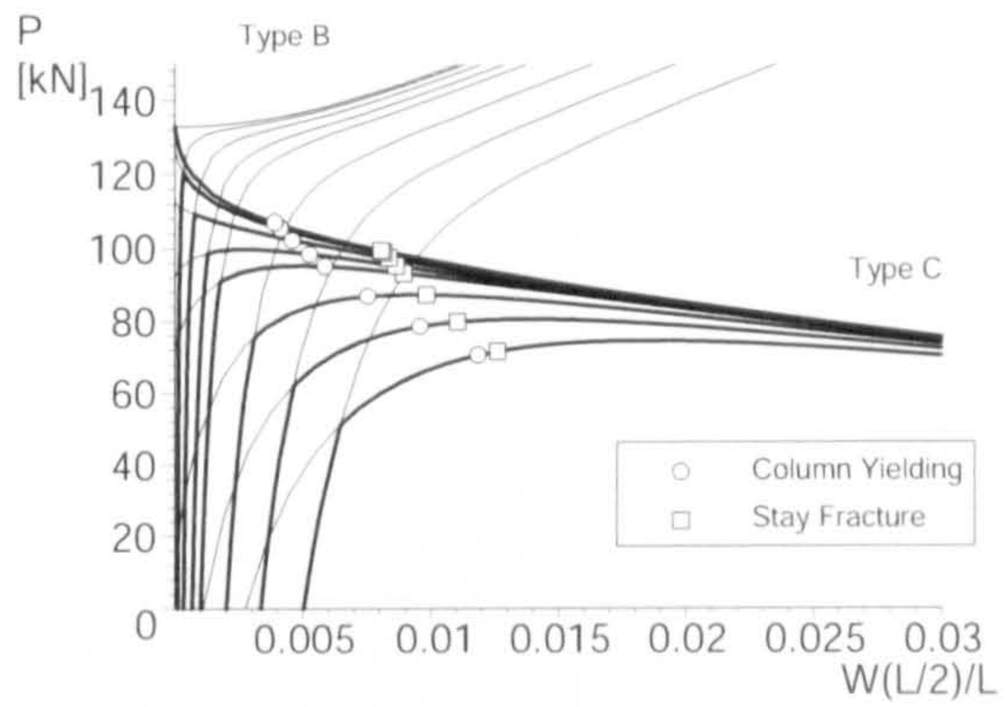

(d) Point 3

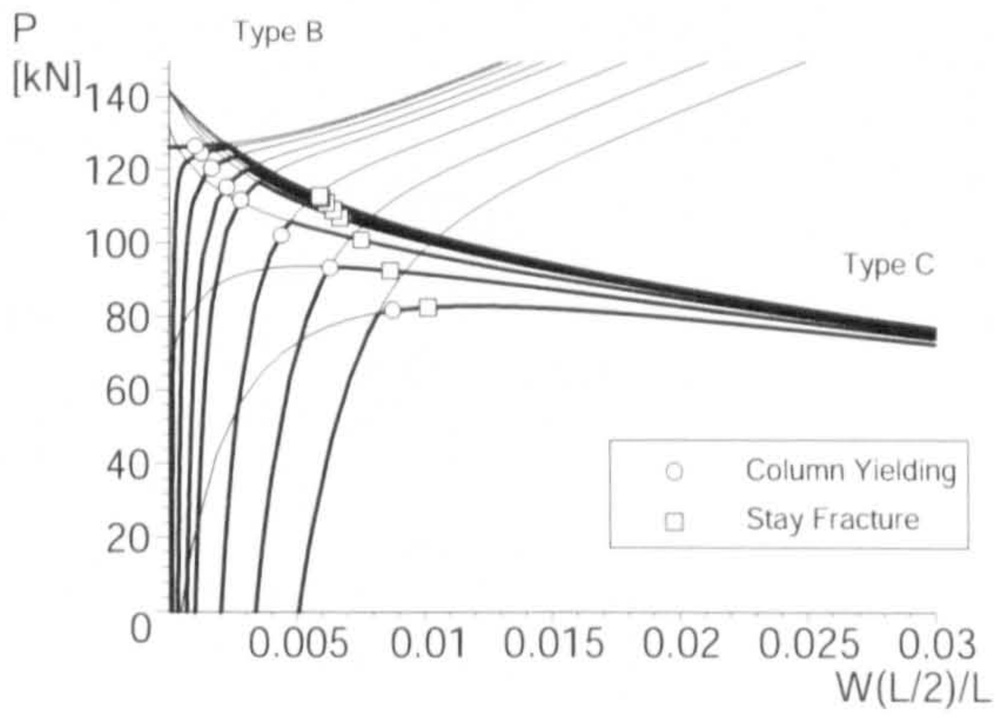

(e) Point 4

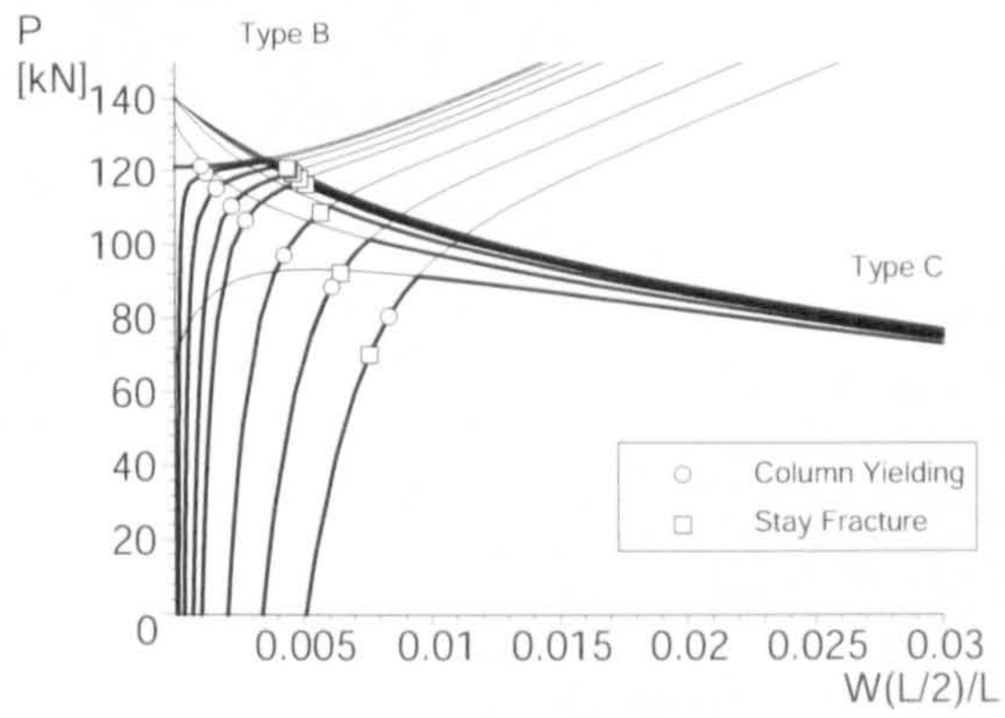

(f) Point 5

Figure 4.9: Equilibrium paths for Mode 1 represented by the axial load P versus midspan displacement $W(L/2)/L$. Note that the highest path in each sub-figure occurs when $\delta = 0$, and the lowest path occurs when $\delta = 1/200$.

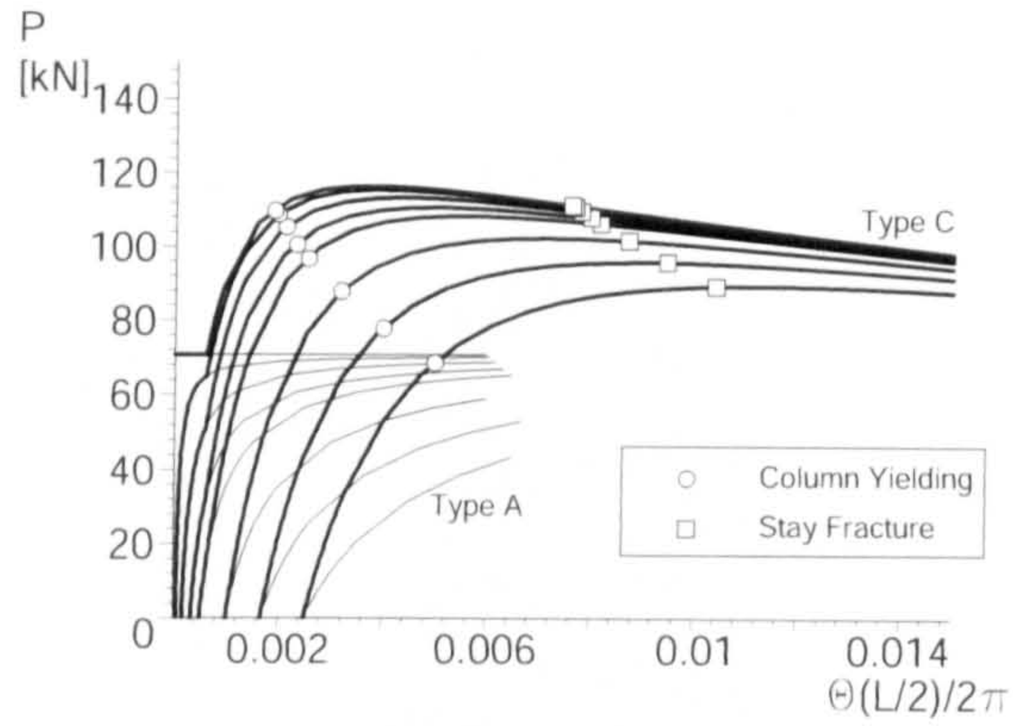

(a) Point 1

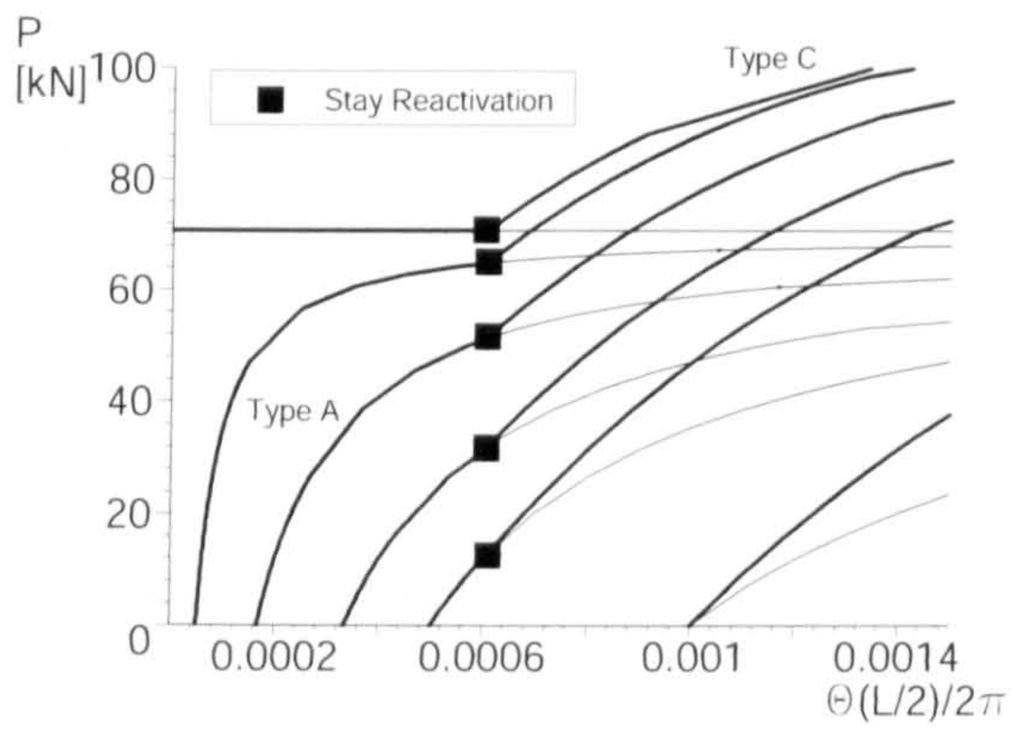

(b) initial part of Point 1

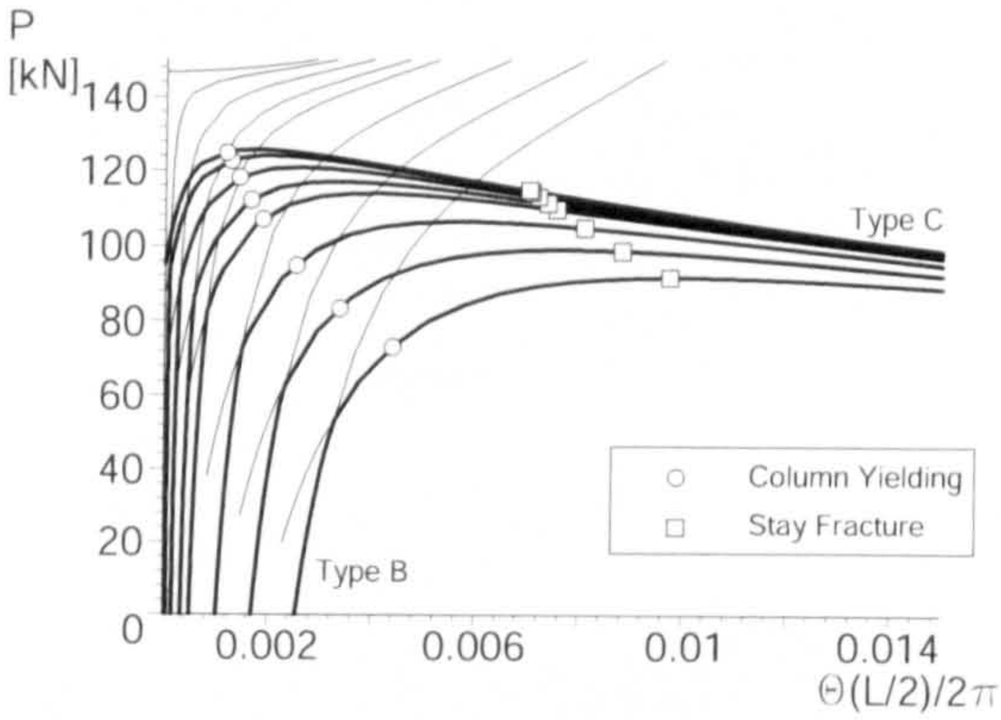

(c) Point 2

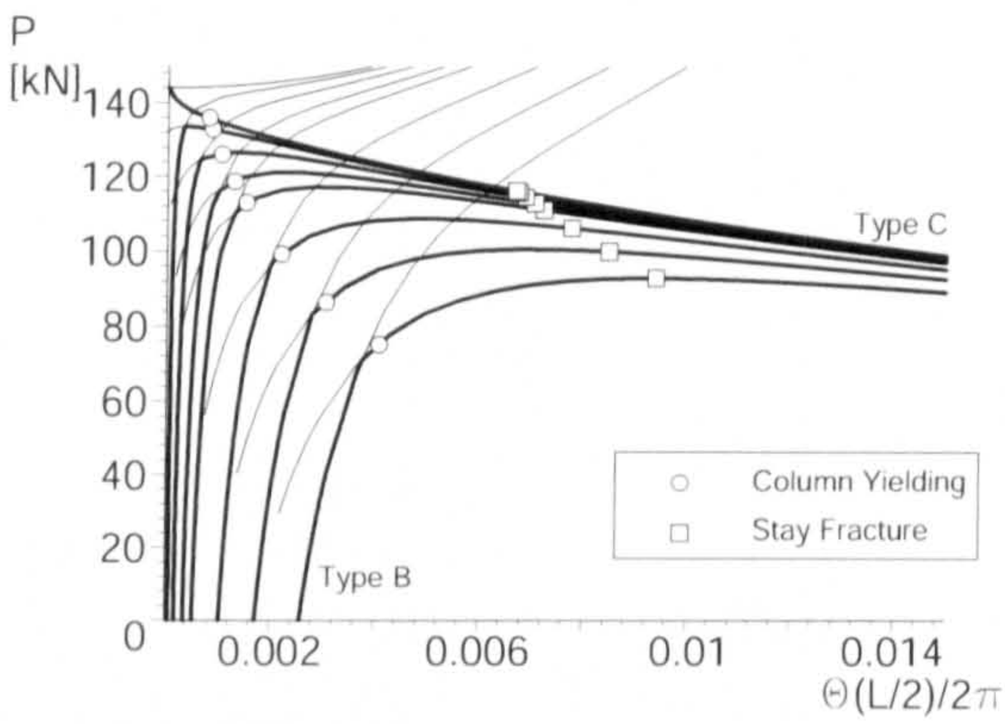

(d) Point 3

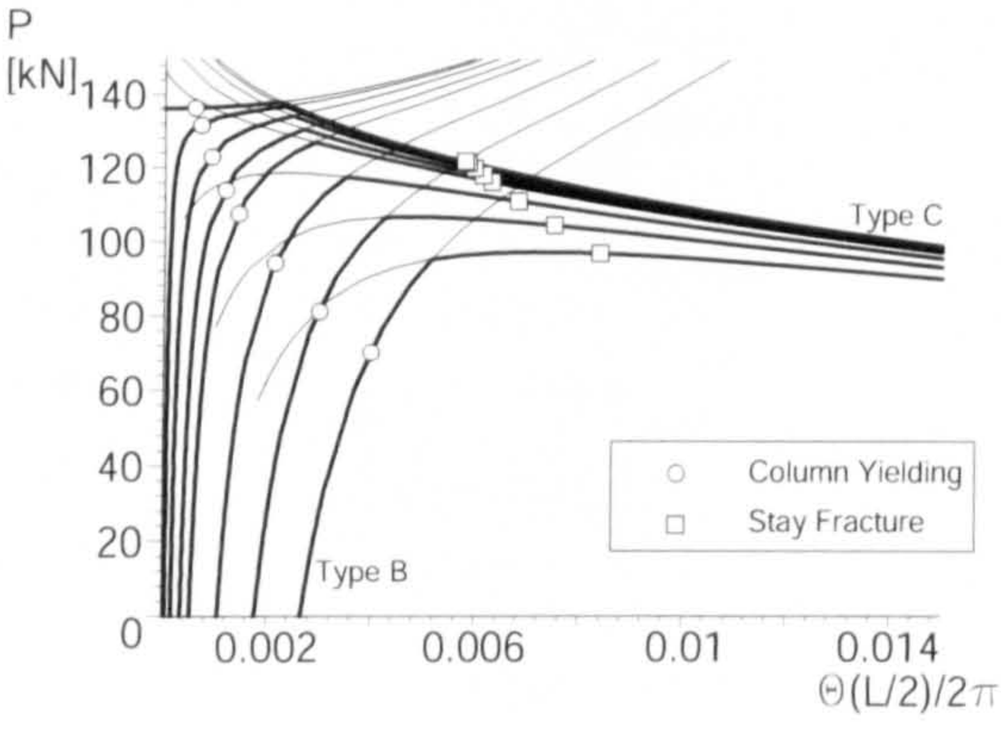

(e) Point 4

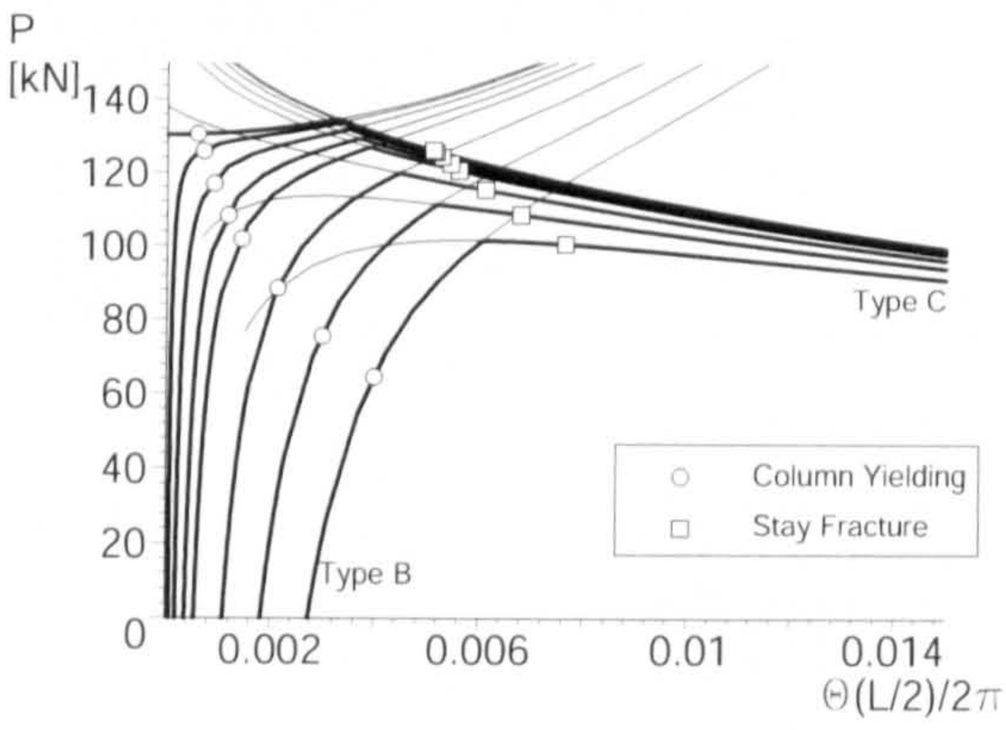

(f) Point 5

Figure 4.10: Equilibrium paths for Mode 2 represented by the axial load P versus midspan buckling rotation $\Theta(L/2)/2\pi$. Note that the highest path in each sub-figure occurs when $\delta = 0$, and the lowest path occurs when $\delta = 1/400$.

Figures 4.9 and 4.10, the more prestress that is applied, the longer the stays are active under loading.

The fracture and column yielding points are also presented in Figures 4.9 and 4.10. In most cases, column yielding is the failure mode: the yielding points occur prior to the stay fracture points in the loading paths. However, at Point 5 in Mode 1 with larger values of the imperfection (1/200), stay fracture becomes the governing failure mode. This phenomenon is perhaps attributed to the following reasons: first, since a large amount of the initial prestress is already applied, there is only a limited capacity available for further stress increase in the stays; second, a large value of the imperfection allows the structure to bend easily, which causes a rapid increase in strain in the stays.

4.4.2 Validation for the tip displacement coefficients

In order to investigate the tip displacement coefficients for the crossarm, the third and fifth order expansions with respect to R_X were formulated for buckling Type B and C respectively. Although this approximation gives significant computational advantages to the analytical model, the accuracy of the process has not yet been evaluated. Hence, in this section, the numerical values of the approximated tip displacements h_X, which can be obtained from equations (4.27) and (4.28), and the exact shape functions for the crossarm $w_{2X}(y)$, which can be obtained from equation (4.12), are presented and then compared against each other.

To examine the actual values of h_X and $w_{2X}(y)$, equilibrium points were selected from the Point 4 post-buckling response with an imperfection value of 1/600, as shown in Figure 4.11. Points EB1–EB4 are from the path in Type B, and Points EC1–EC4 are from the path in Type C.

Figure 4.12 plots h_X and $w_{2X}(y)$ at those selected points from the equilibrium path. As can be seen, although minor discrepancies are observed at EC3 and EC4, in general these two curves have almost the same value at the tip of the crossarm.

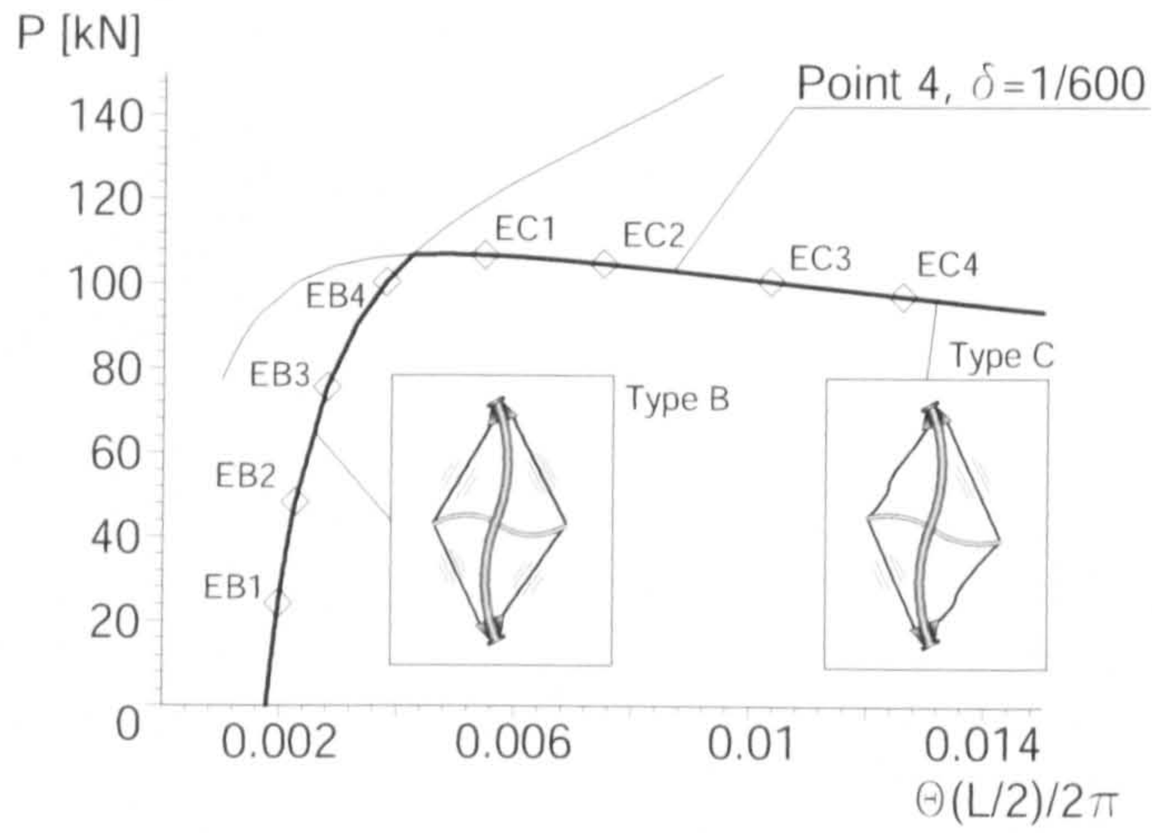

Figure 4.11: Selected points for the validation of the tip displacement coefficients.

Thus, it can be said that the approximations for h_X are appropriate and have been validated with the presented comparison.

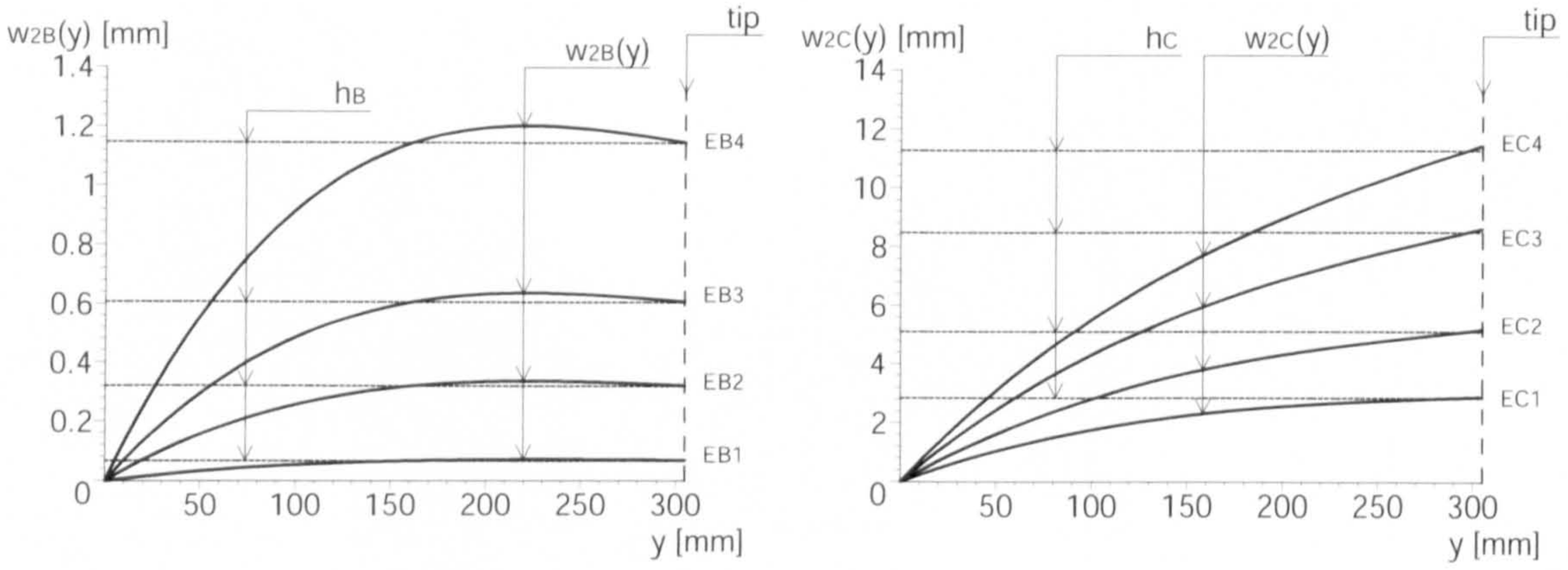

(a) Type B

(b) Type C

Figure 4.12: Comparison of $w_{2X}(y)$ and h_X. Note that the values of $w_{2X}(y)$ and h_X almost coincide at the tip of crossarm, $y = 305\,\text{mm}$.

4.4.3 Finite element validation

Using the FE program ABAQUS, numerical FE models were developed to validate the results from the modified analytical model presented in the previous section. In order to indicate the structural failure points clearly, the following three different

types of FE models were developed: an elastic model, an elastic–plastic model and a stay fracture model. In the elastic model, all of the structural components had purely elastic responses except that the stays were modelled to lose their stiffness under compression. In the elastic–plastic model, although the stays were elastic, the column and the crossarm had elastic–plastic responses, see Figure 4.1(a). In the stay fracture model, although all of the structural components had purely elastic responses, the stay had a failure load in tension at which the stays lost their tension completely, see Figure 4.1(b). As stated in §3.4.3, this analysis was also conducted by a nonlinear Riks analysis using the Euler buckling displacement as an imperfection. The elements adopted were exactly the same as those in the previous FE analysis: truss elements modelled to lose their tension in compression for the stays and beam elements for the column and the crossarm.

Figures 4.13 and 4.14 show the equilibrium paths under axial loading from the FE models along with those from the analytical model using $\delta_1 = 1/300$ and $\delta_2 = 1/600$ at each point for both modes respectively. As can be seen, for Mode 1 the equilibrium buckling paths of the elastic model of the FEM almost coincide with those of the analytical model. For Mode 2, although the equilibrium paths of the FEM and the analytical model are in good agreement in their initial stages, these are in less good agreement once the load reaches the flattened region, which is observed in Type C buckling. Regardless of this less good agreement, the same trend can be still detected from these two models. All of these observations is exactly the same as the one from the perfect cases discussed in the previous chapter. Thus, although a certain level of error has to be admitted in the analytical model for Mode 2, the current modelling is still useful to predict the qualitative buckling behaviour; moreover, at least it can be said that the presented FE model seems reliable.

As for the failure points, in Mode 1, it can be seen without exception that the stay fracture points of the FE model and the analytical model are in good agreement. Despite this correlation, the yielding points in the analytical model involve a certain discrepancy with those in the FEM, especially in the cases with lower values of the

prestress though the level of the failure load is predicted with reasonable accuracy. This discrepancy is possibly attributed to the yielding criterion in the analytical modelling—the column is assumed to have failed when the fibre stress reaches the yield stress. This assumption gives a good prediction when stresses from bending moments in columns are relatively low, but when bending stresses dominate the axial stress, this approach may give a rather poor prediction as high bending stresses do not have much impact on the plastic resistance of a column in practice (Rotter, 2007).

As can be seen, the horizontal deflections at the yielding points are relatively large in Mode 1 when the prestress is low. Therefore, the bending stress in the column may also be relatively large; this is probably the reason for the underestimation of the yield points. Particularly when the prestress is small such as Points 1, 2 and 3, the bending stress tends to become even larger as the constraint against the column movement that is provided from the low prestressing force is relatively low. Therefore, it should be noted that the presented yielding criterion might cause the underestimation of the yielding point especially with lower levels of prestress.

In Mode 2, the stay fracture points of the FEM and the analytical models are in less good agreement. It seems that this error is attributed to less accurate analytical modelling, i.e. it contains fewer degrees of freedom as discussed in the previous chapter. Despite this discrepancy, good agreement can be seen between the yielding points of the FEM and the analytical models. As the yielding points occur at the initial stage of equilibrium paths, it may be reasonable to suppose that the effects from the bending moments and the accuracy of the analytical model did not affect the results.

From these comparisons, it can be said that the presented analytical model and failure criteria are reasonable, though the column failure criterion might be inappropriate when lower values of the prestress are introduced—but it should be noted that low prestress is a practically less relevant case, and the level of the yield load is still predicted well despite the error in displacements. It seems that the major

discrepancies between the two models are attributed to the less accurate analytical modelling of Mode 2, which arises from the lack of sufficient degrees of freedom. Hence, although the analytical model may be thought not to be completely accurate, it can at least be thought that the current FE model is quite reliable.

4.4.4 Sensitivity studies

Figures 4.15(a) and 4.16(a) show the maximum axial load capacity $P_{\text{el,max}}$ for each mode respectively, and Figures 4.15(b) and 4.16(b) show the midspan horizontal displacement for Mode 1 and the midspan rotation for Mode 2 respectively at the maximum loading against various imperfection values. These graphs are plotted from the equilibrium paths through the analytical and elastic FE models, which have already been shown in the previous section.

As can be seen from (a) in Figures 4.15 and 4.16, the maximum axial strength $P_{\text{el,max}}$ increases as the prestress T increases. It can also be seen that the maximum capacity is most sensitive to the imperfections at Point 3, which represents the prestress level of T_{opt} being located at the boundary of Zones 2 and 3. The prestress T_{opt} has been considered to be the optimized prestress in the literature because the highest buckling load can be observed there. However, when T is moderately greater than T_{opt}, the maximum load capacity $P_{\text{el,max}}$ becomes even larger than that for T_{opt}. With these obtained results, it can hardly be said that T_{opt} is the optimized prestress.

As for the horizontal displacement at the maximum load, this value decreases as the prestress increases, as can be seen from (b) in Figures 4.15 and 4.16; the least sensitivity is observed in Zone 3. This result was somewhat expected because of the fact that the structure does not easily bend when it is restrained with a large prestress.

Since the least sensitivity to the imperfections and the highest maximum load capacities are observed in Zone 3, the value of the optimized prestress that allows

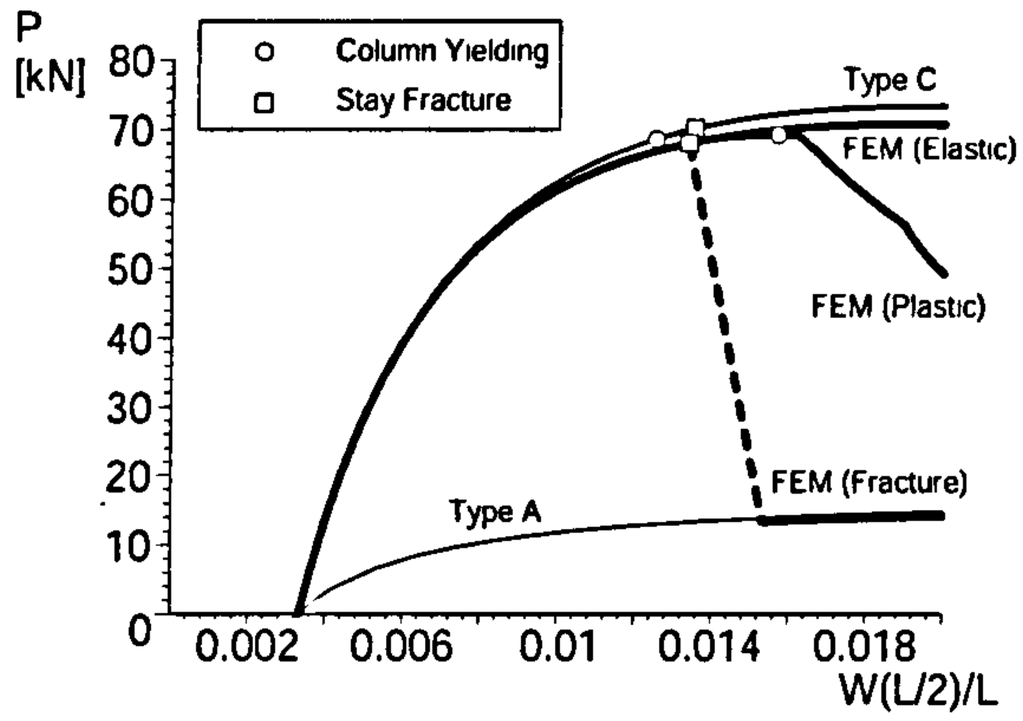

(a) Point 1

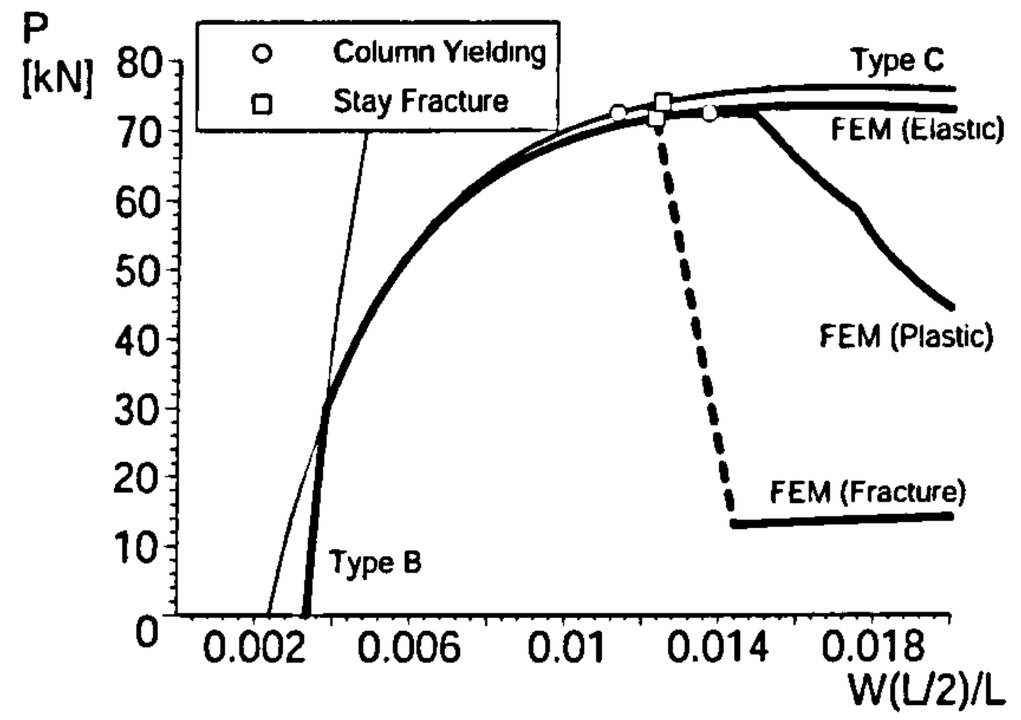

(b) Point 2

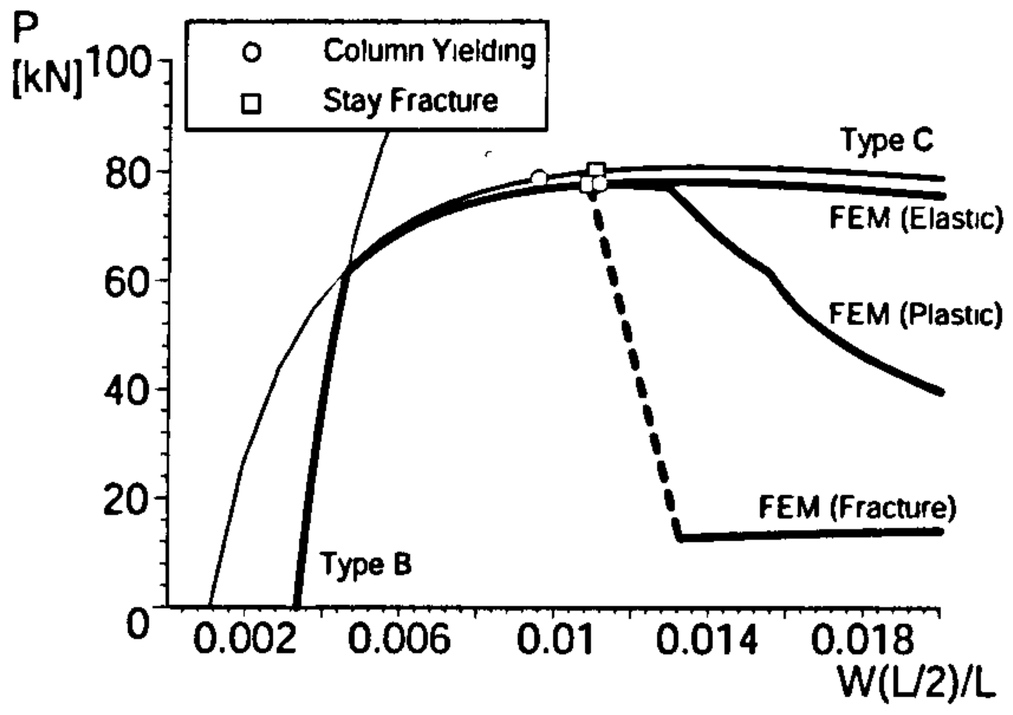

(c) Point 3

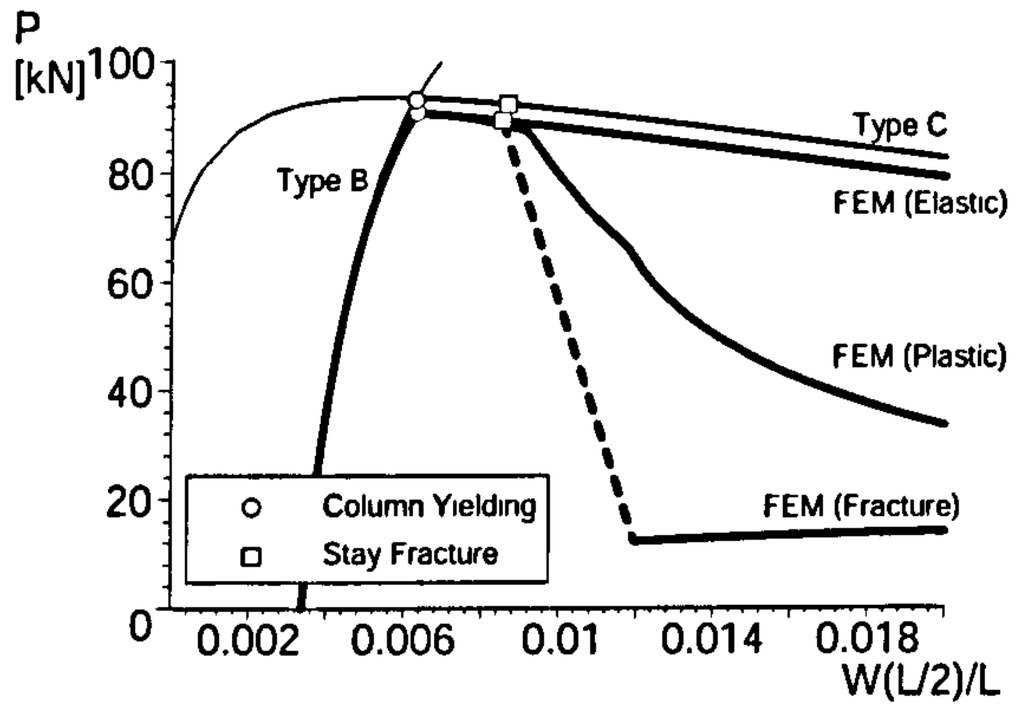

(d) Point 4

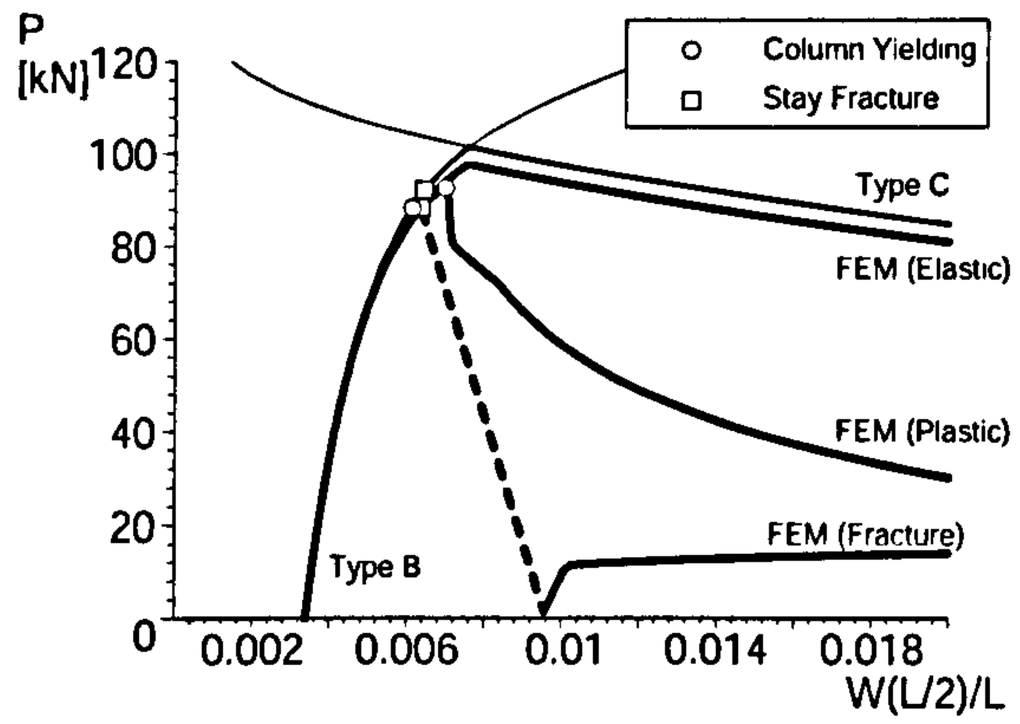

(e) Point 5

Figure 4.13: Equilibrium paths for Mode 1 comparing the FEM and the analytical models for $\delta = 1/300$. Three paths from the FEM are plotted in each sub-figure in order to spot the failure points.

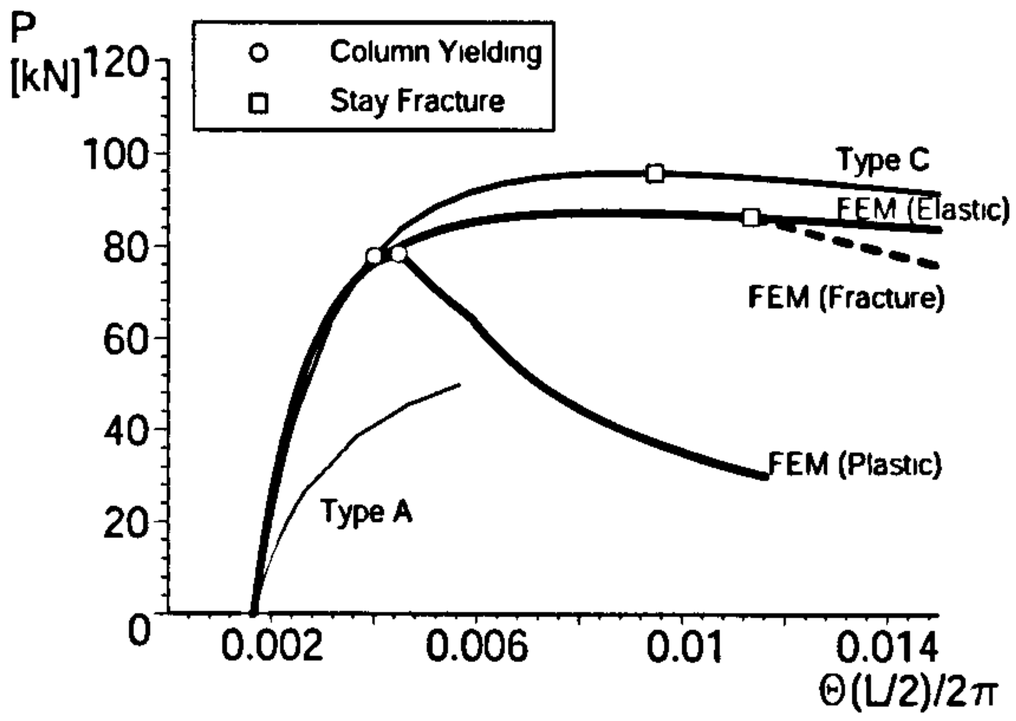

(a) Point 1

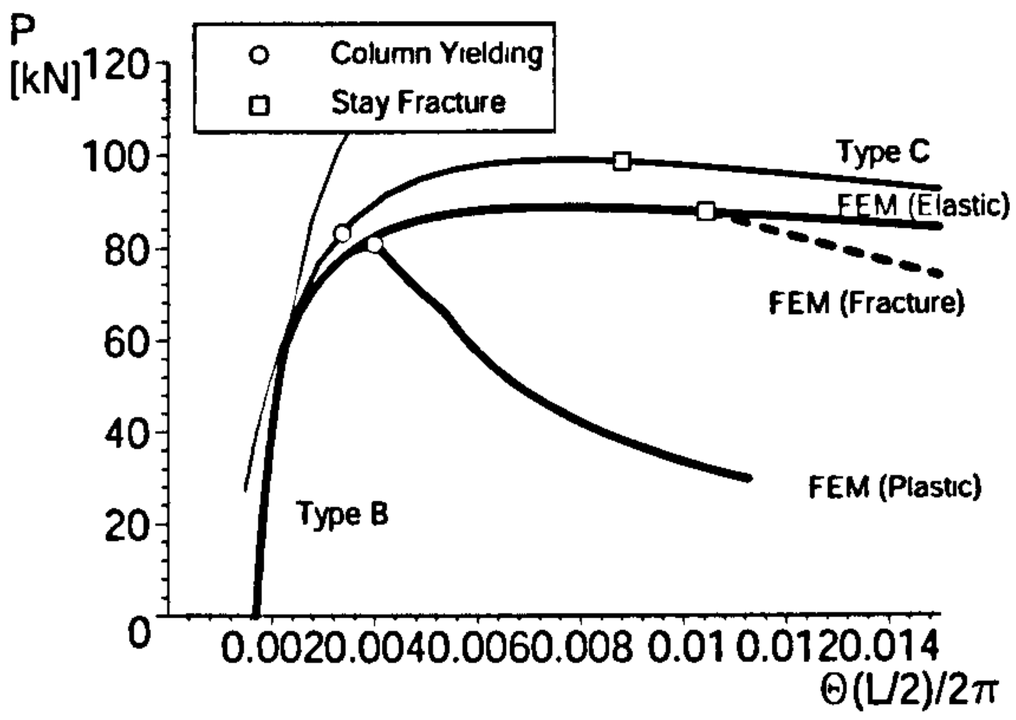

(b) Point 2

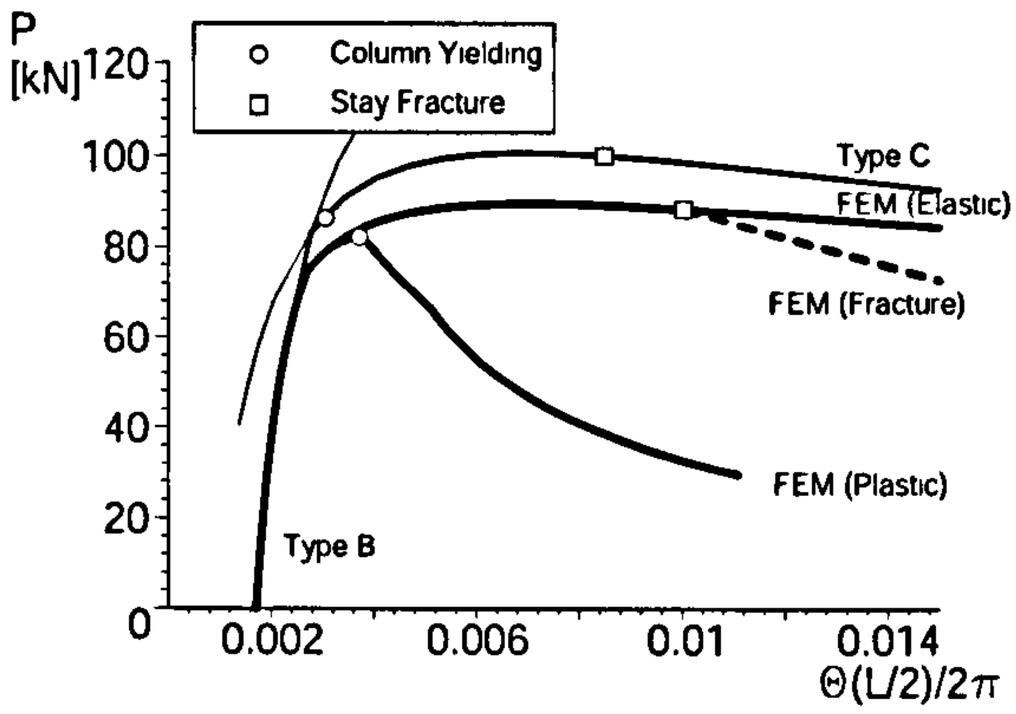

(c) Point 3

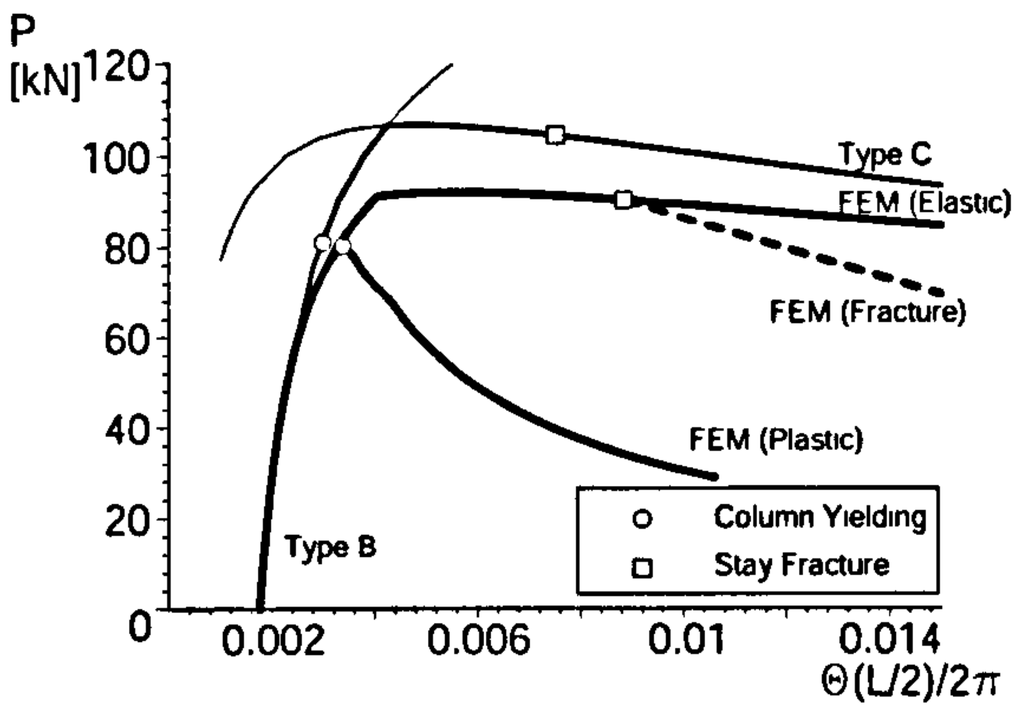

(d) Point 4

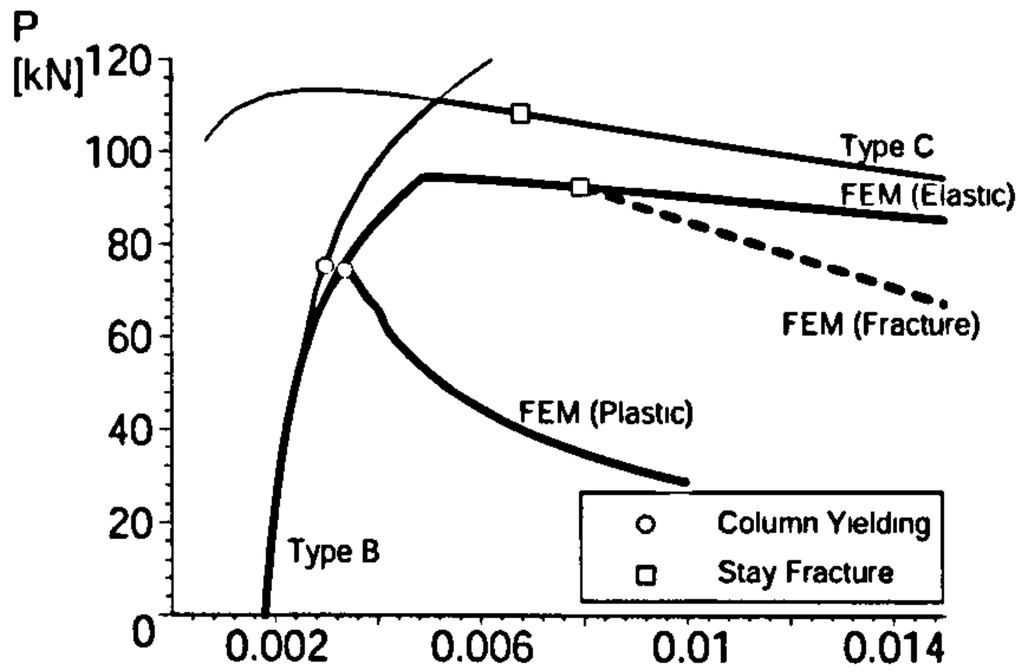

(e) Point 5

Figure 4.14: Equilibrium paths for Mode 2 comparing the FEM and the analytical models for $\delta = 1/600$. Three paths from the FEM are plotted in each sub-figure in order to spot the failure points.

designers to obtain the maximum strength $P_{\text{el,max}}$ with the minimized structural resistance is expected to be somewhere in Zone 3, higher than T_{opt}. Despite this, the exact value of the optimized prestress is still unknown. Although increasing the prestress provides the structure with more axial strength and less sensitivity to imperfections, the greater prestress also requires an increase in the cross sectional area of the structural components to counteract potential plasticity occurring earlier. The optimized prestress has to be found by balancing these two different aspects with certain indicators for optimization; this argument is to be developed in Chapter 6 along with related parametric studies.

4.5 Remarks

This chapter has aimed to investigate more practically realistic structural responses of the stayed column. Previous studies (Wong & Temple, 1982; Temple *et al.*, 1984; Chan *et al.*, 2002) also took into account the geometrical imperfections and successfully located the maximum load capacity. However, the equilibrium behaviour itself and structural failure were not previously examined in detail; in addition, the sensitivities to imperfections and prestress were not satisfactorily investigated.

The equilibrium response under axial loading in conjunction with column yielding and stay fracture has been presented from both the mathematical model and FE analyses. As expected, the current analytical model for Mode 1 has excellent agreement with the FE model; however it is less accurate for Mode 2 when compared with Mode 1 due to the approximation of modelling, i.e. more degrees of freedom are necessary to obtain more accuracy in Mode 2, which was also discussed in Chapter 3. The results indicate that the presented analytical modified model can account for the geometrical imperfection of the column, and that the current FE modelling can be considered to be quite reliable. Owing to this validation, in the interactive buckling and parametric studies that follow in subsequent chapters, the FEM is to be used as the main tool for investigation.

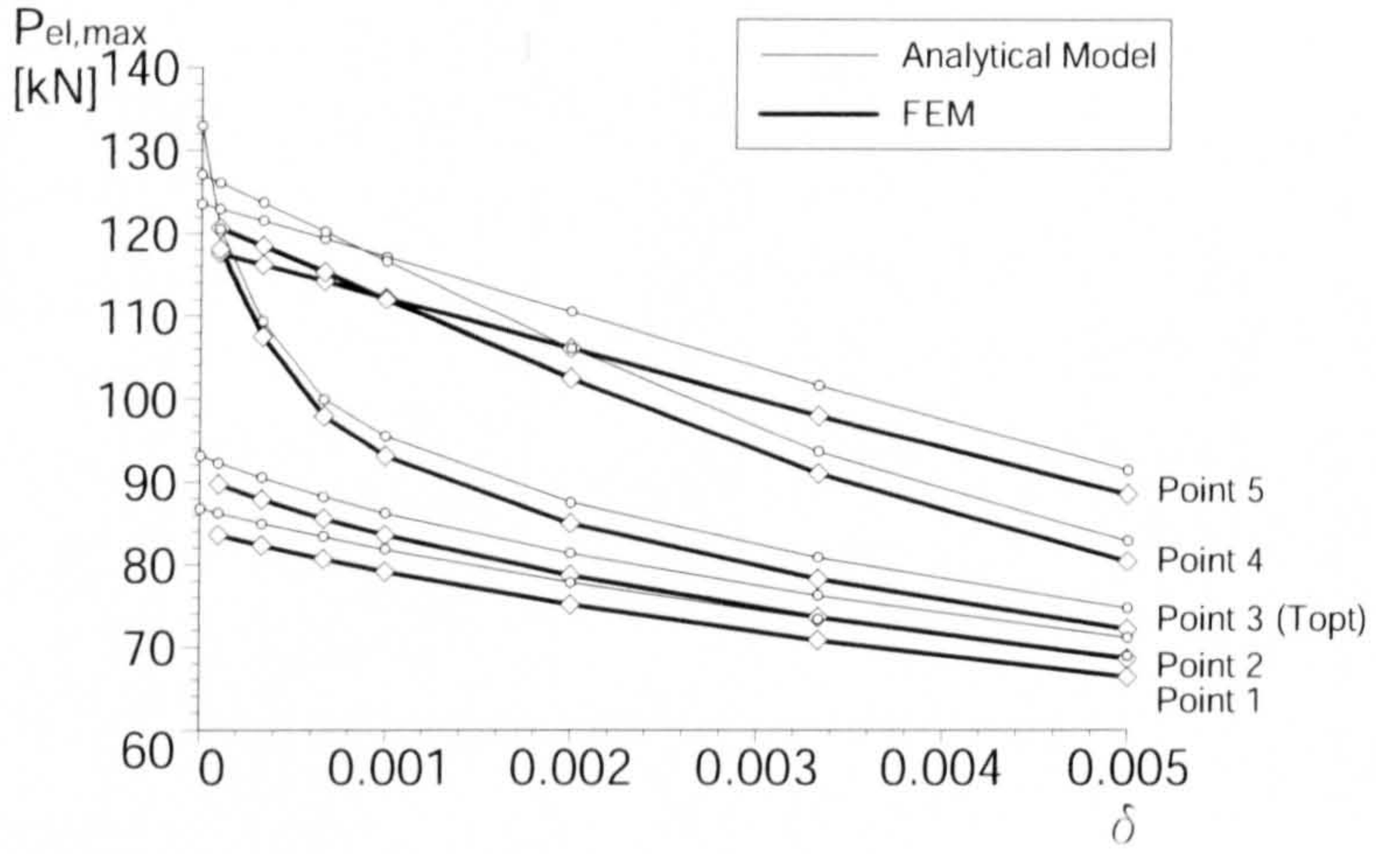

(a) maximum load versus the imperfection

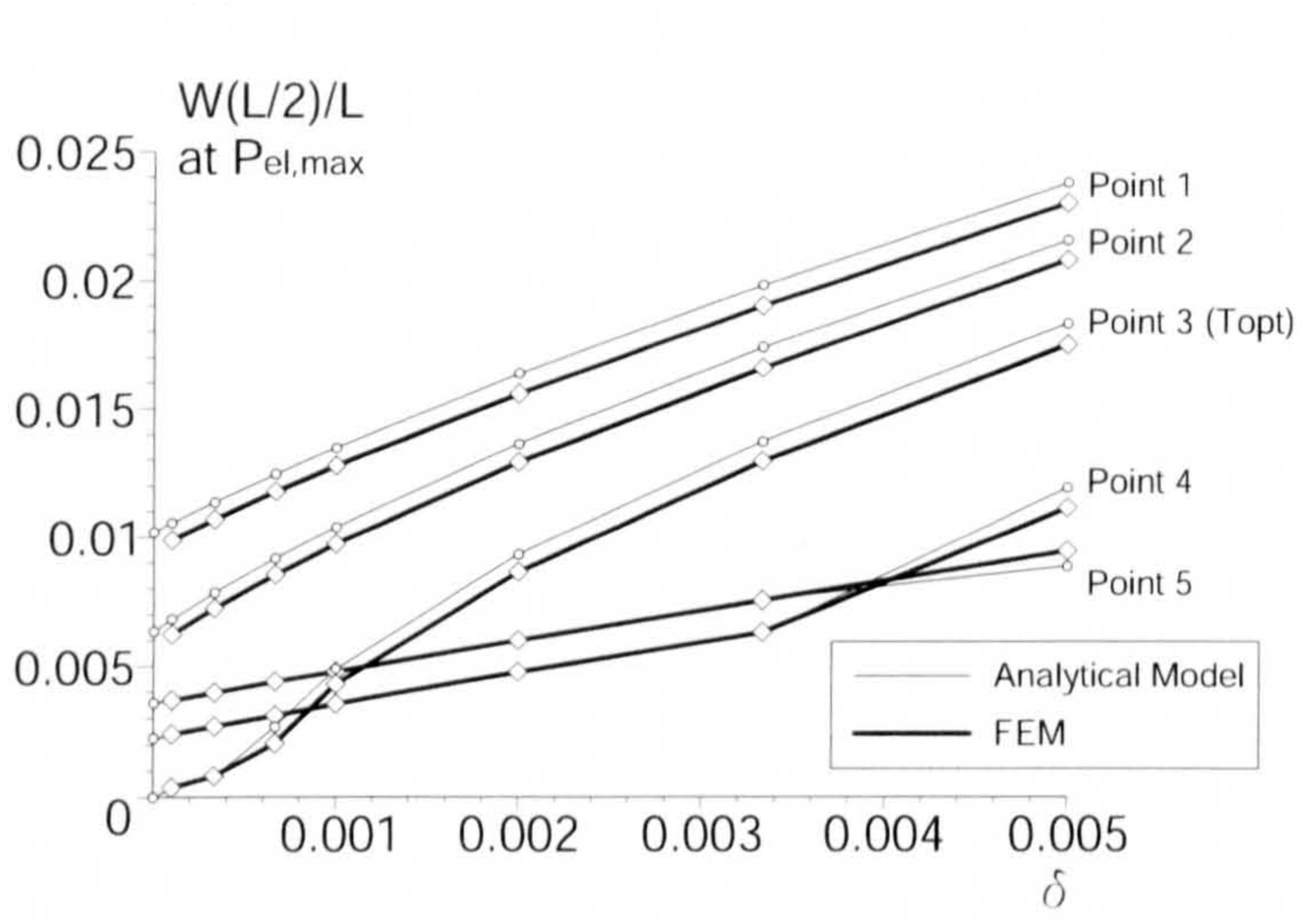

(b) horizontal deflection at the maximum load versus the imperfection

Figure 4.15: Imperfection sensitivities of the system (Mode 1).

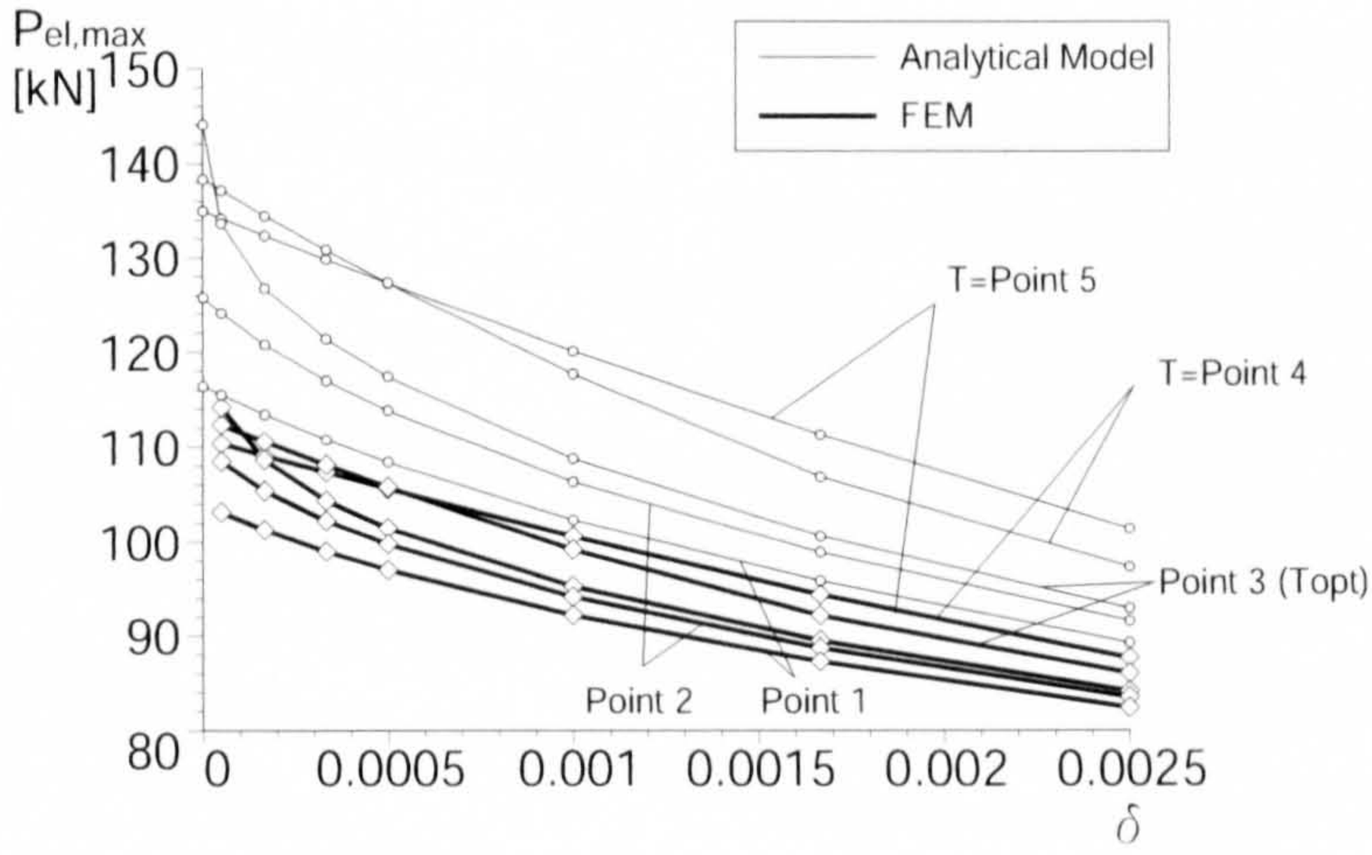

(a) maximum load versus the imperfection

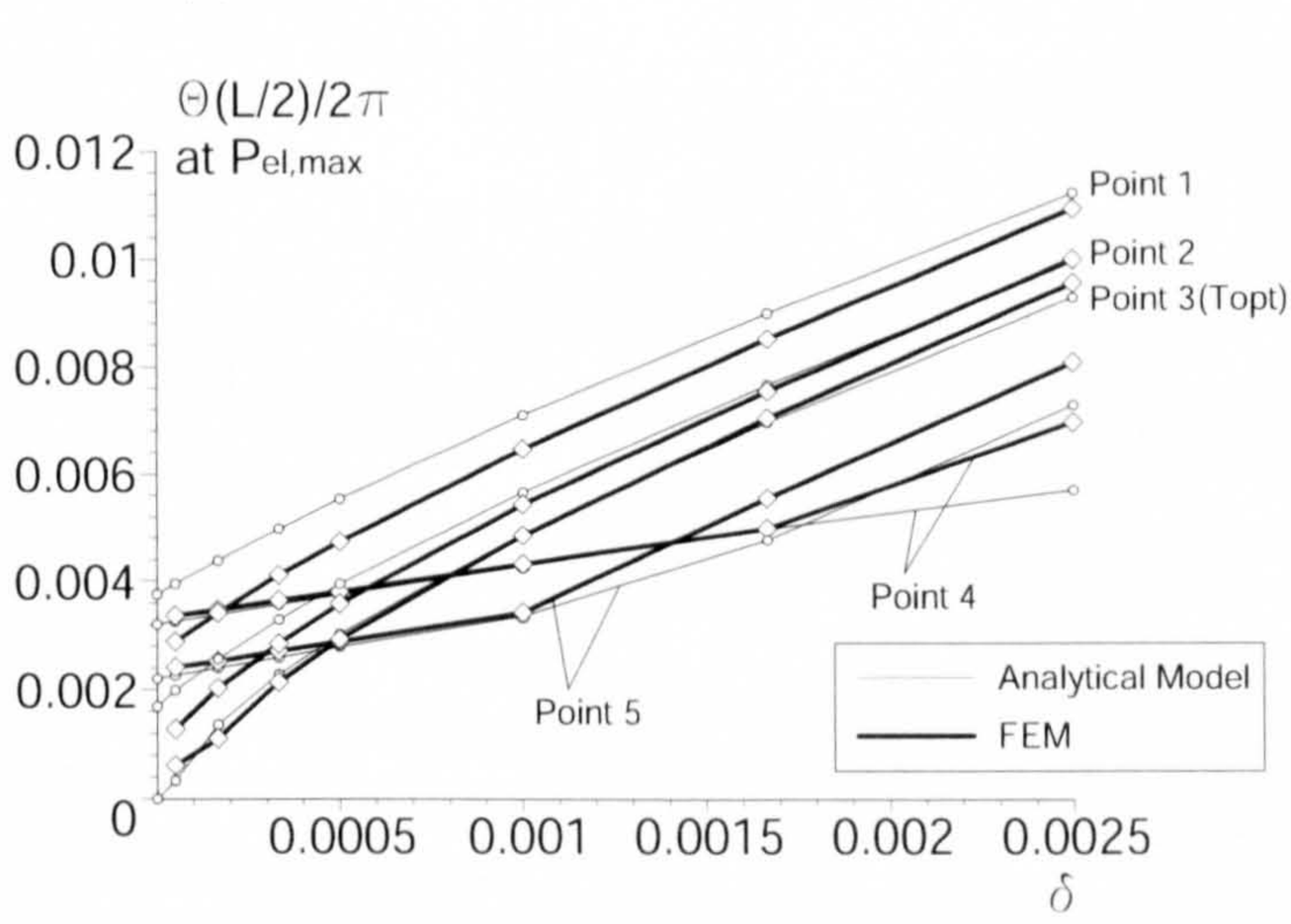

(b) midspan rotation at the maximum load versus the imperfection

Figure 4.16: Imperfection sensitivities of the system (Mode 2).

The sensitivity to geometrical imperfections has also been presented from the investigation. The results indicate that the optimized prestress that allows designers to obtain the maximum strength is located in somewhere in Zone 3, although previously this value has been considered to be at the boundary of Zones 2 and 3 from linear buckling analysis (Hafez *et al.*, 1979). Despite these findings, the exact value of the optimized prestress is still undetermined due to the lack of a rational indicator for optimization; an issue that needs further investigation and is discussed in Chapter 6. However, in the next chapter another important aspect for design, i.e. interactive buckling, is discussed.

Chapter 5

Interactive Buckling

5.1 Introduction

In the previous chapter, the post-buckling behaviour of the stayed column was modelled analytically with geometric imperfections, and possible structural failure points were located on the equilibrium path. Although realistic behaviour of the stayed column was presented for distinct mode buckling, the model still ignores another practical important aspect: interactive buckling. Interactive buckling is a phenomenon in which buckling modes with different wavelengths are triggered simultaneously. It has been reported as quite a notorious phenomenon for structural safety from previous work (Thompson & Hunt, 1984; Hunt, 1986). For the stayed column, the levels of the buckling loads for Modes 1 and 2 are often close together; therefore, interactive buckling would potentially occur as a combination of Modes 1 and 2 (see Figure 5.1); it would be necessary to take into account interactive buckling behaviour in order to achieve structural safety in design. Despite the potential importance of this type of behaviour, interactive buckling in the stayed column has not been investigated at all in previous work.

This chapter describes differences in the buckling responses between distinct mode buckling and interactive buckling. In order to facilitate this comparison, the interac-

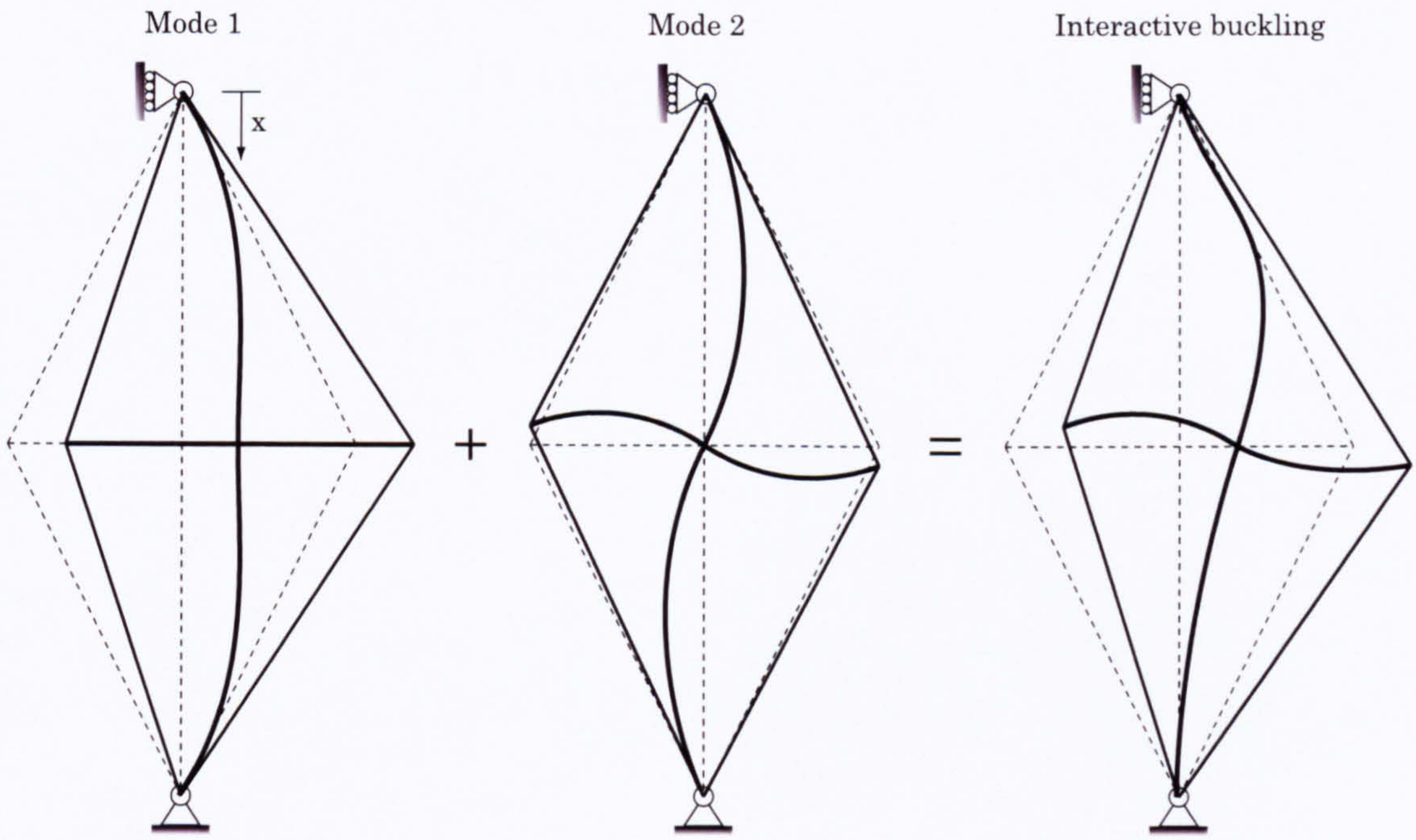

Figure 5.1: Interactive buckling of the stayed column.

tive buckling response was obtained using the code ABAQUS (ABAQUS, 2006). It was revealed that interactive buckling becomes the worst case where Mode 2 governs in the critical load analysis.

5.2 Methodology

5.2.1 Imperfection

The current investigation involves FE analysis; Riks analysis was conducted using the code ABAQUS to reveal equilibrium paths for interactive buckling. Firstly, using FEM, buckling analysis was conducted to obtain values of the critical load for distinct mode buckling, which led to the evaluation of the benchmark prestress T_{opt}; subsequently, the interactive buckling behaviour was investigated with the obtained prestress.

Formulation of the FE model follows the same process stated as in §3.4.3. As mentioned earlier, there are a few examples of post-buckling equilibrium paths for

stayed columns in previous work (Temple *et al.*, 1984; Smith, 1985; De Araujo *et al.*, 2006); however, investigations into interactive buckling have not been attempted.

A more complicated shape of initial out-of-straightness is needed to induce interactive buckling, rather than a simple shape based on a distinct buckling mode, which was adopted in the analysis performed in Chapters 3 and 4. In this study, imperfection shapes were created by combining a half sine wave and a full sine wave, ensuring that the interaction between Modes 1 and 2 behaviour would be induced. Thus, the shape function for the imperfection was expressed as follows:

$$\begin{aligned} W_\delta(x) &= W_{1\delta}(x) + W_{2\delta}(x) \\ &= \delta L \left[\mu_1 \sin \frac{\pi x}{L} + \mu_2 \sin \frac{2\pi x}{L} \right], \end{aligned} \tag{5.1}$$

where μ_1 and μ_2 are coefficients for the components of the imperfection, expressing a proportion of each wave.

In order to investigate the transition from Modes 1 to 2 buckling through interactive buckling, different combinations of magnitudes of a half sine wave and a full sine wave were selected. As already stated in §3.4.3, amplitudes of the imperfection were selected in order that the end-shortening caused by the initial out-of-straightness would be the same (Wadee, 2000), thus

$$\int_0^L \frac{1}{2} \left[W_{1\delta}'^2(x) + W_{2\delta}'^2(x) \right] \mathrm{d}x = \mathcal{E}_0, \tag{5.2}$$

where $\mathcal{E}_0$ is the first order approximation of the end-shortening caused by the initial out-of-straightness, which yields the following equation:

$$\mu_1^2 + 4\mu_2^2 = 1. \tag{5.3}$$

From the above equation, the combinations given in Table 5.1 were obtained. As for the basic amplitude of the imperfection δ, 1/300 was generally selected to obtain the actual level of the design load from the equilibrium path. As mentioned earlier, this

Case	Coefficients	
	μ_1	μ_2
Mode 1	1.000	0
Case 1	0.750	0.3307
Case 2	0.500	0.4330
Case 3	0.250	0.4841
Mode 2	0.000	0.5000

Table 5.1: Selected combinations of μ_1 and μ_2 for the imperfection.

value represents the recommended level of an initial local bow imperfection in the global analysis of frames for hot finished sections in Eurocode 3 (EN1993-1-1, 2005), accounting for the effects of all types of imperfection, including residual stress and geometrical imperfections, such as lack of straightness and any minor eccentricities present in joints.

5.2.2 Prestress

From Zone 3, the two different values of the initial prestress, T_{opt} and $2T_{\text{opt}}$, were selected to investigate changes in the interactive buckling responses. Zones 1 and 2 behaviour were basically not investigated as it was shown that the optimal value of T was located in Zone 3 from the previous chapter; thus, investigating Zones 1 and 2 would be superfluous for practical design.

Although in the previous chapters, T_{opt} was derived through the analytical model, in this section, T_{opt} was obtained from Hafez's work (1979) with assistance from the FEM, which provides more accurate values of T_{opt} as the analytical model involves a certain degree of error especially in Mode 2. According to his analysis, T_{opt} is expressed as

$$T_{\text{opt}} = P_{\text{max}}^{\text{C}} C_{11}, \tag{5.4}$$

where,

$$C_{11} = \frac{\cos\alpha}{2K_c\left(\frac{1}{K_s} + \frac{2\sin^2\alpha}{K_a} + \frac{2\cos^2\alpha}{K_c}\right)}, \tag{5.5}$$

in which K_c K_s and K_a are the axial stiffness of the column, the stay and the crossarm respectively, expressed as follows:

$$K_c = \frac{EA}{L}, \quad K_s = \frac{E_s A_s}{L_s}, \quad K_a = \frac{E_a A_a}{a}, \tag{5.6}$$

and $P^{\mathrm{C}}_{\mathrm{max}}$ is calculated by

$$P^{\mathrm{C}}_{\mathrm{max}} = \frac{P^{\mathrm{C}}_{\mathrm{Zone3,T=0}}}{C_{22}}, \tag{5.7}$$

where $P^{\mathrm{C}}_{\mathrm{Zone3,T=0}}$ is the critical load calculated from FE analysis when $T = 0$, and C_{22} is

$$C_{22} = 1 + \frac{\cos^2\alpha}{K_c\left(\dfrac{1}{K_s} + \dfrac{2\cos^2\alpha}{K_a}\right)}. \tag{5.8}$$

5.2.3 Assumption

The same assumptions were also made for the analysis in this chapter as those shown in §3.1.1 except that the column is perfectly straight. Note that in this chapter, all of the structural components are purely elastic in order to focus on the interactive buckling response.

5.3 Numerical Results

The investigation was conducted with the two parameters, the crossarm length a and the stay diameter ϕ_s, varying. Firstly, using the FEM, buckling analysis was conducted to obtain values of the prestress T_{opt} through equations (5.4) and (5.7). Subsequently, the interactive buckling behaviour was investigated with the obtained prestress.

The same dimensions and properties as in §3.3.1 were also applied. The stay diameter ϕ_s was varied from 1.6 mm to 10.0 mm with a classification of F1 to F6 (see Table 5.2) while the crossarm length a was fixed to $a = 305$ mm, and the crossarm

length a was varied from 76.25 mm to 457.5 mm with a classification of a1 to a6 (see Table 5.3) while the stay diameter was fixed to $\phi_s = 4.8$ mm.

5.3.1 Buckling analysis

Figures 5.2 and 5.3 show the buckling load $P^{\mathrm{C}}_{\mathrm{max}}$ with a variation of ϕ_s and a re-

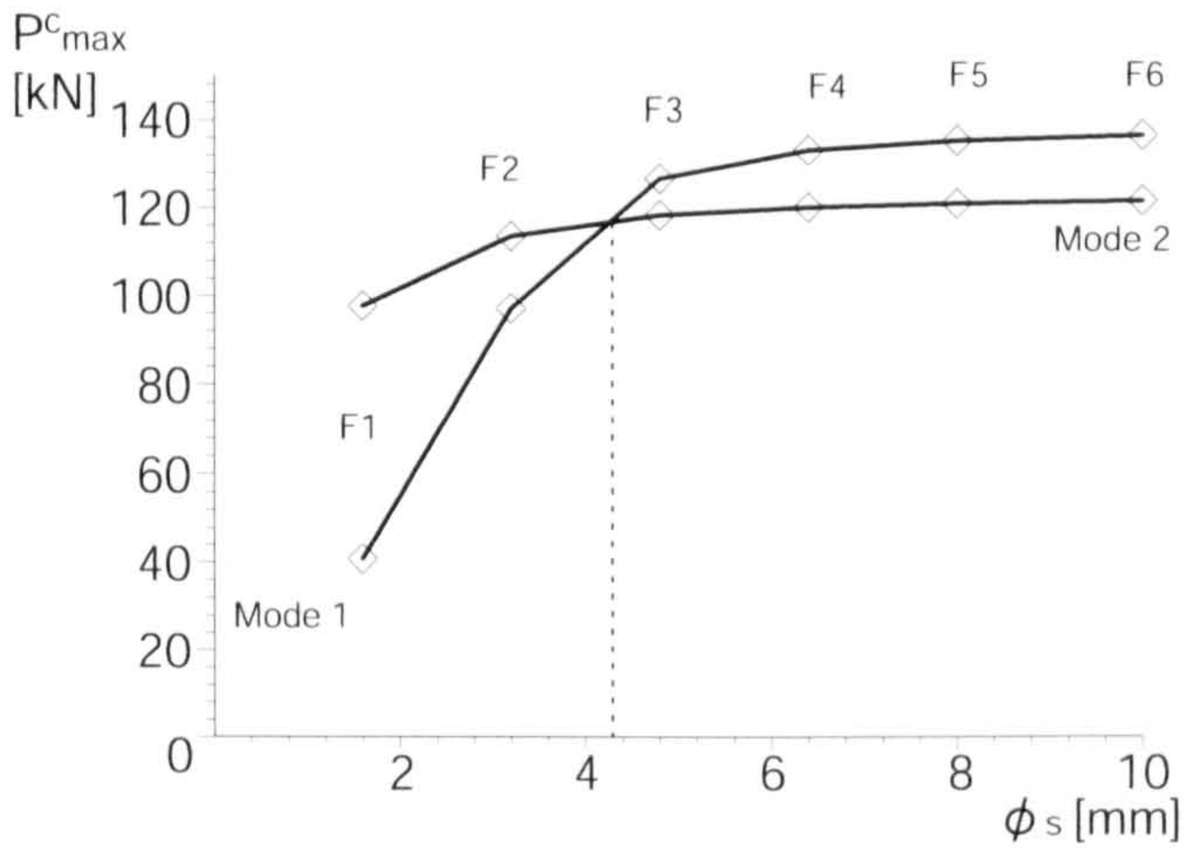

Figure 5.2: Buckling loads with the stay diameter ϕ_s varying.

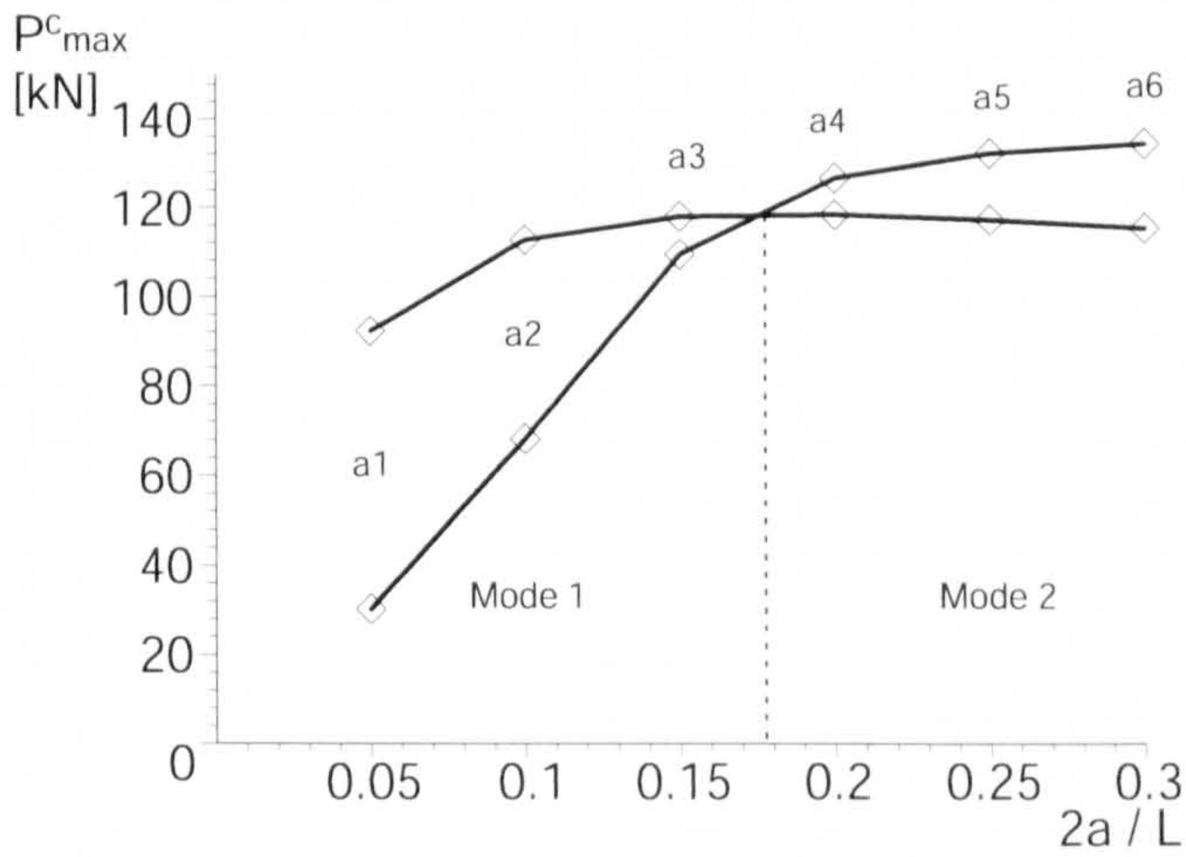

Figure 5.3: Buckling loads with the crossarm length a varying.

spectively. As can be seen, when the stay diameter ϕ_s is small, such as F1 and F2, Mode 1 becomes the governing mode, and when the stay diameter ϕ_s is large, such

as the cases of F3 to F6, Mode 2 becomes the governing mode. Similarly, when the crossarm length a is short, such as a1 to a3, Mode 1 becomes the governing mode, and when the crossarm length a is long, such as a4 to a6, Mode 2 becomes the governing mode. These relationships between the buckling modes and the structural configurations were already reported in previous work (Smith *et al.*, 1975; Hafez *et al.*, 1979; Hathout *et al.*, 1979). Substituting these values of $P_{\max}^{C}$ into equation (5.4), values of T_{opt} were obtained as represented in Tables 5.2 and 5.3.

Case	ϕ_s (mm)	T_{opt} (kN)	Buckling Mode
F1	1.6	0.12	1
F2	3.2	1.16	1
F3	4.8	3.10	2
F4	6.4	5.39	2
F5	8.0	8.08	2
F6	10.0	11.79	2

Table 5.2: Linear optimum prestress T_{opt} and governing buckling mode with the stay diameter ϕ_s varying.

Case	a (mm)	T_{opt} (kN)	Buckling Mode
a1	76.25	0.82	1
a2	152.5	1.84	1
a3	228.75	2.91	1
a4	305	3.10	2
a5	381.25	3.01	2
a6	457.5	2.89	2

Table 5.3: Linear optimum prestress T_{opt} and governing buckling mode with the crossarm length a varying.

5.3.2 Interactive buckling behaviour

In this section, the interactive buckling behaviour was investigated through Riks analysis in ABAQUS with the values of T_{opt} obtained from buckling analysis. It is evident from the results that the interactive buckling has a substantial effect on the buckling behaviour with certain configurations.

Figures 5.4 and 5.5 show the equilibrium paths with a variation of the stay diameter

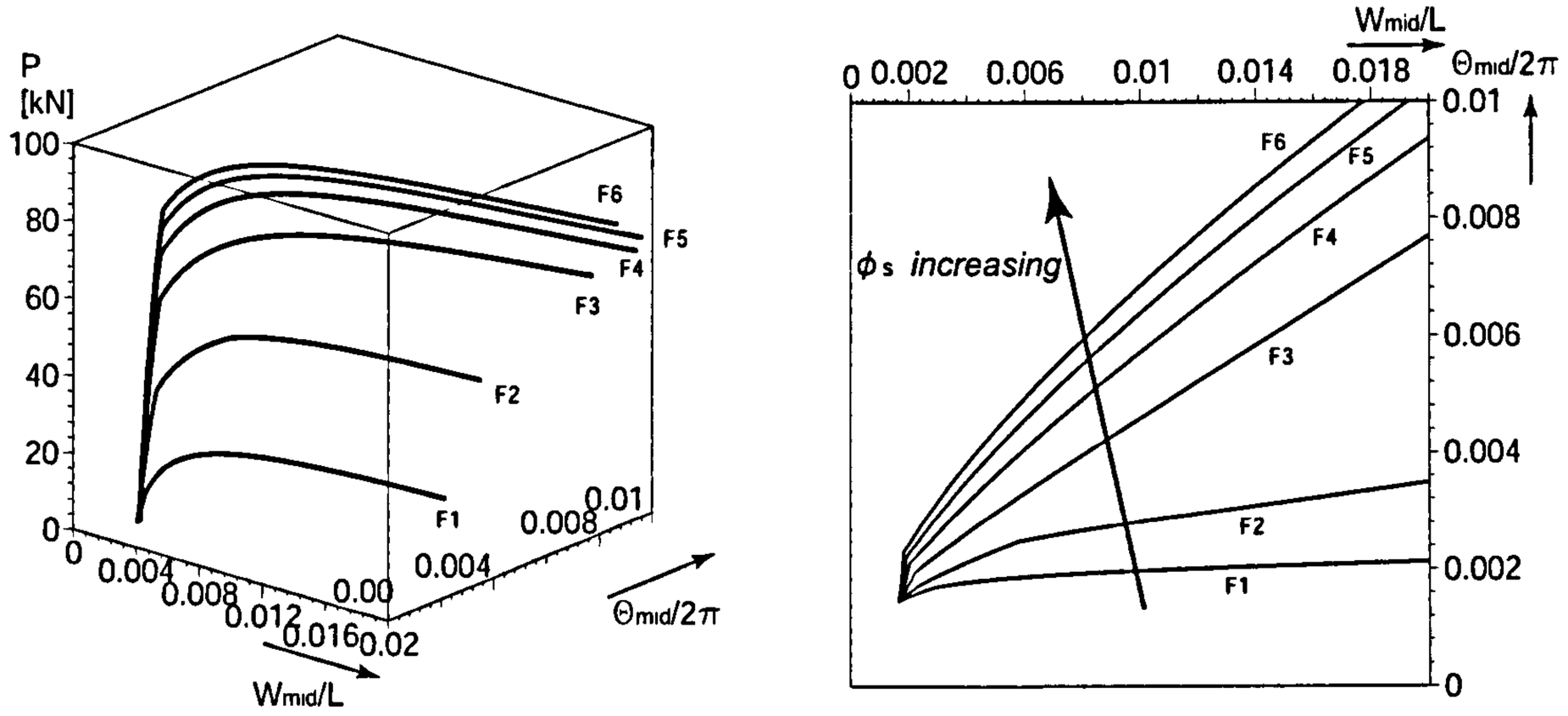

(a) axial load P against the nondimensionalized midspan displacement W_{mid}/L and the nondimensionalized midspan rotation $\Theta_{\text{mid}}/2\pi$

(b) nondimensionalized midspan displacement W_{mid}/L versus the nondimensionalized midspan rotation $\Theta_{\text{mid}}/2\pi$

Figure 5.4: Equilibrium paths with the stay diameter ϕ_s varying when the imperfection combination is Case 2.

ϕ_s and the crossarm length a respectively when the Case 2 imperfection combination was adopted. As can be seen, when the stay diameter ϕ_s is small or the crossarm length a is short, the rotation (Mode 2) component in displacement is rather small, and therefore, the behaviour seems to be rather similar to Mode 1 buckling. However, the larger the stay diameter ϕ_s or the longer the crossarm length a, the larger the midspan rotation component Θ_{mid} in displacement becomes in comparison with the midspan displacement W_{mid}, which apparently leads the buckling to being more interactive.

These results are also observed from Figures 5.6 and 5.7 showing the equilibrium paths represented by the axial load P versus the end-shortening Δ. When the diameter ϕ_s is small or the crossarm length a is short, i.e. Mode 1 is critical, the lowest maximum load capacity is seen from the Mode 1 buckling path such as F2, a2, and a3, implying that Mode 1 is the most important of all of the combinations. However, when the diameter ϕ_s becomes larger or the crossarm length a is longer,

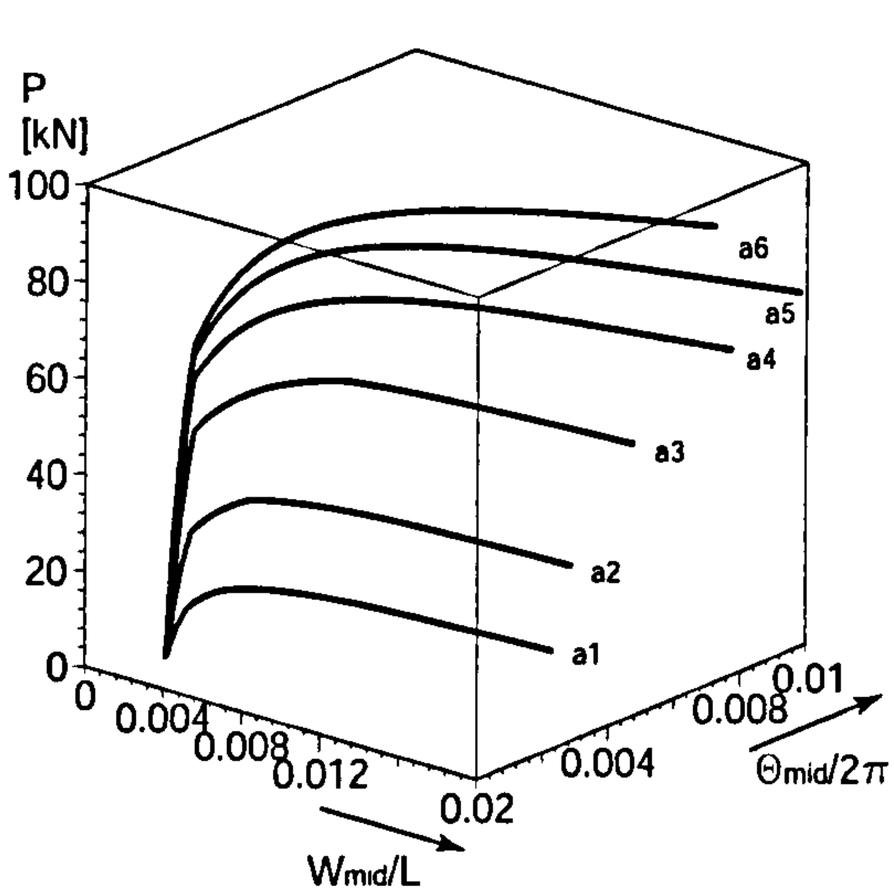

(a) axial load P against the nondimensionalized midspan displacement W_{mid}/L and the nondimensionalized midspan rotation $\Theta_{\text{mid}}/2\pi$

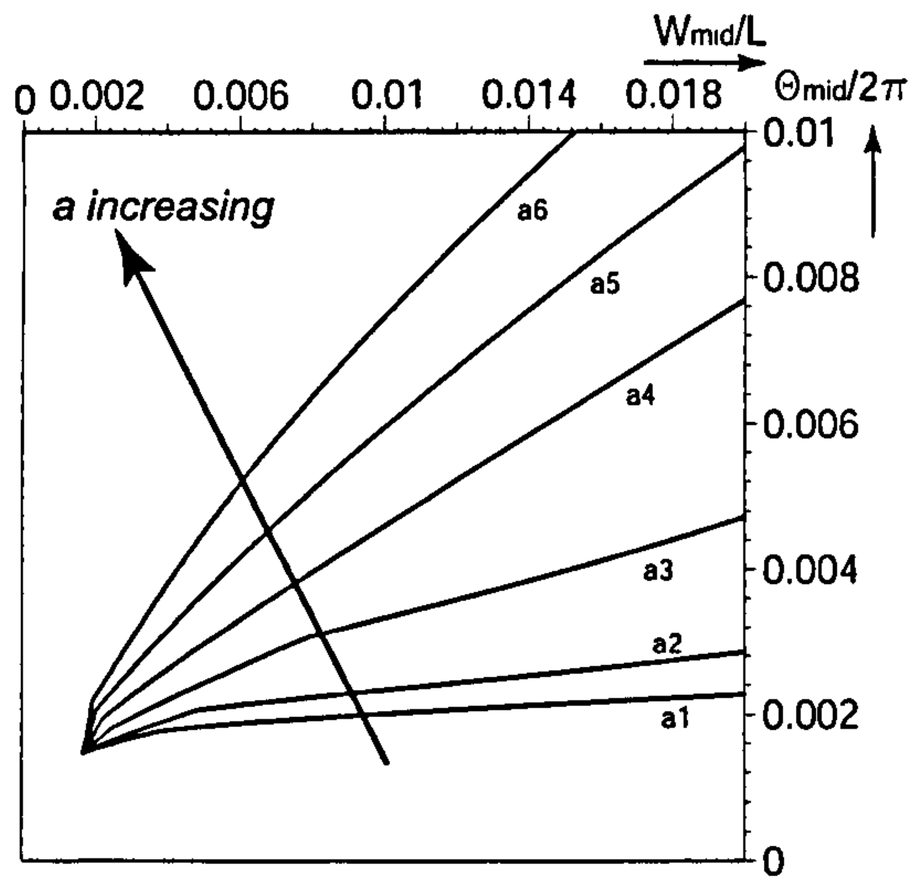

(b) nondimensionalized midspan displacement W_{mid}/L versus the nondimensionalized midspan rotation $\Theta_{\text{mid}}/2\pi$

Figure 5.5: Equilibrium paths with the crossarm length a varying when the imperfection combination is Case 2.

i.e. Mode 2 is critical, the lowest maximum load capacity is seen from one of the interactive buckling cases such as F3, F4, F5, a4 and a5, implying that interactive buckling governs the nonlinear behaviour. The results suggest that when Mode 1 is the governing mode in buckling analysis, interactive buckling behaviour is less important, but when Mode 2 is the governing mode, interactive buckling gains importance, giving a lower maximum load capacity than those with the distinct buckling modes.

These results are summarized in Figure 5.8 showing the maximum load capacity in conjunction with the critical loads P^{C} with a variation of the stay diameter ϕ_s and the crossarm length a respectively, when the Case 2 imperfection combination was adopted for interactive buckling. As can be seen, when Mode 1 is critical, the lowest maximum load capacity can also be seen in Mode 1, whereas when Mode 2 is critical, the maximum load capacity is always seen in the interactive cases. The largest difference in maximum load capacity between distinct and interactive modes can be seen where the curves for the Modes 1 and 2 load capacities are crossing over;

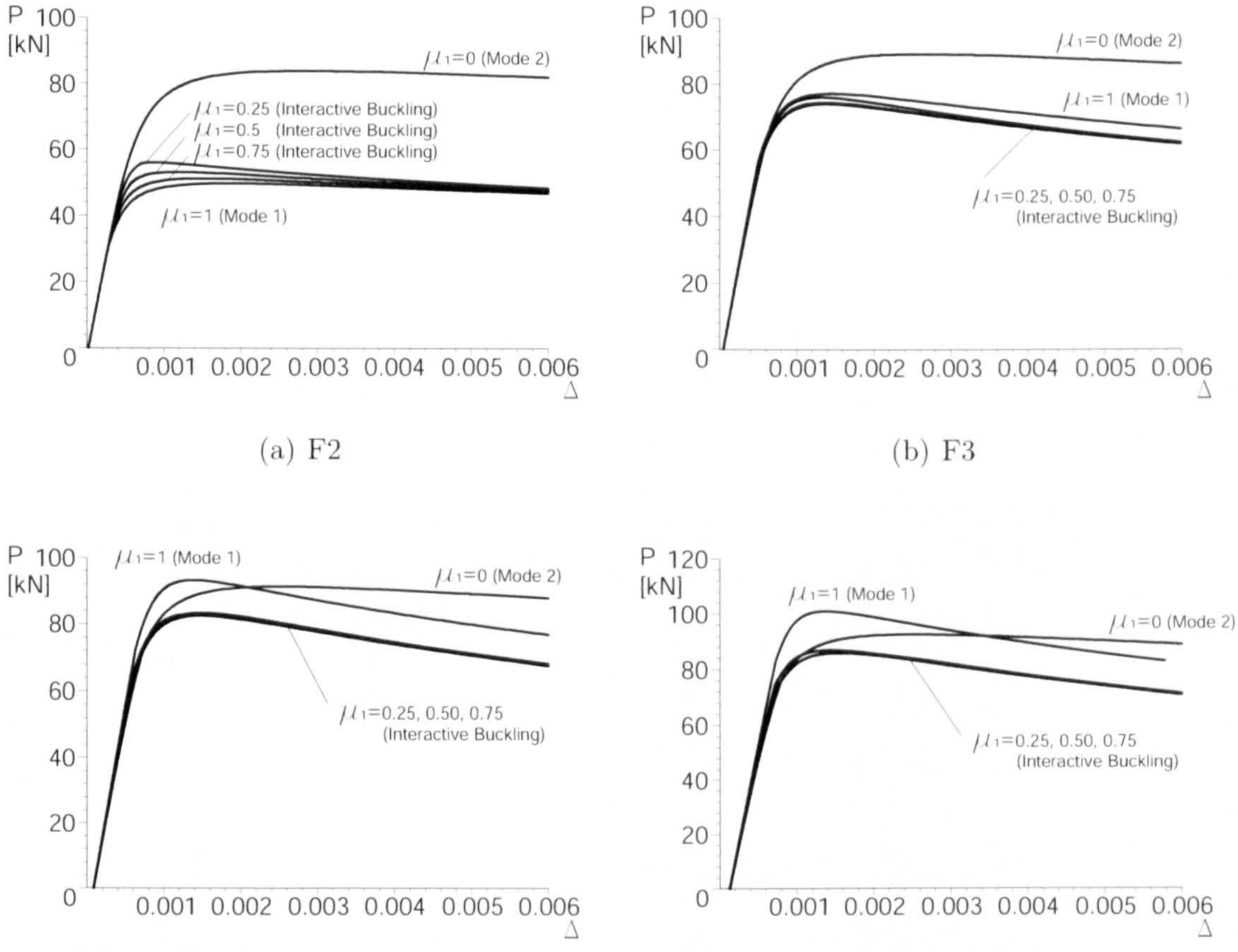

(a) F2

(b) F3

(c) F4

(d) F5

Figure 5.6: Equilibrium paths represented by the axial load P versus the end-shortening Δ with the stay diameter ϕ_s varying.

it appears that this is the place where the effect of interactive buckling is the most significant. It should be noted that as the curves for the maximum load capacity vary with the level of imperfection, the place where interactive buckling is most significant would also change with it.

The difference in the significance of interactive buckling among the different configurations can also be recognized from the stress state in the stays. Figure 5.9 plots the axial force in each stay against the end-shortening Δ, when the Case 2 imperfection combination was adopted. As can be seen from (a), (d) and (e) in Figure 5.9, in the cases of F2, a2 and a3, where Mode 1 is the lowest mode from eigenvalue analysis, Stays 3 and 4 go slack; this suggests that the buckling behaviour is rather close to

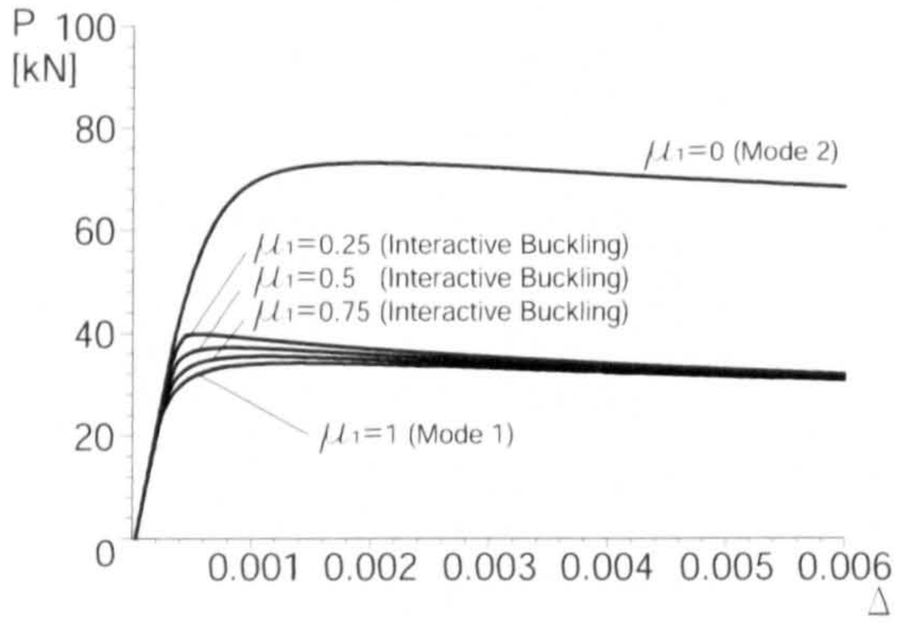

(a) a2

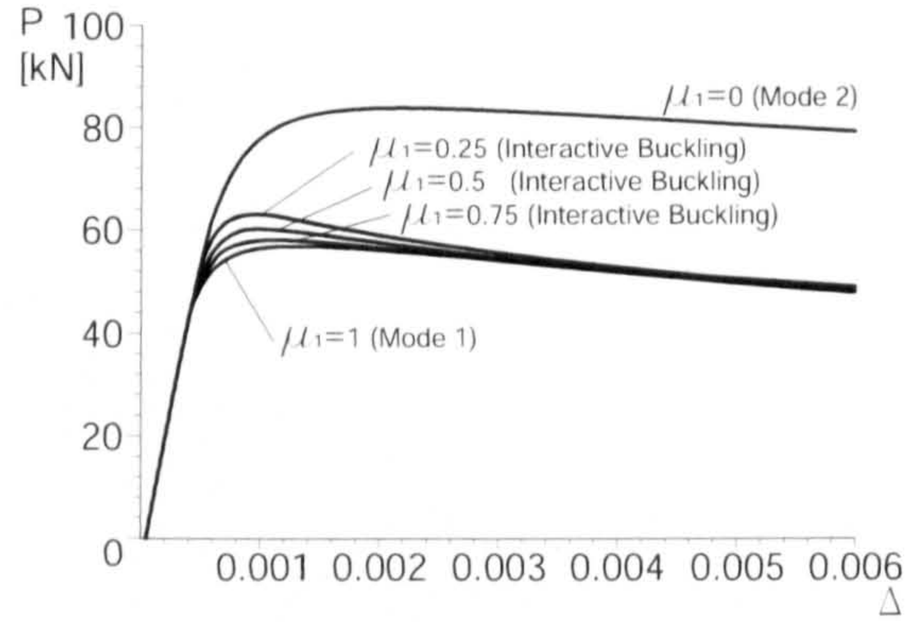

(b) a3

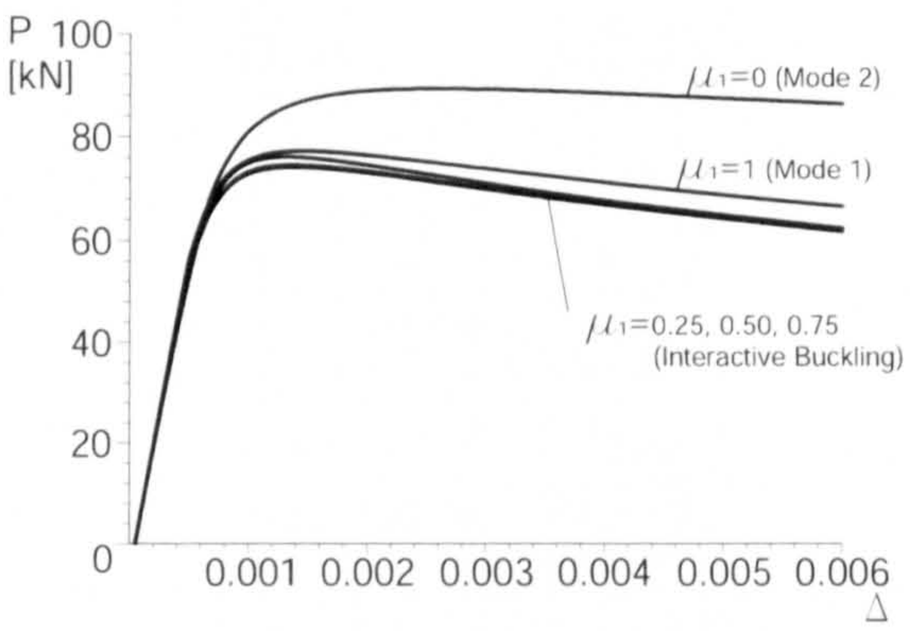

(c) a4

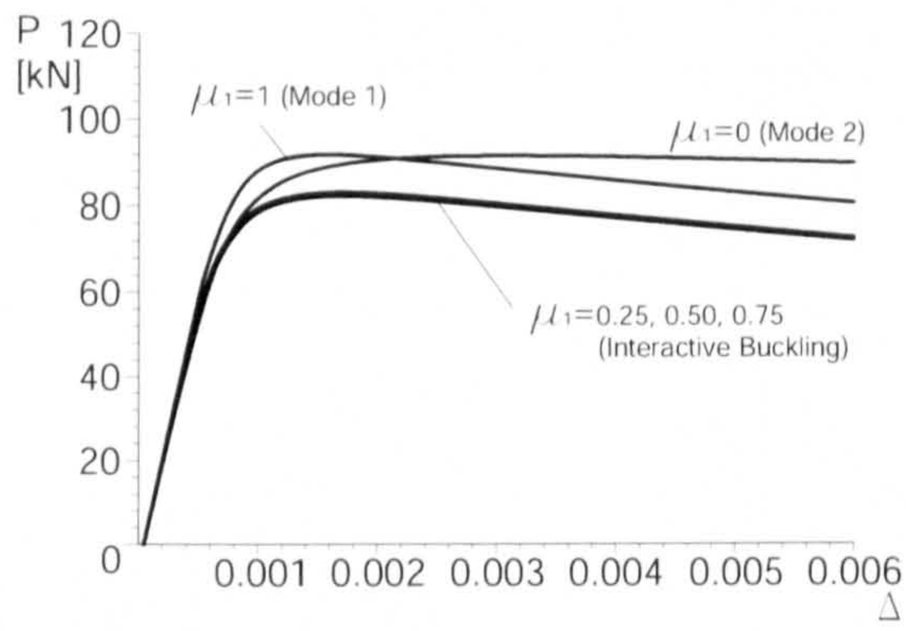

(d) a5

Figure 5.7: Equilibrium paths represented by the axial load P versus the end-shortening Δ with the crossarm length a varying.

Mode 1 although their deflections are in common with interactive buckling to some extent. In the cases of F3, F4, a4 and a5, where Mode 2 is the lowest mode from eigenvalue analysis, only Stay 4 goes slack, and the three stays are active after the slackening, implying that interactive buckling is substantially stronger rather than the cases of F2, a2 and a3. These results suggest that the interactive behaviour is strongly linked to their critical buckling responses.

Figures 5.10 and 5.11 show the maximum load capacity plotted against the different combinations of the initial imperfections, which are presented in Table 5.1, with a variation of the parameter ϕ_s and a respectively. As can be seen, when Mode 1 is critical, the lowest maximum load capacity is also seen in Mode 1; however, when

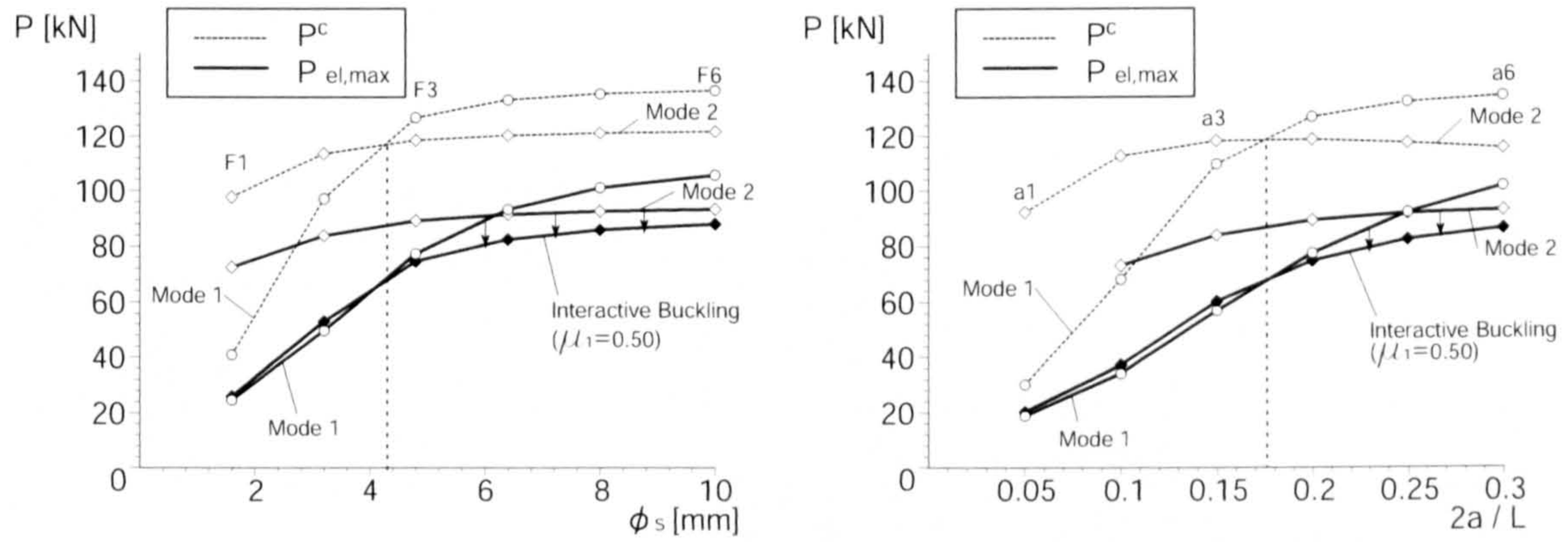

(a) stay diameter ϕ_s varying

(b) crossarm length a varying

Figure 5.8: Maximum load capacity $P_{\mathrm{el,max}}$ in conjunction with critical loads P^{C} at $T = T_{\mathrm{opt}}$.

Mode 2 is critical, the maximum load capacity is always seen in the interactive cases. It can also be observed from the figures that there are only small differences within the interactive buckling region regardless of different combinations of μ_1 and μ_2. This result indicates that the interactive buckling behaviour is relatively insensitive to the combination of the imperfections, but some non-trivial combination appears to be necessary.

In this section, the interactive buckling response has been examined from various aspects when the prestress T is set to T_{opt}. The results presented in this section indicate that interactive buckling behaviour is linked to its configuration rather than the assumed imperfection shapes, and that with the configuration where interactive buckling is important, i.e. Mode 2 is the governing mode in buckling analysis, interactive buckling needs to be examined for design, especially in the place where the maximum load capacities for Modes 1 and 2 coincide, where the interactive effect seems to be the strongest.

5.3.3 Sensitivity to prestress

Since it was revealed from Chapters 3 and 4 that the buckling response is strongly linked to the magnitude of the prestress, the effect of an increase in the initial prestress was also investigated; FE analysis was conducted, adopting two different levels of the prestress, T_{opt} and $2T_{\text{opt}}$. It is evident from the results that an increase in the prestress from T_{opt} would be advantageous for designers. Figures 5.12 and 5.13 compare that the buckling responses with $T = T_{\text{opt}}$ and $T = 2T_{\text{opt}}$.

The diagrams are represented by the axial load P versus the end-shortening Δ with a variation of the parameters ϕ_s and a respectively, while the Case 2 imperfection combination was adopted. Clearly, the diagram indicates that increasing the prestress allows a rise in the maximum load capacity even for the case of interactive buckling. This trend has already been seen in the distinct mode buckling results in Chapter 4. It should, however, noted that after the peak loads the response is more unstable at $T = 2T_{\text{opt}}$ than at $T = T_{\text{opt}}$. Although this type of instability is not favourable in structural stability, "snap-back", a sudden reduction in the load carrying capacity during the rigid loading, is not observed; therefore, the maximum load capacity would be still used as the design load without adopting an additional safety factor, i.e. the increase in the maximum load is simply thought to be an advantage.

Figures 5.14 and 5.15 show the maximum load capacity with a variation of the parameter ϕ_s and a respectively when $T = T_{\text{opt}}$ and $T = 2T_{\text{opt}}$. It can also be observed that increasing the prestress results in a rise in the maximum load capacity in every combination of the imperfections.

As mentioned earlier in the thesis, although the maximum buckling load $P^{\text{C}}_{\text{max}}$ can be seen at $T = T_{\text{opt}}$, T_{opt} is not the true optimal prestress value, and introducing the level of prestress to be greater than T_{opt} would be recommended in practice in terms of the post-buckling response and the maximum load capacity for distinct mode buckling. As an increase in T from T_{opt} also increases the maximum load

capacity for the interactive buckling cases (Mode 2 critical), this recommendation also appears to apply to interactive buckling currently being considered.

5.3.4 Sensitivity to imperfections

Since the sensitivity to imperfections is also considered to be an important factor to account for the interactive buckling response, the effect of the level of the imperfection was examined, comparing the cases adopting different basic values of the imperfection. A variation of the basic amplitude of the imperfection δ was selected from Table 4.2 with the Case 2 imperfection combination being chosen. Imperfection combination Cases 1 and 3 were not investigated as it has already been shown in this chapter that the post buckling response is relatively insensitive to the combination of the imperfections; thus investigating those combinations would be superfluous. As for the structural configuration, a4/F3, which is the basic configuration used in the analysis in Chapters 3 and 4, was adopted. With these input values, FE analysis was conducted to reveal the buckling response for each imperfection. In general, the sensitivity to the imperfection size is very similar to the cases for distinct mode buckling. Figure 5.16 shows the buckling behaviour with different levels of the imperfection.

The diagrams are represented by the axial load P versus the end-shortening Δ with a variation of the basic imperfection δ and the prestress T when the Case 2 imperfection combination was adopted. Comparing Figure 5.16 with Figures 4.9 and 4.10, it is obvious that the buckling response is very similar to the distinct mode cases. It should be noted that when $T = T_{\text{opt}}$ and $\delta = 1/10000$, which presents a nearly perfect state in FE analysis, the most significant drop can be seen from the peak load. This result is parallel to the finding in Chapter 3, which shows that the prestress $T = T_{\text{opt}}$ yields the most unstable post-buckling response in a perfect case. It is therefore conjectured that the introduction of the prestress $T = T_{\text{opt}}$ also promotes the most unstable path in the interactive post-buckling behaviour in a perfect state as well.

Figure 5.17 shows the maximum load capacity $P_{\text{el,max}}$ against the amplitude of the basic imperfection δ. As can be seen, the maximum strength is the most sensitive to the imperfection at $T = T_{\text{opt}}$, and this significant sensitivity is apparently mitigated by increasing the level of the prestress. The increase in the prestress also contributes to yielding higher values of the maximum load capacity. These results also correlate with those from Figures 4.15 and 4.16, which present the distinct buckling mode cases. These results also support the recommendation that the initial prestress should be greater than T_{opt}.

In this section, the effect of a variation of the imperfection has been presented to observe the sensitivity to the amplitude of the imperfection in interactive buckling behaviour. It seems that the sensitivity to imperfections is quite similar to that of the distinct modes, which leads to the suggestion that the introduction of the prestress to be greater than T_{opt} would be beneficial when designing against both distinct and interactive buckling.

5.4 Remarks

To the best knowledge of the author, this is the first study to investigate the interactive buckling behaviour of the stayed column. Although previous studies (Temple *et al.*, 1984; Smith, 1985; De Araujo *et al.*, 2006) also examined the buckling behaviour, their focus was only the distinct buckling response. It has been shown from the current study that interactive buckling has a substantial influence on the buckling behaviour.

The results indicate that the interactive buckling behaviour becomes crucial with lower levels of the maximum load capacity when the lowest buckling load is seen in Mode 2, especially where the maximum load capacities for Modes 1 and 2 coincide and the interactive effect seems to be the strongest. From previous studies, the convention has been that when Mode 2 is critical, designing the stayed column against Mode 2 buckling is enough to ensure the safety of the structure; however,

the presented results imply that the interactive buckling behaviour should be taken into account to ensure safety.

It has also been shown that increasing the prestress T from T_{opt} increases the maximum load capacity in interactive buckling and renders the system less imperfection sensitive. Furthermore, it has been postulated from the analysis that the prestress level T_{opt} causes the most unstable response. These results imply that introducing a greater amount of the prestress than T_{opt} would be beneficial to increase the efficiency of the structure. This conclusion is in line with the results obtained in Chapters 3 and 4, which also described that introducing a greater amount of the prestress than T_{opt} would be recommended in terms of the post-buckling response and the maximum load capacity.

Despite these suggestions on the optimal level of the prestress, the exact value of the optimal prestress which allows the best efficiency of the stayed column has not yet been pinpointed due to the lack of a rational indicator for optimization that successfully accounts for nonlinear buckling, which is discussed in the next chapter with all of the information obtained so far including the interactive buckling behaviour.

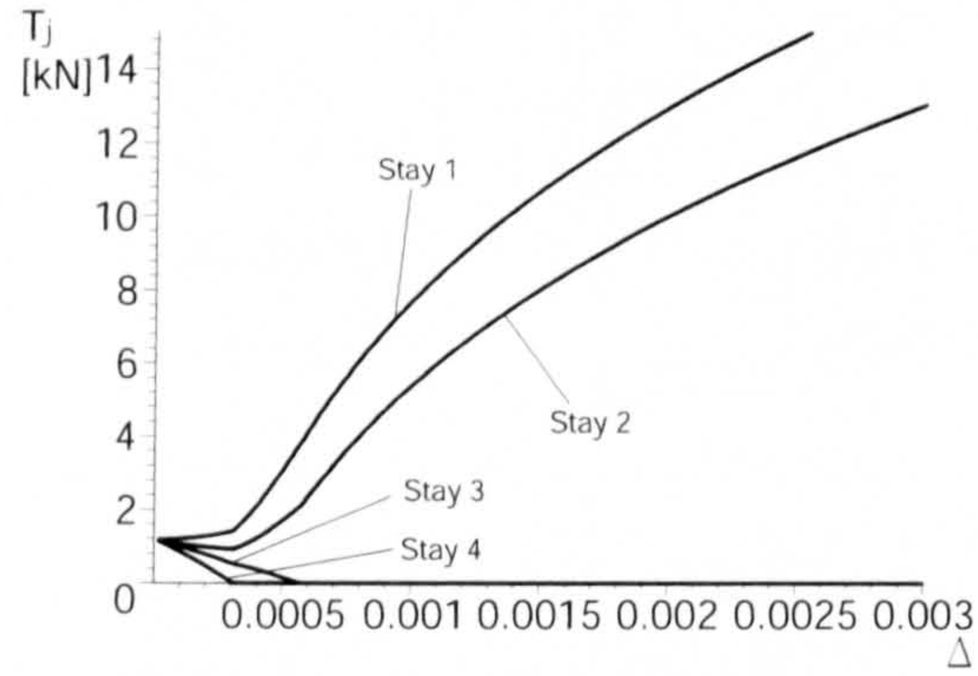

(a) F2 (Mode 1)

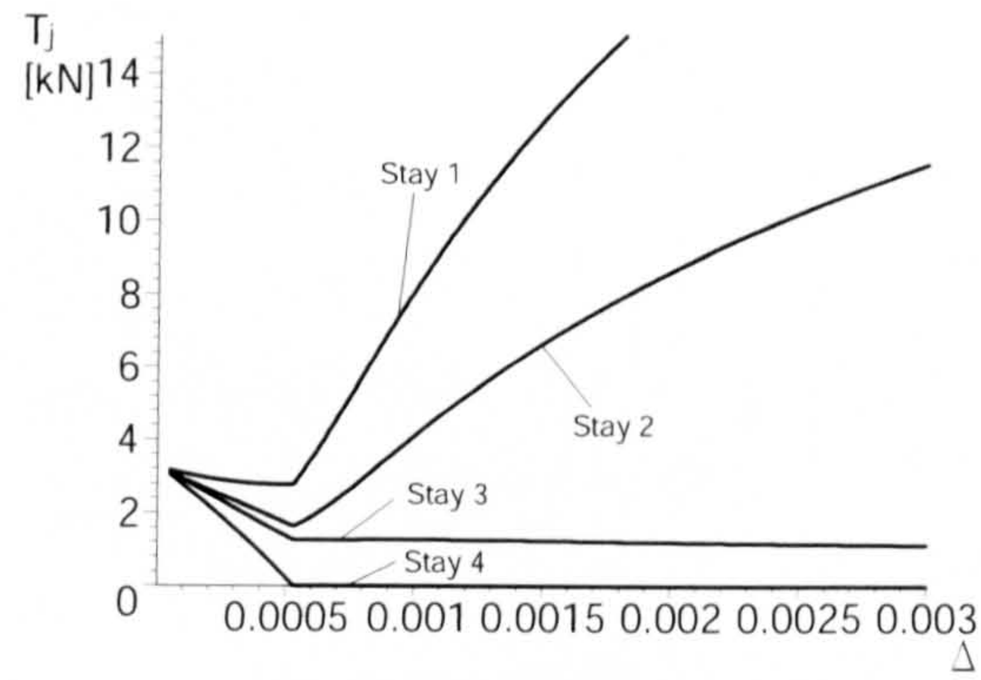

(b) F3/a4 (Mode 2)

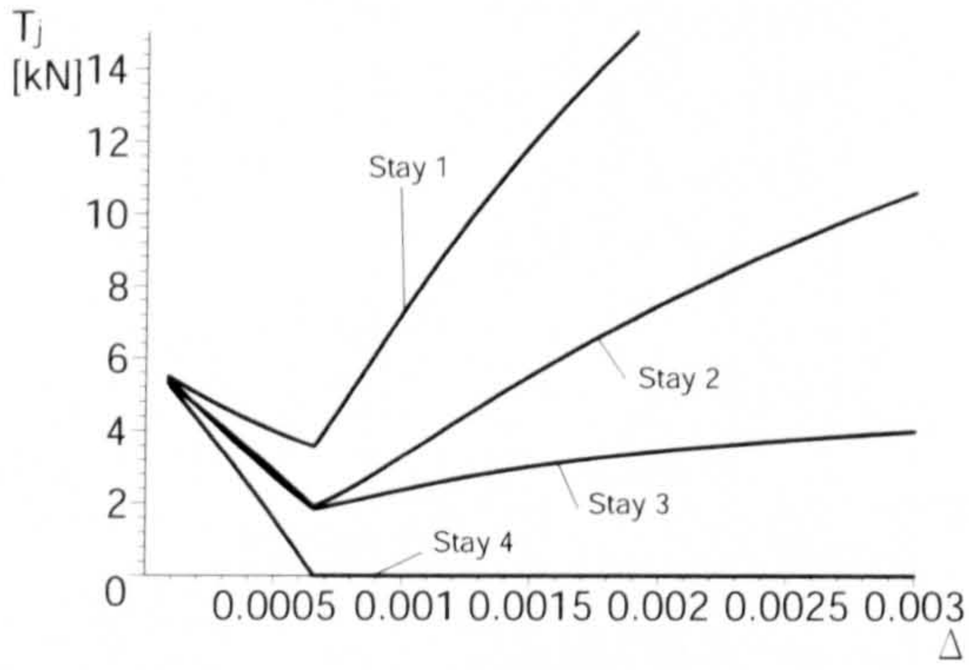

(c) F4 (Mode 2)

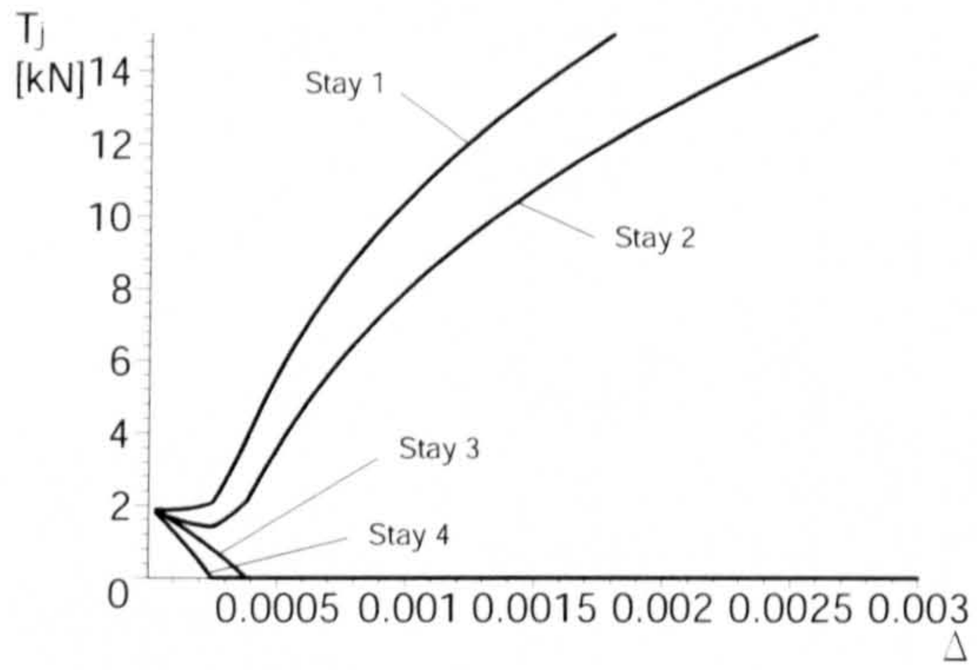

(d) a2 (Mode 1)

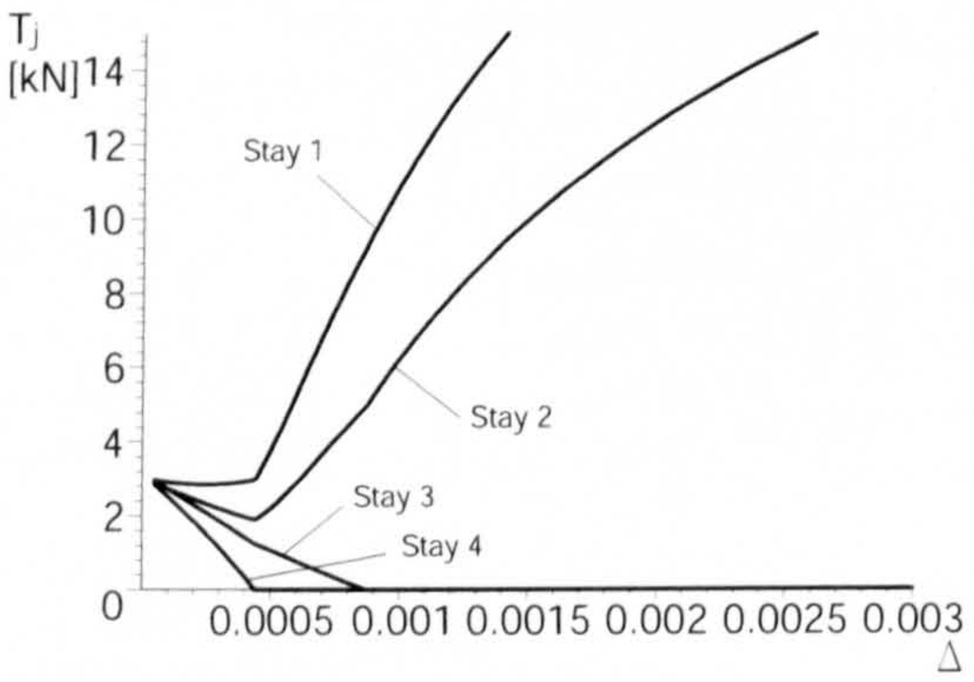

(e) a3 (Mode 1)

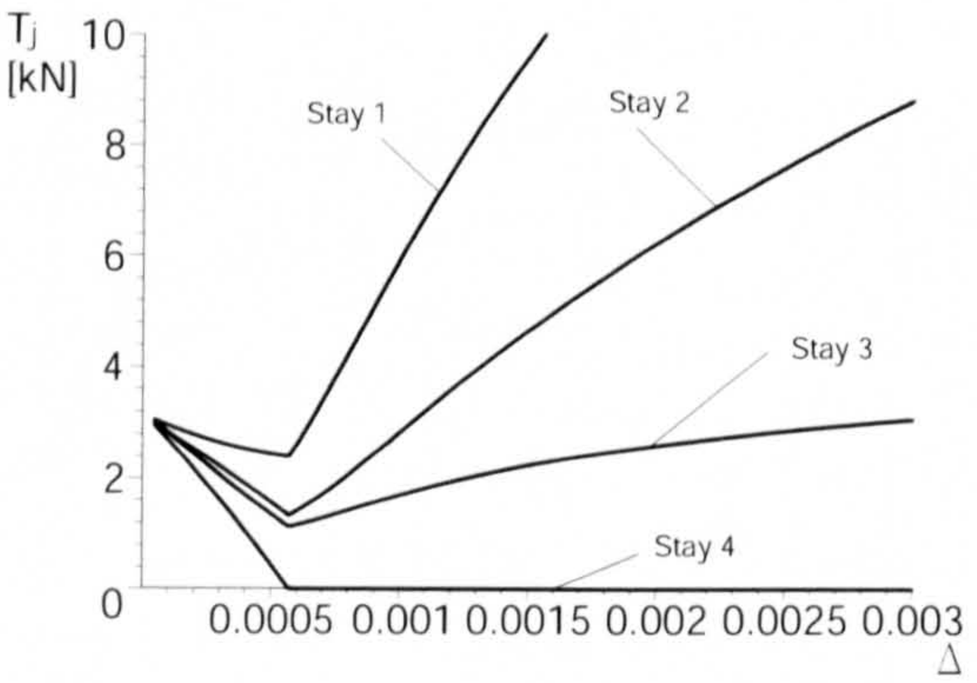

(f) a5 (Mode 2)

Figure 5.9: Transition of the axial forces in the stays T_j when $T = T_{\text{opt}}$, and $\mu_1 = 0.5$. The given modes in the parentheses show the critical buckling mode.

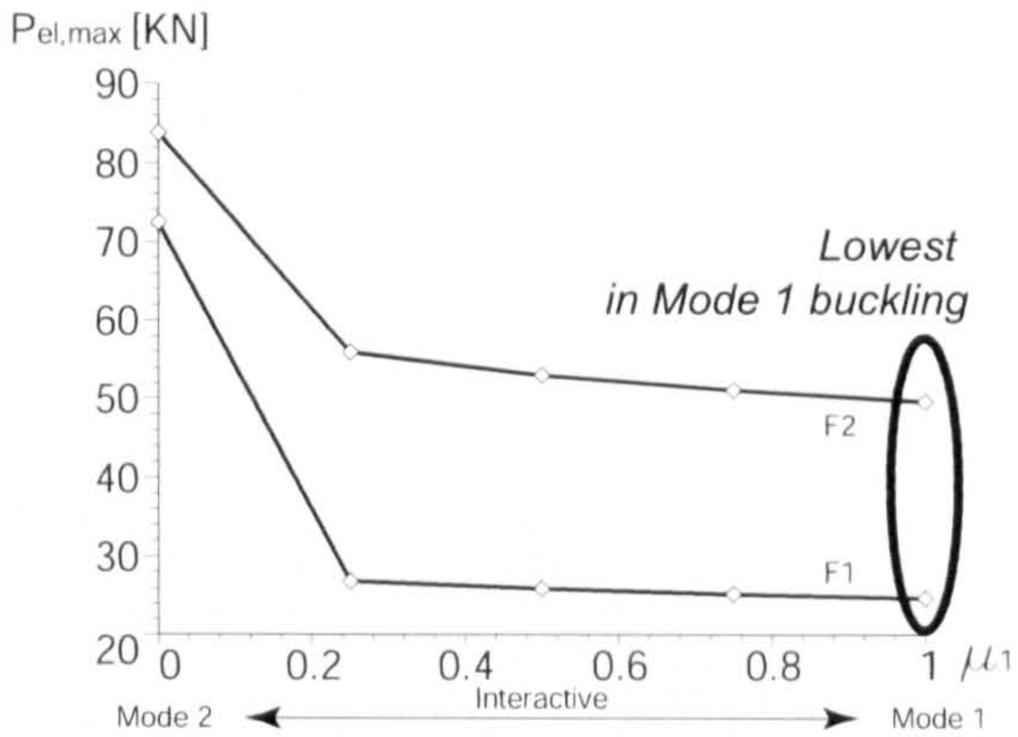

(a) F1–F2

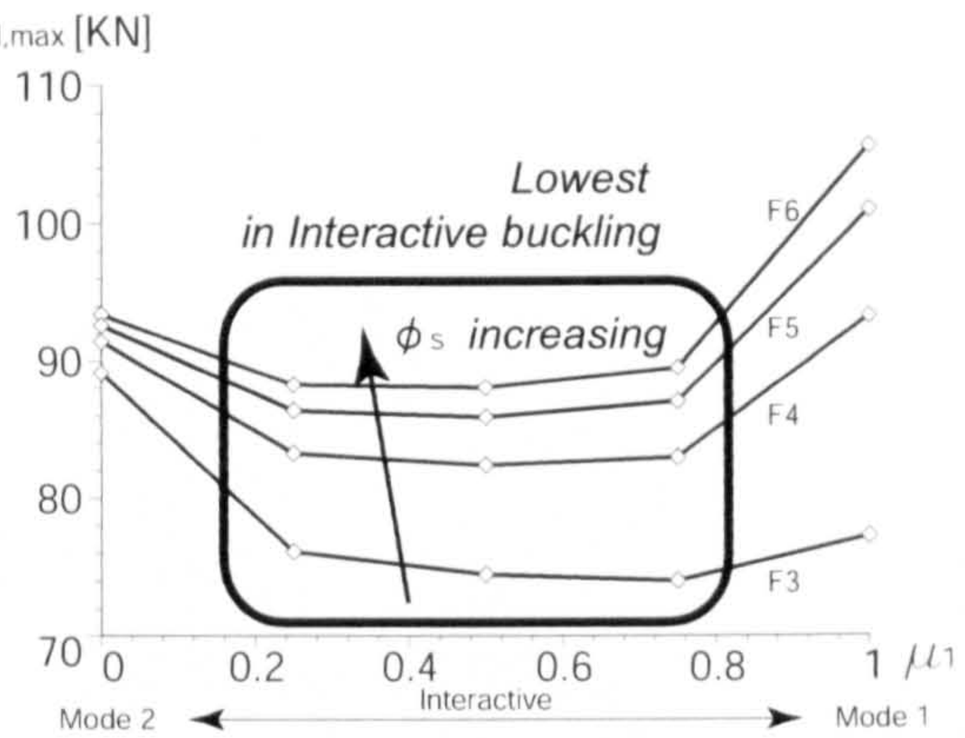

(b) F3–F6

Figure 5.10: Sensitivity to the imperfection combination represented by the maximum load capacity $P_{\max}$ versus μ_1 with the stay diameter ϕ_s varying.

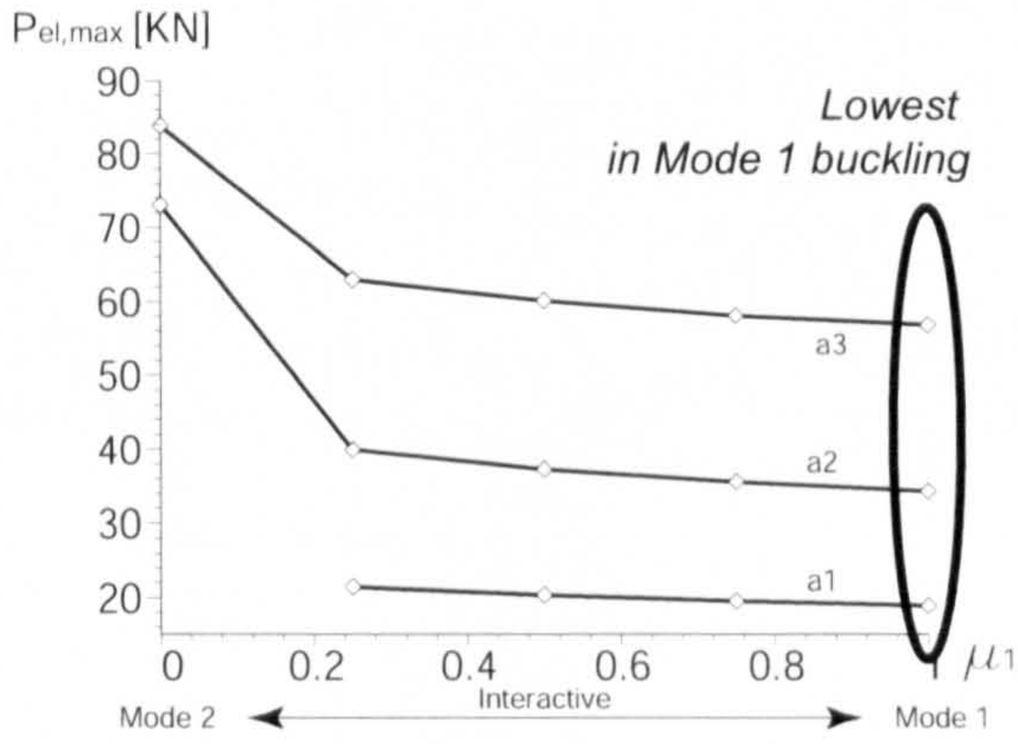

(a) a1–a3

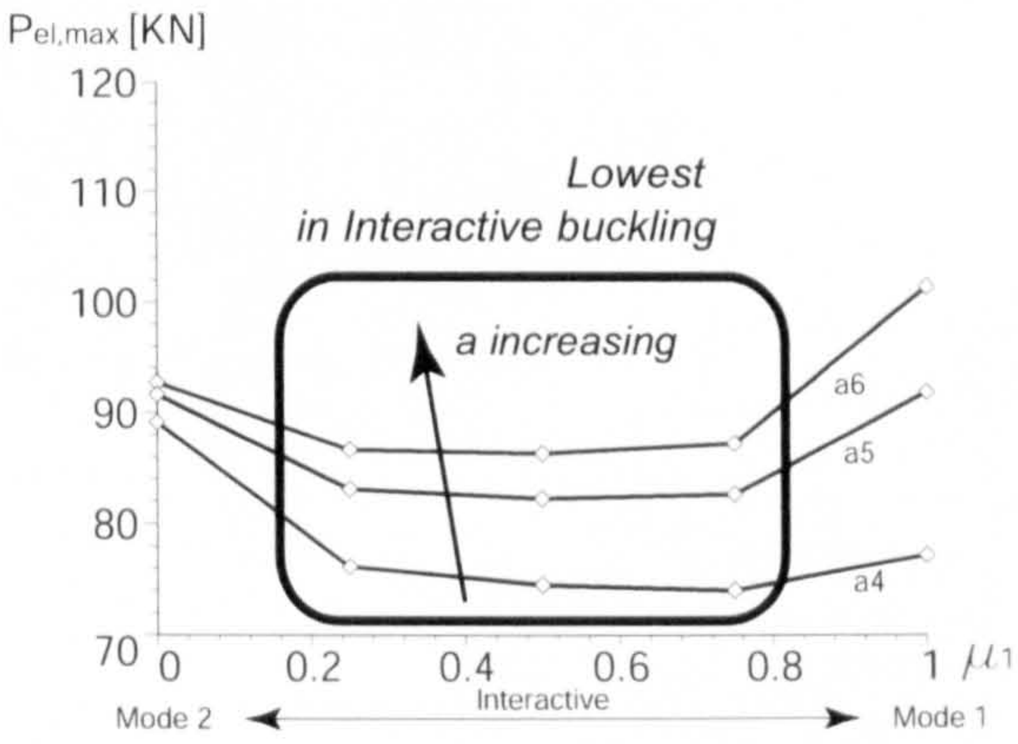

(b) a4–a6

Figure 5.11: Sensitivity to the imperfection combination represented by the maximum load capacity $P_{\mathrm{el,max}}$ versus μ_1 with the crossarm length a varying.

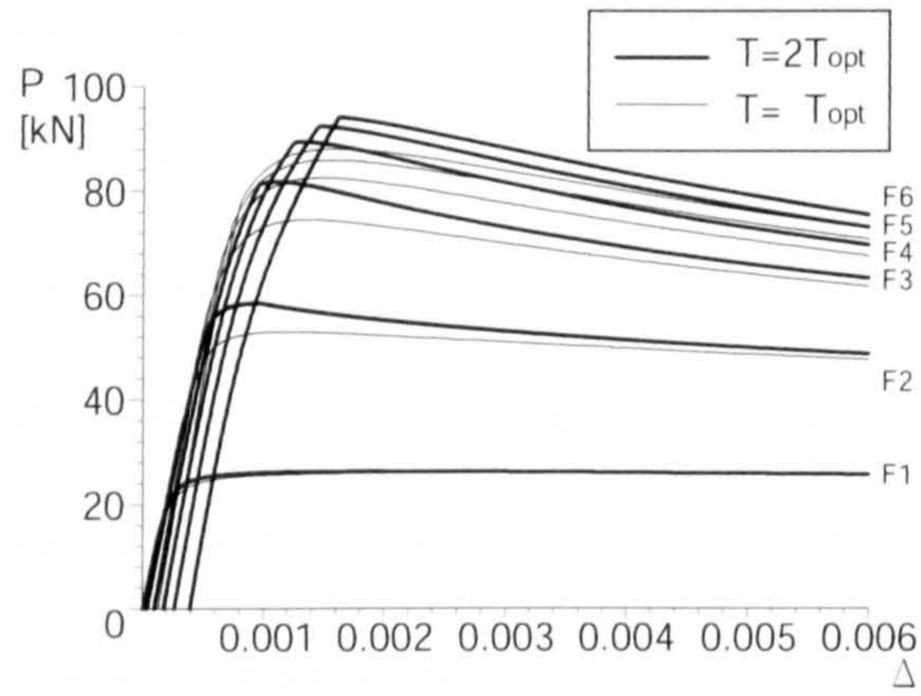

Figure 5.12: Equilibrium paths represented by the axial load P versus the end-shortening Δ with the stay diameter ϕ_s varying when $T = T_{\text{opt}}$ and $T = 2T_{\text{opt}}$, and $\mu_1 = 0.5$.

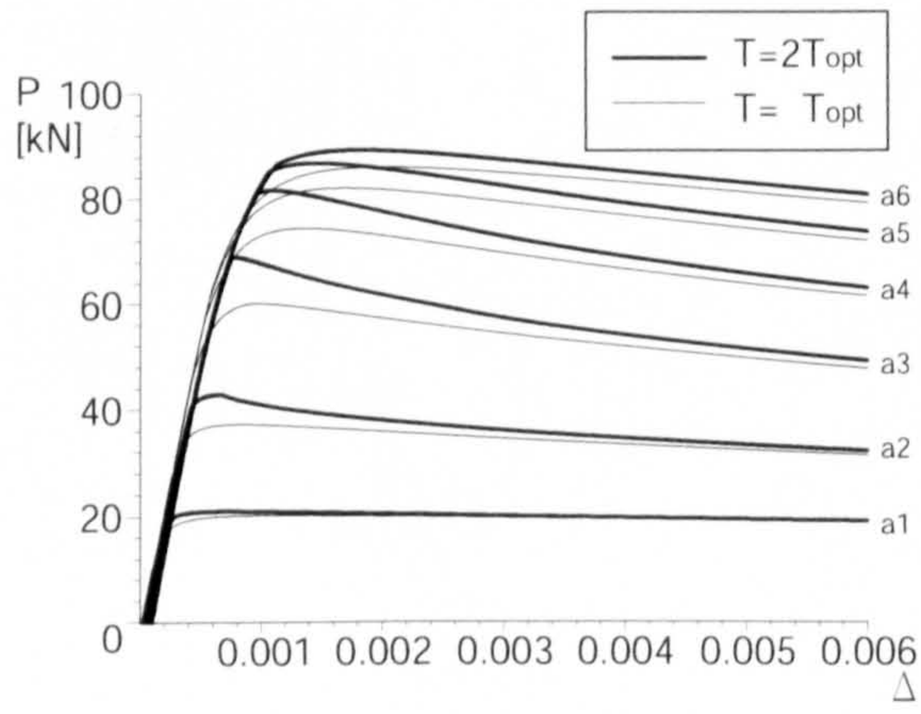

Figure 5.13: Equilibrium paths represented by the axial load P versus the end-shortening Δ with the crossarm length a varying when $T = T_{\text{opt}}$ and $T = 2T_{\text{opt}}$, and $\mu_1 = 0.5$.

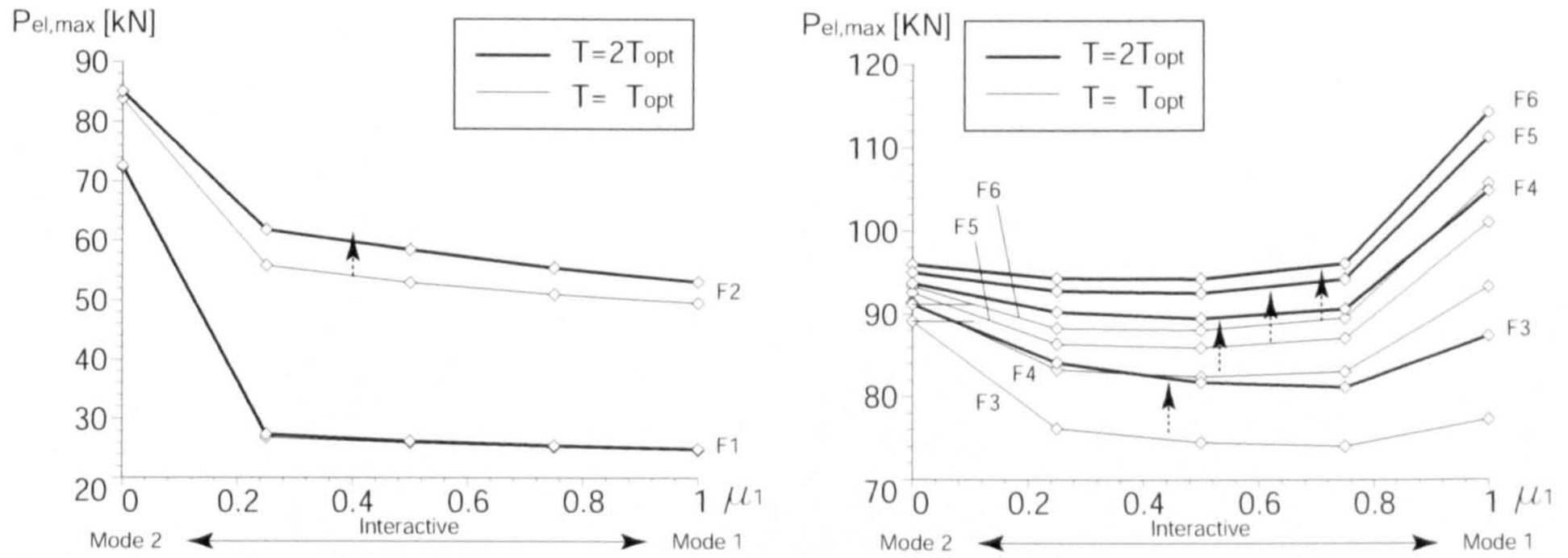

(a) F1–F2

(b) F3–F6

Figure 5.14: Sensitivity to the imperfection combination represented by the maximum load capacity $P_{\mathrm{el,max}}$ versus μ_1 with the stay diameter ϕ_s varying when $T = T_{\mathrm{opt}}$ and $T = 2T_{\mathrm{opt}}$. The arrow with the doted line show an increase in the maximum load capacity from T_{opt} to $2T_{\mathrm{opt}}$.

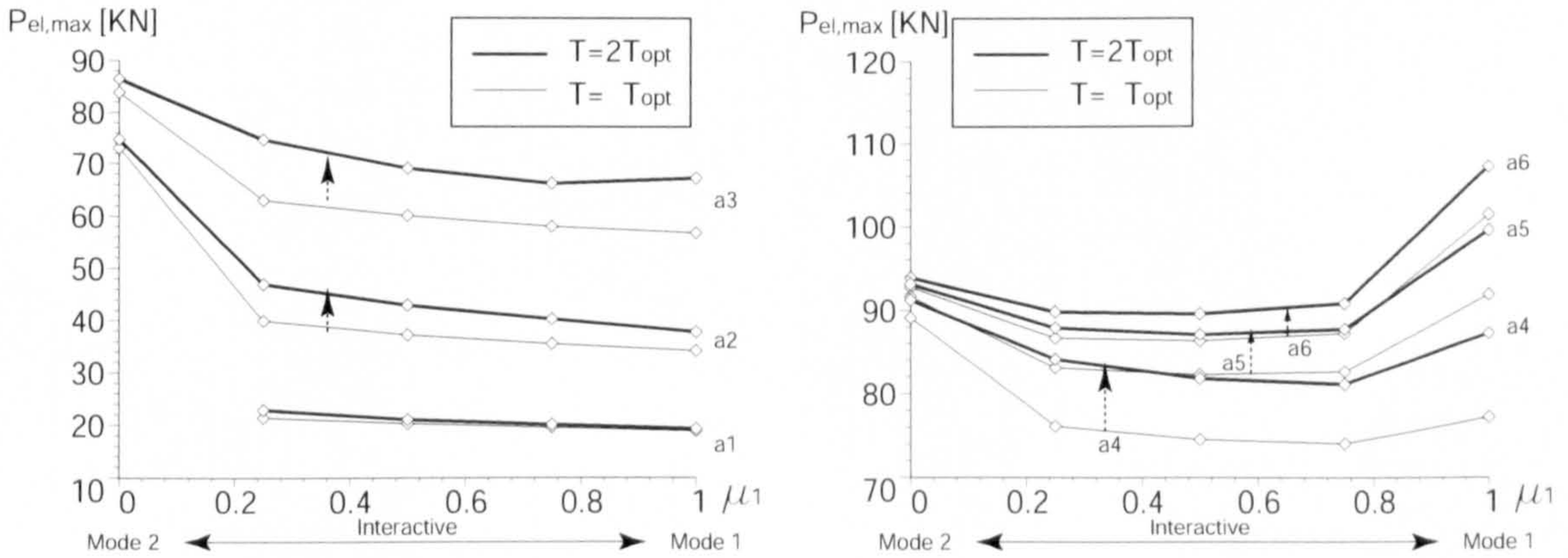

(a) a1–a3

(b) a4–a6

Figure 5.15: Sensitivity to the imperfection combination represented by maximum loading capacity $P_{\mathrm{el,max}}$ versus μ_1 with the stay diameter a varying when $T = T_{\mathrm{opt}}$ and $T = 2T_{\mathrm{opt}}$. The arrow with the doted line show an increase in the maximum load capacity from T_{opt} to $2T_{\mathrm{opt}}$.

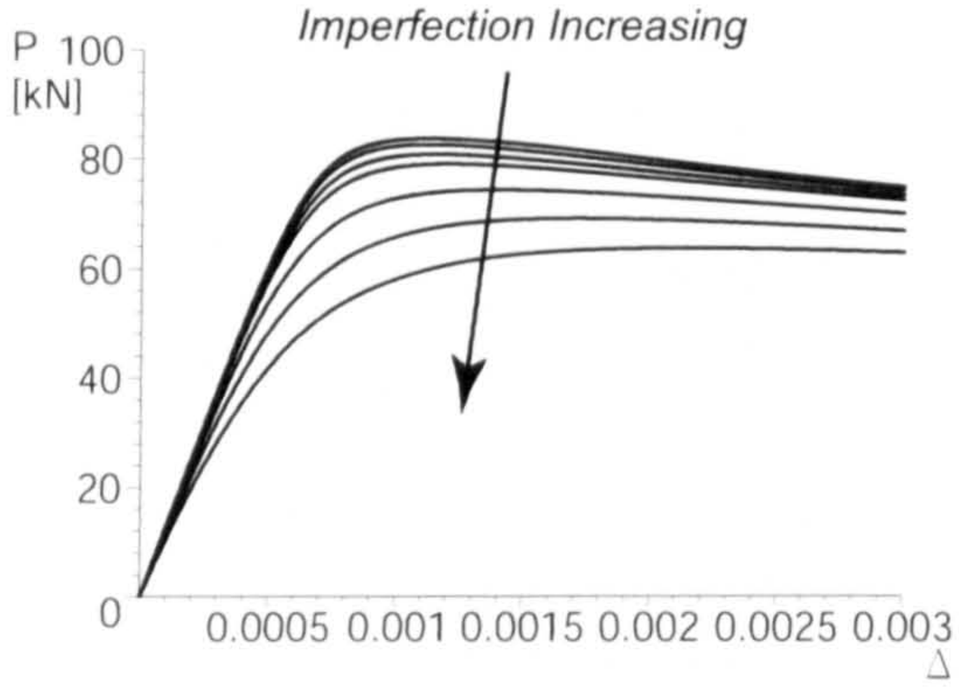

(a) $T = 0$

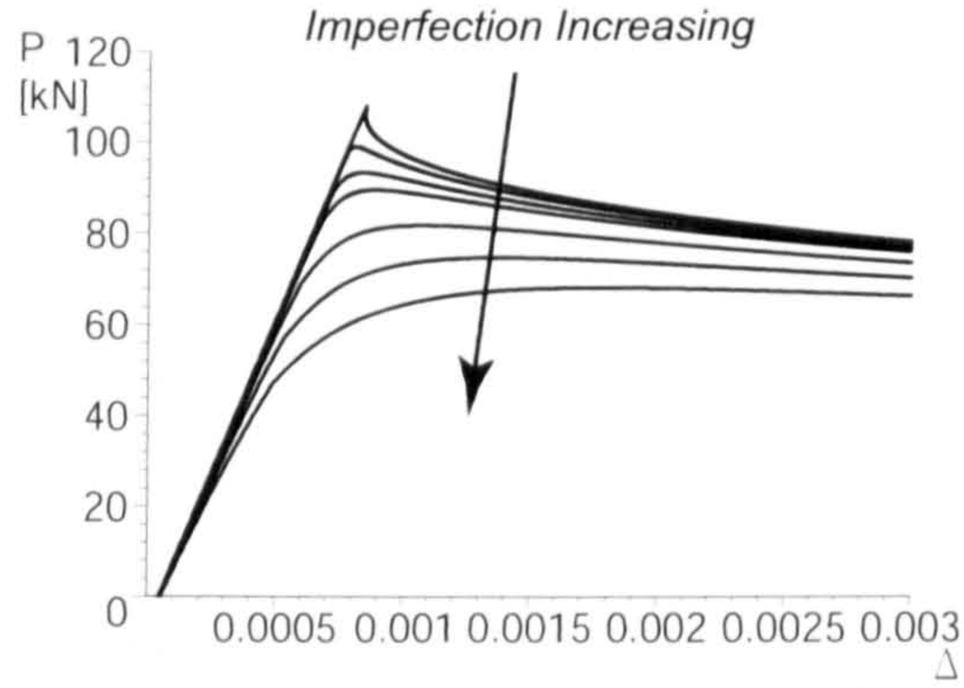

(b) $T = T_{\text{opt}}$

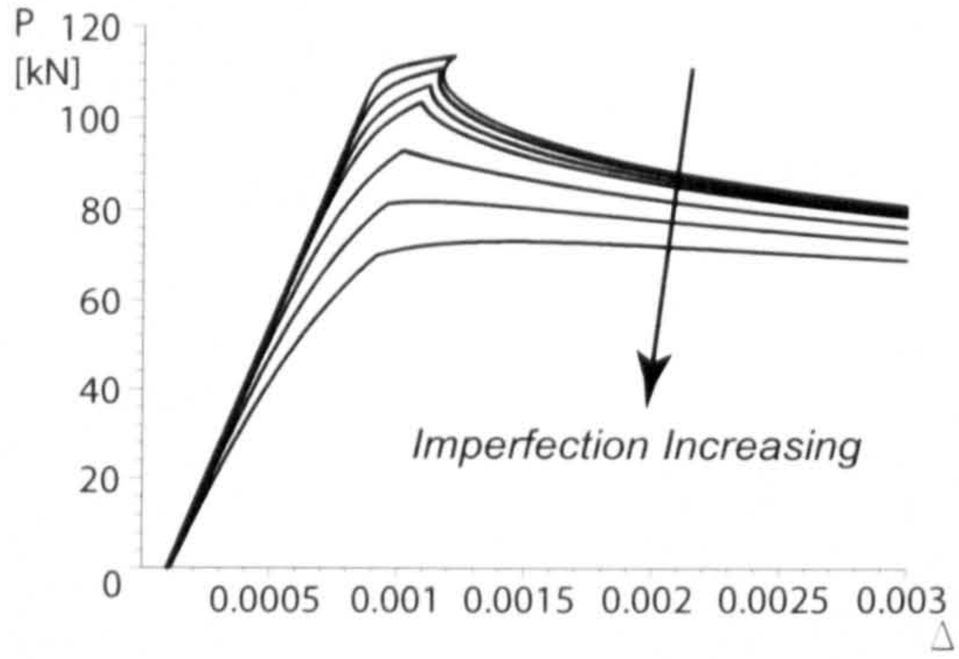

(c) $T = 2T_{\text{opt}}$

Figure 5.16: Equilibrium paths represented by the maximum load capacity $P_{\text{el,max}}$ versus the end-shortening Δ with a variation of the imperfection δ when $\mu_1 = 0.5$ and the case of a4/F3 were adopted.

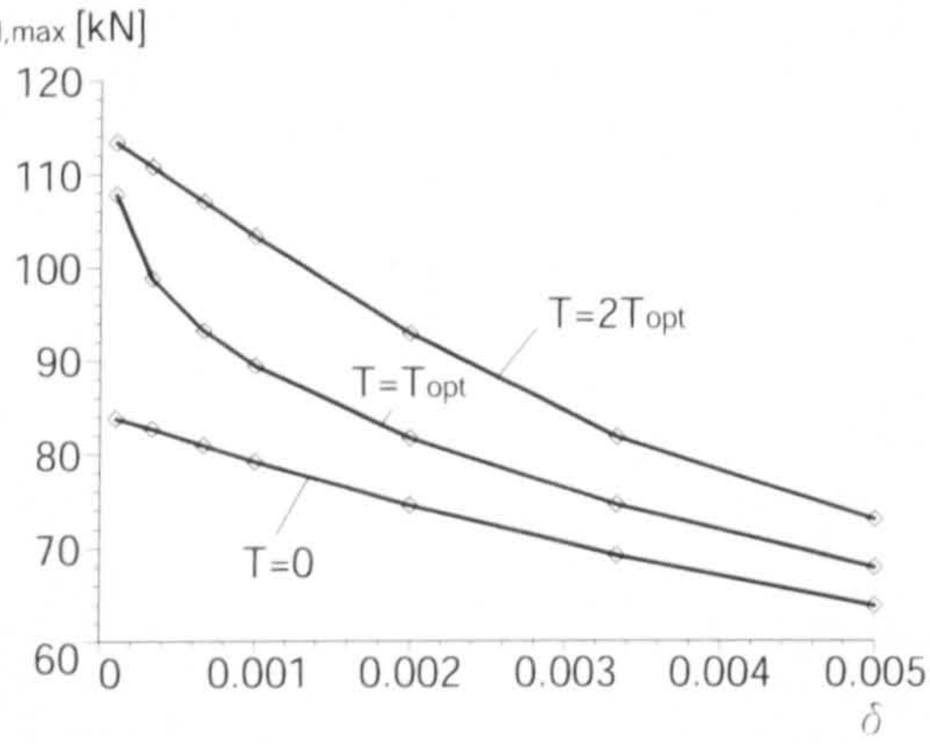

Figure 5.17: Maximum load capacity $P_{\text{el,max}}$ versus the imperfection δ with a variation of the prestress T when $\mu_1 = 0.5$.

Chapter 6

Optimal Prestressing and Configuration

6.1 Introduction

In the last three chapters, it has been repeatedly stated that the level of the prestress T_{opt}, which allows the maximum buckling load $P_{\text{max}}^{\text{C}}$ to be exhibited, is not the actual optimum; the real optimum level of the prestress would be greater than T_{opt} if the post-buckling strength and stability are taken into consideration. The use of the real optimal level of prestress T_{ropt} would potentially allow designers to make substantial economic savings; investigations into the optimized prestress T_{ropt} is therefore considered to be very important for practical designs. Despite this potential importance, the exact value of the optimal prestress T_{ropt}, which maximize the axial load carrying efficiency, has not yet been investigated satisfactorily.

There have been few studies of investigating the maximum load capacity at different levels of the prestress (Smith, 1985; Liew & Li, 2006). Certainly, the maximum load capacity becomes an indicator for the optimal value of the prestress for a particular configuration; however, the maximum load capacity does not always correspond to the most efficient of the system. Although the level of the prestress which achieves

the maximum load capacity in a particular configuration may be used, if the correct configuration were not selected in the first instance, the system could hardly be called an efficient axial load carrier. For instance, in the case of a1 in Chapter 5, the maximum load capacity cannot be increased regardless of the level of the prestress due to the lack of sufficient restraints attributed to its configuration.

Considering that selecting an adequate configuration is also an important issue for designers, it would be of great assistance to present an indicator representing the structural efficiency, which allows us to compare the cases having different structural configurations and different levels of the prestress concurrently.

The study in the current chapter presents the level of the optimal prestress T_{ropt} through investigations into the ratios of the maximum elastic load capacity to the required structural resistance for the column η and for the stay η_s.

These ratios are considered to represent the structural efficiency of the structural components in terms of the load carrying capacity to the required structural resistance. Using the code ABAQUS (ABAQUS, 2006), FE analysis was conducted with the stay diameter ϕ_s and the crossarm length a varied. Numerical examples for the real optimal level of prestress T_{ropt} are presented, and suggestions for the structural configurations for improving the structural efficiency are obtained through parametric studies.

6.2 Methodology

The current investigation involves FE analysis with a number of different levels of prestress. This process allows us to find the real optimal level of the prestress T_{ropt} by comparing indicators for structural optimization. These are the ratios of the elastic maximum load capacity $P_{\mathrm{el,max}}$ to the required structural resistance for the column $Af_{\mathrm{y,req}}$ and that for the stay $A_s f_{\mathrm{s,Rd,req}}$, which are defined as η and η_s respectively. In FE analysis, Riks analysis was conducted using the code ABAQUS,

which produced the necessary component to calculate the values of η and η_s, i.e. the maximum elastic load capacity $P_{\text{el,max}}$ and the required structural resistance for the column $Af_{\text{y,req}}$ and for the stay $A_s f_{\text{s,Rd,req}}$.

6.2.1 Model development

The development of the FE model follows the same process stated as in §3.4.3. Note that the FE model was already validated through the comparison with the analytical model. The imperfection shape follows equation (5.1), which accounts for distinct mode buckling as well as interactive buckling. The basic amplitude of the imperfection δ was selected to be 1/300 to obtain the actual level of the design load from the equilibrium path (EN1993-1-1, 2005). All of the structural components are purely elastic in order to obtain the maximum elastic load capacity.

6.2.2 Analysis procedure

The study was conducted with two parameters varying, the crossarm length a, and the stay diameter ϕ_s. Only the Mode 1 and interactive buckling equilibrium paths were investigated. The reason for not investigating the distinct Mode 2 equilibrium path stems from the results obtained in Chapter 5, which indicates that when Mode 2 is the lowest mode in buckling analysis, the maximum load capacity in interactive buckling is normally lower than those in Modes 1 and 2. As for the imperfection combination for interactive buckling, Case 2 from Table 5.1 was selected. As it was already shown that the interactive behaviour is relatively insensitive to the combination of the imperfections, it is considered to be superfluous to investigate different cases of the imperfection combinations.

From each analysis, the level of the required material strength for the column and the stay were recorded in order to achieve the maximum elastic load capacity $P_{\text{el,max}}$ (See Figure 6.1). For the column, it is required that the yield stress $f_{\text{y,req}}$ is more than

the maximum fibre stress along the column at the level of the maximum elastic load capacity. This approach is based on the Perry–Robertson theory, which is adopted in the current version of Eurocode 3 (EN1993-1-1, 2005). For the stay, the maximum stress in all of the stays at the level of the elastic maximum load capacity becomes the required design stress for the stay $f_{\mathrm{s,Rd,req}}$. In the case of the stay, the required design stress is not simply equal to the yield stress nor the proof stress of the stay due to the more complicated design procedures and safety regulations for cables and rods than those for the column (EN1993-1-11, 2006). For instance, if the design is conducted to Eurocode 3 and the stays are constructed from and the stays are constructed from strand rope, the design values of the tension stress is the lesser of the breaking stress divided by a factor of 1.5 and by the partial factor γ_{R}, γ_{R} being the partial factor accounting for any bending stress at the end of the stay.

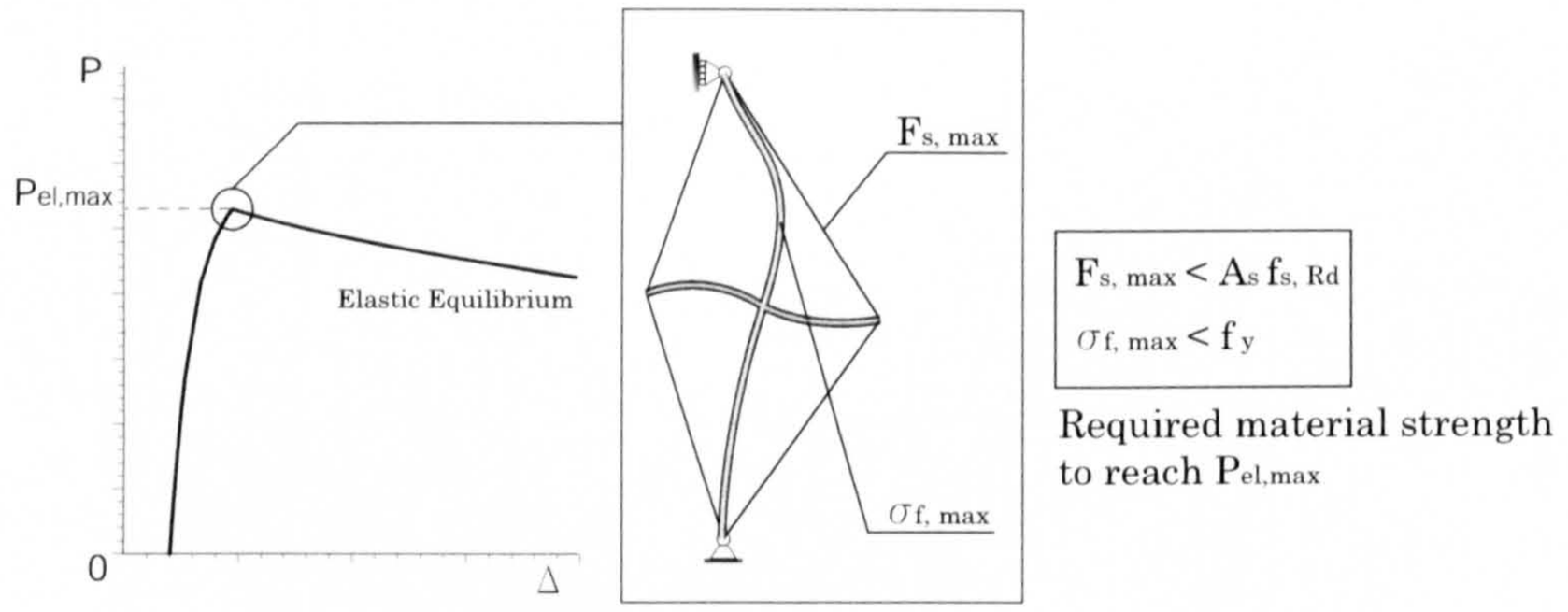

Figure 6.1: Required material resistance to achieve the elastic maximum load capacity $P_{\mathrm{el,max}}$.

From the above definition of the required material strength, the required structural resistance for the column and the stay is simply expressed as $Af_{\mathrm{y,req}}$ and $A_s f_{\mathrm{s,Rd,req}}$ respectively. Thus, the ratio of the maximum elastic load capacity to the required structural resistance for the column η is expressed as

$$\eta = \frac{P_{\mathrm{el,max}}}{Af_{\mathrm{y,req}}}. \tag{6.1}$$

Similarly, the ratio of the elastic maximum load capacity to the required structural

resistance for the stay η_s is expressed as

$$\eta_s = \frac{P_{\text{el,max}}}{A_s f_{\text{s,Rd,req}}} \frac{L/2}{L_s}, \tag{6.2}$$

where $L/2L_s$ represents a correction on the stay length as this changes with the crossarm length a.

The value of η represents the reduction factor in the design load from the required compression resistance of the column, which enables η to be used as an indicator for structural efficiency in terms of the load carrying capacity to the required structural resistance of the column. The greater the value of η, the smaller the influence of buckling becomes. Hence, in the limit when $\eta = 1$, effectively elastic buckling becomes negligible in calculating the resistance of cross-sections. The value of η_s is also an indicator for structural efficiency in terms of the load carrying capacity to the required structural resistance. The greater the value of η_s, the less structural resistance of the stay is required for the system to support a given load.

The real optimal value of the prestress was sought by comparing values of η and η_s at different levels of prestress. For distinction, the optimal prestress obtained from a comparison of η was defined as T_{ropt1} and the one from a comparison of η_s was defined as T_{ropt2}. In order to find the levels of T_{ropt1} and T_{ropt2}, the value of T_{opt} expressed in equation (5.4), which represents the previous idea of the optimal prestress as being the maximum buckling load of the system (Hafez *et al.*, 1979), was used as the basis from which the prestress was increased. Note that as the values η and η_s are nondimensional, although the structural configurations are different, these values are mutually comparable. Hence, comparing values of η and η_s would help designers to select the adequate structural configuration as well as the adequate level of the prestress.

In fact, the ratio of η represents the upper limit of the buckling reduction factor χ

in Eurocode 3, where the reduction factor χ is used thus:

$$N_{\mathrm{b,Rd}} = \frac{\chi A f_{\mathrm{y}}}{\gamma_{\mathrm{M1}}} \quad \text{for class 1, 2 or 3 cross-sections,} \tag{6.3}$$

where $N_{\mathrm{b,Rd}}$ is the design value of the resistance to compression forces; γ_{M1} is a partial safety factor, which is recommended to be taken as unity for buildings. If $\gamma_{\mathrm{M1}} = 1$ is adopted, the expressions for η and χ are exactly the same, apart from the fact that the different forms of the yield stresses are used, $f_{\mathrm{y,req}}$ and f_{y} respectively. As $f_{\mathrm{y,req}}$, which represents the lower limit of the yield stress, is used in place of the actual value of yield stress of steel f_{y} in the expression of η, it can be said that η represents the upper limit of the buckling reduction factor χ.

Note that higher values of η and η_s do not necessarily guarantee that the structure is cost-effective as the cost for the system is also strongly dependent on the grades of steel and the stays, i.e. the required design stress also becomes an important factor. For instance, the use of steel tension rods for the stays would be less expensive than the use of wire strand. In order to adopt steel rods, the design stress for the stay must be sustained at a relatively low value; however, high values of η and η_s do not necessarily guarantee a low value of $f_{\mathrm{s,Rd,req}}$. For the same reason, higher values of η and η_s do not necessarily guarantee that maximum load capacity of the system. When it is strongly required to support a heavy load even at the expense of material costs, these indicators might not be useful either—the maximum critical load $P^{\mathrm{C}}_{\mathrm{max}}$ would be a better indicator for the design; certainly, a greater level of the prestress than T_{opt} is still required. Despite these shortcomings, obtaining high levels of the buckling resistance with minimum stay supports is the aim of this structural system; therefore, η and η_s, which represent structural efficiency in terms of the load carrying capacity to the required structural resistance, are important indicators for structural efficiency that are linked to the factor of cost-effectiveness. If η and η_s are used in conjunction with required material weights and types, the cost-effectiveness could be more accurately estimated—this however, is beyond the scope of this thesis.

As for basic assumptions, the same assumptions were also made for the analysis in

this chapter as those shown in §3.1.1 except for the assumption that the column is perfectly straight.

6.3 Numerical Results

As stated earlier, the equilibrium response with imperfections was investigated using the FEM at different levels of the prestress. The same dimensions and properties as in §3.3.1 were also applied for the analysis, with the stay diameter, $\phi_s = 4.8\,\text{mm}$ being chosen. The stay diameter ϕ_s was varied from 1.6 mm to 10.0 mm with a classification of F1 to F6 (see Table 5.2) while the crossarm length a was fixed to 0.305 m, and the crossarm length a was varied from 76.25 mm to 457.5 mm with a classification of a1 to a6 (see Table 5.3) while the stay diameter was fixed to $\phi_s = 4.8\,\text{mm}$.

Firstly, the results of the buckling analysis conducted in Chapter 5 were examined to reveal which mode is the lowest critical load and to obtain the value of the prestress T_{opt}. This was used as the benchmark for the minimum prestress. Subsequently, the optimal prestress was investigated through a comparison of the ratios η and η_s, which were obtained from Riks analysis. As stated earlier, the level of the prestress which maximizes both η and η_s becomes the true optimal prestress.

6.3.1 Buckling analysis

The results of buckling analysis have already been shown in Figures 5.2 and 5.3. In the cases of F1, F2, a1, a2, a3, Mode 1 is critical; hence, the characteristic Mode 1 post-buckling would normally become critical in these cases. For the rest of the cases, the interactive buckling would generally govern in the equilibrium response as Mode 2 becomes critical. Note that buckling analysis was conducted only with the prestress level of T_{opt}; therefore, the buckling mode at T_{opt} does not necessarily correspond to the buckling behaviour at the other levels of the prestress. Hence, in

this chapter, changes in the governing equilibrium behaviour is focused upon more rather than changes in the buckling modes as buckling analysis was only conducted with the prestress level of T_{opt} in the earlier discussion. However, the buckling mode at T_{opt} is still thought to give a good prediction in the governing equilibrium behaviour with different levels of the prestress. The levels of T_{opt} was also presented in Tables 5.2 and 5.3, which become the basis from which the prestress was increased in Riks analysis.

6.3.2 Riks analysis

Using the prestress based on the value of T_{opt}, the real optimal level of prestress was investigated for each case through Riks analysis using ABAQUS. Previous work (Smith, 1985; Liew & Li, 2006) also made a comparison of cases at different levels of prestress using the maximum load capacity as an indicator for effectiveness; however, the maximum load capacity is not a mutually comparable indicator with different configurations. In the current study, the optimal value of the prestress is clearly presented by comparing the values of η and η_s representing the column element and the stay efficiencies respectively, which are mutually comparable with different configurations and would therefore help designers to choose an adequate structural configuration as well as to investigate the optimal prestress.

Figure 6.2 shows the maximum elastic load capacity $P_{\text{el,max}}$ of the system, which is one of the required components to obtain η and η_s as shown in equations (6.1) and (6.2) respectively. Note that the maximum "elastic" load capacity does not become an indicator for the level of the optimal prestress even within the same configuration due to the lack of consideration for plasticity and design strength. Figure 6.3 displays the required the column yield stress for the column $f_{\text{y,req}}$ to obtain the maximum elastic load at each level of the prestress for each case. As can be seen, the required yield stress $f_{\text{y,req}}$ varies with the prestress. The level of the prestress which minimizes the value $f_{\text{y,req}}$ does not represent the optimal level of the prestress even within the same configuration either because different levels of

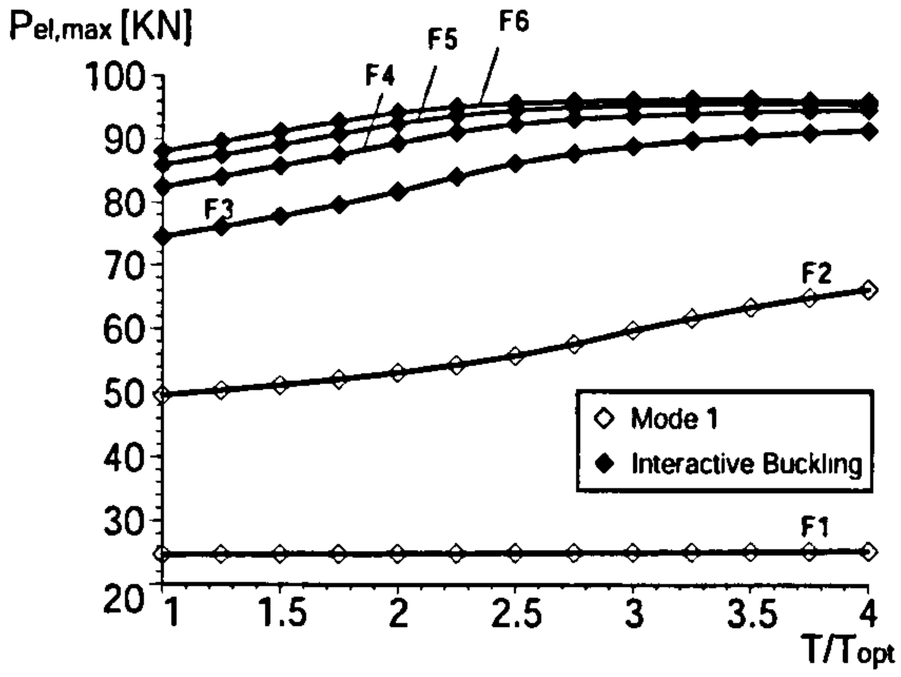

(a) stay diameter ϕ_s varying

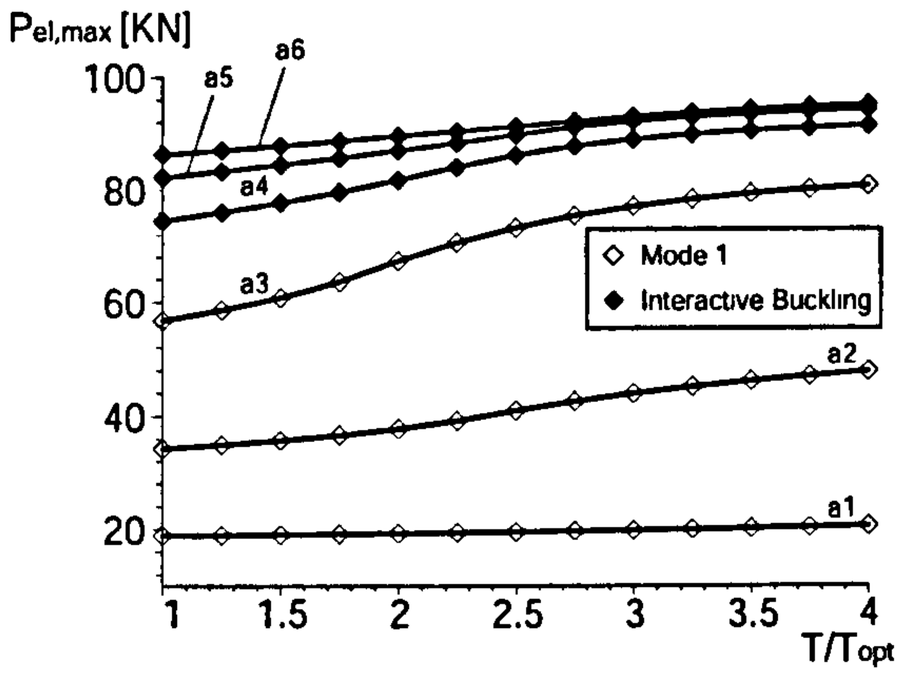

(b) crossarm length a varying

Figure 6.2: Maximum elastic load capacity $P_{\text{el,max}}$.

$P_{\text{el,max}}$ can be found at each level of the prestress. To locate the optimized prestress, the maximum load capacity should be taken into account as well as the required structural resistance.

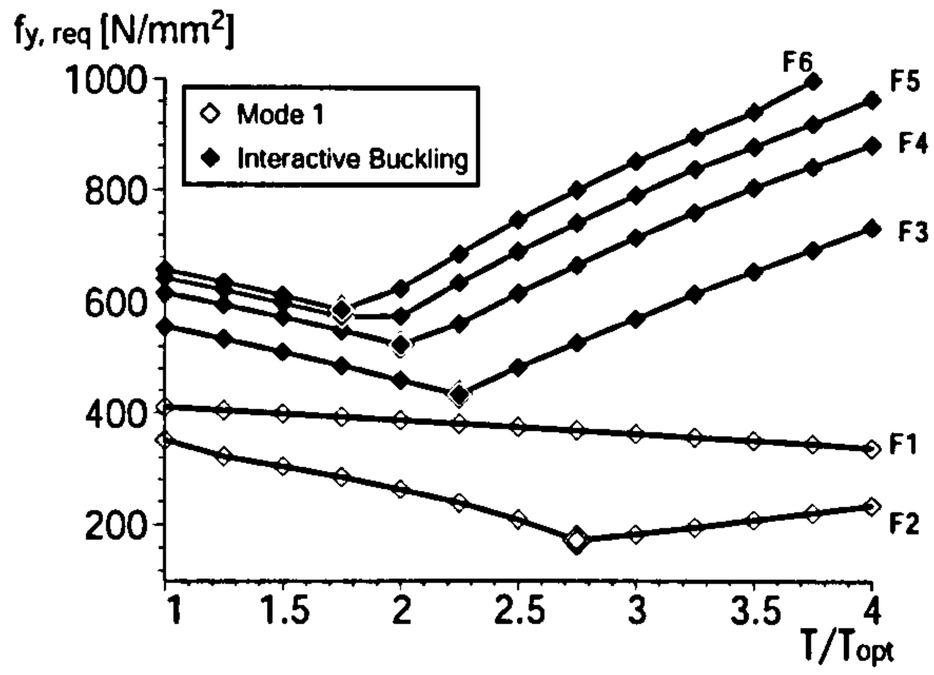

(a) stay diameter ϕ_s varying

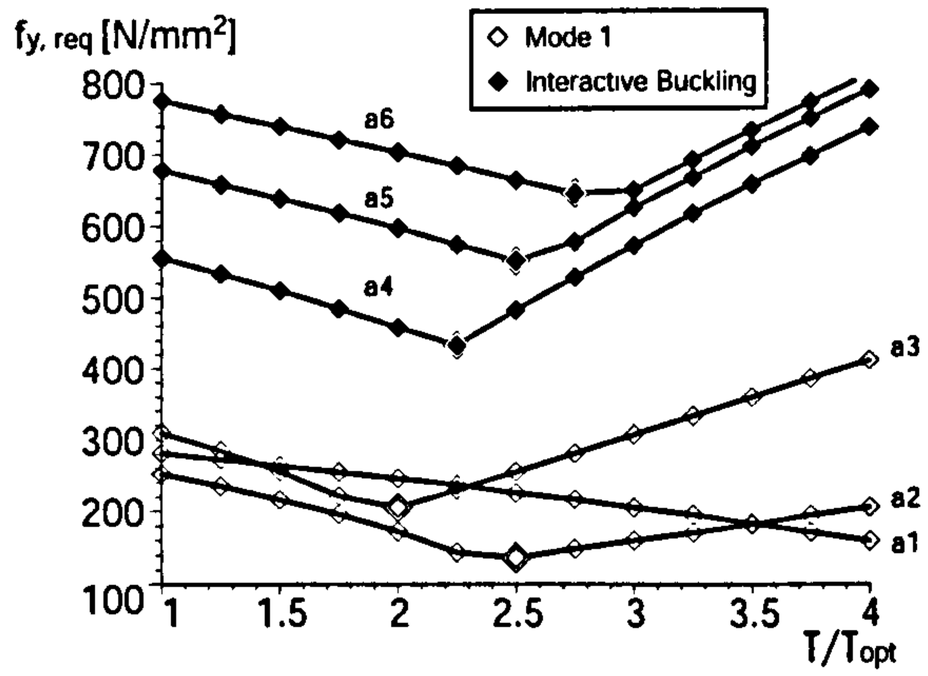

(b) crossarm length a varying

Figure 6.3: Required column yield stress $f_{\text{y,req}}$ to reach the maximum elastic load capacity $P_{\text{el,max}}$.

Figure 6.4 shows the ratio of the maximum elastic load capacity to the required structural resistance, which defines η. As stated earlier, when the value of η is high, the structural efficiency in terms of the load carrying capacity to the required structural resistance of the column also becomes high. The level of the prestress

that maximizes η for each configuration represents the optimal level of the prestress for each case. This optimal level of the prestress T_{ropt1} obtained from a comparison of values of η for each case is presented in Tables 6.1 and 6.2. As can be seen, the nondimensionalized optimal level of prestress $T_{\mathrm{ropt1}}/T_{\mathrm{opt}}$ becomes lower as the stay diameter ϕ_s increases, and as the crossarm length a approaches a configuration where the transition of the governing behaviour from Mode 1 to interactive buckling is seen.

The best efficiency is found for F2 with $T/T_{\mathrm{opt}} = 2.75$ when the stay diameter ϕ_s is varied and for a3 with $T/T_{\mathrm{opt}} = 2.5$ when the crossarm length a is varied. Both of these are located at the point where the governing behaviour is Mode 1 and yet is close to the transition from Mode 1 to the interactive mode. Therefore, it can be conjectured that, if it is necessary to increase the structural efficiency in terms of the load carrying capacity to the required structural resistance of the column, it would be recommended for designers to choose a configuration that achieves this type of behaviour. Despite the suggestions above, further investigations are considered to be necessary in order to validate them, as the number of the cases investigated for this section is rather limited. Further parametric studies are presented in the next section.

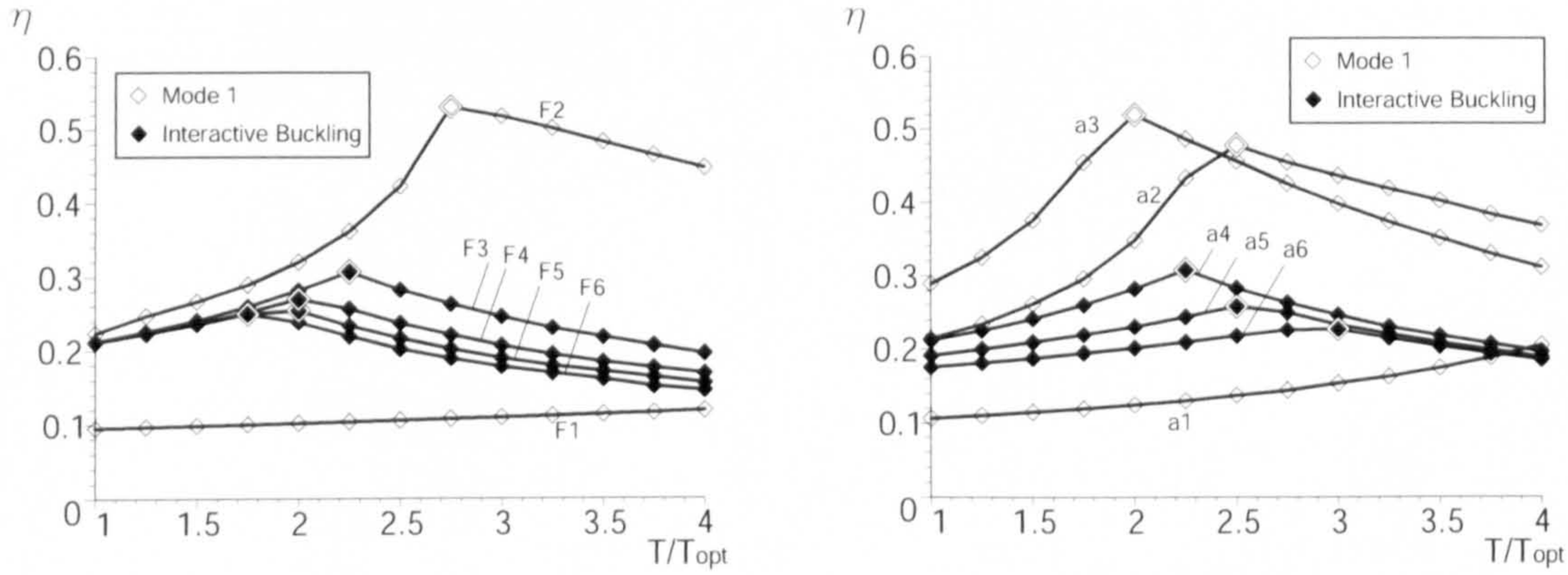

(a) stay diameter ϕ_s varying

(b) crossarm length a varying

Figure 6.4: Ratio of the maximum elastic load capacity to the required structural resistance for the column η—the higher a value of η, the more effective buckling resistance the column has.

Case	ϕ_s (mm)	T_{ropt} (kN) T_{ropt1}	T_{ropt2}	Buckling Mode	Governing Equilibrium Behaviour
F1	1.6	—	—	1	Mode 1
F2	3.2	2.28 ($2.75T_{\text{opt}}$)	2.28 ($2.75T_{\text{opt}}$)	1	Mode 1
F3	4.8	6.55 ($2.25T_{\text{opt}}$)	6.55 ($2.25T_{\text{opt}}$)	2	Interactive
F4	6.4	11.03 ($2.00T_{\text{opt}}$)	11.03 ($2.00T_{\text{opt}}$)	2	Interactive
F5	8.0	16.62 ($2.00T_{\text{opt}}$)	16.62 ($2.00T_{\text{opt}}$)	2	Interactive
F6	10.0	21.29 ($1.75T_{\text{opt}}$)	21.29 ($1.75T_{\text{opt}}$)	2	Interactive

Table 6.1: Real optimal levels of prestress T_{ropt} and governing buckling mode with the stay diameter ϕ_s varying.

Case	a (mm)	T_{ropt} (kN) T_{ropt1}	T_{ropt2}	Buckling Mode	Governing Equilibrium Behaviour
a1	76.25	—	—	1	Mode 1
a2	152.5	4.59 ($2.5T_{\text{opt}}$)	4.59 ($2.5T_{\text{opt}}$)	1	Mode 1
a3	228.75	5.83 ($2.0T_{\text{opt}}$)	5.83 ($2.0T_{\text{opt}}$)	1	Mode 1
a4	305	6.55 ($2.25T_{\text{opt}}$)	6.55 ($2.25T_{\text{opt}}$)	2	Interactive
a5	381.25	7.52 ($2.5T_{\text{opt}}$)	7.52 ($2.5T_{\text{opt}}$)	2	Interactive
a6	457.5	8.67 ($3.0T_{\text{opt}}$)	8.67 ($3.0T_{\text{opt}}$)	2	Interactive

Table 6.2: Real optimal levels of prestress T_{ropt} and governing buckling mode with the crossarm length a varying.

Figure 6.5 shows the required resistance stress for the stay $f_{\text{s,Rd,req}}$ to achieve the maximum elastic load capacity $P_{\text{el,max}}$ for each case. The level of the required resistance stress $f_{\text{s,Rd,req}}$ affects the selection of cable grades, which strongly affects the cost and the mechanical properties of the stay (EN1993-1-11, 2006). Therefore, carefully examining the required resistance for the stay is essential for designers in practice as well as increasing the structural efficiency in terms of both η and η_s.

Figure 6.6 shows the ratio of the maximum elastic load capacity to the required structural resistance for the stay η_s. As stated earlier, when the value of η_s is high, less stay resistance is required to support a unit load; hence, the structural efficiency in terms of the load carrying capacity to the required structural resistance of the stays becomes high. The level of the prestress that maximizes η_s for each configuration becomes the optimal level of the prestress for the stay T_{ropt2}, which is

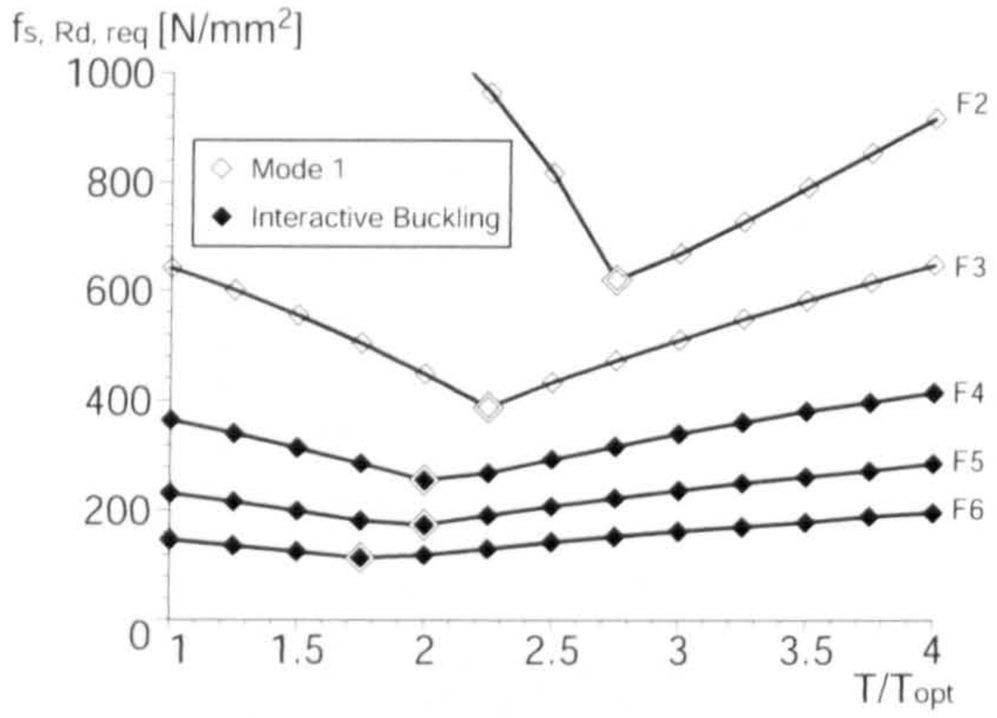

(a) stay diameter ϕ_s varying

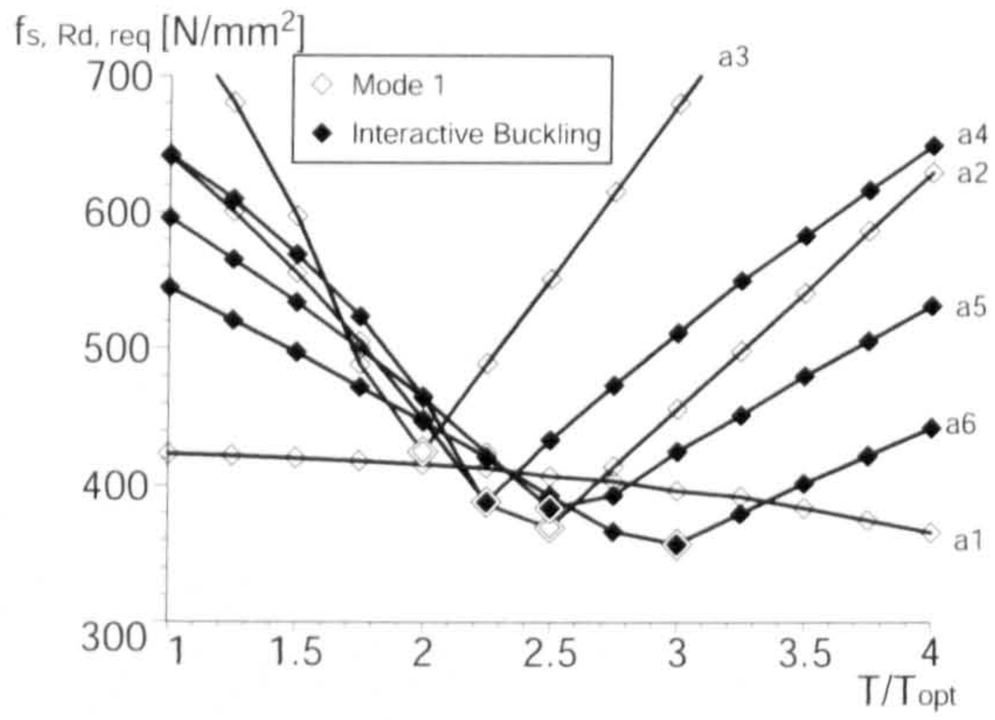

(b) crossarm length a varying

Figure 6.5: Required stay resistance to reach the maximum elastic load capacity $P_{\mathrm{el,max}}$.

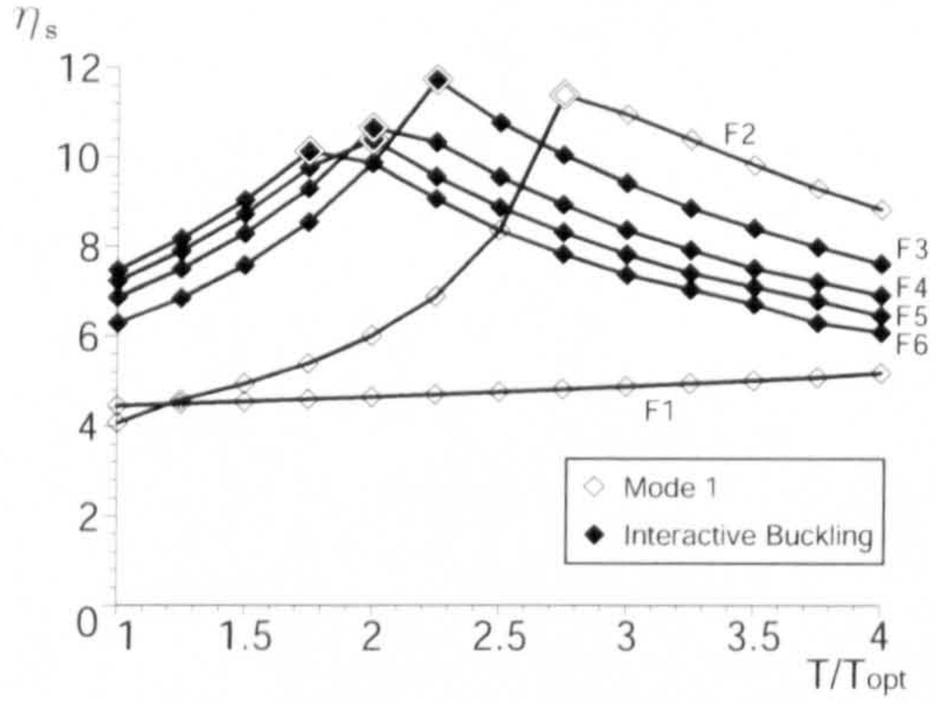

(a) stay diameter ϕ_s varying

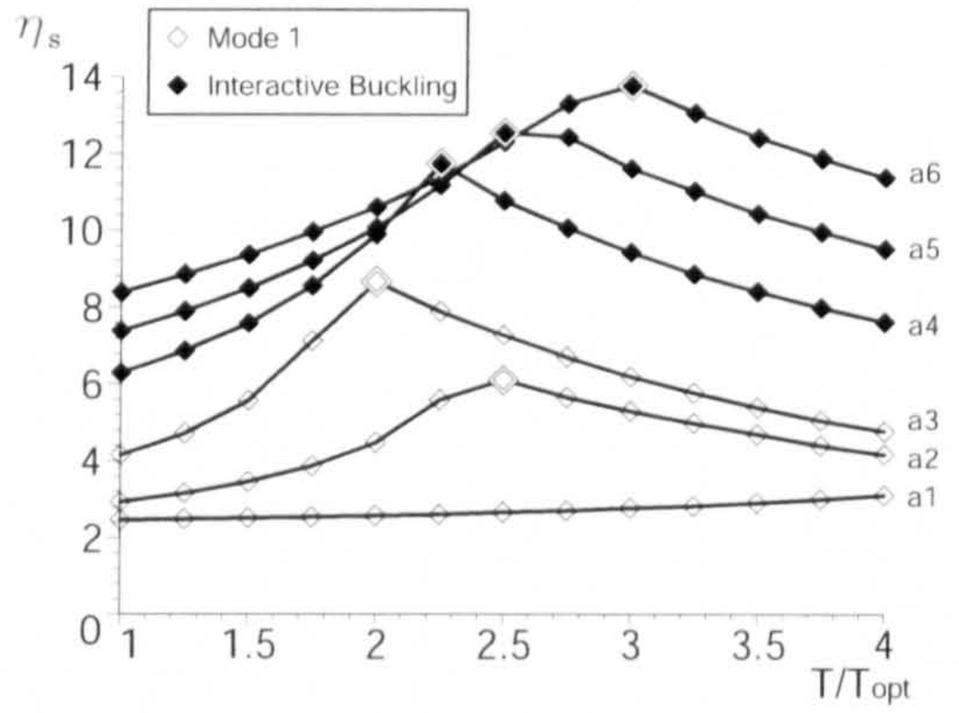

(b) crossarm length a varying

Figure 6.6: Ratio of the maximum elastic load capacity to the required structural resistance for the stays η_s—the higher a value of η_s, the more efficiency the stays have.

As can be seen, the optimal levels of the prestress for the column T_{ropt1} coincides with the prestress which the optimal levels of the prestress for the stay T_{ropt2}, implying that designers do not have to be concerned with balancing the true optimal prestress for the column T_{ropt1} and for the stay T_{ropt2} when they decide the level of prestressing. The best efficiency for the stay is located at F3 with $T/T_{\mathrm{opt}} = 2.25$ when the stay diameter ϕ_s is varied and at a6 with $T/T_{\mathrm{opt}} = 3$ when the length of the crossarm a

varied. Both of these are located at points where interactive buckling is the governing behaviour. Furthermore, F3 is located at a point where the governing behaviour is the interactive mode and is yet close to the transition from Mode 1 to the interactive mode, see Table 6.1; a6 is the longest possible length from the selection. Therefore, it can be conjectured that, if it is necessary to increase the structural efficiency in terms of the load carrying capacity to the required structural resistance of the stay, it would be recommended for designers to: (1) increase the crossarm length; (2) choose the stay diameter which renders the governing behaviour interactive and yet close to the transition from Mode 1 to interactive buckling. However, to validate the statements above, more investigations would be necessary, and these are presented in the next section.

6.4 Further Parametric Studies

As stated earlier, the purpose of the current work was to present the numerical optimal level of the prestress and suggestions for the structural configurations. Although these attempts were made in the previous section, the number of the examined cases were limited to make definitive suggestions on the real optimal level of prestress and the structural configuration.

Table 6.3 lists the combination of the stay diameter and the crossarm length that was investigated for this section. The symbol "√" represents the combinations that were already investigated for the previous section; 36 cases were investigated in total including the 11 cases that are presented in the previous section.

The analysis process is exactly the same as in the previous section. Firstly, the buckling analysis was conducted to investigate which mode would be critical and to obtain the value of the prestress T_{opt}, which was used as the benchmark for the minimum prestress. Subsequently, the level of the optimal prestress was investigated through a comparison of the ratios η and η_s, which were obtained from Riks analysis.

Case	a1	a2	a3	a4	a5	a6
F1				√		
F2				√		
F3	√	√	√	√	√	√
F4				√		
F5				√		
F6				√		

Table 6.3: Examined combinations of the stay diameter and the crossarm length a—"√" represents the combination that were presented in §6.3.

6.4.1 Buckling analysis

Figure 6.7 shows the buckling load P^{C}_{max} at $T = T_{opt}$ with a variation of ϕ_s and a respectively. As can be seen, the governing mode is influenced from both the stay diameter ϕ_s and the crossarm length a. When either the stay diameter ϕ_s is small or the crossarm length is short, Mode 1 tends to become the critical buckling mode, and when either the stay diameter ϕ_s is large or the crossarm length is long, Mode 2 tends to become the critical buckling mode. From these values of P^{C}_{max}, T_{opt} was obtained through equation (5.4).

6.4.2 Riks analysis

In order to calculate values of η and η_s, the maximum elastic load capacity $P_{el,max}$ was examined. Figure 6.8 shows the maximum elastic load capacity $P_{el,max}$ against different levels of the prestress with a variation of the crossarm length a and the stay diameter ϕ_s. It should be noted that in the results from the previous section, if the governing mode in buckling analysis at $T = T_{opt}$ is Mode 1, the governing equilibrium behaviour is always Mode 1, and if the governing mode in buckling analysis at $T = T_{opt}$ is Mode 2, the governing equilibrium behaviour is always interactive buckling. However, as can be seen, the governing modes at $T = T_{opt}$ in buckling do not always correspond to governing equilibrium behaviour at the other levels of the prestress, such as (a2, F5) and (a5, F2). As stated earlier, this might be

attributed to the phenomenon in which the buckling mode possibly changes with the level of the prestress. Nevertheless, as can be seen, buckling analysis with $T = T_{\text{opt}}$ still gives good predictions in investigating the governing behaviour for higher levels of the prestress.

With the values of $P_{\text{el,max}}$ and the required structural resistance for the column $Af_{\text{y,req}}$, the level of η was calculated for each case. Figure 6.9 plots the maximum η for different levels of prestress for each configuration. As can be seen, when either the crossarm length a or the stay diameter ϕ_s is fixed, the greatest value of η is found in a configuration where Mode 1 governs and yet is close to the transition from Mode 1 to interactive buckling.

With the values of $P_{\text{el,max}}$ and the required design stress for the stay $A_s f_{\text{s,Rd,req}}$, the level of η_s was calculated for each case. Figure 6.10 presents the maximum η_s for different levels of prestress for each configuration. As can be seen in Figure 6.10(a), when the crossarm length a is fixed for comparison, the greatest value of η_s can be found in a configuration where interactive buckling is the governing behaviour, and which is close to the transition from Mode 1 to interactive buckling. When the stay diameter ϕ_s is fixed for comparison, the greatest value of η_s can be found for a6, which is the longest crossarm length in the examined combination as shown in Figure 6.10(b).

The level of the real optimal prestress from the above analysis was also recorded from each analysis as shown in Tables 6.4 and 6.5. From a comparison of these two tables, the optimal levels of the prestress for the column T_{ropt1} almost coincide with the optimal levels of the prestress for the stay T_{ropt2} though there are slight differences between the two for some cases. For instance, in the case of (a5, F2), a difference of $0.5T_{\text{opt}}$ is observed; the reason for this discrepancy seems to be attributed to discontinuous changes in the values of η and η_s with the prestress in this specific configuration (see Figures C.3 and C.4). This discontinuity apeears to be related to buckling behaviour transitions accompanied with prestress level changes, which might require further investigation.

It should also be noted that the nondimensionalized optimal level of prestress $T_{\text{ropt}}/T_{\text{opt}}$ becomes lower as the stay diameter ϕ_s increases, and as the crossarm length a approaches a configuration where the transition of the governing mode from Mode 1 to interactive is seen.

Case	a1	a2	a3	a4	a5	a6
F1						
F2			2.90 ($3.50T_{\text{opt}}$)	2.28 ($2.75T_{\text{opt}}$)	3.66 ($2.75T_{\text{opt}}$)	4.19 ($3.25T_{\text{opt}}$)
F3		4.59 ($2.50T_{\text{opt}}$)	5.83 ($2.00T_{\text{opt}}$)	6.55 ($2.25T_{\text{opt}}$)	7.52 ($2.50\ T_{\text{opt}}$)	8.67 ($3.00T_{\text{opt}}$)
F4	5.02 ($2.75T_{\text{opt}}$)	7.70 ($1.75T_{\text{opt}}$)	9.65 ($1.75T_{\text{opt}}$)	11.03 ($2.00T_{\text{opt}}$)	11.69 ($2.25T_{\text{opt}}$)	13.71 ($2.75T_{\text{opt}}$)
F5	6.90 ($2.00T_{\text{opt}}$)	7.95 ($1.00T_{\text{opt}}$)	14.54 ($1.75T_{\text{opt}}$)	16.62 ($2.00T_{\text{opt}}$)	17.50 ($2.25T_{\text{opt}}$)	18.64 ($2.50T_{\text{opt}}$)
F6	9.65 ($1.50T_{\text{opt}}$)	15.44 ($1.25T_{\text{opt}}$)	18.25 ($1.50T_{\text{opt}}$)	21.29 ($1.75T_{\text{opt}}$)	22.71 ($2.00\ T_{\text{opt}}$)	24.52 ($2.25T_{\text{opt}}$)

Table 6.4: T_{ropt1} for each case—the dividing line represents the boundary between Mode 1 and interactive buckling, where above the horizontal line is Mode 1 and below it is interactive buckling.

As expected, all of the results presented in this section are almost identical to the results presented in §6.3. Thus, the following statements have been successfully validated with the further parametric studies presented in this section:

1. The levels of the optimal prestress obtained from η and η_s are in good agreement.

2. The level of η can be improved by choosing a configuration where the governing behaviour is Mode 1 and yet close to the transition from Mode 1 to interactive buckling.

3. The level of η_s can be improved either by choosing a configuration where the governing behaviour is interactive behaviour and yet is close to the transition from Mode 1 to interactive buckling or increasing the crossarm length.

Case	a1	a2	a3	a4	a5	a6
F1						
F2			2.90 ($3.50T_{opt}$)	2.28 ($2.75T_{opt}$)	3.66 ($2.75T_{opt}$)	4.19 ($3.25T_{opt}$)
F3		4.59 ($2.50T_{opt}$)	5.83 ($2.00T_{opt}$)	6.55 ($2.25T_{opt}$)	7.52 ($2.50\ T_{opt}$)	8.67 ($3.00T_{opt}$)
F4	5.02 ($2.75T_{opt}$)	7.70 ($1.75T_{opt}$)	9.65 ($1.75T_{opt}$)	11.03 ($2.00T_{opt}$)	11.69 ($2.25T_{opt}$)	13.71 ($2.75T_{opt}$)
F5	6.90 ($2.00T_{opt}$)	11.93 ($1.50T_{opt}$)	14.54 ($1.75T_{opt}$)	16.62 ($2.00T_{opt}$)	17.50 ($2.25T_{opt}$)	18.64 ($2.50T_{opt}$)
F6	9.65 ($1.50T_{opt}$)	15.44 ($1.25T_{opt}$)	18.25 ($1.50T_{opt}$)	21.29 ($1.75T_{opt}$)	22.71 ($2.00\ T_{opt}$)	27.24 ($2.5T_{opt}$)

Table 6.5: T_{ropt2} for each case—the dividing line represents the boundary between Mode 1 and interactive buckling, where above the horizontal line is Mode 1 and below it is interactive buckling.

From the above arguments, it can be conjectured that η and η_s are maximized at the transition point from Mode 1 to interactive buckling in the governing behaviour with a relatively long length of the crossarm that does not diminish the value of η. However, when the crossarm length a is fixed, a long crossarm length allows a small diameter of the stay ϕ_s at the highest values of η or η_s, which requires a high design stress for the stay for the system to reach the elastic maximum (see Figures 6.9(a), 6.10(a) and C.2). This is not favourable for the design; it should therefore be noted that the crossarm length cannot be extended without limit. Hence, in addition to the values of η and η_s, it would be also necessary for designers to examine the actual value of resistance whether the required resistance allows the use of reasonably inexpensive steel and stays.

As for the best configuration among all, high values of η can be found in the following combinations with a certain level of the prestress: (a2, F4), (a3, F5), (a4, F1), (a5, F2). Of these combinations, the greatest value of η_s can be seen with the case of (a5, F2). Thus, in terms of the structural efficiency, it can be concluded that this combination would be the optimal design for all the cases presented. In fact, this configuration has a relatively long crossarm length and is located at a

point near the transition point in the governing behaviour; this satisfies the above statement for maximizing the levels of η and η_s. In reality, the actual yield stress and required stress are different, thus the configuration which have high η and η_s do not always become the optimal design. As stated before, it would also be necessary for designers to check the actual value of resistance whether the required resistance allows material cost-effectiveness. Despite these points, the concept of η and η_s would give the theoretical optimal design in terms of the load carrying capacity to the required structural resistance, which could be expected to be used as a benchmark for designers.

6.5 Remarks

This is the first study to investigate the optimal level of prestress simultaneously with examination of the adequate structural configuration. The results indicate that the nondimensionalized optimal level of prestress $T_{\mathrm{ropt}}/T_{\mathrm{opt}}$ becomes lower as the stay diameter ϕ_s increases and as the crossarm length a approaches a configuration where the transition of governing equilibrium behaviour from Mode 1 to the interactive is seen. It has also been revealed that the level of the optimal prestress for the column T_{ropt1} coincides with the level of the optimal prestress for the stay T_{ropt2}, implying that designers do not have to adjust the level of prestress to balance these two.

It has also been shown that the best efficiency in terms of the load carrying capacity to the required structural resistance of the column can be found in a configuration where the governing equilibrium behaviour is Mode 1 and yet is close to the transition point from Mode 1 to interactive buckling. As for the stay, the best efficiency can be seen with a configuration where the governing behaviour is interactive buckling and is yet close to the transition point from Mode 1 to interactive buckling. It has also been presented that the efficiency can be improved with an increase in the crossarm length. Certainly, to achieve the best efficiency, the use of the real optimal level of prestress is needed.

From previous studies (Smith, 1985; Liew & Li, 2006), numerical examples of the optimal prestress for a few specific cases were presented using the maximum load capacity as an indicator. Certainly, the maximum load capacity becomes an indicator for the optimal value of the prestress for a particular configuration; however, the maximum load capacity would not become a valid indicator if the configuration of the structure were varied. In the current study, the idea of the ratios of the maximum elastic load capacity to the axial resistance for the column η and for the stay η_s are presented as indicators for optimization, which allows designers to compare the cases with different configurations as well as different levels of the prestress.

Although the values of η and η_s are indicators for cost-effectiveness, high values of η and η_s do not always guarantee that the structure is cost-effective as the cost for the system is also strongly dependent on the grades of steel and the stays. It would also be necessary for designers to examine them carefully to achieve true cost-effectiveness.

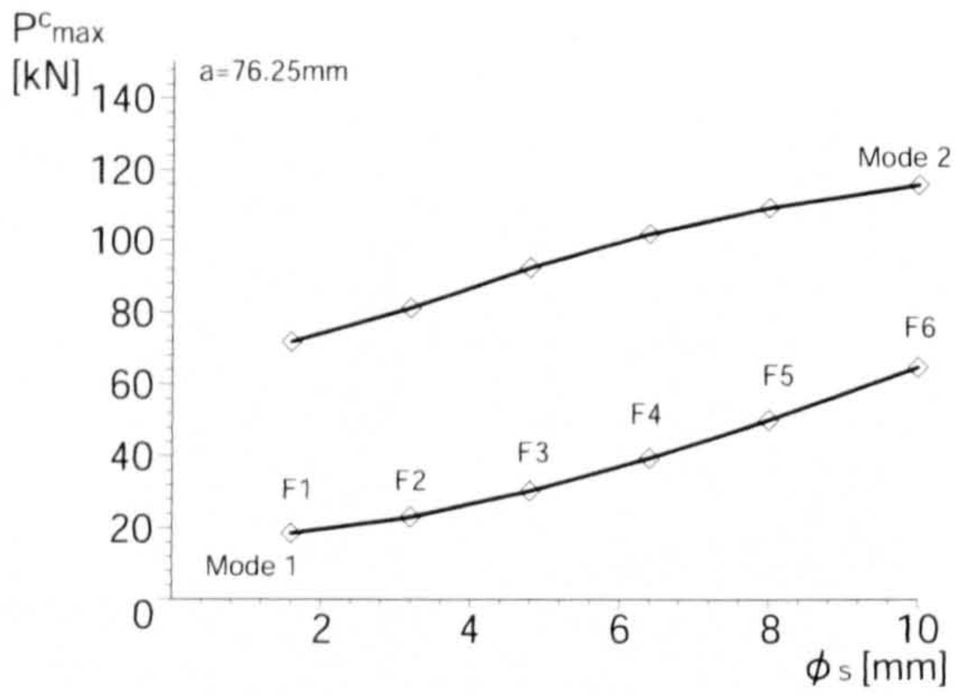

(a) a1

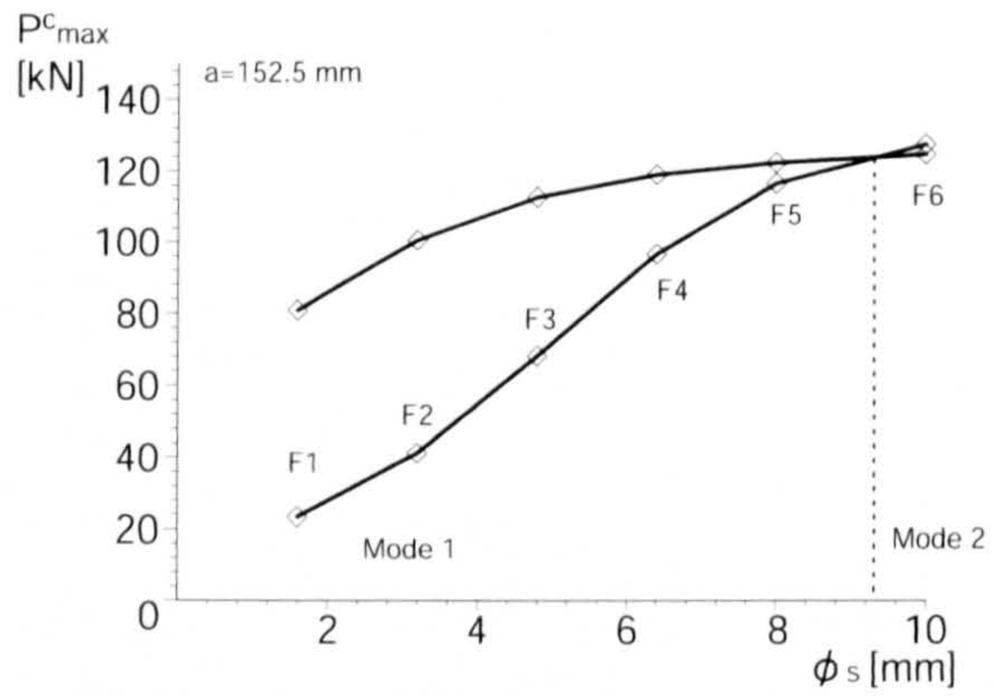

(b) a2

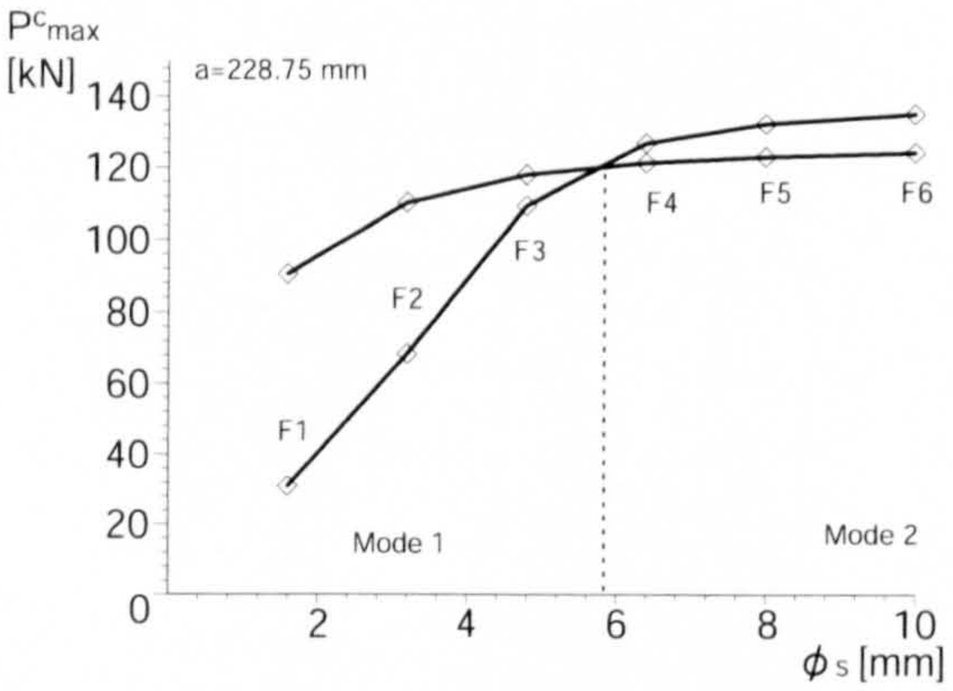

(c) a3

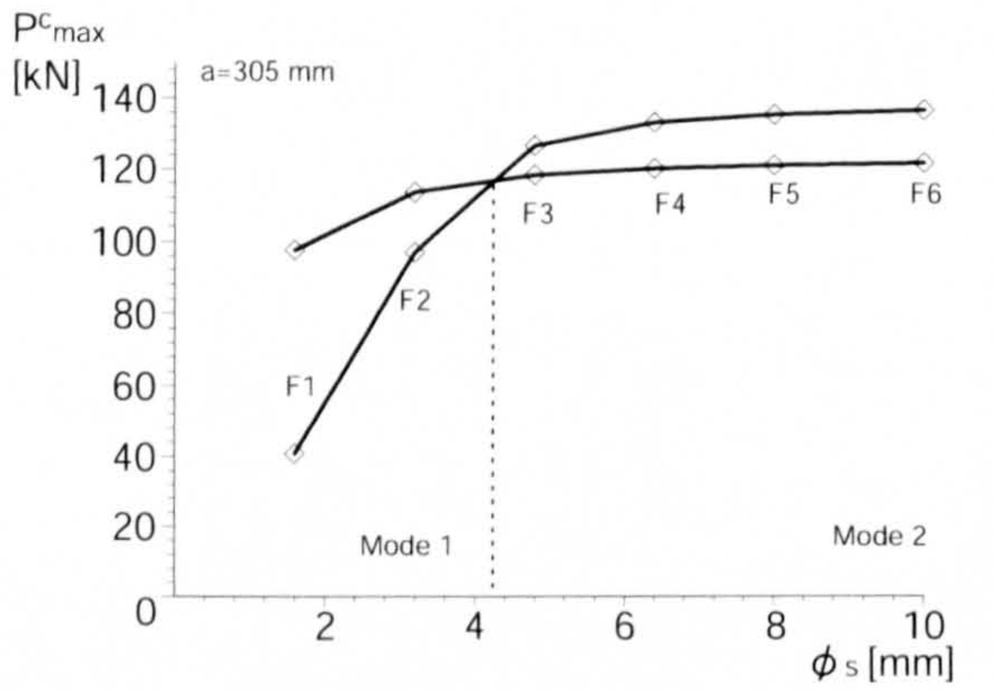

(d) a4

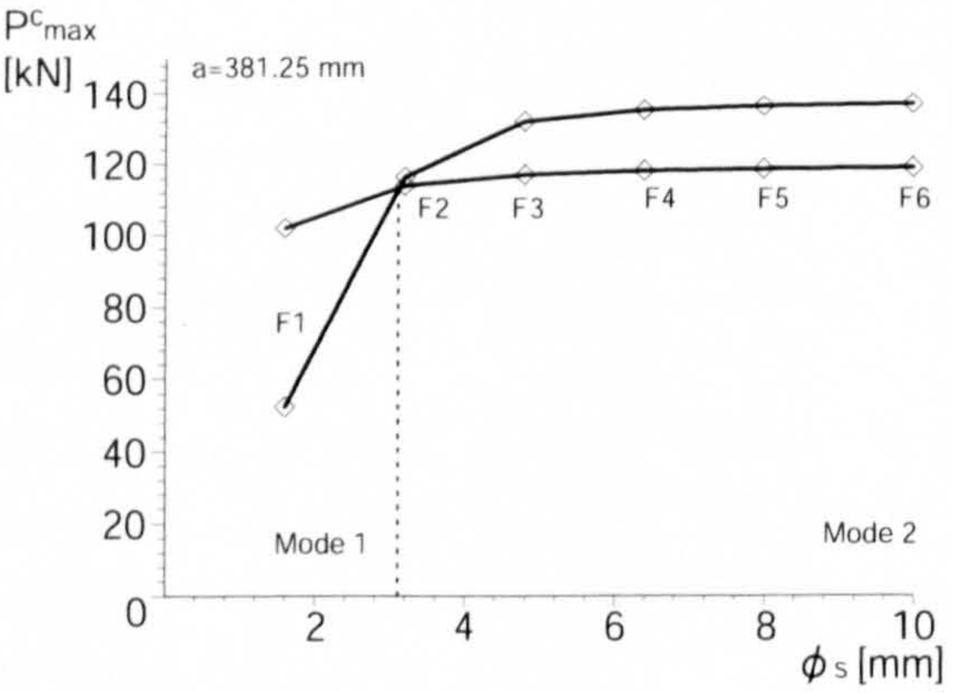

(e) a5

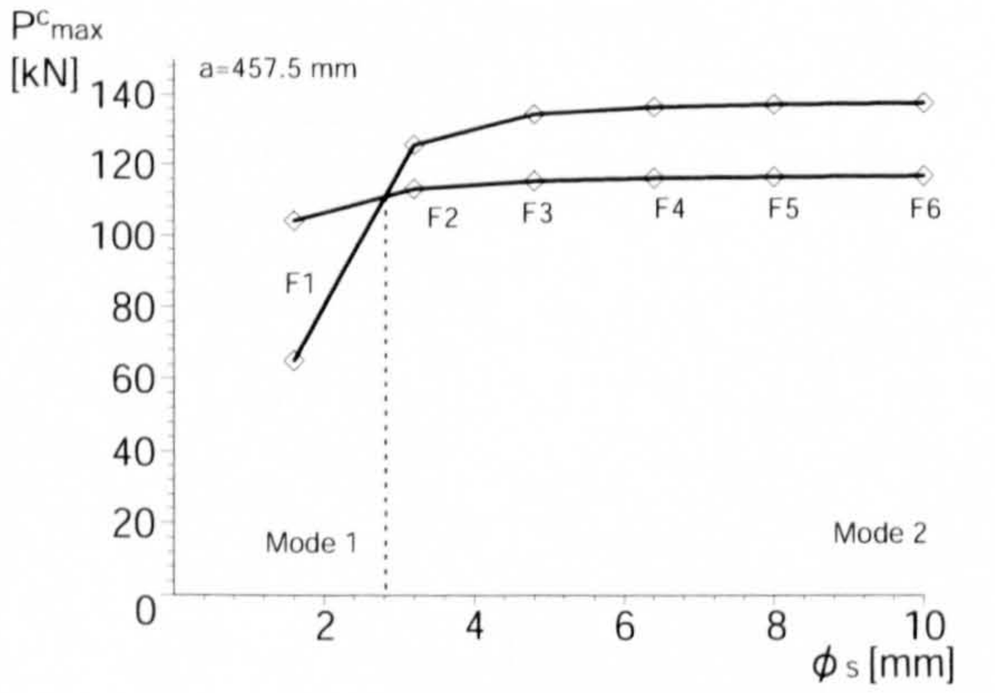

(f) a6

Figure 6.7: Buckling loads at T_{opt} with a variation of the crossarm length a and the stay diameter ϕ_s.

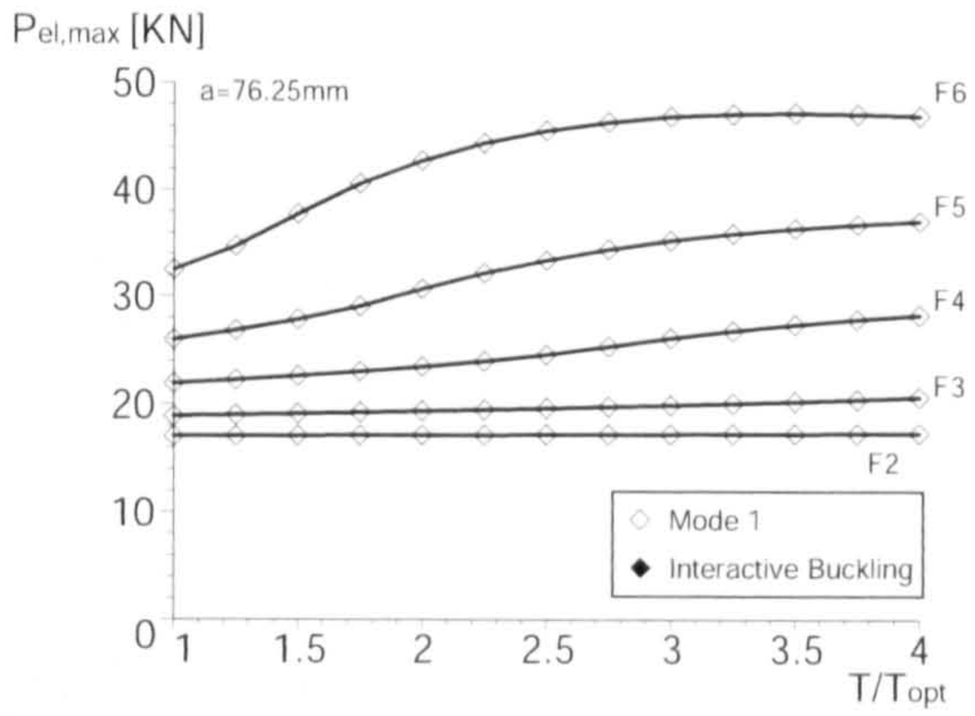

(a) a1

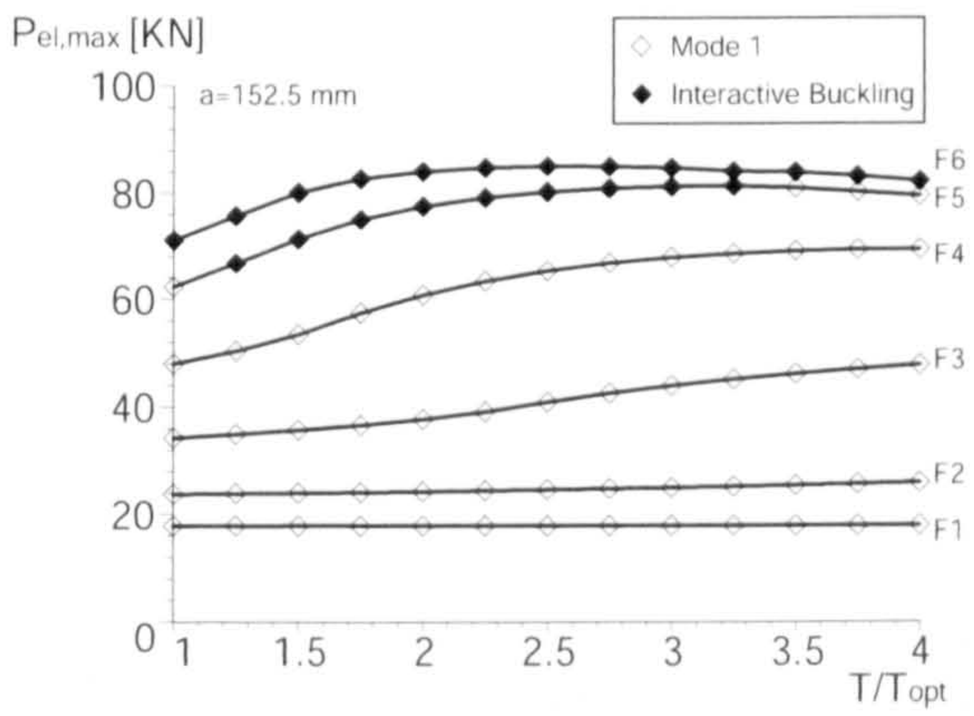

(b) a2

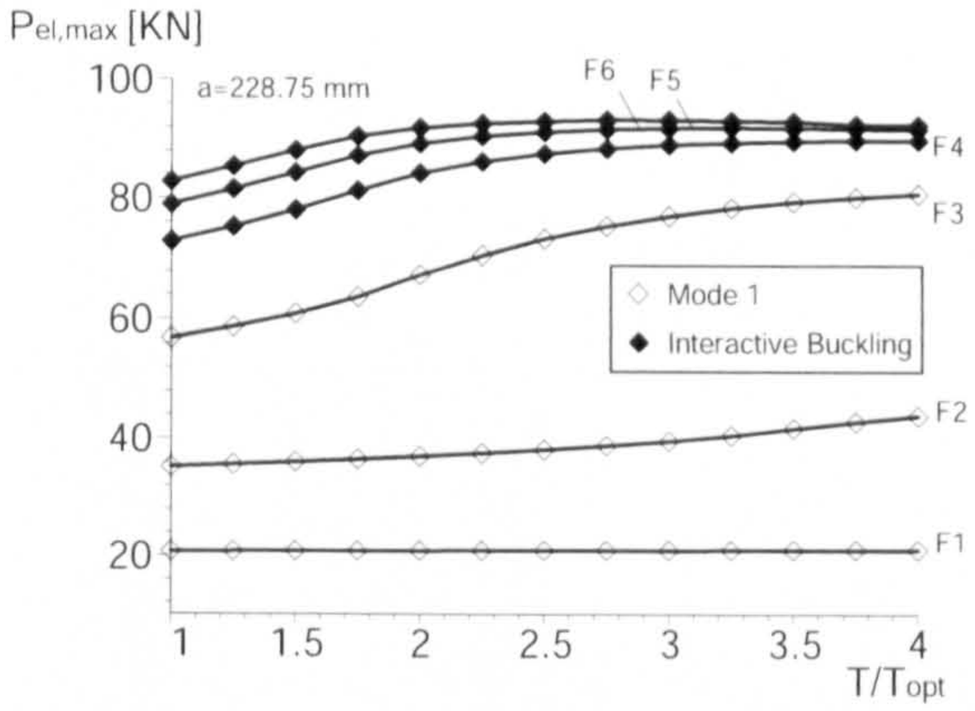

(c) a3

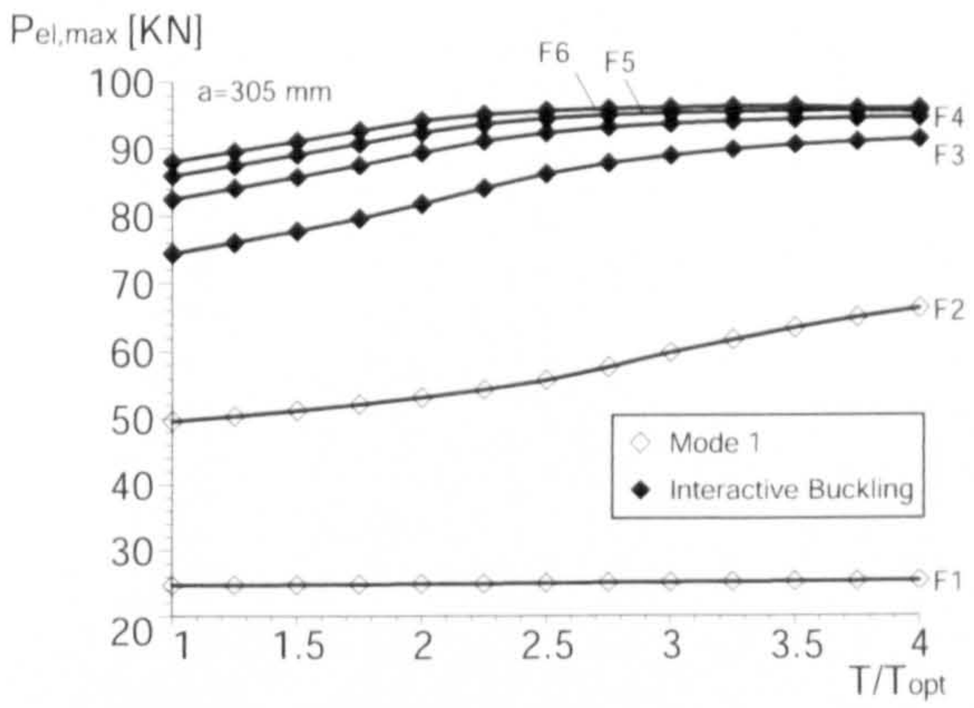

(d) a4

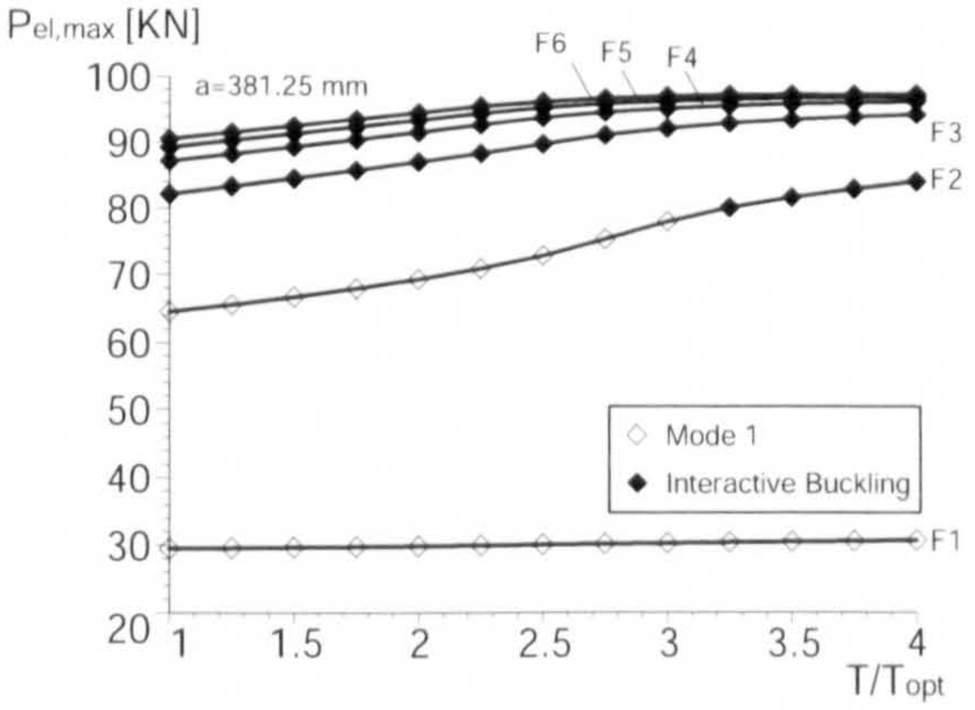

(e) a5

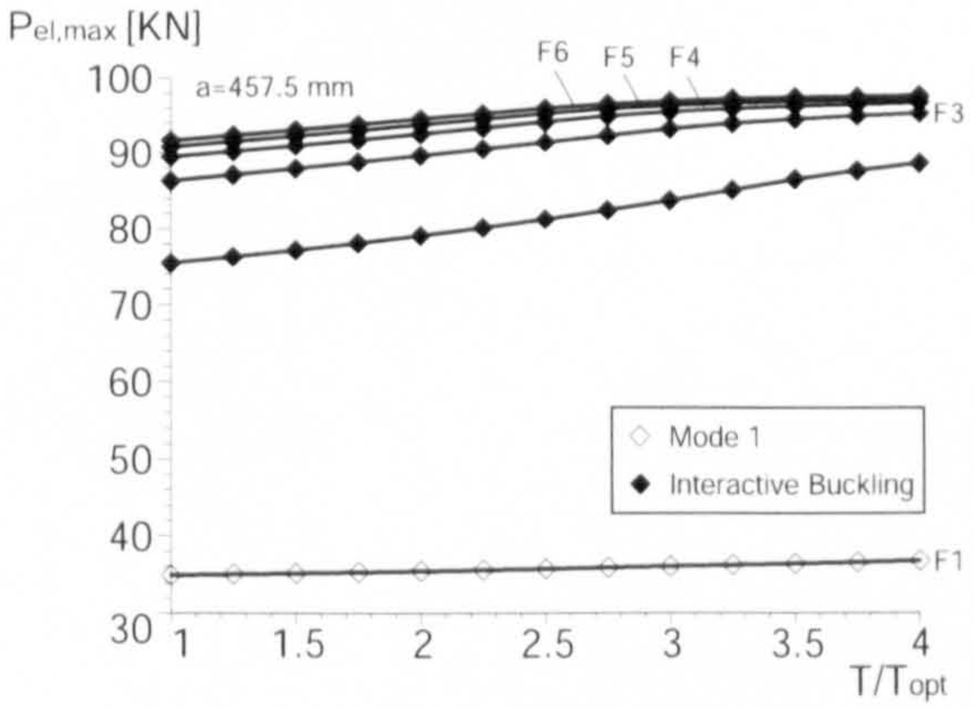

(f) a6

Figure 6.8: Maximum elastic load capacities against prestress with a variation of the crossarm length a and the stay diameter ϕ_s.

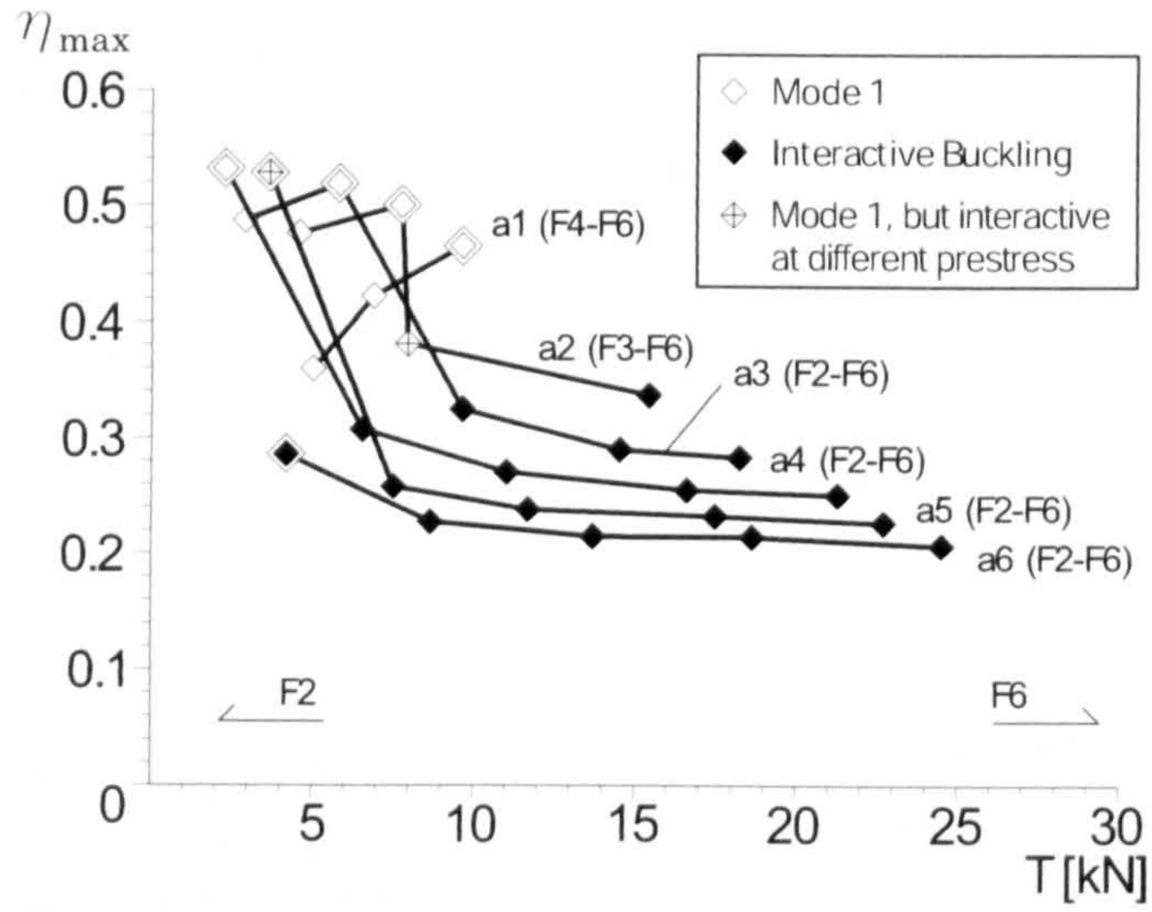

(a) comparing effects from varying the stay diameter with the crossarm length a fixed

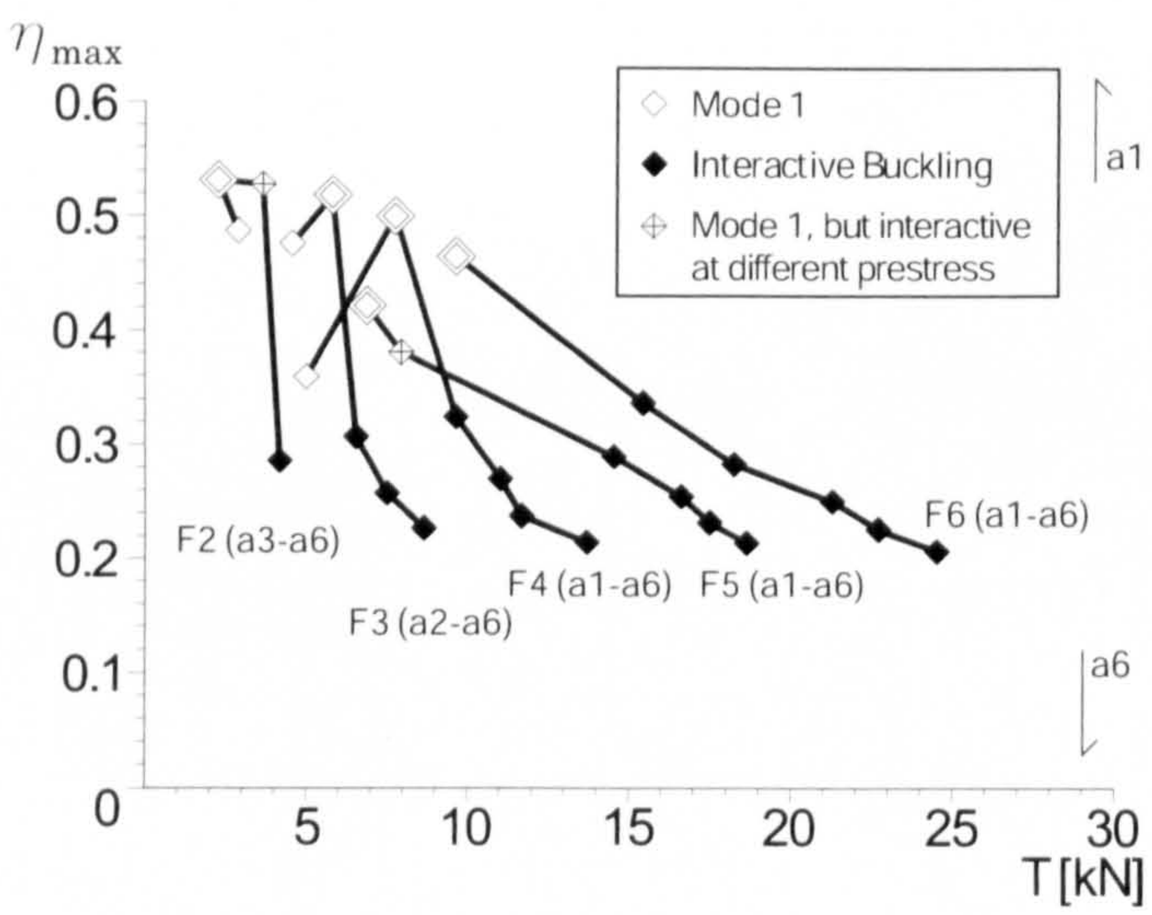

(b) comparing effects from varying the crossarm length with the stay diameter ϕ_s fixed

Figure 6.9: Maximum η for each case—the higher the value of η, the more efficiency in terms of the load carrying capacity to the required structural resistance of the column. Note that the double diamond shows the highest value in each sequence.

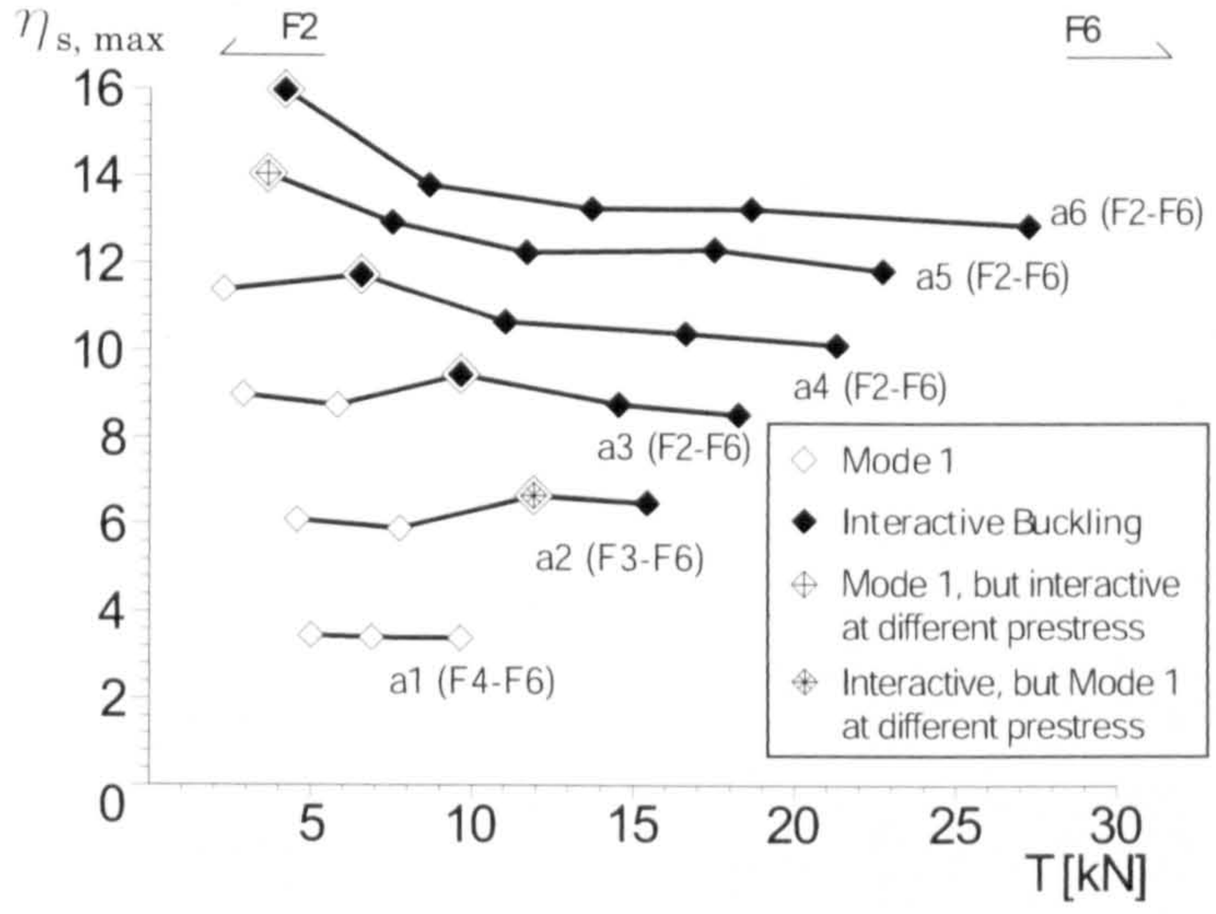

(a) comparing effects from varying the stay diameter ϕ_s with the crossarm length a fixed

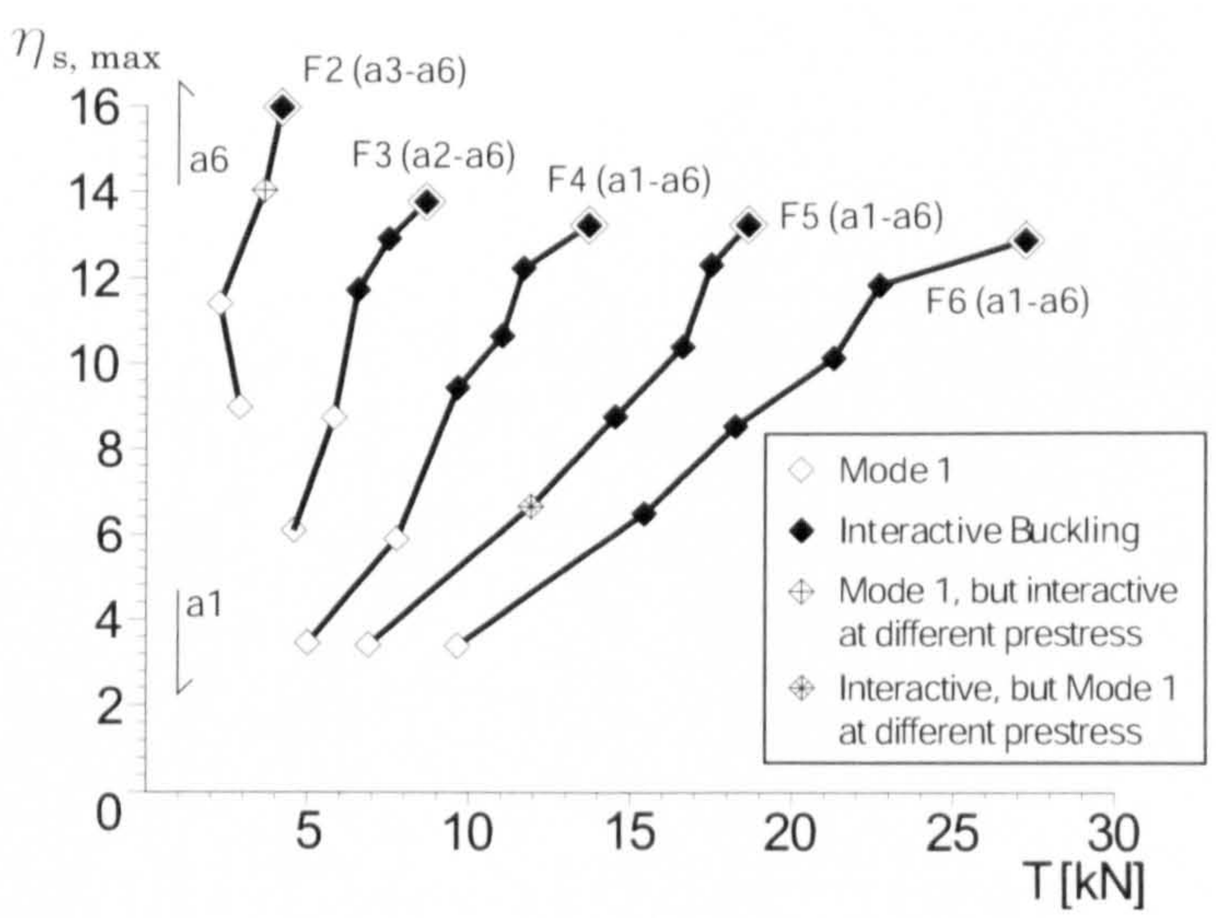

(b) comparing effects from varying the crossarm length a with the stay diameter ϕ_s fixed

Figure 6.10: Maximum η_s for each case—the higher a value of η_s, the less structural resistance is required to support a given load. Note that the double diamond shows the highest value in each sequence.

Chapter 7

Conclusions and Suggestions for Further Work

7.1 Concluding Remarks

This section summarizes the important findings from the research and presents the overall concluding remarks. More detailed conclusions may be seen at the end of each individual chapter.

Comprehensive theoretical post-buckling behaviour of stayed columns had not been investigated to any great extent before. Information on the post-buckling response is considered to be crucial for designers to ensure safety; therefore, it was important to investigate the post-buckling behaviour of stayed columns and to obtain rational methods to evaluate the structural efficiency. Thus, the primary objective of the research was to develop the analytical model to account for the post-buckling behaviour of a single crossarm type of prestress stayed column. Certainly, FE analysis could also illuminate the buckling behaviour; however, the introduction of geometrical imperfections is required, which hinders observing the post-buckling response in a perfect state. Hence, the research was initiated with the analytical work, which can account for the buckling behaviour in a perfect state, and the FEM was mainly

adopted for validation purposes at the initial stage.

In Chapter 3, the theoretical post-buckling behaviour of the prestressed steel stayed column was investigated using the Rayleigh–Ritz method with the standard component in a perfect state. The symbolic computation software MAPLE was adopted for computation. As the previous study (Hafez *et al.*, 1979) revealed that the critical load varies with the prestress, the analysis was conducted with this variation. FE analysis was also conducted to validate the modelling with an introduction of a small value of out-of-straightness, where a nearly perfect state of the column was simulated in the FEM.

The results showed that the post-buckling response was strongly linked to the zone distinction of the critical loads that was found by Hafez et al. (1979) for the first two buckling modes. Also the presented analytical model for Mode 1 had excellent agreement with the FE model; however, it was less accurate for Mode 2 when compared to Mode 1, but it was still considered to be useful to estimate approximate post-buckling responses for Mode 2. It was also shown that the most unstable path occurred with the prestress located at the boundary between Zones 2 and 3 (T_{opt}), although this prestress value gives the highest critical load. This implies that this level of the prestress is not favourable in terms of structural stability; hence, the greater level of the prestress than T_{opt} would be recommended, as a stable path occurs with a higher level of the prestress.

In Chapter 4, initial geometrical imperfections and failure criteria for each structural component were incorporated into the analytical model to account for more realistic behaviour of the stayed column. The model was therefore modified from that in Chapter 3, which previously considered perfect geometries. In order to investigate sensitivity to the out-of-straightness, the level of the imperfection was varied in the analysis.

With the modified model, the equilibrium path which accounted for initial out-of-straightness, column yielding and stay fracture was presented. The results were validated by the FEM. Again, it was revealed that the modified analytical model for

Mode 1 had excellent agreement with the FE model; however, it was less accurate for Mode 2 when compared to Mode 1, but it might be still useful to estimate approximate responses for Mode 2. At least, the current FE model was validated through this comparison. Sensitivity studies to the imperfection indicated that the true optimized prestress, which allows designers to obtain the maximum strength with minimized materials, is located in somewhere in Zone 3, although previously this value has been considered to be at the boundary between Zones 2 and 3, defined as T_{opt} from linear buckling analysis (Hafez *et al.*, 1979).

Chapter 5 described the interactive buckling behaviour of the stayed column with the FE model, which was validated through the comparisons made in Chapters 3 and 4. The levels of Modes 1 and 2 buckling loads were close together; the effect of interactive buckling, which normally gives an adverse effect on structures, was therefore thought to be significant. Despite this potential importance, research on the interactive buckling of the stayed had never been attempted. Analysis was conducted with a variation of the stay diameter and crossarm length, which gave cases which had different pairs of the Modes 1 and 2 buckling loads; thereby, the interactive buckling effect was investigated with the pairs of the buckling loads being varied.

The results indicated that the interactive buckling behaviour became crucial with lower levels of the maximum load capacity when Mode 2 is critical, especially in a region just after the transition in buckling modes from Modes 1 to 2, implying that the interactive buckling behaviour also needs to be taken into account to ensure safety. It was also shown that increasing the prestress from T_{opt} increased the maximum elastic load capacity in interactive buckling. This implied that introducing an amount of prestress greater than T_{opt} would be beneficial in increasing the efficiency of the structure. This design implication is in line with the findings in Chapters 3 and 4, which dealt with distinct mode buckling.

It was found from the investigation into the theoretical post-buckling behaviour conducted until Chapter 5 that the optimal prestress should be greater than the

previously suggested value of T_{opt}. Therefore, in Chapter 6, the optimal level of prestress was sought through parametric studies using the FEM. In addition to the prestress, the stay diameter and the crossarm length were varied in the analysis to examine the ideal configuration for the stayed column. In order to measure the structural efficiency, the ratios of the maximum elastic load to the required structural resistance for the column η and for the stay η_s were calculated as indicators for the structural efficiency. The required resistance was based on the necessary design strength that enabled the structure to reach the maximum elastic load. The use of these ratios enabled a comparison of each case even among cases which had different structural configurations as the ratios are nondimensionalized. An investigation into this type of indicator had never been attempted before.

The results indicated that the nondimensionalized optimal level of prestress $T_{\text{ropt}}/T_{\text{opt}}$ became lower as the stay diameter increases, and as the crossarm length a approached a configuration where the governing equilibrium behaviour changed from Mode 1 to interactive buckling. It was also revealed that the level of the optimal prestress for the column basically coincided with the level of the optimal prestress for the stay. This implies that designers are unlikely to need to adjust the level of prestress to balance these two.

It was also shown that the best efficiency in terms of the material use of the column could be found with a configuration where the governing equilibrium behaviour was Mode 1 and yet was close to the transition from Mode 1 to interactive buckling. As for the stay, the best efficiency could be seen with a configuration where the governing behaviour was interactive buckling and yet was close to the transition from Mode 1 to interactive buckling. It was also presented that the efficiency for the stay could be improved with an increase in the crossarm length a. Certainly, to achieve the best efficiency, the use of the optimal level of prestress was required. These results suggest that the configuration of the stayed column should be determined such that the buckling behaviour would be located at the transition from Mode 1 to interactive buckling with an adequate crossarm length.

This is the first study that deals with the comprehensive theoretical post-buckling behaviour of a single crossarm type, including interactive buckling. Overall, the importance of the post-buckling response has been recognized, and all of these obtained implications could be applicable for designers, which would be expected to contribute to making the design safer and more efficient. Despite these achievements, there are further potential avenues of research to explore in the future, and these are presented in the next section.

7.2 Suggestions for Further Work

As stated, this research provides the basic but comprehensive post-buckling theory and design recommendations for the stayed column to some extent. The current studies, however, do not account for the effect of stress relaxation that may occur due to creep and changes in the ambient temperature with the stays and the column changing their lengths, and thereby their internal forces, causing a change in their stress state. In Zone 3, where the optimal prestress is considered to be located, relaxation may change the response of the column by reducing the prestress from where the column has a relatively stable initial post-buckling response (Zone 3 buckling behaviour) to purely unstable post-buckling responses (towards where $T = T_{\text{opt}}$). This adverse effect from stress changes would be a key sensitivity to focus on in future work. If this sensitivity is significant, it would also be suggested that designers should take into account both the initial prestress and the effective value of prestress after a long time period. Of course, the situation would become more complicated if materials of different coefficients of thermal expansion are used in the column and the stays respectively, or if the temperature changes are non-uniform within the whole component.

Experimental studies focusing on the buckling response are also necessary in order to validate the analytical and numerical models. In the current studies, following Eurocode 3, it was assumed that the basic imperfection value δ of 1/300 covers

the effects of all types of imperfections, including residual stress and geometrical imperfections, which was considered to lead to the appropriate value of the design load. Certainly, this assumption has to be validated through experimental work.

Recent work (De Araujo *et al.*, 2006) presented full-scale three-dimensional experimental test results. Their work showed that the actual full-scale stayed columns could provide more strength than ordinary columns. Despite their achievement, there are a few points which have to be improved in further experimental work. Firstly, their tests were performed in the horizontal plane for the simplification of the measurements and the installation. This layout caused a considerable amount of the initial deflection from the dead weight of the system. As the current work revealed, the initial deflection strongly affects the buckling response including the interactive behaviour. This point may have to be improved to gain more accurate responses in experimental tests. Possible solutions would be to precamber the column to counteract dead load deflections. Secondly, an added support at the mid-span of the column was added to their test by including an additional stay in order to counteract the dead load of the column. However, this support might have contributed to distorting the test results as this support could act as a spring, which also could store the axial energy. In fact, a negative deflection was observed from one of their tests at the initial stage of loading results, which is unlikely in the real case. The third point concerns support conditions for the column. Because of space restrictions, they could not present the ideal support conditions—neither ideal hinges nor rigid supports—in their performed tests. Eventually, semi-rigid supports were provided, which hindered them from developing FE models to simulate their actual experimental work. For practical reasons, the number of the feasible experimental tests would be limited, and FE analysis would therefore be required to complement experimental data in most circumstances. Hence, the support conditions also probably need improvement. Boundary conditions would not be a significant issue if there were no stays in the system as ordinary structural components, because adopting the concept of the effective length enables the use of contraflexure points as virtual pin-ends. However, in the case of the stayed column, this concept cannot be adopted

due to the presence of the stay anchor system at the end of the column element, at which reasonably accurate and ideal boundary conditions have to be provided. It should be noted that improvements in these points would give substantial benefits in further experimental work.

Moreover, the current modelling is limited to two-dimensional (2D) behaviour, it may become important to develop three-dimensional (3D) models. Recent work (Liew & Li, 2006; De Araujo *et al.*, 2006) has used 3D modelling to address 3D collapse responses with a variety of structural configurations and boundary conditions, and with different levels of the prestress. In addition to these, other stability issues also should be investigated in 3D such as the effect of the ovalization of the tube section (Brazier, 1927; Wadee *et al.*, 2006), and torsional effects if, for example, open sections are used instead of closed sections for the main column component.

The results obtained from the current research and the further work outlined above could be used as a basis to produce comprehensive design guidance. Currently, codes of practice, such as Eurocode 3, are lacking in the design procedures for such potentially efficient and cost-effective structures; consequently, case and sensitivity studies in conjunction with engineering judgement are necessary to design stayed columns in practice. Establishing such guidance for stayed columns would facilitate designers to adopt this structural component more effectively.

Appendix A

Hessian Matrix for Zone 3

When the number of degrees of freedom is two in Mode 1, the critical load for Zone 3 can be obtained through calculating the following determinant of the Hessian Matrix:

$$\begin{vmatrix} \dfrac{\partial^2 V_{1B}}{\partial q_1^2} & \dfrac{\partial^2 V_{1B}}{\partial q_1 \partial q_3} \\ \dfrac{\partial^2 V_{1B}}{\partial q_3 \partial q_1} & \dfrac{\partial^2 V_{1B}}{\partial q_3^2} \end{vmatrix} = 0. \tag{A.1}$$

Each component of the matrix can be expressed as

$$\frac{\partial^2 V_{1B}}{\partial q_1^2} = \chi_{p11} P + \chi_{t11} T + \chi_{11}, \tag{A.2}$$

$$\frac{\partial^2 V_{1B}}{\partial q_1 \partial q_3} = \frac{\partial^2 V_{1B}}{\partial q_3 \partial q_1} = \chi_{p13} P + \chi_{t13} T + \chi_{13}, \tag{A.3}$$

$$\frac{\partial^2 V_{1B}}{\partial q_3^2} = \chi_{p33} P + \chi_{t33} T + \chi_{33}. \tag{A.4}$$

The coefficients of the above equations are as follows:

$$\chi_{p11} = \frac{a\left[8b_{pB}E_sA_s\left(b_{11B} - 2\cos^2\alpha\right)\cos^3\alpha + b_{pB}EA\left(4b_{11B} - \pi^2\right) - 4b_{11B}\right]}{\tan\alpha}, \quad \text{(A.5)}$$

$$\chi_{t11} = \frac{2a\left(8\cos^2\alpha - \pi^2\right)\cos\alpha}{\tan\alpha}, \quad \text{(A.6)}$$

$$\chi_{11} = \frac{\left(64a^2E_sA_s\cos^3\alpha + EI\pi^4\right)\tan\alpha}{4a} \quad \text{(A.7)}$$

$$\chi_{p13} = \frac{2a\left[2b_{pB}E_sA_s\left(4\cos^2\alpha + b_{13B}\right)\cos^3\alpha + b_{13B}\left(b_{pB}EA - 1\right)\right]}{\tan\alpha}, \quad \text{(A.8)}$$

$$\chi_{t13} = \frac{-16a\cos^3\alpha}{\tan\alpha}, \quad \text{(A.9)}$$

$$\chi_{13} = -16aE_sA_s\sin\alpha\cos^2\alpha, \quad \text{(A.10)}$$

$$\chi_{p33} = \frac{a\left[8b_{pB}E_sA_s\left(b_{33B} - 2\cos^2\alpha\right)\cos^3\alpha + b_{pB}EA\left(4b_{33B} - 9\pi^2\right) - 4b_{33B}\right]}{\tan\alpha}, \quad \text{(A.11)}$$

$$\chi_{t33} = \frac{2a\left(8\cos^2\alpha - 9\pi^2\right)\cos\alpha}{\tan\alpha}, \quad \text{(A.12)}$$

$$\chi_{33} = \frac{\left(64a^2E_sA_s\cos^3\alpha + 81EI\pi^4\right)\tan\alpha}{4a}, \quad \text{(A.13)}$$

where:

$$b_{11B} = \left[4E_sA_s\left(3\cos^2\alpha - 2\right)\cos^3\alpha - \pi^2\left(\frac{\pi^2EI}{L^2} - \frac{EA}{4}\right)\right]\left[2E_sA_s\cos^3\alpha + EA\right]^{-1}, \quad \text{(A.14)}$$

$$b_{33B} = \left[4E_sA_s\left(3\cos^2\alpha - 2\right)\cos^3\alpha - 9\pi^2\left(\frac{9\pi^2EI}{L^2} - \frac{EA}{4}\right)\right]\left[2E_sA_s\cos^3\alpha + EA\right]^{-1}, \quad \text{(A.15)}$$

$$b_{13B} = -2\left[4E_sA_s\left(3\cos^2\alpha - 2\right)\cos^3\alpha + \frac{15\pi^4EI}{L^2}\right]\left[2E_sA_s\cos^3\alpha + EA\right]^{-1}. \quad \text{(A.16)}$$

The critical load for Mode 2 can also be obtained by following the same process as that for Mode 1, but it should be noted that the expressions for Mode 2 are more complicated, reflecting the extra complexity in the model for that buckling mode.

Appendix B

Error Evaluation and Imperfection Amplification

B.1 Error Evaluation and Error Increase in Mode 2

The buckling responses with imperfections from the analytical and the FE models were already shown in Figures 4.13 and 4.14. Although the models were validated against each other, the error between the two was not precisely evaluated.

Figure B.1 shows the difference of maximum loading capacity between the analytical and the FE models when $\delta = 1/300$ for Mode 1 and $\delta = 1/600$ for Mode 2. The error was calculated using the following:

$$\text{Error}\,[\%] = \frac{(P_{\text{el,max}})_{\text{AM}} - (P_{\text{el,max}})_{\text{FEM}}}{(P_{\text{el,max}})_{\text{FEM}}}, \tag{B.1}$$

where $(P_{\text{el,max}})_{\text{AM}}$ and $(P_{\text{el,max}})_{\text{FEM}}$ represent the maximum loads for the analytical model and the FEM respectively when it is assumed that all of the components in the models are purely elastic. The graph clearly shows that, although the error remained around 4 % for Mode 1, this value increases from 10 to 15 % for Mode

2 as the initial prestress T increases. It was already discussed in Chapter 4 that the reason for less accuracy in Mode 2 is caused by the lack of the numbers of degrees-of-freedom; nevertheless, a reason for this error increase in Mode 2 have not yet been investigated. Hence, in this appendix, some possible reasons for this error

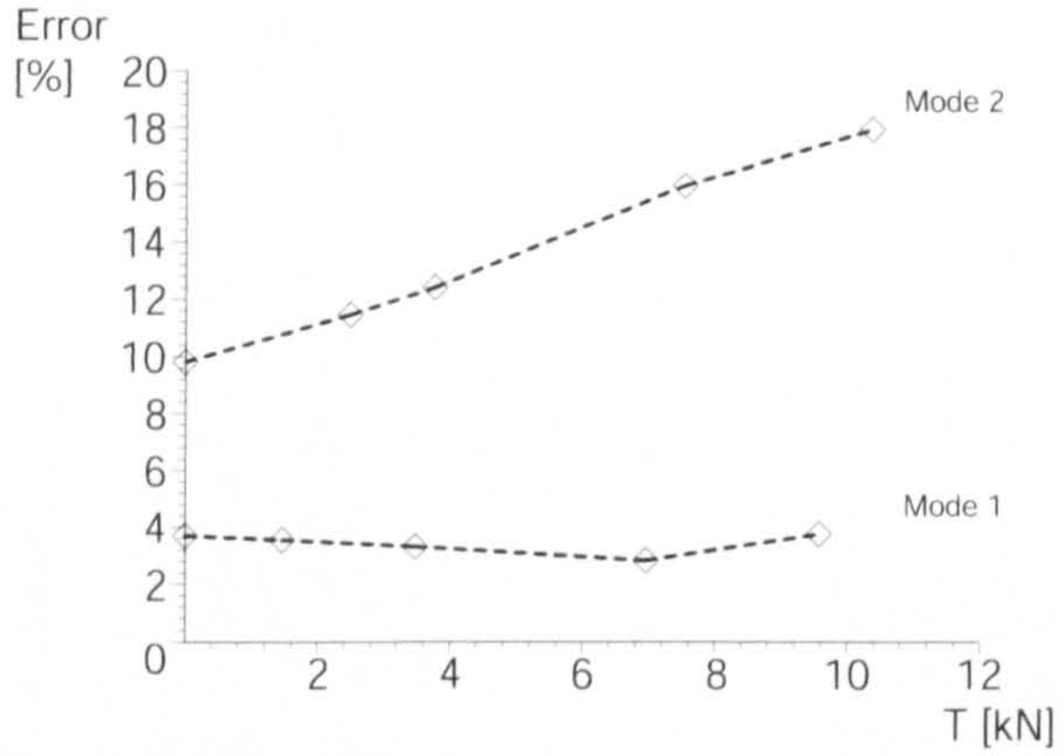

Figure B.1: Error between the analytical and the FE models, when $\delta = 1/300$ for Mode 1 and $\delta = 1/600$ for Mode 2.

increase are presented; the results may illuminate necessary improvements in the current analytical model.

B.2 Hypothesis and Methodology for Investigation

One of the reasons for this increase in the discrepancy in Mode 2 might be attributed to the fact that in the FEM, the amplitude of the out-of-straightness is increased from the initial compression force in the column. In fact, it was assumed that the initial configuration is kept after the introduction of the initial prestress, i.e. the effect of the imperfections being amplified by the application of the prestress was neglected in the current analytical model.

In order to assess the effect of the imperfection amplification, the level of this imperfection amplification was investigated using both the analytical modelling and

the FEM. Then, with obtained amplified imperfection values, the current analytical model was recalculated, which led to corrected results.

B.3 Effect of Imperfection Amplification

The level of the imperfection amplification was obtained using the equilibrium equation (4.40). As all of the stays are active in this case, Type B was the buckling type. The same analytical model can be used in the calculation, except that Δ needed to be re-evaluated by substituting $P = 0$ into equation (3.33) and, similarly, P needed to be equated to zero in the energy expressed in equation (4.39). Furthermore, for Mode 2, it was necessary for the energy to be expanded to the 2nd order as a Taylor series with respect to T in order to render the equilibrium equation tractable. FE analysis was also conducted to validate the analytical model for the selected values of prestress represented in Table 4.1. Figure B.2 shows the relationship between the

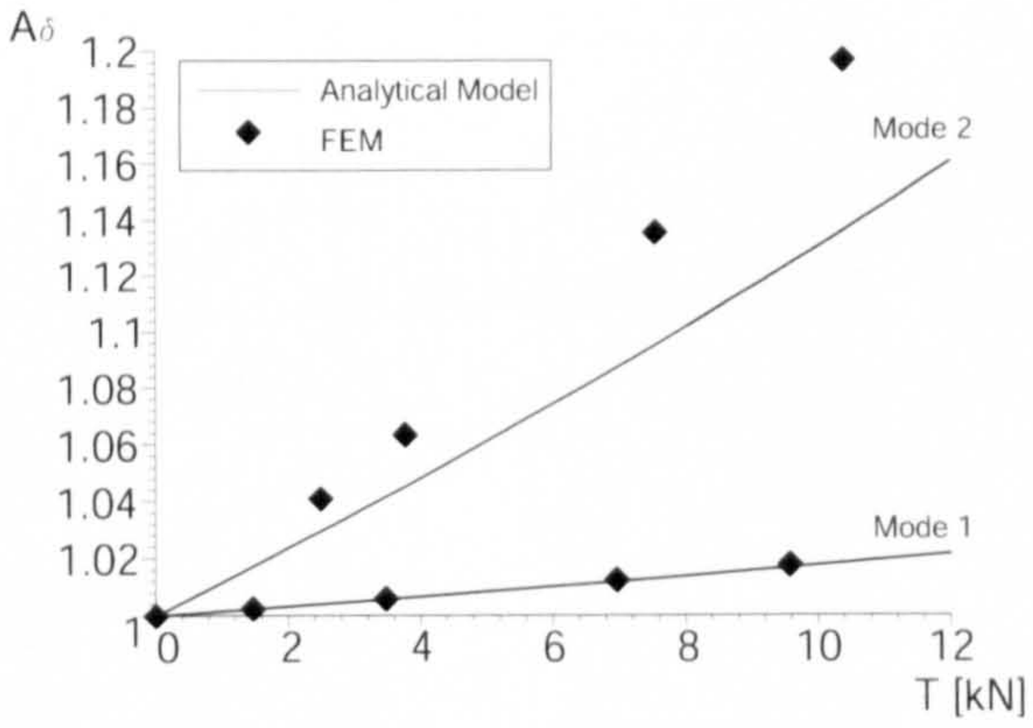

Figure B.2: Imperfection amplification ratio A_δ, when $\delta = 1/300$ for Mode 1 and $\delta = 1/600$ for Mode 2.

initial prestress T and the imperfection amplification ratio A_δ, which is defined as

$$A_\delta = \frac{\delta_T}{\delta}, \tag{B.2}$$

where δ_T is the amplitude of the nondimensional imperfection after prestressing. The amplitude of δ_T was measured at the mid-height for Mode 1 and at the quarter

point for Mode 2 respectively. As expected, the level of imperfection amplification becomes larger as the prestress increases. Also it can be seen that the Mode 2 imperfection is much more sensitive to the prestress—an increase of 18% in the out-of-straightness can be seen with the level of the Point 5 prestress from FE analysis. Despite this significant sensitivity in Mode 2, in Mode 1 this amplification is around only 2% at the maximum; therefore, this amplification is considered to be negligible in Mode 1. Therefore, it can be said that in Mode 2, the current analytical modelling underestimates the level of imperfection especially at higher levels of the prestress, which can be thought to be one of the reasons that the errors increase seen in Figure B.1. In order to confirm this hypothesis, the concept of imperfection amplification from the prestress was introduced into the current analytical model to correct the Mode 2 buckling behaviour and is reported below.

B.4 Corrected Analytical Response

The modified value of the imperfection is necessary to reflect the effect of imperfection amplification in the current model; this value can be calculated by multiplying the initial imperfection by the amplification ratio A_δ. Using these corrected values of the imperfection when $\delta = 1/600$, which were derived from Figure B.2, the analytical model for Mode 2 was recalculated.

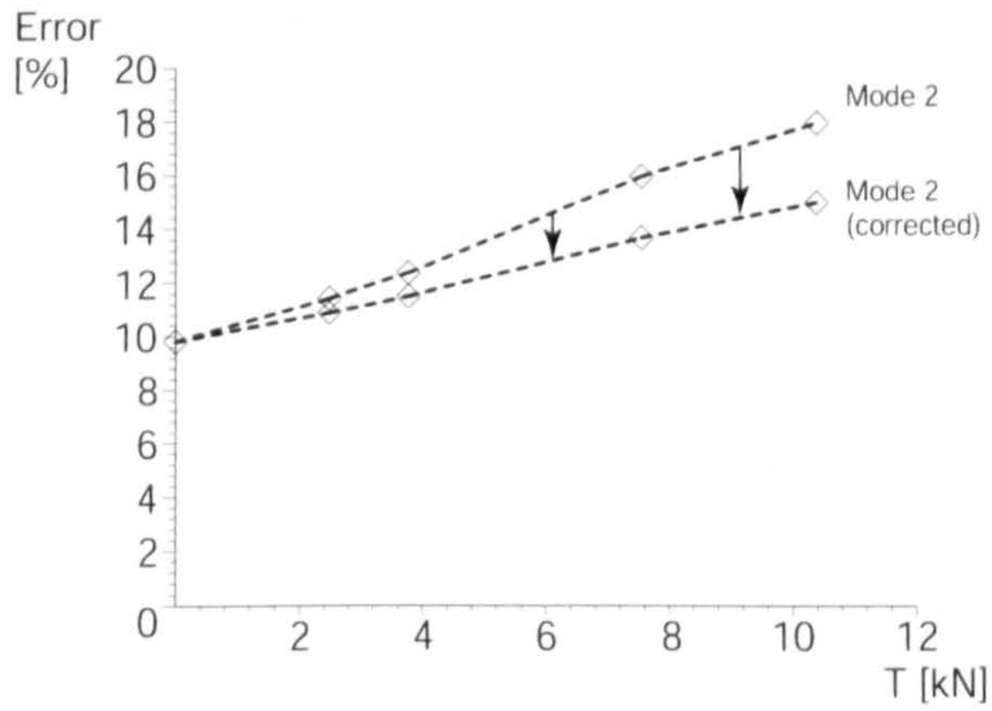

Figure B.3: Error between the analytical and the FE models in Mode 2 when $\delta = 1/600$.

Figure B.3 shows that the difference of the maximum elastic load capacity between the corrected analytical and the FE models. For comparison purposes, the case in which the effect of the imperfection amplification was neglected is also plotted. As expected, a substantial improvement in the error is seen; nevertheless, it should be noted that a type of error which increases as the initial prestress T increases still exists. A part of the reason for this remaining error increase is thought to be attributed to the fact that the Mode 2 amplification ratio was underestimated compared with that obtained from the FEM, as can be seen from Figure B.2, i.e. the effect of imperfection amplification is not fully reflected in the obtained results. However, this underestimation does not seem to explain everything about this error increase as the degree of the underestimation is not significant.

The results indicate that the imperfection amplification is one of the important reasons for the increase in the discrepancy between the two models as T increases, although introducing imperfection amplification into the current analytical model cannot explain everything on this error increase. Further investigation and model modification might be necessary to explain this phenomenon, although this modification would probably make the current analytical model even more complicated.

B.5 Summary

In this Appendix, possible reasons for an increase in the error between the analytical model and the FEM for Mode 2 buckling response as the prestress T increases has been examined. In order to account for this phenomenon, the effect of the imperfection amplification was taken into account in the current analytical modelling. To the knowledge of the author, the concept of the imperfection amplification has never been considered in previous work.

It has been shown that including the effect of the imperfection amplification reduces this error increasing substantially. Thus, it can be concluded that imperfection amplification is one of the important reasons for the increase in the discrepancy

between the two models as T increases, However, it has also been shown that this error increase is not solely attributed to the imperfection amplification. Further investigation and model modification might be necessary to explain this phenomenon, although this modification would probably make the current analytical model even more complicated.

Appendix C

Supplementary Data for Parametric Studies

For §6.4, parametric studies were conducted to obtain the maximum values of η and η_s for each case, which are presented in Table 6.3. However, all of the data were not presented in that section to gain the maximum value of η and η_s. Although the maximum elastic load capacities were presented in the main text, the required yield stress for the column $f_{\mathrm{y,req}}$, the required design stress for the stay $f_{\mathrm{s,Rd,req}}$, and values of η and η_s at different levels of the prestress were not presented for brevity. In this Appendix, these values are presented to clarify where the results originated.

C.1 Required Stress

Figure C.1 shows the required yield stress for the column $f_{\mathrm{y,req}}$, which is one of the components to obtain values of η, at each level of the prestress for each case. Figure C.2 plots the required design stress for the stay $f_{\mathrm{s,Rd,req}}$, which is one of the components to obtain values of η_s, at each level of the prestress for each case.

C.2 Column Element Efficiency η and Stay Efficiency η_s

Figure C.3 shows values of η for all of the considered configurations and prestress. As can be seen, the maximum value of η in each diagram is basically observed on a curve where the governing equilibrium behaviour is Mode 1 but close to the transition from Mode 1 to interactive buckling. Figure C.4 shows values of η_s for all of the considered configurations and prestress. The maximum value of η_s for each diagram is also observed at a curve where the governing equilibrium behaviour is interactive but close to the transition from Mode 1 to interactive buckling. Note that these points were already discussed in the main chapter.

APPENDIX C. SUPPLEMENTARY DATA FOR PARAMETRIC STUDIES

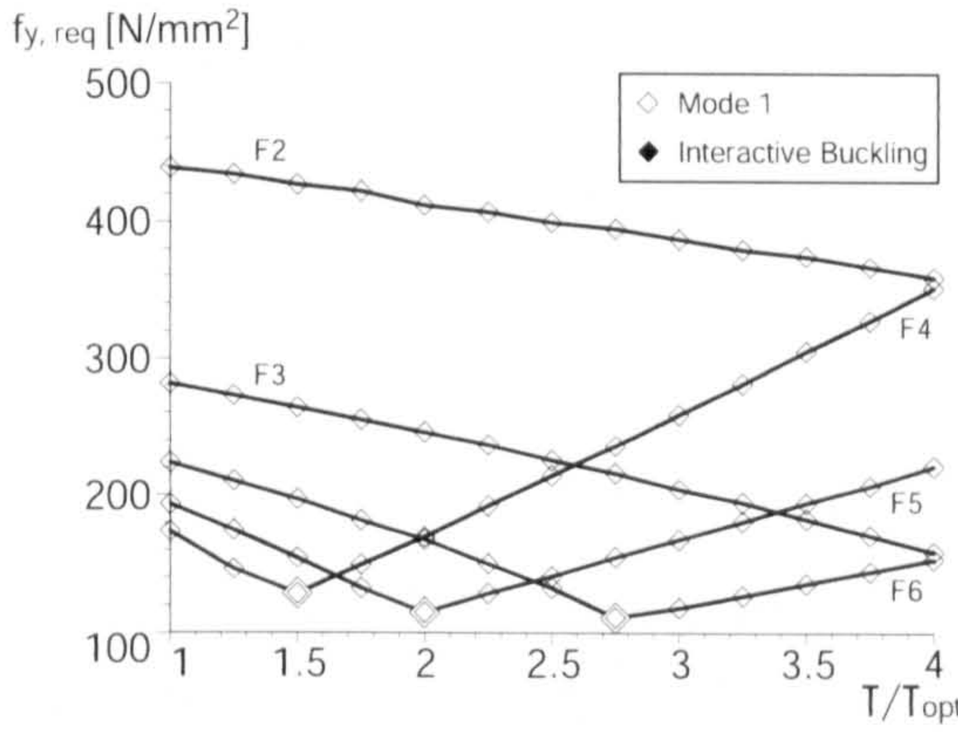

(a) a1

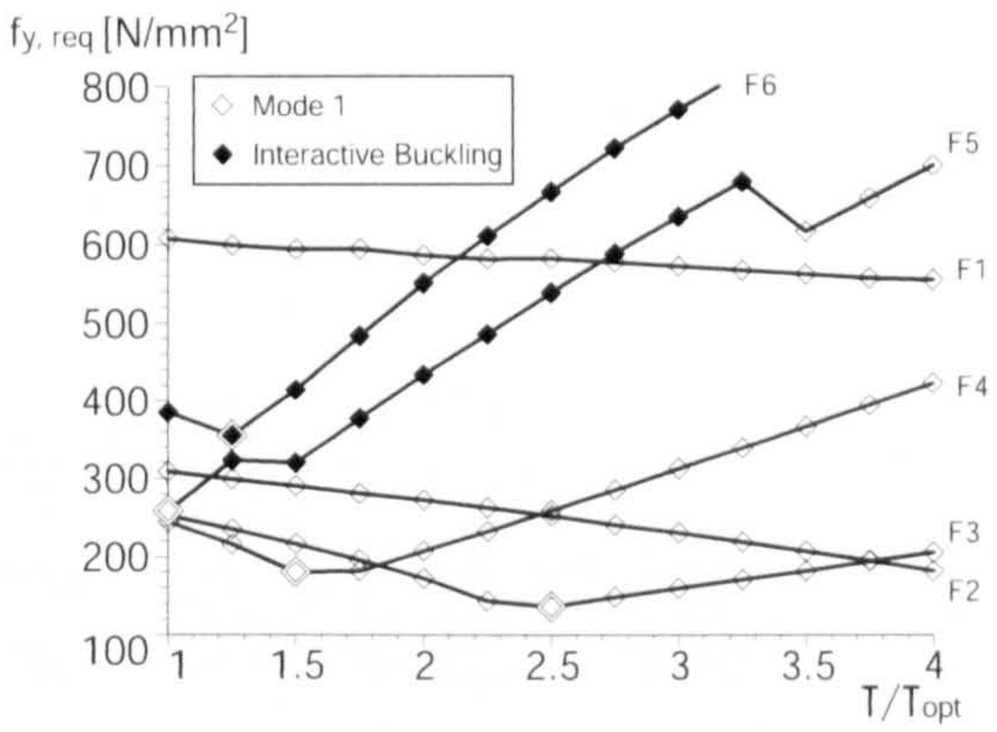

(b) a2

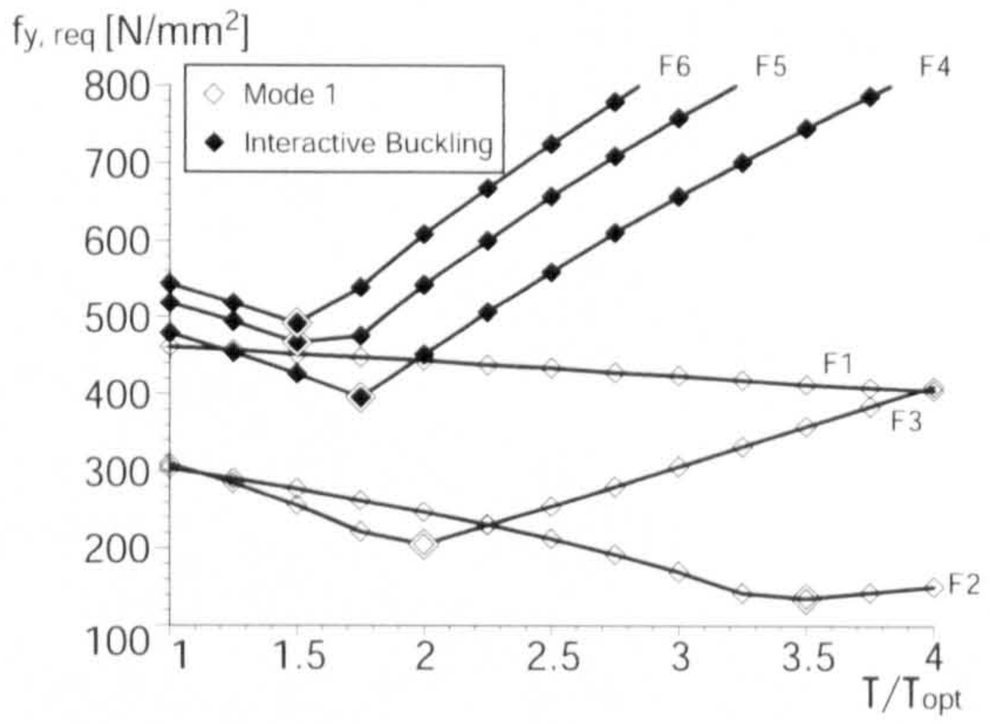

(c) a3

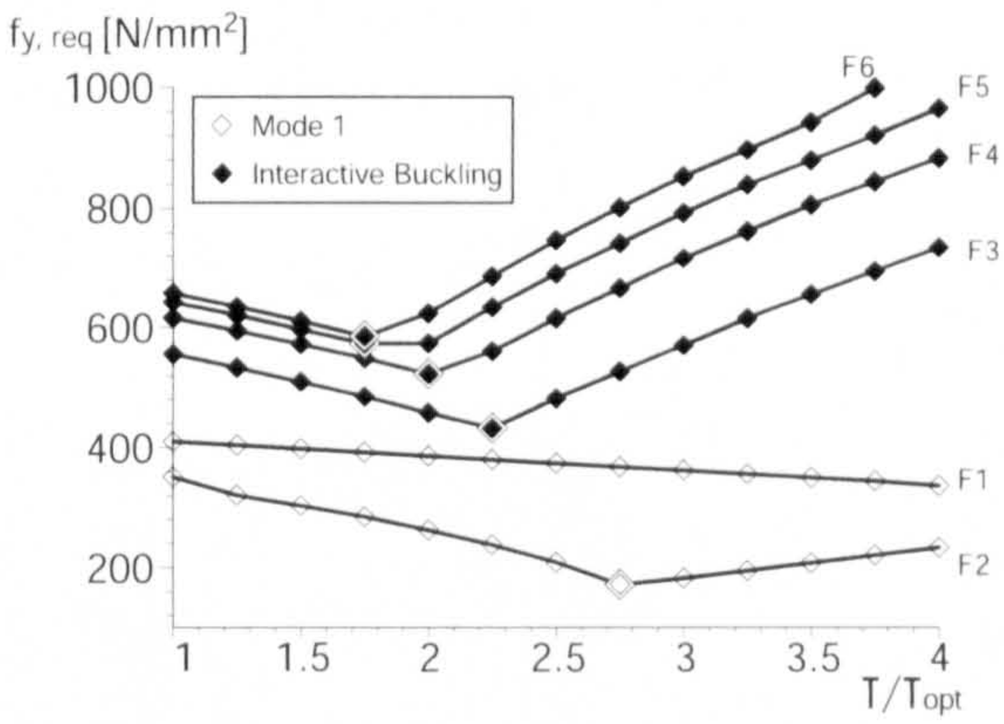

(d) a4

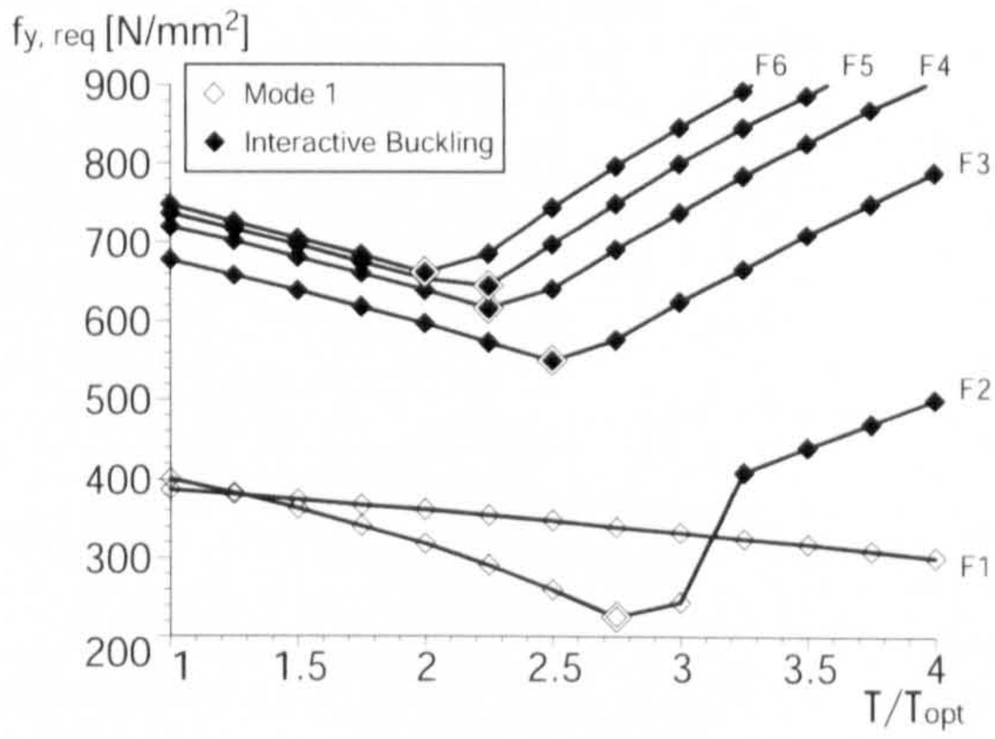

(e) a5

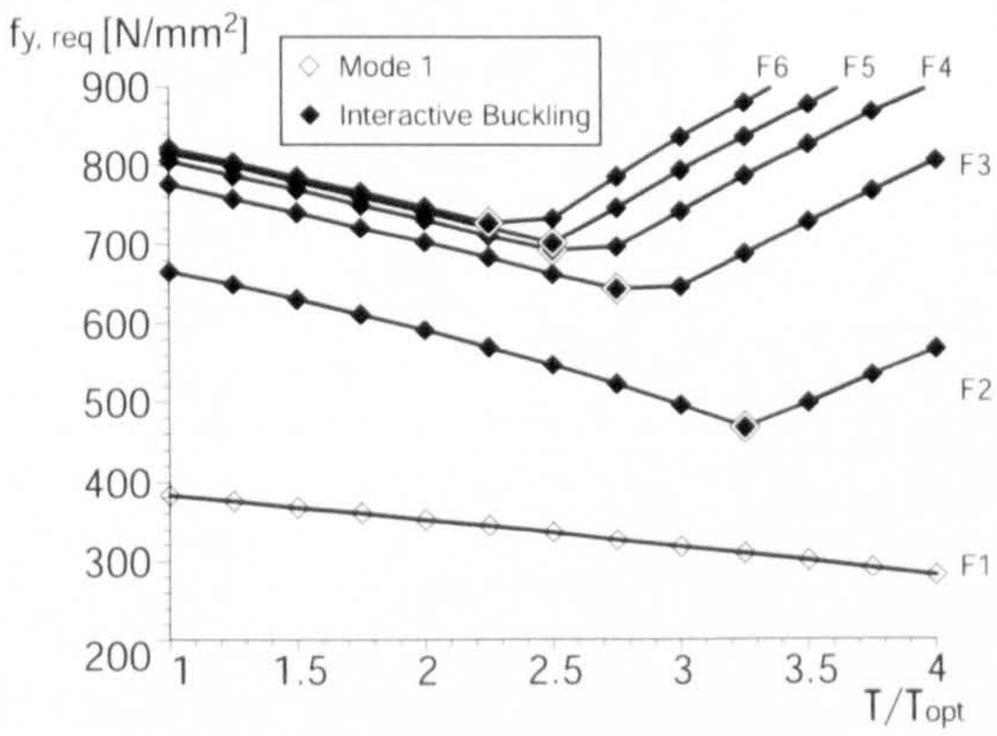

(f) a6

Figure C.1: Required column yield stress $f_{y,req}$.

APPENDIX C. SUPPLEMENTARY DATA FOR PARAMETRIC STUDIES

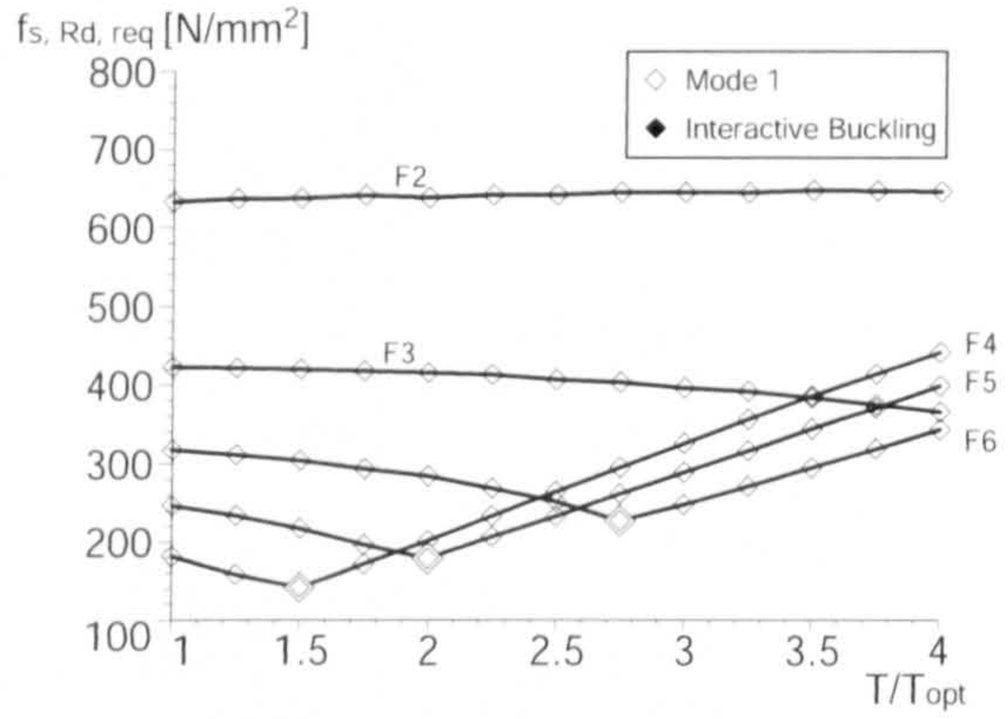

(a) a1

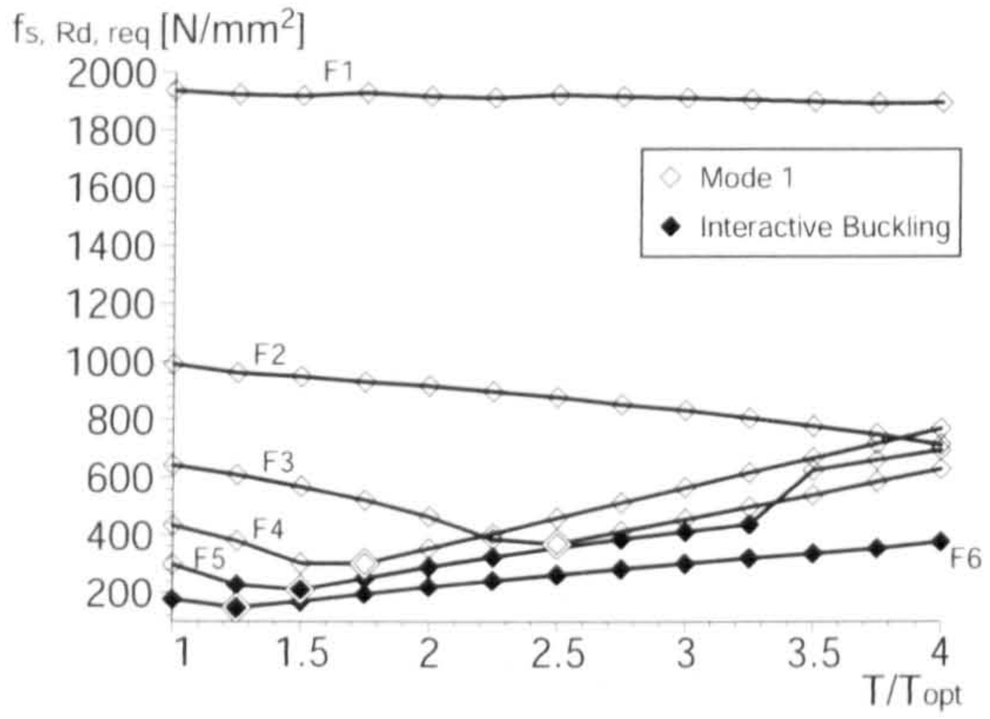

(b) a2

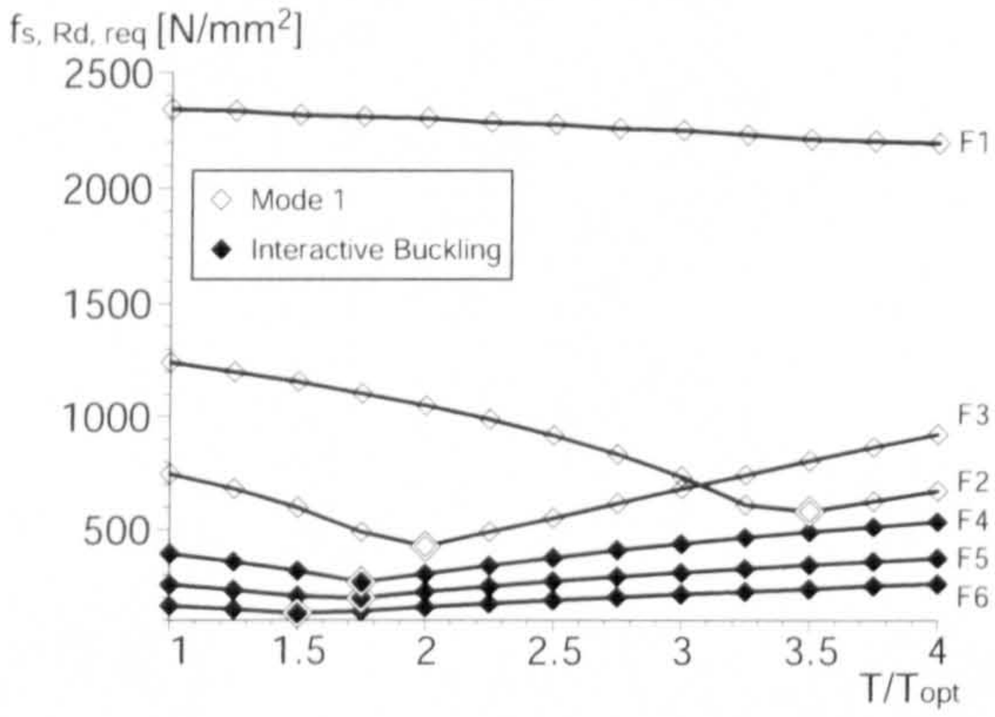

(c) a3

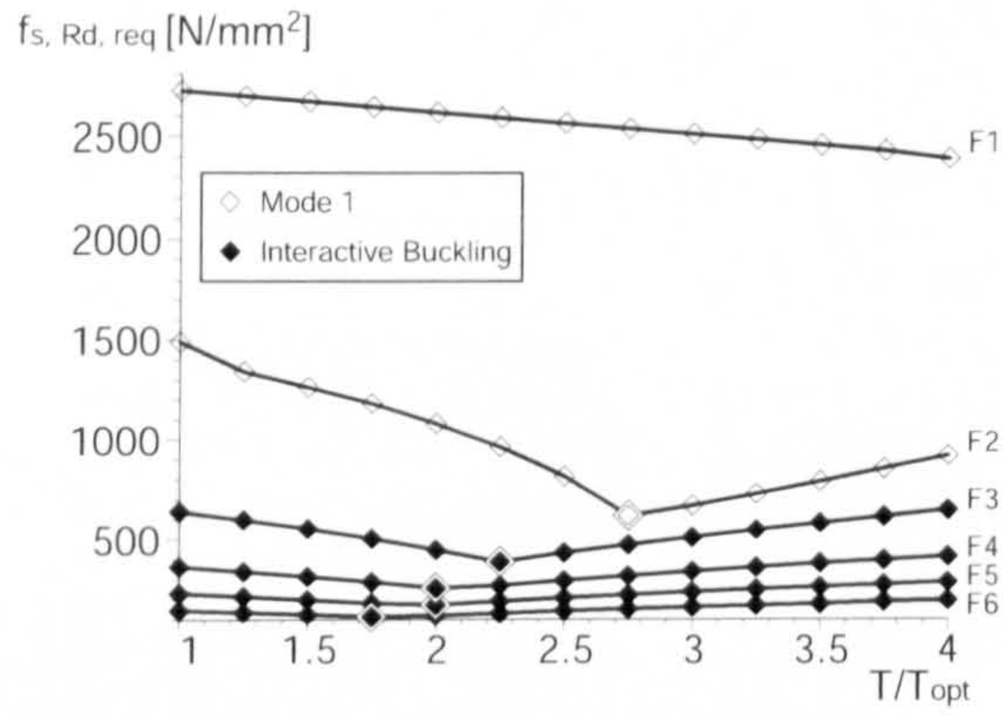

(d) a4

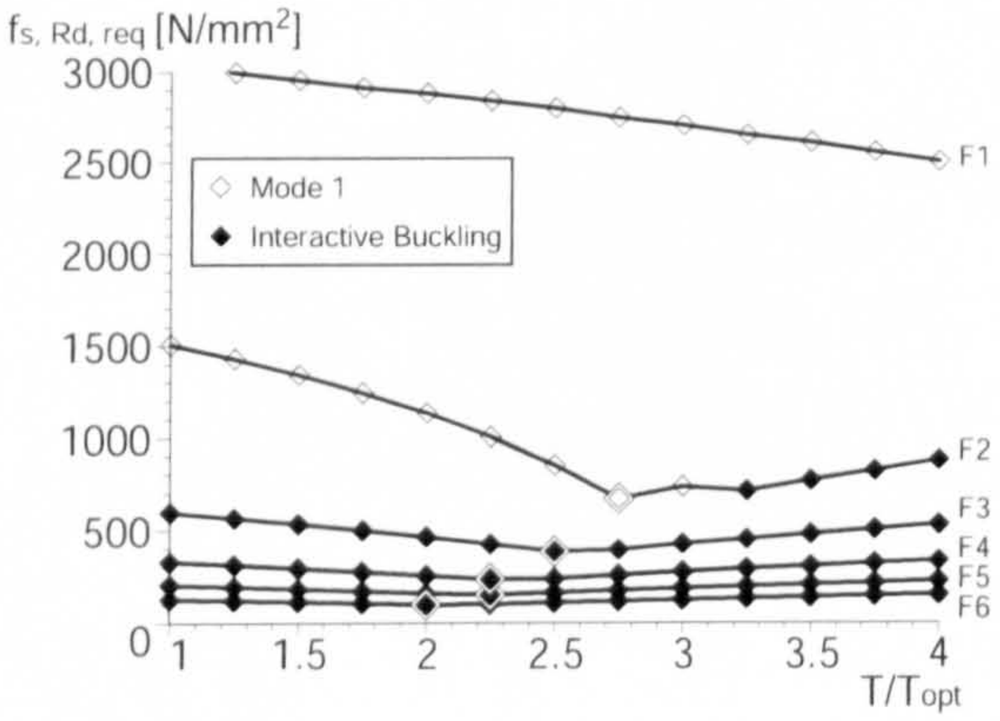

(e) a5

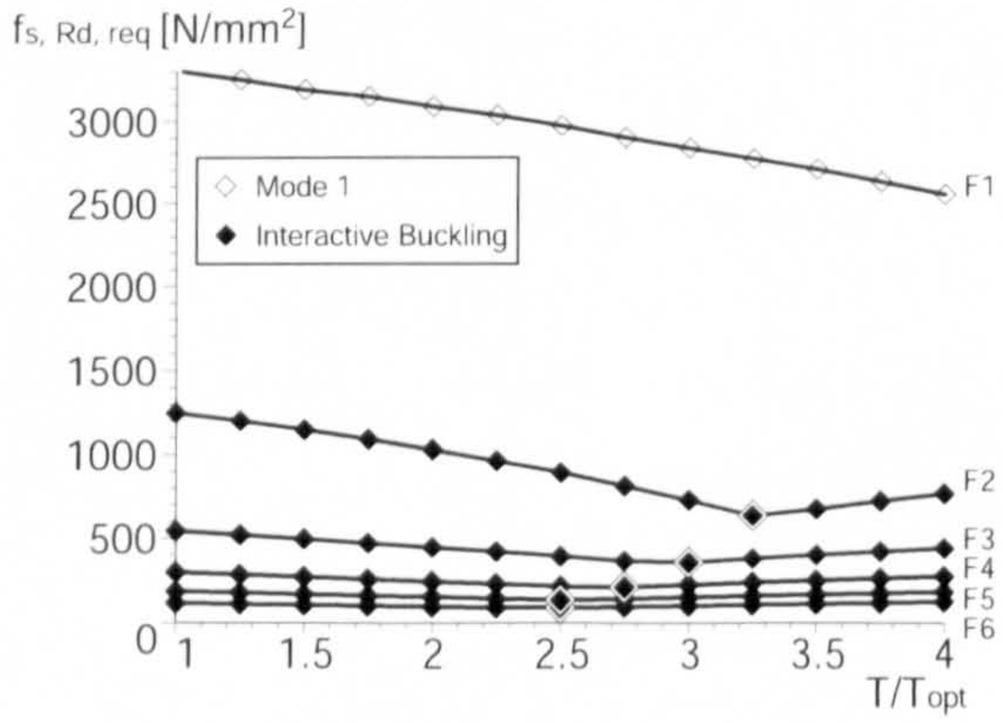

(f) a6

Figure C.2: Required stay design stress $f_{\mathrm{s,Rd,req}}$.

APPENDIX C. SUPPLEMENTARY DATA FOR PARAMETRIC STUDIES

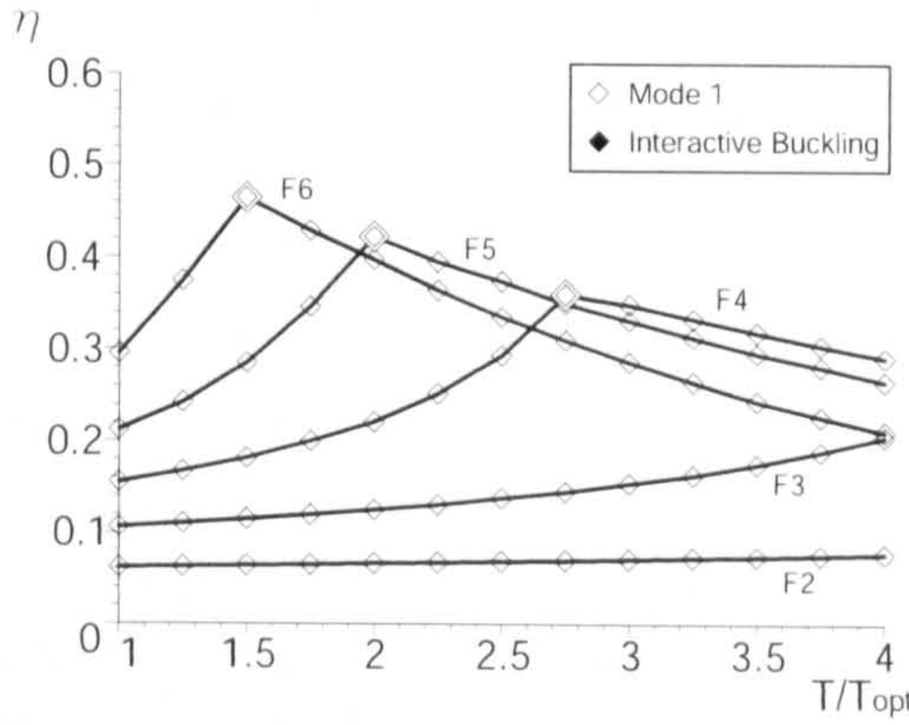

(a) a1

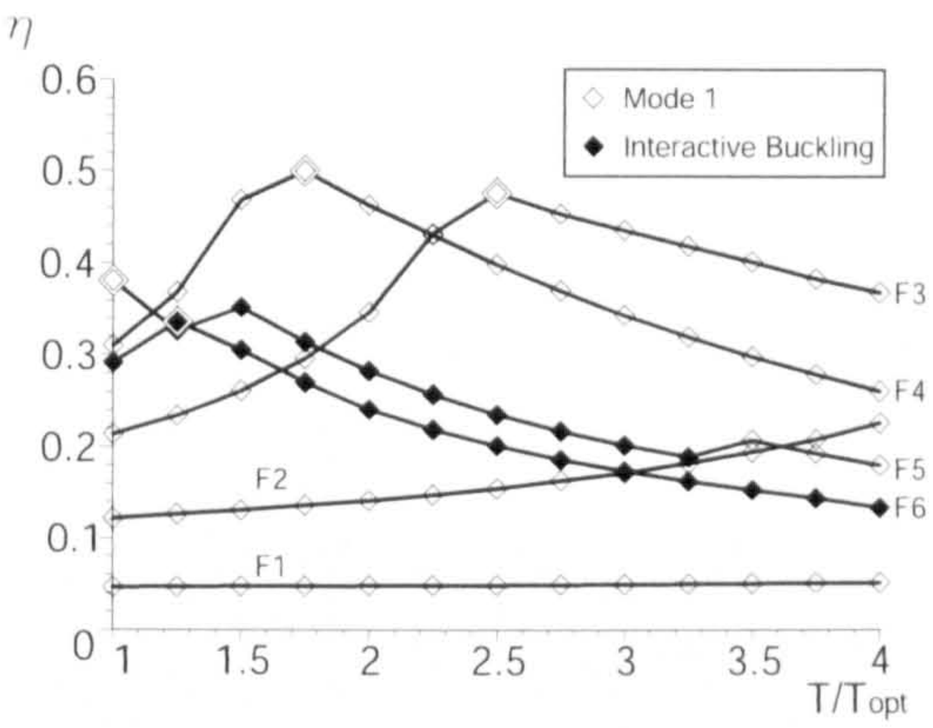

(b) a2

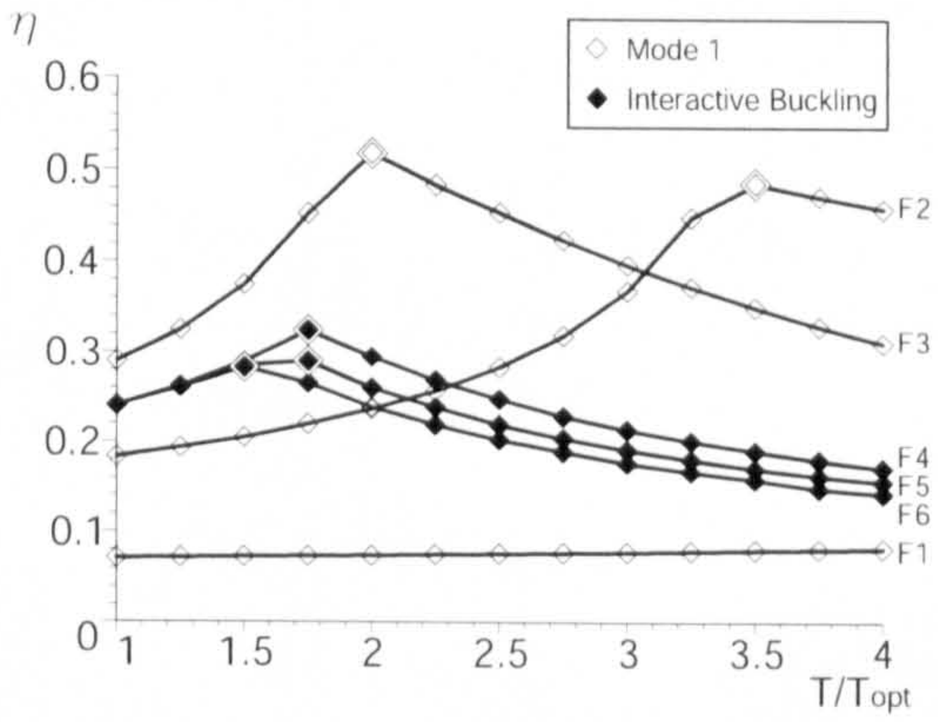

(c) a3

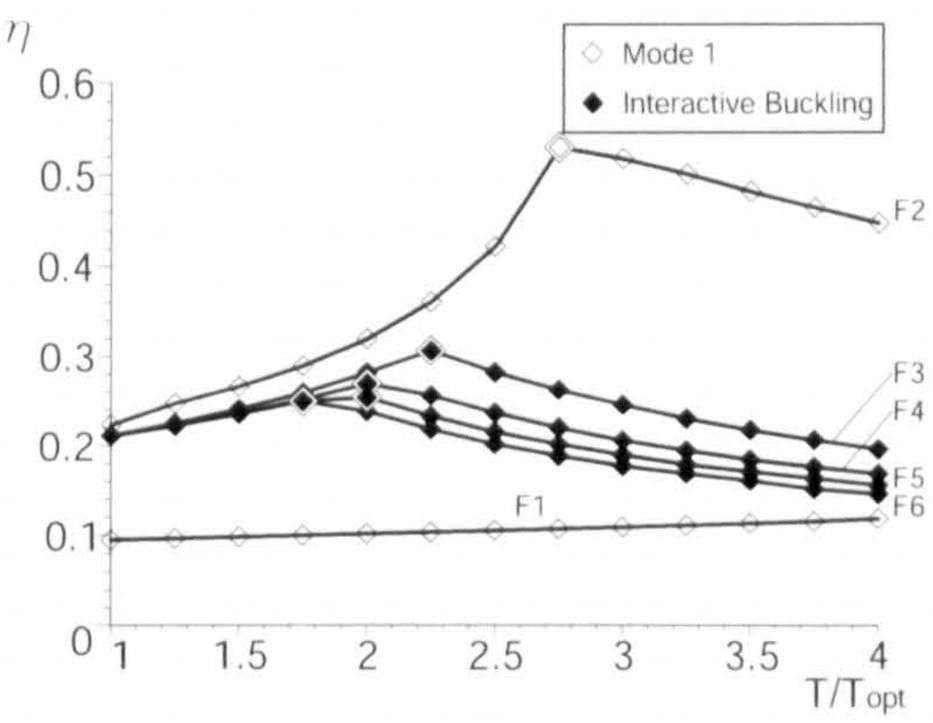

(d) a4

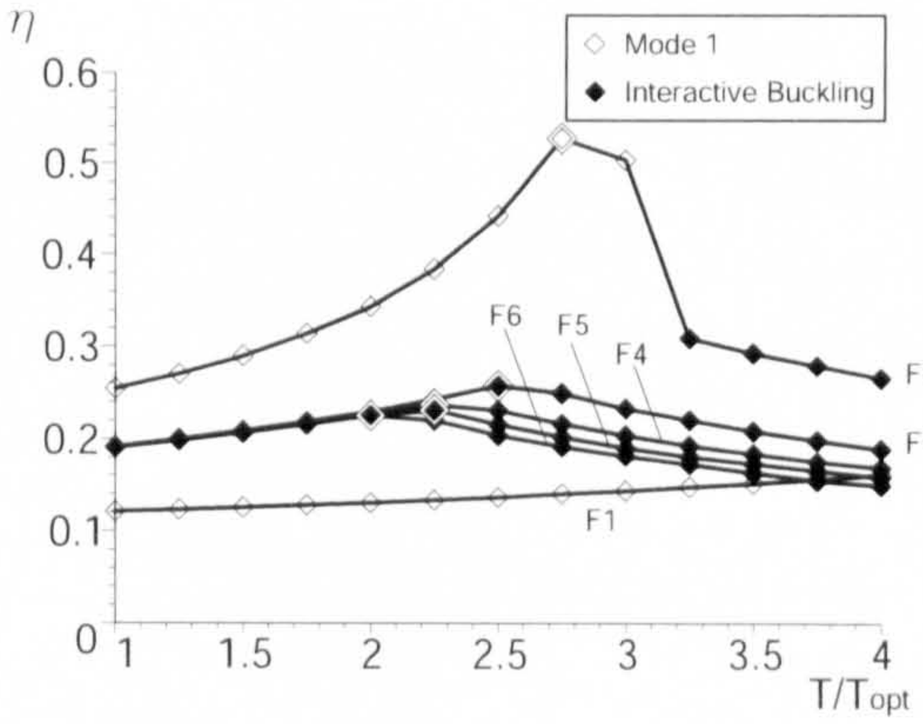

(e) a5

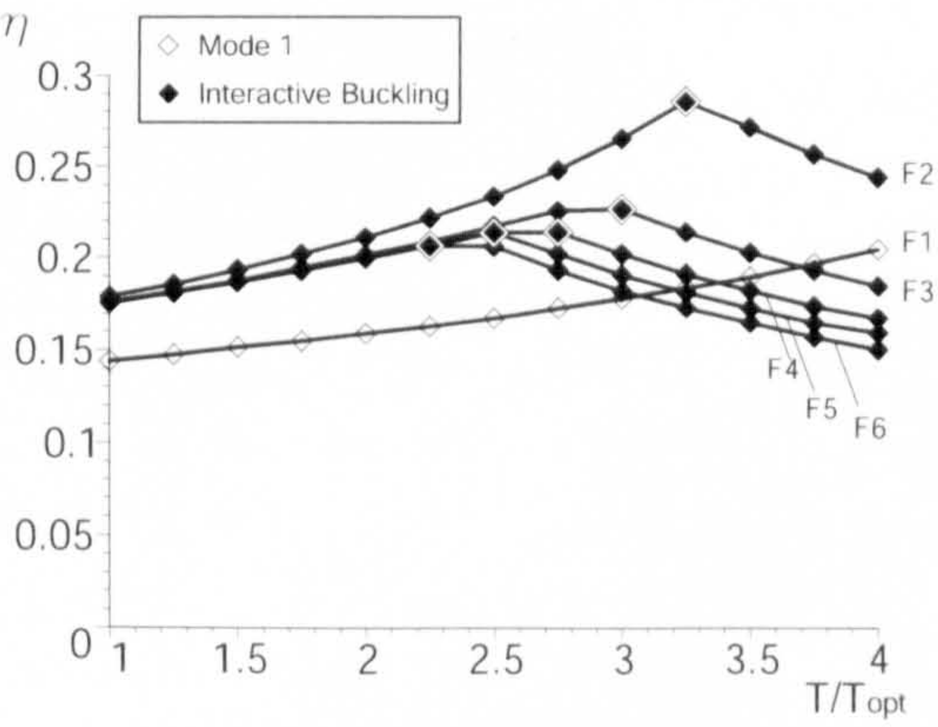

(f) a6

Figure C.3: Values of the column element efficiency η.

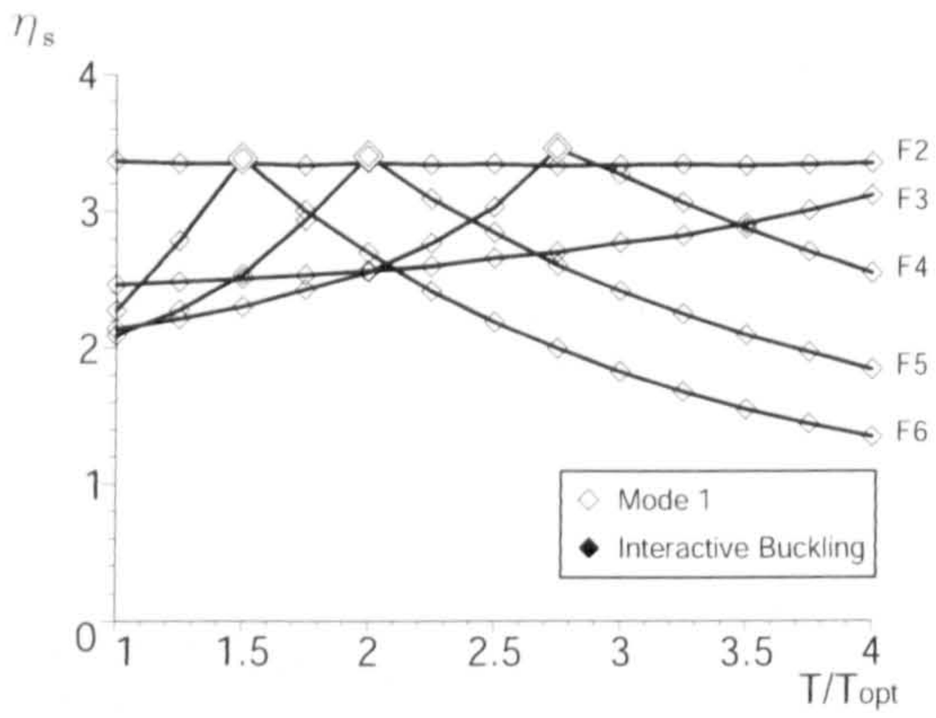

(a) a1

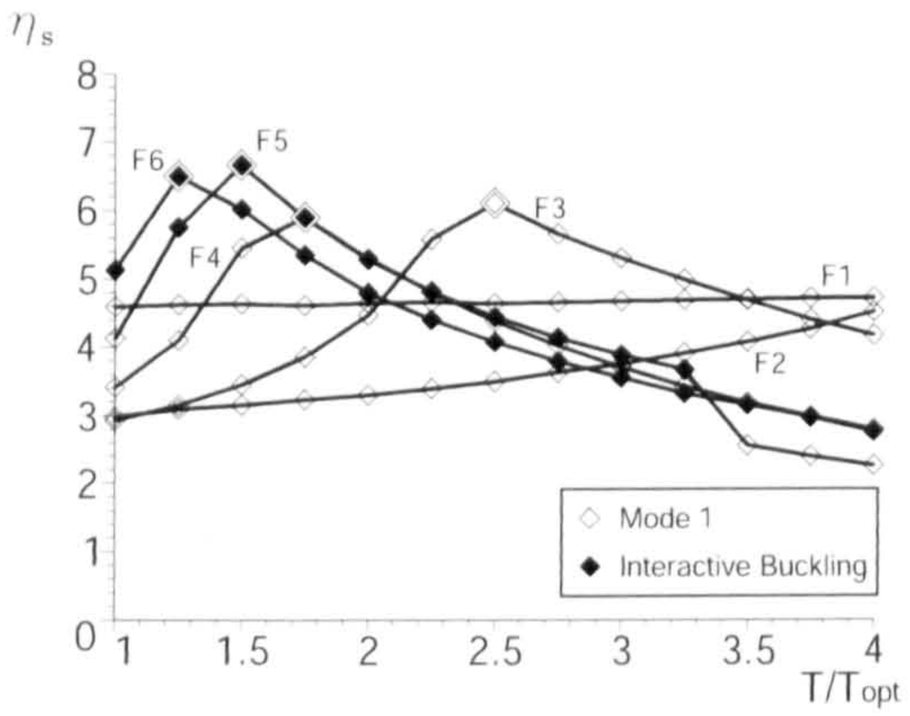

(b) a2

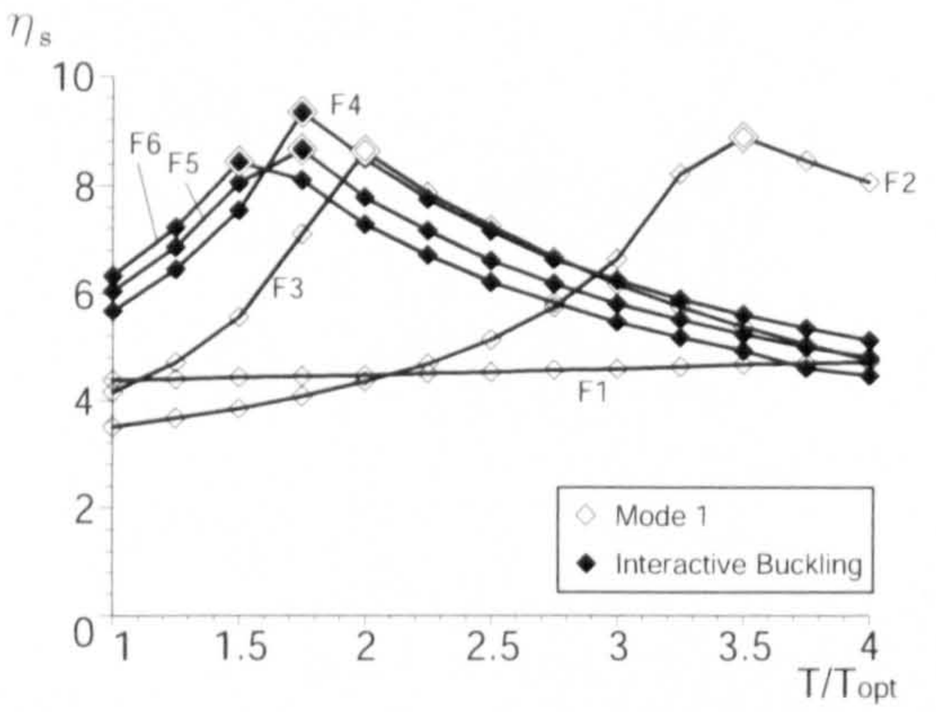

(c) a3

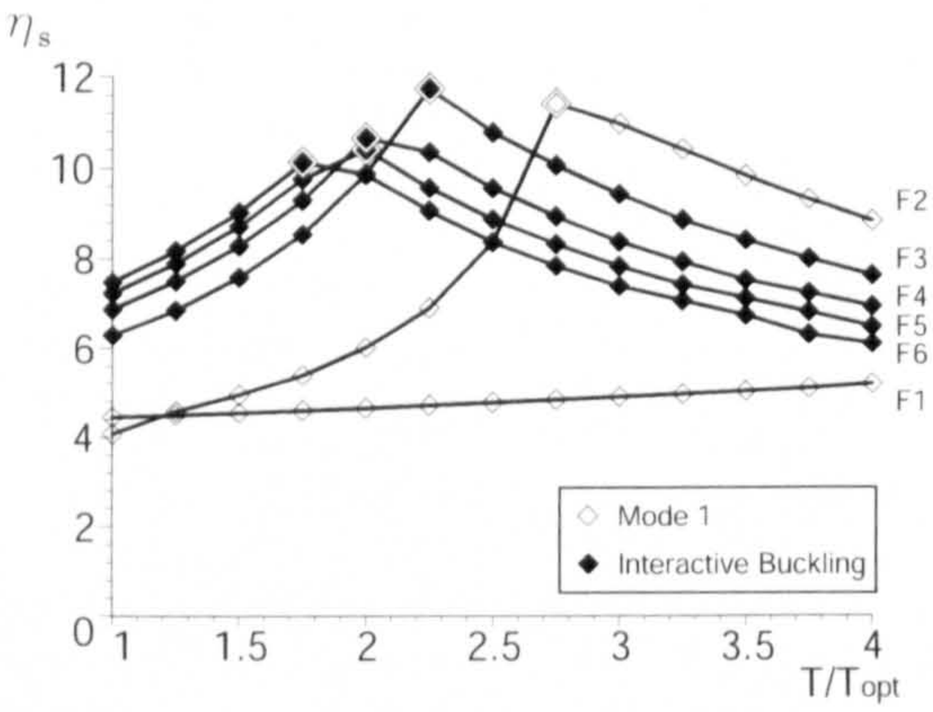

(d) a4

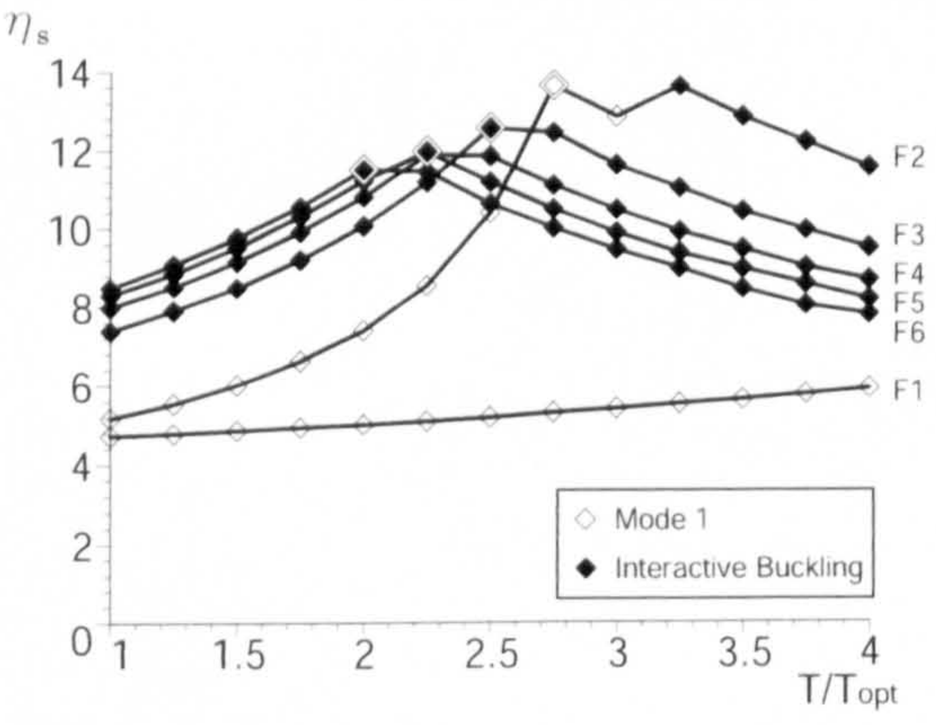

(e) a5

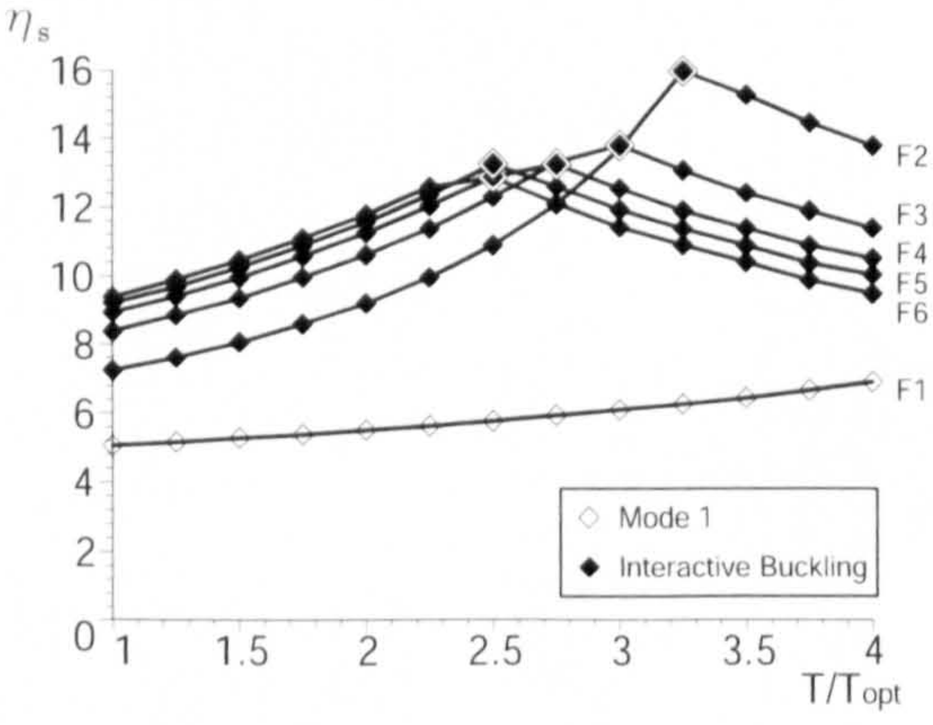

(f) a6

Figure C.4: Values of the stay efficiency η_s.

References

ABAQUS. 2006. *Abaqus/standard: User's manual version 6.6.* Pawtucket, USA: Hibbitt, Karlsson & Sorensen, Inc.

Allen, H. G. 1969. *Analysis and design of structural sandwich panels.* Oxford: Pergamon.

Allen, H. G., & Bulson, P. S. 1980. *Background to buckling.* Maidenhead: McGraw-Hill.

Azhari, M., & Bradford, M. A. 1995. The use of bubble functions for the postlocal buckling of plate assemblies by the finite strip method. *Int. J. Num. Meth. Eng.*, **38**(6), 955–968.

Bažant, Z. P., & Cedolin, L. 1991. *Stability of structures: Elastic, inelastic, fracture and damage theories.* Oxford: Oxford University Press.

Belenya, E. 1977. *Prestressed load-bearing metal structures.* Moscow: Mir Publishers.

Brazier, L. G. 1927. On the flexure of thin cylindrical shells and other thin sections. *Proc. R. Soc. A*, **116**, 104–114.

Chan, S. L., Shu, G., & Lü, Z. 2002. Stability analysis and parametric study of pre-stressed stayed columns. *Eng. Struct.*, **24**, 115–124.

Chu, K-H., & Berge, S. S. 1963. Analysis and design of struts with tension ties. *J. Struct. Div. ASCE.*, **89**(ST 1), 127–163.

Coates, R. C., Coutie, M. G., & Kong, F. K. 1988. *Structural analysis.* London, UK: Chapman and Hall Ltd. Third Edition.

De Andrade, S. A. L., Vellasco, P. C. G. da S., & Da Silva, J. G. S. 2003a. Concepcão e projecto estrutural do palco principal do Rock in Rio III. *Construçao Magazine*, **6**, 4–11. (in Portuguese).

De Andrade, S. A. L., Vellasco, P. C. G. da S., & Da Silva, J. G. S. 2003b. Sistema construtivo e montagem estrutural do palco principal do Rock in Rio III. *Construçao Magazine*, **7**, 30–35. (in Portuguese).

De Araujo, R. R., De Andrade, S. A. L., Vellasco, P. C. G. da. S., Da Silva, J. G. S., & De Lima, L. R. O. 2006. Structural response of pre-stressed stayed steel columns. *Stability and Ductility of Steel Struct.*, 241–248.

Dowling, P. J., Knowles, P., & Owens, G. W. 1988. *Structural steel design.* Sevenoaks, Kent, UK: Butterworths.

EN10210-2, BS. 2006. *British standard: Hot finished structural hollow sections of non-alloy and fine grain steels part 2: Tolerances, dimensions and sectional properties.* British Standards Institution.

EN1993-1-1, BS. 2005. *Eurocode 3: Design of steel structures - part 1-1: General rules and rules for buildings.* British Standards Institution.

EN1993-1-11, BS. 2006. *Eurocode 3: Design of steel structures - part 1-11: Design of structures with tension components.* British Standards Institution.

Everall, P. R. 1999. *Mode jumping and quasi-periodicity in nonlinear elastic structures.* Ph.D. thesis, University of Bath.

Everall, P. R., & Hunt, G. W. 1999. Arnold tongue predictions of secondary buckling in thin elastic plates. *J. Mech. Phys. Solids.*, **47**, 2187–2206.

Falzon, B. G., & Cerini, M. 2006. An automated hybrid procedure for capturing mode-jumping in postbuckling composite stiffened structures. *Composite Struct.*, **73**, 186–195.

Fox, C. 1987. *An introduction to the calculus of variations.* New York: Dover.

Hafez, H. H., Temple, M. C., & Ellis, J. S. 1979. Pretensioning of single-crossarm stayed columns. *J. Struct. Div. ASCE.*, **105**(ST 2), 359–375.

Hathout, I. A., Temple, M. C., & Ellis, J S. 1979. Buckling of space stayed columns. *J. Struct. Div. ASCE.*, **105**(ST 9), 1805–1822.

Heck, A. 2003. *Introduction to Maple.* New York, USA: Springer.

Howson, W. P., & Williams, F. W. 1980. A parametric study of the initial buckling of stayed columns. *Proc. Instn Civ. Engrs.*, **69**, 261–279.

Howson, W. P., & Williams, F. W. 1984. Stayed column design for optimum initial buckling. *Pages 706–712 of:* Nooshin, H. (ed), *3rd. Int. Conf. Space Struct.* London: Elsevier Applied Science Publishers.

Hunt, G. W. 1986. Hidden (a)symmetries of elastic and plastic bifurcation. *Appl. Mech. Rev.*, **39**(8), 1165–1186.

Hunt, G. W. 1989. Bifurcations of structural components. *Proc. Instn Civ. Engrs*, **87**, 443–467.

Hunt, G. W., & Wadee, M. A. 1998. Localization and mode interaction in sandwich structures. *Proc. R. Soc. A*, **454**, 1197–1216.

Hunt, G. W., Williams, K. A. J., & Cowell, R. G. 1986. Hidden symmetry concepts in the elastic buckling of axially-loaded cylinders. *Int. J. Solids Struct.*, **22**(12), 1501–1515.

Hunt, G. W., Da Silva, L. S., & Manzocchi, G. M. E. 1988. Interactive buckling in sandwich structures. *Proc. R. Soc.*, A **417**, 155–177.

Hunt, G. W., Mühlhaus, H-B., & Whiting, A. I. M. 1997. Folding processes and solitary waves in structural geology. *Phil. Trans. R. Soc.*, A **355**, 2197–2213.

Huseyin, K. 1974. *Nonlinear theory of elastic stability.* Leyden: Noordhoff.

Hutchinson, J. W., & Koiter, W. T. 1970. Postbuckling theory. *Appl. Mech. Rev.*, **23**, 1353–1366.

Jemah, A. K., & Williams, F. W. 1990. Parametric experiments on stayed columns with slender bipods. *Int. J. Mech. Sci.*, **32**(2), 93–100.

Johns, K. C., & Chilver, A. H. 1971. Multiple path generation at coincident branching points. *Int. J. Mech. Sci.*, **13**, 899–910.

Koiter, W. T. 1945. *On the stability of elastic equilibrium.* Ph.D. thesis, Technische Hogeschool, Delft (Technological University of Delft), The Netherlands. English translation issued as NASA, *Tech. Trans.*, **F10**, 833, 1967.

Koiter, W. T., & Pignataro, M. 1976. *A general theory for the interaction between local and overall buckling of stiffened panels.* Tech. rept. WTHD 83. Delft University of Technology, Delft, The Netherlands.

Liew, J. Y. R., & Li, J-J. 2006. Advanced analysis of pre-tensioned bowstring structures. *Int. J. Steel Struct.*, **6**(2), 153–162.

Luongo, A., & Pignataro, M. 1988. Multiple interaction and localization in the postbuckling of compressed thin-walled members. *AIAA J.*, **26**(11), 1395–1402.

Mauch, H. R., & Felton, L. P. 1967. Optimum design supported by tension tension ties. *J. Struct. Div. ASCE.*, **93**(ST 3), 201–220.

Murray, N. W. 1973. Buckling of stiffened panels loaded axially and in bending. *The Structural Engineer*, **51**(8), 285–301.

Ronalds, B. F. 1989. Torsional buckling and tripping strength of slender flat-bar stiffeners in steel plating. *Proc. Instn Civ. Engrs, Part 2*, **87**, 583–604.

Rotter, J. M. 2007. Recent advances in the philosophy of the practical design of shell structures, implemented in eurocode provisions. *Pages 26–31 of:* Zingoni, A. (ed), *Recent Developments in Structural Engineering, Mechanics and Computation, 2007.* Rotterdam: Millpress.

Simitses, G. J. 1976. *An introduction to the elastic stability of structures.* Englewood Cliffs: Prentice-Hall.

Smith, E. A. 1985. Behavior of columns with pretensioned stays. *J. Struct. Div. ASCE.*, **111**(5), 961–972.

Smith, R. J., McCaffrey, G. T., & Ellis, J. S. 1975. Buckling of a single-crossarm stayed column. *J. Struct. Div. ASCE.*, **101**(ST 1), 249–268.

Southwell, R. V. 1932. On the analysis of experimental observation in problems of elastic stability. *Proc. R. Soc. A*, **135**(828), 601–616.

Sridharan, S., & Peng, M-H. 1989. Performance of axially compressed stiffened panels. *Int. J. Solids Struct.*, **25**(8), 879–899.

Steirteghema, J. V., De Wildea, W. P., Samyn, P., Verbeecka, B. P., & Wattel, F. 2005. Optimum design of stayed columns with split-up cross arm. *Adv. Eng. Soft.*, **36**, 614–625.

Supple, W. J. 1970. Changes of waveform of plates in the post-buckling range. *Int. J. Solids Struct.*, **6**, 1243–1258.

Temple, M. C. 1977. Buckling of stayed columns. *J. Struct. Div. ASCE.*, **103**(ST 4), 839–851.

Temple, M. C., Prakash, M. V., & Ellis, J. S. 1984. Failure criteria for stayed columns. *J. Struct. Div. ASCE.*, **110**(11), 2677–2689.

Thompson, J. M. T., & Hunt, G. W. 1973. *A general theory of elastic stability.* London: Wiley.

Thompson, J. M. T., & Hunt, G. W. 1984. *Elastic instability phenomena.* Chichester: Wiley.

Thompson, J. M. T., & Lewis, G. M. 1972. On the optimum design of thin-walled compression members. *J. Mech. Phys. Solids.*, **20**, 101–109.

Thompson, J. M. T., & Supple, W. J. 1973. Erosion of optimum designs by compound branching phenomena. *J. Mech. Phys. Solids.*, **21**, 135–144.

Trahair, N. S., Bradford, M. A., & Nethercot, D. A. 2001. *The behaviour and design of steel structures to BS5950.* London, UK: Spon Press. Third Edition.

Tsien, H. S. 1942. A theory for the buckling of thin shells. *J. Aero. Sci.*, **12**, 373–384.

Wadee, M. A. 1999. Experimental evaluation of interactive buckle localization in compression sandwich panels. *J. Sandw. Struct. Mater.*, **1**(3), 230–254.

Wadee, M. A. 2000. Effects of periodic and localized imperfections on struts on nonlinear foundations and compression sandwich panels. *Int. J. Solids Struct.*, **37**(8), 1191–1209.

Wadee, M. A. 2007. Nonlinear mathematics in structural engineering. *Math. Today*, **43**(3), 104–108.

Wadee, M. K., Wadee, M. A., Bassom, A. P., & Aigner, A. A. 2006. Longitudinally inhomogeneous deformation patterns in isotropic tubes under pure bending. *Proc. R. Soc. A*, **462**, 817–838.

Wong, K. C., & Temple, M. C. 1982. Stayed column with initial imperfection. *J. Struct. Div. ASCE.*, **108**(ST 7), 1623–1640.

Zeeman, E. C. 1977. *Catastrophe theory.* London, UK: Addison-Wesley.